Crystallization and Enthalpic Relaxation Studies on A Copolymer of Lactic Acid

By

Azizan Abdul Aziz

UNIVERSITY OF BIRMINGHAM

A thesis submitted to the University of Birmingham

For the degree of

DOCTOR OF PHILOSOPHY

School of Metallurgy and Materials
College of Engineering and Physical Sciences
University of Birmingham

December 2016

Synopsis

The effect of thermal behaviour and properties such as enthalpic relaxation, degree of crystallinity, development of crystallization, crystallization kinetics and melting behaviour of Co-poly (lactic acid) were studied using differential scanning calorimetry (DSC), FTIR spectroscopy and hot stage microscopy. Co-poly (lactic acid) was chosen for this study since unlike poly (L-lactic acid) it was very slow to crystallize, the comonomer inhibiting the crystallization, and it was well suited to test the technique of FTIR-TA to measure the development of crystallinity over extended periods up to and beyond 1000 min. and to produce material with very different degrees of crystallinity.

Both glass formation and enthalpic relaxation have been measured on amorphous and partially crystalline samples produced by controlled cooling from the melt and the effect of the degree of crystallinity measured. The reduction in the enthalpic relaxation at equilibrium was primarily due to the change in $\Delta c_p(T_g)$ and increase in T_g with crystallinity attributed to the reinforcing effect of the hard crystalline phase on the soft mobile liquid phase. Kohlrausch-William-Watts equation was used to analyze the kinetics of the enthalpic relaxation but there was little change of the parameters with the degree of crystallinity.

In measuring isothermal crystallization, four procedures were adopted using a thermostated oven and DSC to follow the development of crystallinity with time over a wide temperature range from the glass transition to the melting point (m.pt). However, the results were dependent on the experimental conditions but gave some indication that the samples crystallized on cooling to room temperature and on re-heating to the m.pt. Last trace of crystallinity m.pts which were characteristic of the crystallization temperature were obtained by rapid reheating and correcting for thermal lag. These were analysed by the Hoffman-Weeks's relationship to determine the equilibrium melting temperature. Furthermore by

modifying a model proposed by Flory and Vrij the m.pts were used to calculate the stem lengths of the lamellae with time at each isothermal temperature. The stem length increased in thickness with the square root of time from the initial onset of crystallization and the rate increased with temperature obeying an Arrhenius relationship. This was considered to be evidence for the mechanism of secondary crystallization being diffusion controlled and occurring concurrently with primary.

Observation of the crystallization in thin films by hot-stage microscopy confirmed that the mechanism was that of the growth of heterogeneously nucleated disc spherulites. Both nucleation density and radial growth rates were measured but they exhibited different temperature dependence. The growth rate exhibited the characteristic bell shaped dependence which has been explained by the Hoffman and Lauritzen relationship in terms of nucleation control at temperatures close to the m.pt. and diffusion control at temperatures near the glass transition. The derived nucleation constant K was consistent with growth nucleation occurring in Regime 11, and enabled the surface energy terms to be determined.

FTIR spectroscopy has been used to study and characterize the change in structure of Co-PLA with temperature and time. Many of the IR absorptions bands change position and intensities with heating and cooling process consistent with crystallizing and melting reversibly. Isothermal crystallization kinetics analysis of Co-PLA conducted in the temperature range from 120 to 136 °C from these changes in the absorption of the IR bands and in particular the intensities of the crystalline and amorphous bands of the carbonyl ester group. In this way it was possible to analyse the kinetics of both primary and secondary crystallization directly from the relative crystallinity over extended periods with sufficient accuracy to test the validity of the Avrami equation.

Modifications have been made to the Avrami equation to account for the simultaneous presence of secondary crystallization and the additional crystallinity produced by the secondary processes is sufficient to account for the observation of fractional constant n values on analysing the data assuming that primary and secondary crystallization could be separated by their different time dependences.

The rate constants determined were consistent with the primary process occurring by growth of heterogeneous disc spherulites growing linearly with time and obeying an Avrami equation with n=2.0. The secondary process occurred by the thickening of the lamellae with the square root of time, the rate of thickening being diffusion controlled.

Acknowledgement

First and foremost, I am grateful to my supervisors, Dr Michel J. Jenkins and Professor James N. Hay for their guidance, patience, tolerance and insight over the period of this research but for their persistence this project would not have come to fruition.

I would also like to give a very special thanks to Mr. Frank Biddlestone for his technical support. His broad experience, logical thinking and constructive comment have been of great value to me in carrying out the experimental part of the research.

I would like to express my sincere gratitude to Dr Samsudin S. Amril for his helpful comments and guidance during the latter years of my studies and I must not forget to thank my many friends who have supported me and shared their knowledge; these precious friendships have made my life in UK most enjoyable and will last a lifetime.

I gratefully acknowledge the assistance from Dato' Dr Zainal Abidin Mohd Yusuf (President and Group Chief Executive of SIRIM Berhad, Malaysia) and the Director General of MARA, Malaysia for providing the opportunity for this postgraduate study.

Finally, I would like to express my special appreciation to my wife, Siti Azurah Ahmad, my children, Norman Adam and Mikael Alif, and also my parents, brothers and sisters for their love, moral support and continuous encouragement during my long absences during my studies in the U.K.

CONTENTS

List of Figures

List of Tables

Abbreviations

Co-PLA	*Co-poly(lactic acid)*
CCD	*Charge-coupled devices*
DSC	*Differential scanning calorimetry*
FTIR	*Fourier transform infrared spectroscopy*
IR	*Infrared*
KBr	*Potassium bromide*
m.pt.	*Melting point*
mW	*Milliwatts*
PET	*Poly(ethylene terephthalate)*
PEK	*Polyether ketone*
PEEK	*Polyether ether ketone*
PLA	*Poly (lactic acid)*
PS	*Polystyrene*
ROP	*Ring Opening Polymerization*
TGA	*Thermogravimetric analysis*

Symbols

%	Percentage
σ	Surface free energy
σ_e	Fold surface free energy of the critical size nucleus
π	Circumference ratio
°C	Degree Celsius
μm	Micron 10^{-6} m
A	Surface area / Absorbance / a pre-exponential factor
A_o	Absorbance of the amorphous band at initial time
A_t	Absorbance of the amorphous band at time t
A_∞	Absorbance at end of crystallization
A_c	Absorbance of a totally crystalline sample
a	Unit cell dimension along the growing plane
b	Lateral side of the unit cell / monomolecular layer thickness
c	Unit cell dimension along the lamella thickness / velocity of light / concentration of the substance
c_p	Specific heat
d	constant thickness of disc
ΔE	Activation energy of viscous flow
g	Steady state growth rate of a crystal / radial growth rate / Temperature independent constant
g^o	a pre-exponential factor
Δg_v	Difference in free energy between the solid and liquid per cm^{-3}
ΔG_f	Free energy of nucleus per mol

ΔG^*	Free energy of formation of a critical size nucleus per monomer mol.
ΔH_f	Heat of fusion of the sample per monomer mol.
ΔH^o_f	Heat of fusion of the totally crystalline sample per monomer mol.
Δh_v	Enthalpy of fusion per cm^3
Δs_v	The entropy change on crystallization per cm^3
Δh_m	Heat of fusion per g.
Δh_m^o	Enthalpy of fusion of totally crystalline sample per g
Δh_∞	Maximum enthalpy change per g.
Δg_p	Change of specific heat J per g.
ΔE_A	Activation energy of enthalpic relaxation, per monomer mol.
Δh_t	Enthalpy change at Tg per g
Δh_∞	Difference between enthalpy of the quenched glass and liquid per g.
h_o	Enthalpy of the quenched glass per g
h_∞	Extrapolated enthalpy of the liquid
K	Kelvin / equilibrium constant / Nucleation constant
ks	Secondary crystallization rate constant
k	Boltzmann constant
L	Nucleation density
l	Film thickness / lamellae thickness / nucleation rate
N	Density of heterogeneous nuclei
n	Avrami exponent / number repeat monomer units / an integer constant
R_h	Rate of heating
R_c	Rate of the imposed factor / the crystallization rate
R	Gas constant (8.314JK-1 mol-1)
R^2	Sum of the square of the residuals

T_A	The ageing temperature
C_p	Heat capacity per mol
$c_{p,g}$	The specific heats of the glass per g
$c_{p\,l}$	The specific heats of the liquid per g
r	Constant radius of rods / radius of spherulite
T	Temperature ^oC
Tc	Crystallization temperature
Tg	Glass transition temperature
Tm	Melting temperature
T_m^o	Equilibrium melting temperature
T_∞	Temperature below which the motion of crystallisable segment
t	Time
$t_{1/2}$	Crystallization half-life
ΔT	Degree of supercooling ($\Delta T = T_m^o - T_c$)
W	Wavenumber
Xa	Amorphous weight fraction,
Xa,t	Amorphous weight fraction at time t
X_c	Crystalline weight fraction
X_p	Relative primary crystallinity
X	Relative crystallinity
$X_{c,t}$	Fractional crystallinity at time t
$X_{p,t,}$	Fractional primary crystallinity at time t
$X_{p\infty}$	Fractional primary crystallinity at the end of the process
$X_{p,f}$	Residual crystallinity left after partial melting
$X_{s\infty}$	Fractional secondary crystallinity at the end of process

Xt	Fractional crystallinity at time t
P_o	Probability of a point on a surface is uncovered by expanding circles
T_2	Thermodynamic glass transition temperature
ν	Frequency / growth rate
v_o	Temperature independent constant
v_t	Total area of the expanding circles at time t
U*	Activation energy for viscous flow (6300 J per mol)
α_t	The degree of conversion towards equilibrium at time t
τ_o	Average relaxation time
dT/dt	Heating rate, $^oC\ s^{-1}$
dH/dt	Heat flow, watts
$\Phi(t)$	Extent of enthalpic relaxation
β	Inverse measure of the breadth of the relaxation spectrum
γ	Under equilibrium conditions of no annealing or re-crystallization
ξ	Lamellae fold length/ thickness of the lamellae
ξ_e	Equilibrium lamellae fold length
Z	Avrami composite rate constant
Z_p	Avrami composite rate constant for primary process

1.0. Introduction

Poly (lactic acid), PLA, is one of the most important commercial bio-polymers. Since it is biodegradable and readily produced from annually renewable resources it is considered to be a possible replacement for oil based plastics, such as polyethylene and polypropylene, especially in packaging.[1-6]. It is biocompatible and has good mechanical properties and has been extensively used in many medical devices and applications especially drugs delivery, scaffolds and tissue engineering [7, 8].

PLA is produced from natural resources and being biodegradable its application in food packaging has become appropriate because it does not require or at least very minimum usage of the landfill for disposal [9, 10]. It has the required clarity and rigidity as a film and comparable to materials such as poly (ethylene terephthalate) (PET) and polystyrene (PS). It has excellent shaping and moulding properties [11]. Recently, the large scale and economic production of PLA has been developed by Nature Work LLC but it has been reported that PLA is relatively brittle and due to that it has limitations in the range of its applications [12].

The monomer repeat unit and chain structure of PLA is shown in Figure 1.1

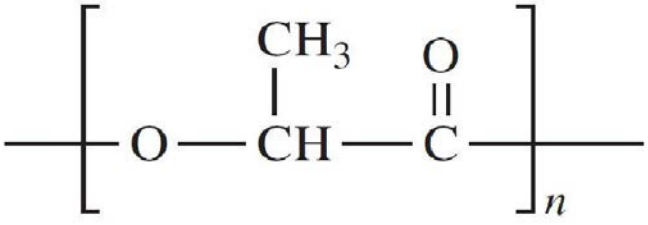

Figure 1.1. Poly-lactic acid (PLA) repeated unit

It has an asymmetric carbon atom and as such can exist in two geometric isomers, i.e. D and L forms, which gives rise to stereoregular polymers which differ only in stereoregularity of the monomer sequences along the chain.

PLA is a linear aliphatic polyester of lactic acid (2-hydroxy propionic acid) and can be produced from the condensation polymerization of lactic acid or the ring opening polymerization (ROP) of the three cyclic dimers of lactic acid, see Figure 1.2. The cyclic dimer of PLA possesses two asymmetric carbon atoms and generally exists in three different forms i.e. L-lactide, D-lactide and Meso-lactide as shown in Figure 1.2. In the D- and L- lactides both asymmetric carbons atoms possess the same configuration, while the meso-lactide has one L and the other D configurations.

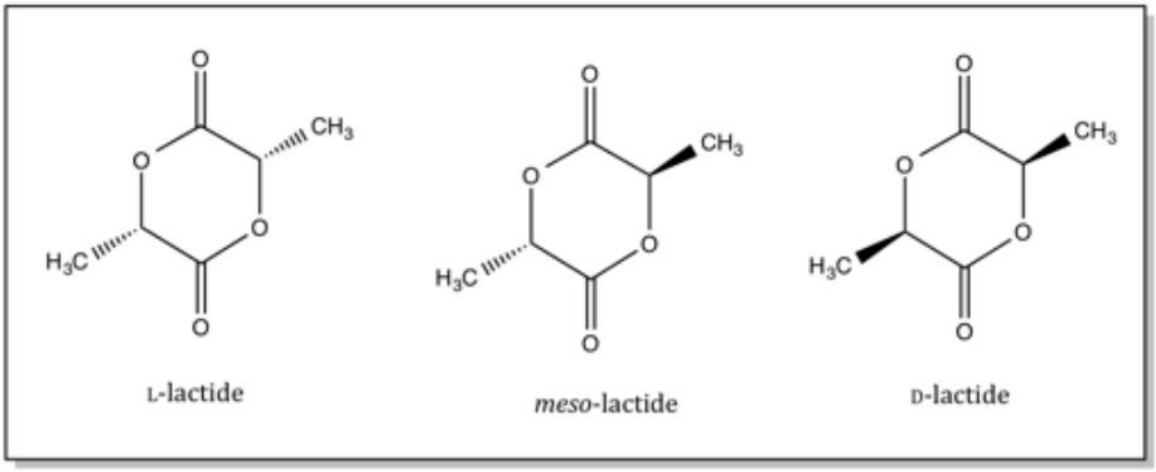

Figure 1.2. Three different chiral stereoisomers of PLA: L-lactide, D-lactide and meso-lactide

It was reported that if more than 90% of the L content exists in the polymer it can crystallize to a limited extent but with lower stereoregularity the polymers are amorphous and form glasses with transition temperatures, Tg, between 50 – 57 °C [13-14] depending on the stereoregularity. It has also been reported that generally the crystallinity of poly (L-lactide) can reach 45% [15]. Addition of small amounts of D-lactide in a random copolymer reduces the rate of

crystallization and crystallinity. This reduction increases with increasing D-content of the copolymers [16]. Studies on the influence of addition of the meso-lactide show that there is a reduction in melting point of 3 °C for every 1% added [17]. These observations show that significant changes can be made to the physical properties of PLA by the introduction of imperfections in the stereoregularity. It was also reported that imperfections can be seen in the form of twists in the configuration of the chain that hinder closed packing within the crystalline regions and this depends on the amount of D or meso-lactide content in the copolymer [18]. It is also been reported that in tailoring polymer properties such as crystallinity, thermal stability and melting point as well as mechanical properties, the stereoregularity of PLA should be controlled [19, 20].

In this study a copolymer of L- lactic acid with 4% D- lactide was studied to reduce the rate of crystallization. It exhibited a T_g in the range 50–60 °C. Below this temperature, Co-PLA is rigid and brittle. Developing high crystallinity in PLA tends to increase the elastic modulus and reduce the elongation at break as well as the service temperature [21].

1.1. Polymer Morphology

Thermoplastic polymers can be divided into two groups of materials, amorphous and partially crystalline. Polymers crystallized from the melt are not completely crystalline and the crystallinity can vary from 10 to 80% [22]. They always contain some amorphous regions. Polymers which cannot crystallise are completely amorphous and exist as mobile liquids above the glass transition temperature and as immobile liquids which appear to be “solid-like” below the glass transition.

In amorphous polymers the molecules are disordered with a liquid-like structure (Figure 1.3) whereas in the crystalline regions of a partially crystalline polymer the chains pack together to form ordered regions, frequently with a lamellar structure. These grow length-wise and by branching splay out into a spherical array called spherulites [22]. (Figure 1.4).

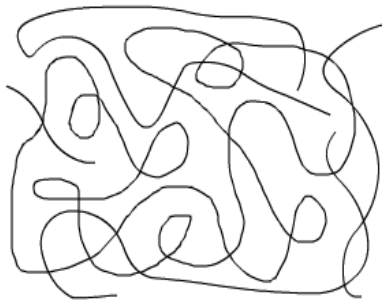

Figure 1.3. Amorphous [23]

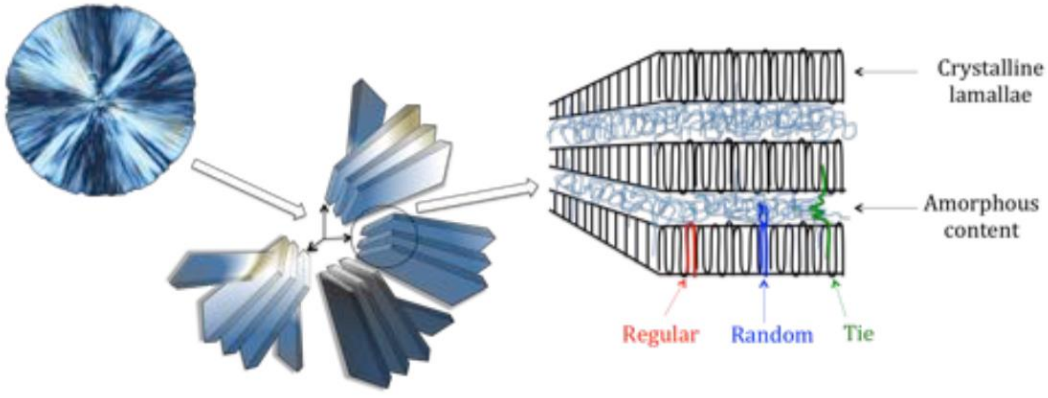

Figure 1.4. An idealised representation of the structure of a polymer spherulite emphasising the structure of the branching lamellae and the direction of the molecular chains perpendicular to the spherulite radius.

1. 2. Polymer Crystallization

The crystallization of polymers is a transition from a highly disordered array of the chains, characteristic of the amorphous phase into three-dimensional ordering of the chains within the lamellae in which the chains are aligned parallel to one another [24, 25]. The micro-structure of the crystalline polymers is built up from arrays of lamellae, locally parallel with the polymer chains perpendicular to the length of the lamellae. The lamellae are separated from one another by amorphous regions which remote from the surface of the lamellae have liquid structure of amorphous materials but close to the surface and emerging from the surface retain some of the crystal structure or form irregular folds by returning to the lamella. The lamellae by repeated branching develop into spheres, called spherulites which grow linearly with time until they impinge with one another. Once a spherical contour is achieved the molecular chains within the lamellae are perpendicular to the expanding radii of the spherulite. The thickness of the lamellae and their linear growth rates are dependent on the crystallization temperature. The size of the final spherulites depend on the number of nuclei which initiate the growth of the spherulites and depends on the previous thermal history of the polymer and processing conditions such as crystallisation temperature, rate of change of temperature with respect to time, molecular weight of the polymer and any inclusions [25, 26]. Therefore only partially crystallinity can develope due to the many entanglements preventing the entire polymer chains arranging into the three-dimensional array required for crystallinity and a 100% crystalline polymer is not possible on crystallizing from the melt [25].

PLA can be either amorphous or crystalline depending on its molecular order but also on the processing conditions in the melt i.e an amorphous polymer is achieved by rapidly quenching from the melt to below Tg if the crystallization rate is inhibited by reducing its stereoregularity. However, by using a slow cooling rate from the melt or by retaining it at the appropriate temperature the same polymer can be obtained crystalline [27–29].

1.2.1. Nucleation

Two distinct processes are involved in crystallization; these are nucleation and growth. Three types of nucleation have been postulated to account for the behaviour of crystallization and its temperature dependence; these are primary, secondary and tertiary nucleation.

In primary nucleation, an isolated crystalline region is produced from the melt and a small ordered region i.e. a nucleus is produced by random alignment of chain segments or on the surface of a foreign particle, i.e. an inorganic or dust particles; this is strictly speaking secondary nucleation but since it involves production of a polymer crystal nucleus we will treat it as a primary nucleation process. The first is homogeneous nucleation and occurs by the chance alignment and clustering of chain segments until a stable entity is produced which can grow rather than dissipate into the amorphous material. The second is heterogeneous nucleation and is usually associated with crystalline impurities present in the polymer. Above the melting temperature, the nuclei are unstable due to the free energy of the liquid being lower than that of the crystalline state. Nucleation is controlled by the free energy of formation of the nucleus, which involves the surface free energy term, σ, as well as the difference between the bulk free energy of the liquid and the crystal Δg_v, per unit volume.

For a rectangular nucleus of dimensions a, b and c, the free energy of formation of the nucleus is

$$\Delta G_f = abc\Delta g_v + (2ab + 2ac + 2bc)\,\sigma \qquad (1.1)$$

assuming the surfaces have the same free energy.

For growth of the nucleus, ΔG_f has to be negative and for this to occur Δg_v has to be negative. since σ is always positive. This is the case below the equilibrium melting point and once a, b and c have achieved critical.

For $\Delta G_f = 0$

$$\Delta g_v = -\{(2ab + 2ac + 2bc)/abc\}\sigma \qquad (1.2)$$

The critical size of the nucleus a, b and c depends on the values of σ and Δg_v.

Since from classical thermodynamics Δg_v is defined by

$$\Delta g_v = \Delta h_v - T \Delta s_v$$

where Δh_v and ΔS_v are the enthalpy and entropy change on crystallization per unit volume of material at temperature T, respectively.

At the equilibrium thermodynamic melting point, T_m^o, $\Delta g_v = 0$. It follows that

$$T_m^o = \Delta h_v / \Delta s_v \qquad (1.3)$$

And

$$\Delta g_v = \Delta h_v (T_m^o - T_c) / T_m^o = \Delta h_v (\Delta T)/T_m^o \qquad (1.4)$$

where ΔT is the super-cooling from the equilibrium melting point.

It follows from the equation that Δg_v gets larger as ΔT increases and as a consequence ΔG_f smaller as well as a, b and c. It follows that the critical nucleus size decreases at lower crystallization temperature. Also the critical nucleus size is infinite at the thermodynamic melting point.

Hoffman and Lauritzen [30], extended this nucleation theory to polymer crystallization recognizing that the fold surfaces, a and b had a much larger surface energy, σ_e than the lateral surfaces structure, σ and equation 1.2 simplifies to

$$\Delta g_v = - (2/\xi)\sigma_e \qquad (1.5)$$

where ξ replaces c as the thickness of the lamellae.

This is the fundamental equation of Hoffman and Lauritzen theory of nucleation of polymer crystallization as it predicts the dependence of the thickness of lamellar crystals on crystallization temperature, the dependence of crystal growth on the degree of supercooling and the dependence of the melting point of polymers on crystallization temperature.

1.2.2. Growth

The second stage in crystallisation is growth of the crystal faces; this occurs by secondary nuclei forming on the growth surface by clustering and alignment of the chain segments until a stable nuclei is produced. Since the free energy of formation of the critical nucleus size is less than the primary nucleus involving fewer surface energy terms growth will normally occur after primary nucleation. Growth is observed to be a nucleation controlled process with a dependence on super-cooling, decreasing as the crystallization temperature increases towards the melting point. Spherulites are produced by growth branching of the lamellae.

Spherulites are observed to grow linearly with time such that the radius, r,

$$r = v\,t \tag{1.6}$$

where v is the growth rate and t is the time.

The growth rate has a bell shaped dependence on temperature in that the rate is zero close to the melting point and the glass transition temperature, see Figure 1.5. This is a result of two competing processes, nucleation at high temperature close to the melting point, when the rate is nucleation controlled and diffusion controlled at low temperature when the motion of the chain segments slow down as the glass transition is approached.

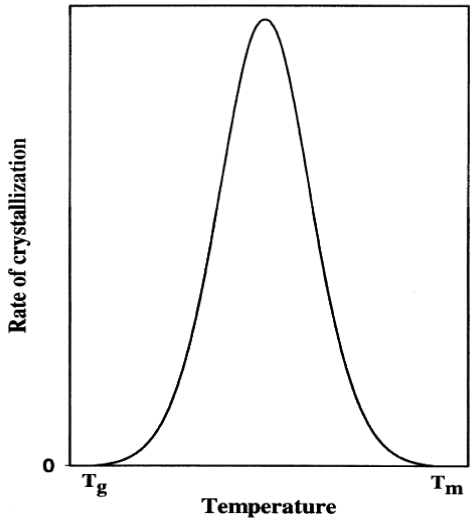

Figure 1.5. Dependence of crystallisation rate on temperature [31]

Turnbull and Fisher [32] have combined these two processes to derive the overall temperature dependence of the growth rate from the melt. The equation has been written as in the form of crystal growth rates as

$$v = v_o \exp(-\Delta E/RT).\exp(-\Delta G/RT) \qquad (1.7)$$

where v is the growth rate of a crystal at the crystallization temperature, T, v_0 is a temperature independent constant, ΔE represents the activation energy for viscous flow, i.e. the energy barrier for the transport of material to the crystal-liquid interface, ΔG is free energy of formation of a critical size nucleus and R is the gas constant (8.314 JK^{-1} mol^{-1}).

Hoffman and Lauritzen [33-40] modified the equation to

$$v = v_o.\exp(-U/R(T_c - T_2))\exp(-K/T_c.\Delta T f) \qquad (1.8)$$

where U is the activation energy of viscous flow (assigned a value of 6300 $Jmol^{-1}$ by Hoffman), T_c the crystallization temperature, T_2 the thermodynamic glass transition temperature, ΔT the degree of supercooling ($T_m^o - T_c$), R the gas constant and f is the correction for the temperature dependence, such that $f = 2T_c/(T_c + T_m^o)$. K is the nucleation constant the value which depends on the type of nucleation adopted and includes molecular structure information, i.e.

$$K = jb\sigma\sigma_e T_m^o / k\Delta H_v \quad (1.9)$$

where b is the monomolecular layer thickness, σ and σ_e the side and fold surfaces free energies, T_m^o the equilibrium melting point, k Boltzmann constant and ΔH_v the enthalpy of fusion per unit volume.

Equation (1.9) has been used to analyse the dependence of the radial growth of spherulites on the degree of supercooling, ΔT, provided it grew at the same rate as the radial expansion of the spherulite, no imperfect growth of crystal face and no crystal thickening.

According to Lauritzen and Hoffman, there are three regimes which describe three different secondary nucleation mechanisms called regime I, II and III; these are shown in Figure 1.6. The j value of equation 1.9 depends on the nucleation regime as defined by Lauritzen and Hoffman [30, 40, 41] where j = 4 for regimes 1 and lll, and 2 for regime ll. It is the relative rates of the secondary nucleation on the surface and extension of the polymer chain growth along the surface after nucleation was occurred.

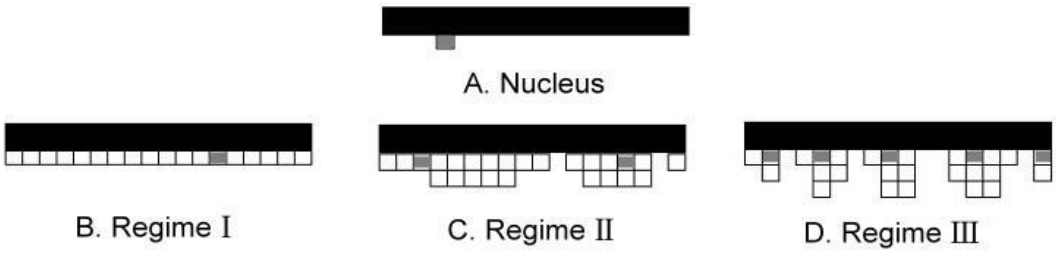

Figure 1.6. The model of secondary nucleation on the growth face of crystal. [42]

Where:

A. Isolated secondary nucleation.

B. Nucleation followed by covering of crystal face by crystalline material. (Smooth growth face.)

C. Further nucleation before face is completely cover. (Irregular growth face.)

D. Multiple nucleation before face is covered. (Rough growth face)

The regimes are separated by the degree of supercooling; in regime 1 it is small and surface nucleation is low compared with the rate of covering the surface. The j value is 4 and secondary nucleation rate dominates crystal growth. This implies that the growth surface is smooth.
In regime II the degree of supercooling is higher and the nucleation rate is comparable to rate of the surface being covered. The value of j is 2 and the growth surface is quite rough and irregular with prominences, see C in Figure 1.6. In regime III the degree of supercooling is even larger and the nucleation rate is faster than the surface is covered. The j value is also 4. Figure 1.6 illustrates the change in surface profile as the regimes change from I to III while Figure 1.7 illustrates the change in the nucleation constant, K.

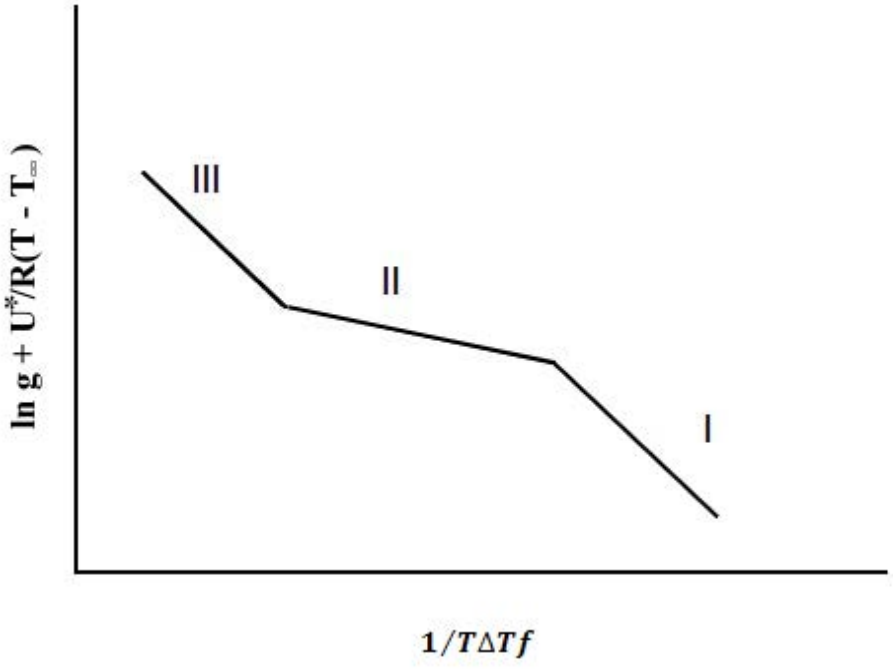

Figure 1.7. Three Regimes in the Nucleation [42].

1.3. Polymer Crystallization Kinetics – the Avrami Equation

The Johnson-Mehl-Avrami [43, 44] equation has been widely used to study polymer crystallization kinetics. Its derivation is more readily understood by a procedure adopted by Evans [45] using the pattern of expanding circles produced by raindrops on the surface of a smooth pond as one model of spherulite crystallization in thin films. The problem which had been solved by Poisson was to determine the probability, P_o, that a particular point on the surface was uncovered by any of the expanding circles. This was

$$P_o = \exp(-V_t) \qquad (1.10)$$

Where V_t is the total area of the expanding circles at time t.

Evans generalised this approach by considering all of the crystallization models adopted by Avrami [43, 44] to evaluate the kinetics of crystallization of metals, and derived what has

become to be known as the Avrami equation, relating the volume fractional crystallinity, X_t, to time.

$$1 - Xt = \exp(-Zt^n) \qquad (1.11)$$

where Xt is the volume fractional crystallinity, which has developed at time t, Z is a composite rate constant incorporating nucleation characteristics and growth rate, t is time and n is an integer constant characteristic of the crystallization mechanism and the geometry of the growing crystal.

Since $P_o = 1\text{-}X_t$ (1.12)

i.e. the volume fraction of material uncrystallised at time t.

The volume occupied by the crystalline entities is

$$V_t = Zt^n \qquad (1.13)$$

The values of Z and n are listed for each crystallization mechanisms adopted by Avrami. (Table 1.1).

Table 1.1. The Avrami Rate Parameters for different Crystallization Mechanisms.

Crystallization Mechanism	Nucleation	n Value	Z / t^{-n}	Geometric restriction
Spheres	Homogeneous	4.0	$2/3\pi v^3 l$	3-dimensional
Spheres	Heterogeneous	3.0	$4/3\pi v^3 L$	3-dimensional
Discs	Homogeneous	3.0	$1/3\ \pi v^2 ld$	2-dimensional
Discs	Heterogeneous	2.0	$\Pi v^2 Ld$	2-dimensional
Rods	Homogeneous	2.0	$1/4\ \pi l r^2 l$	1-dimensional
Rods	Heterogeneous	1.0	$1/2\ \pi v r^3 L$	1-dimensional

Growth rate v; nucleation rate l; nucleation density L; sample thickness d; rod radius r.

The Avrami equation has been widely adopted to analyse the crystallization kinetics of polymers [43, 44, 46-54] and the growth of spherulites in 3-dimensions has been observed by microscopy. For this mechanism, n should be 4.0 for homogeneous nucleation or 3.0 for heterogeneous nucleation but invariably fractional values between 3 and 4 are observed. The mechanisms chosen by Avrami for crystallization do not allow for constant fractional n values and many authors have doubted the validity of the application of the equation to polymer crystallization kinetics. The Avrami equation has many limitations which have been cited as the cause of fractional n values among which the variation in the crystalline density within the spherulite boundary throughout the crystallization process has been suggested as the cause for fractional n values. Others are that assumptions made in deriving it are not valid; the following have been identified [33, 54, 55]:

1. Nucleation and growth rate are not constant with time
2. The equation only accounts for primarily and not secondary crystallization process
3. The volume of the system is not constant
4. The growth does not cease on impingement.
5. Only rods, discs and spheres are considered.
6. An induction time before crystallization starts is present.

Despites these limitations the Avrami equation is still universally used to analyse the crystallization kinetics of polymers and the rate parameters are widely quoted.

1.4. The Melting of Polymers

Melt crystallized polymers generally melt over a range of 5 to 20 ^{o}C and tends to increase with increasing crystallization temperature. The value is also dependent on thermal history; in particular annealing at higher temperatures increases the melting point progressively with time. The melting point is not characteristic of the polymer in the same way as it is for

low molecular weight material. In measuring the m.pt. of a polymer by DSC it is convenient to define two different m.pts; one at which most of the crystalline regions are melting, i.e. T_{max} corresponding to the temperature of the maximum in the endotherm and one which defines the last trace of crystallinity, T_m, correponding to the end temperature when the thermal response returns to the baseline.

Polymer lamellae are very thin 10-20 nm thick and their m. p. is determined by the thickness which varies with crystallization and annealing temperatures according to the nucleation theory of Hoffman and Lauritzen [56]. T_{max} corresponds with the melting of lamellae with average thickness and T_m to the thickest lamellae present [56]. The range of melting corresponds with the distribution of lamellae thicknesses present.

The melting temperature of lamellar crystals which are infinitely thick and not suppressed by surface energy terms corresponds with the equilibrium melting temperature, T_m^o [57].

However, it is not measured directly by experiment since lamellar crystal grows with a finite thickness during the crystallization process determined by the size of the critical nucleus.

T_m^o is determined by extrapolation experimentally determined m.pts of lamellae of finite infinite thicknesses. T_m^o, is determined using the Hoffman-Week's relationship, derived from their theory of nucleation, [56] in which the observed melting point T_m is related to crystallization temperature, T_c by

$$T_m = T_m^o (1 - 1/2\gamma) + T_c/2\gamma \qquad (1.14)$$

Where $\gamma = (\sigma_e^* \xi / \sigma_e \xi^*_e)$, σ_e is the surface free energy of the top surface of the lamellae, ξ the lamella thickness, and * indicates equilibrium values.

Under equilibrium conditions of no annealing or re-crystallization, $\gamma = 1.0$. T_m^o is determined from a plot of T_m against T_c which is linear with a slope of ½ if T_m has been determined under

equilibrium conditions of no re-crystallization on heating to melt. The extrapolated line of T_m against T_c intersects the equilibrium line of $T_m=T_c$ at T_m^o.

1.5. Previous Study on Poly(Lactic acid)

PLA is considered to be an important industrial material with properties which have been commercialised, such as biodegradability, biocompatibility and recyclability. It is produced from renewable resources which will be required to replace oil based polymers in the future. Accordingly there has been much effort in measuring its mechanical properties and improving these by copolymerization, blending and by the addition of fillers to improve thermal stability and crystallinity. There is a very extensive literature on PLA but a review by Donald Garlotta [9] and a book on Poly (Lactic Acid), by R. Auras et al [11] are excellent summary of what has been achieved, industrially and in academia.

There are a few factors that influence the thermal properties, crystallization and degree of crystallinity of PLA material, i.e polymer molecular weight, polymerization conditions, thermal history, stereoregularity and purity. It has been reported in the literature that the melting enthalpy of PLLA is 93.6 Jg^{-1} adopted by Fisher et al. [11, 58] which is the most commonly used.

The addition of compounds containing hydroxyl groups, (i.e., lactic acid, water, alcohols) reduces the molecular weight of PLA by hydrolysis and the stereoregularity is easily controlled by copolymerizing with the D- or L-lactide, and the D, L-lactide, or meso- or polymerization conditions and amount of meso-, D-, lactide, to form random or block stereocopolymers [9, 59]. The stereo chemical architecture is also important as it helps to control the rate and extent of crystallinity, mechanical properties and processing conditions. It has been reported, that besides the molecular weight and the concentration of L- conformer the presence or absence of nucleating agent alters the rate and extent of crystallization [9, 60]. It has been shown that

annealing the PLA copolymers with various L– and D- content, allows the crystallization to occur between 75 °C and the melting point and often produces materials with double melting peaks [9, 60]. Annealing at higher temperature e.g. 135 °C, close to melting temperature, produces incomplete crystallization and produces lamellae with the highest melting points. Annealing for longer periods enables further crystallization to occur and enables them to be more perfect with higher melting points.

It has been reported that PLA is slow to crystallize with the fastest rates in the temperature range of 110–130 °C [9, 17, 61-68]. Kalb and Pennings [9, 69] showed that spherulites grew after 1 minute and the growth rate was 10.6 mm/min. at 125 °C. They also determined using DSC that the crystallinity of PLLA did not exceed 60%. Studies on the crystallization kinetics of copoly(L-co-*meso*-lactide) by Kolstad [9, 17] showed that the crystallization half-lives increased approximately 40% for every 1 wt% increase in the *meso*-lactide content. They also found that the addition of 6% talc increased the nucleation density and reduced the crystallization half-live in line with it being a nucleating agent. Further kinetics studies by Vasanthakumari and Pennings [9, 70] used the Hoffman–Weeks equation to determine the equilibrium m.pt., T_m^o. Urbanovici *et al.* [9, 71] performed isothermal rate measurements on PLLA using DSC at six crystallization temperatures in the range of 90–130 °C and analysed the data using the Avrami equation. Fractional n values are observed with n values between 3 and 4. With a wide range of grades and different levels of crystallinity of copolymers of LA have different performance and a wider range of physical properties than PLA itself. Generally with higher crystallinity better properties are observed with improved thermal stability and increased elastic modulus [13].

Lim et al. [14] have focused on structural composition, thermal properties, crystallization behaviour, rheological properties, and thermal degradation as well as the processing of PLA and has shown that they are all greatly dependent on the L and D composition. They found that

if the L content was more than 90 % a crystalline structure would develop but if it dropped to less than 90 % the copolymer was amorphous; increasing the D content to the decreased the m.pt. and Tg of PLLA. They also reported that Tg was higher with L-lactide copolymer in copolymer than the same amount of D-lactide. Similar findings have been reported by Tsuji and Ikada [72].

It has been reported by Ahmed et al [13] that the thermal properties i.e. melting, glass transition and crystallization as a function of molecular mass, isomer content and microstructure shows that the Tg of PLLA material was higher than PDLLA samples. Similar observation was reported by Ahmed in that partially crystalline sample exhibited higher Tg compare to amorphous sample with similar molecular weights. They also found that there were no melting or crystallization transitions with low molecular weight samples. However, high molecular weight samples readily crystallised [13].

Study by He et al [73] at different crystallization temperature between 90 and 125 °C found that multiple melting peaks were observed on crystallizing at the lower temperatures (105, 110 and 115 °C) while single peaks were observed at the higher temperature i.e. 120 and 125 °C. This observation was supported by Yasuniwa et al [74] where double melting peaks were observed at lower temperatures and low heating rates. This was attributed to melting and recrystallization of small or less perfect lamellae on heating to melt [73].

Di Lorenzo [75] also found that at low crystallization temperatures small defect lamellae are formed when PLA samples were crystallised. On melting these exhibited endothermic peaks, due to recrystallization and reorganization with a second endothermic peak observed on melting. He also found that recrystallization and reorganization were not observed at higher crystallization temperatures where only a single melting was observed.

1.6. The Glass Transition

Amorphous materials have a random array of molecules which is characteristic of a liquid while crystalline solids are characterised by long ranged three dimensional ordering of the molecules. Crystalline materials which do not decompose or sublime melt to form liquids above the melting point which should crystallize on cooling below the m.pt. However, not all liquids crystallize on cooling; if their molecular structure is disordered or if the crystallization rate is very slow. At a sufficiently low temperature these liquids harden and become glasses which have the rigidity of a solid and the three dimensional random structure of a liquid.

The temperature at which the glass, T_g, forms depends on the rate of cooling of the liquid, the external pressure, and any constraint on the liquid. It is accompanied by a change in mechanical properties; an increase in elastic modulus, and yield stress and a decrease in fracture toughness and brittleness. It is thus an important material parameter determining the ultimate use of a commercial material. In polymers it represents a change from a hard material to a soft, rubbery material on heating through the transition.

Unlike melting and crystallization, the glass transition is not accompanied by changes in enthalpy, entropy or volume but is accompanied by a step change in the temperature dependence of properties such as specific heat, and coefficient of thermal expansion. There is no change in free energy or entropy so the transition is not accompanied by any change in order. Thermodynamically it has been described as a second order transition involving chain segment mobility decreasing to zero. However, the measured value of Tg depends on the cooling rate [76] since on cooling the polymer through the transition at a constant pressure from the equilibrium liquid is no longer able to remain in a state of equilibrium in the time scale of cooling and a glass is produced [77, 78]. This retains the chain configuration of the liquid at the temperature when segments stopped rearranging. The adopted chain configuration defines the Tg as it is ‘frozen in’ at time-scale imposed by the rate of cooling [79, 80]. If a

higher cooling rate is used the configuration at a higher temperature is locked in and a higher T_g is obtained; if a lower cooling rate, a lower T_g is obtained. If the material is stored close to T_g but below Tg, the configuration will change towards the equilibrium one, if sufficient time is allowed and a lower T_g will result with changes to volume and enthalpy [24, 81, 82]. Long ranged segmental mobility is reduced to zero when the polymer is below its Tg compared to that above the Tg when the mobility is relatively high.

The glass transition of PLA has been well studied; Wunderlich et al. [11, 83-85] measured the glass transition of amorphous and semi-crystalline PLA by using adiabatic calorimetry, differential scanning calorimetry, and temperature-modulated DSC (TMDSC). From these experiments they found that the Tg shifted to higher temperature with increasing crystallinity on annealing.

Studies on commercial PLLA by DSC at 10 °C min^{-1} showed that the initial crystalline polymer exhibited a Tg at 73 °C but in a subsequent run it was 64 °C. This shows that on the first heating, the Tg value was higher due to the high crystalline content (crystalline domains hinder the mobility of amorphous chains). They suggested that the different value of Tg measured are due to the kinetics effect that depends on the molecular weight of the polymer [9].

The effect of molecular weight and crystallinity on the mechanical properties of PLA, prepared by polymerizing L- D- and L-lactide to produce amorphous or semi-crystalline polymers have been studied by Perego et al, and they reported that there no significant effect of stereo-isomer content on the value of Tg or molecular weights in the range tested [9, 86]. The value of Tg measured by Jamshidi [9, 87] using different molecular weight shows that PLA with a molecular weight of 22,000 g/mole has a Tg of 55 °C but the overall difference was only 4–5 °C lower than that predicted for PLA of infinite molecular weight.

1.7. Physical Ageing and Enthalpic Relaxation in Polymers

There are many types of ageing that polymers undergo under different conditions, e.g. oxidative, degradative, on irradiation with ion beams etc. which result in the material properties changing with time and invariably as a result of chemical or structural changes. Physical ageing is unique in that the process is associated with changes below the glass transition and is totally reversible on heating to above the T_g [88]. Physical ageing is a general phenomenon and a basic feature of the glass state. It occurs as the glass is in a non-equilibrium state and ageing is caused by the glass relaxing towards equilibrium as defined by the extrapolation of the liquid properties to the ageing temperature [88]. It is called physical ageing as most physical properties change and the change can be used to measure the extent of relaxation. If dilatometry is used to follow the volume with time the process has been called volume relaxation and if the change in enthalpy is measured it is called enthalpic relaxation. It is, however, generally accepted that all three are measuring different aspects of the same phenomenon. Due to the change in material properties on physical ageing and the importance of defining material properties this phenomenon has been widely investigated, particularly in commercially important polymers such as PEEK, polycarbonate, polystyrene, poly (ethylene terephthalate) and PLA. In the case of PLA the calculated enthalpic relaxation rate at 40 °C i.e. β_H = 1.77 J/g per decade, and the apparent activation energy Δh^* = 1107 kJ/mol. [11, 89].

Enthalpic relaxation is commonly studied using conventional DSC [90-92]. The glass has a higher enthalpy at the ageing temperature than the extrapolated value for the liquid, see Figure 1.8 and ageing at a temperature close to but below T_g allows the chain segments to relax to the equilibrium configuration [90]. During this process, the polymer chains still have some mobility but on a time scale greater than that adopted in cooling to form the glass. On re-heating an aged glass the excess enthalpy, (ΔH), is released as an exotherm on the step change in heat

capacity at the T_g, see Figure 1.8 and is a measure of the extent of relaxing of the glass towards equilibrium.

The maximum enthalpy change, ΔH_∞, is the difference between the enthalpy of the quenched glass, H_o, and the extrapolated enthalpy of the liquid, H_∞,

$$\Delta H_\infty = H_o - H_\infty$$

$$= \{H_o(T_g) - c_{pg}(T_g - T_a)\} - \{H_\infty(T_g) - c_{p.l}(T_g - T_a)\} \quad (1.15)$$

Where $H_o(T_g)$ and $H_\infty(T_g)$ are the corresponding enthalpies at T_g and $c_{p,g}$ and c_{pl} the specific heats of the glass and liquid respectively. Since by the definition of T_g, (see Figure 1.8)

$$H_o(T_g) = H_\infty(T_g) \quad (1.16)$$

Then $$\Delta H_\infty = c_{pl}(\Delta T) - c_{p.g}(\Delta T) = \Delta c_p \, \Delta T \quad (1.17)$$

where $\Delta T = ((T_g - T_g)$, and $\Delta c_p = c_{pl} - c_{pg}$

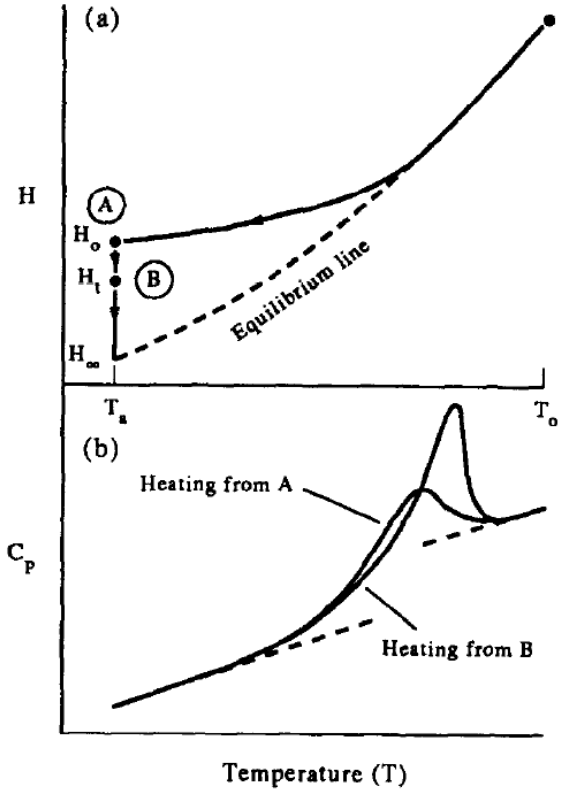

Figure 1.8. "Schematic illustration of (a) enthalpy vs temperature plot, and (b) specific heat vs temperature curves. State A is reached by cooling at constant rate from equilibrium at T_o; state B is reached after subsequently aging at T_a, for time t. The lower figure shows typical DSC traces on heating from each of these states. The dashed line in the upper figure represents the equilibrium enthalpy-temperature curve, and H, is the value of the enthalpy in equilibrium at T_a." [93], {Hutchinson J. M, 1995}.

The concept of enthalpic relaxation on ageing and its subsequent recovery as an endothermic peak on a DSC trace is best represented schematically in Figure 1.8. In DSC, the initial enthalpic state can be seen to deviate from the equilibrium line at Tg as the material is cooled to A at a controlled rate. On storing at this temperature the enthalpy decreases towards the equilibrium value but at time, t, it is reduced to H_t at B.

The loss in enthalpy between A and B is found from the enthalpy evolved on re-heating through the glass transition, from the area under these curves between T_a and T_o. The DSC traces of B which is the aged sample has more pronounced enthalpic peak on Tg [93].

1.8. Present Study on Copoly (lactic acid) - Aims and Objectives

While PLA as a biodegradable material has received much attention from industry and academia as a substitute for film forming petroleum-based thermoplastics the many studies made on the PLA are on a highly crystalline material and little has been done to investigate amorphous and the effect of change in the degree of crystallinity on the material properties. Conventional studies on physical ageing, on the effect of cooling rate on the glass transition temperature as well as the effect of fractional crystallinity on glass transition temperature have not been studied, presumably because it is difficult to produce amorphous samples with low degrees of crystallinity. The quoted glass transition temperatures are in the region of 50-60 ^{o}C PLA devices in vitro or at room temperature must age extensively and the material properties become dependent on time as well as fractional crystallinity.

Co-PLA is a random copolymer of L-lactide with 4% of the D-monomer and at this degree of copolymerization the rate of crystallization is reduced greatly. It should be possible by controlling thermal history to produce amorphous samples as well as those with low fractional crystallinity in order to see the effect on glass formation, physical ageing, crystallization and melting. The copolymer is less well studied than PLA and has the potential to control the morphology better than the homo-polymers. The kinetics of glass formation and enthalpic relaxation will be measured by DSC on a series of samples which are amorphous and with different degrees of crystallinity.

The effect of the degree of crystallinity and crystallization temperature on the observed m.p. will be analysed using the Hoffman-Weekes equation model in order to determine the equilibrium m.pt. and this in turn used to predict the temperature dependence of the rates of crystallization.

DSC has been used widely to study the isothermal crystallization rate of PLA but the lack of sensitivity of the technique may limit its application to measure the crystallization of the copolymer, and in particular to separate primary from secondary crystallization. However, thermal analysis Fourier transform infrared spectroscopy (TA-FTIR) has been shown to separate the two processes in two polyesters [11, 94] and has the potential to do this in with the copolymer. This technique will be compared with DSC to determine the most accurate method of determine the extent of crystallization with time of the Co-PLA which has not been studied previously.

Other techniques such as hot-stage optical microscopy will be used to investigate the variation of radial growth of spherulites with temperature to compare the crystallization rate constants and mechanism with those predicted by application of a modified Avrami equation.

In these ways it is hoped to have a better understanding of the parameters which determine the glass transition temperature, the extent of enthalpic relaxation and the crystallization of PLA copolymers and the effect of stereo-isomer content in inhibiting the crystallization.

2.1. Materials

2.1.1. Poly Lactic Acid (Co-PLA)

The material used in this study was a co-poly (L-lactic acid) with 4% D-lactic acid. It was supplied as PLA2002D in pellet form by NatureWorks LLC, Minnetonka, MN, USA. It is a semi-crystalline L-lactic acid co-polymer with 4 % D-lactide to reduce its rate of crystallization. It's molecular weight (Mw) was194 kg mol^{-1}.

The physical properties listed by NatureWorks for PLA2002D are shown in table 1 below:

Table 2.1. Physical Properties of PLA2002D

Physical Properties	PLA 2002D
Glass transition temperature, Tg,	55 °C
Melting Point, Tm,	154 °C
Crystallization Temperature, Tc,	- °C
Crystallinity,	37%
Molecular Weight,	194 kg mol^{-1}
D-lactide Content,	4%

2.2. Reagents

2.2.1. Potassium bromide

Potassium bromide (KBr) powder, of FTIR grade, was supplied by Sigma Aldrich (Dorset, UK), and pre-dried in an air-oven for at least 12 hours at 120 °C, before being pressed into IR discs.

2.2.2. Chloroform

Chloroform, of research grade, was used as a solvent for Co-PLA. It was supplied as 99.5% pure by Sigma Aldrich (Dorset, UK) and used as received.

2.3. Sample Preparation and Conditioning

2.3.1. Compression Moulding

About 10.0 g of Co-PLA was hot pressed into sheets (100 x 100 x 1 mm) from pellets using a Moore Hydraulic Press, see Figure 2.1. The pellets were heated to 200°C, held under 10 tonnes pressure for 3 minutes, and subsequently slow cooled to room temperature while the pressure was maintained. The thin sheet was then cut into small pieces and used in DSC experiments.

Figure 2.1. Moore Hydraulic Press

2.3.2. Oven

A Gallenkamp laboratory air oven, model (OV – 335), was used to condition polymer samples. An external thermocouple, together with a temperature reader Digitron model 2751 – K was used to monitor the oven temperature and maintained it as required at the conditioning temperature.

2.4. Experimental Techniques

2.4.1. Differential Scanning Calorimetry (DSC)

A Perkin-Elmer, model DSC 7, differential scanning calorimeter, interfaced to a PC and controlled by Perkin-Elmer Pyris Management Software, was used to characterise the physical properties of Co-PLA. It was connected to a Grant Intracooler which controlled the

temperature of the DSC down to 3 ^{o}C and enabled the calorimeter to be cooled to room temperature while maintaining cooling at 50 ^{o}C min^{-1}.

DSC is s dynamic calorimeter and is widely used to characterise materials by measuring their specific heat as a function of temperature and rate of heating or cooling. It does this by comparing the instantaneous heat flow of sample and reference cells as shown in Figure 2.2. The sample cell contains the sample of material sealed in an aluminium pan and lid, and the reference an empty aluminium pan and lid. DSC is an important technique to study the thermal response and the transitions of polymer by changes in heat capacity of the material. This technique measures the difference in heat input required to keep the temperatures of the sample and reference cells the same at a frequency of a fiftieth of a second [95]. Therefore any variation in heat flow that occurs between the sample and reference cell is due to thermal transitions in the sample. The heat flow between sample and reference cell is recorded in milliwatts (mW) as a function of time and temperature.

If the sample takes in energy an endothermic transition is occurring and if the sample releases heat an exothermic transition is occurring as shown in Figure 2.3. Much information can be gained by using DSC to study the glass formation, crystallisation and melting of polymers, as well as curing and other chemical processes which may occur. The glass transition is observed as a step change in the heat flow-temperature plot while crystallization is observed as an exothermic and melting as an endothermic process. The temperature range in which these occur is characteristic of a polymer.

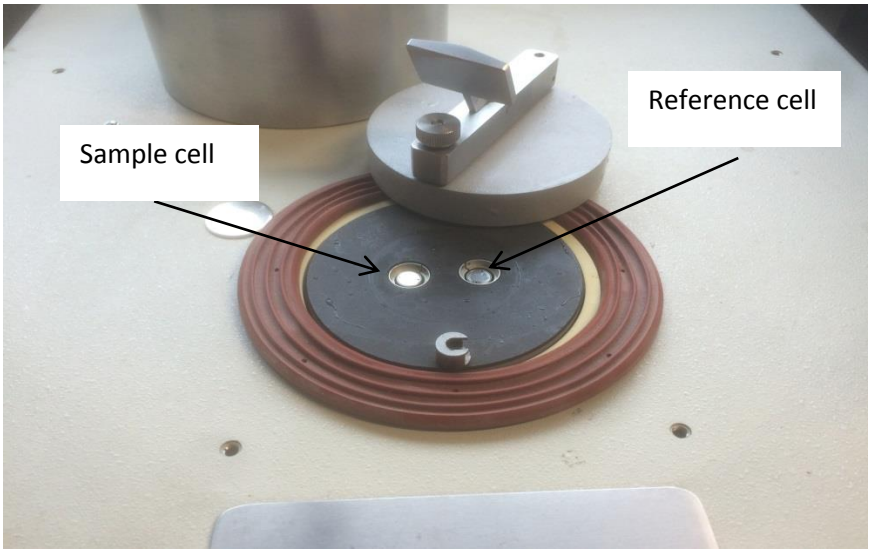

Figure 2.2. DSC sample and reference cell

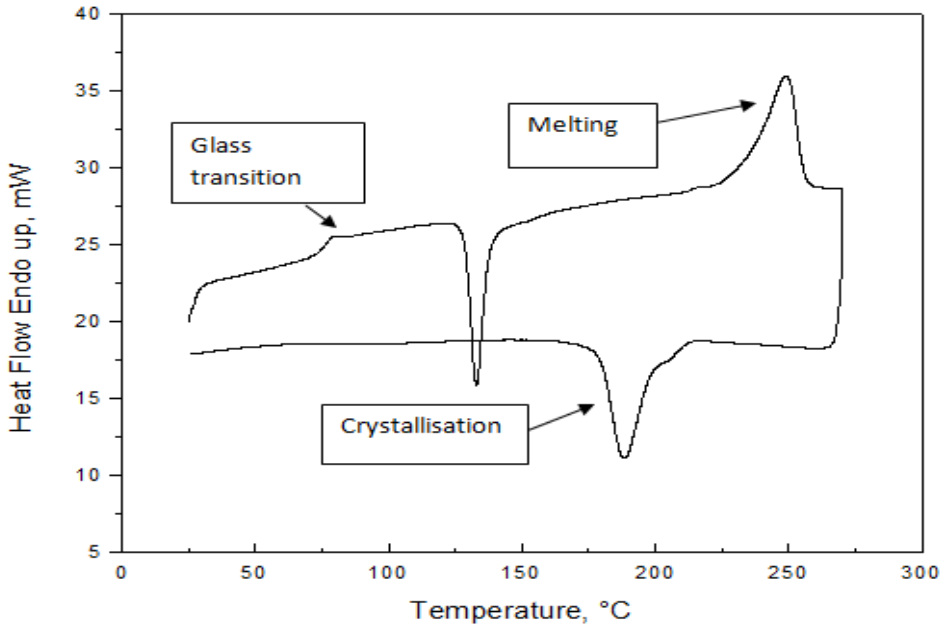

Figure 2.3. DSC scan of a partially crystalline polymer on heating and cooling

2.4.2. Experimental Procedure

The temperature and thermal response of the calorimeter was calibrated from the melting point and the enthalpy of fusion of ultra-pure indium and tin (99.999%). Calibration of indium was set by heating from 140 to 170 °C at 5 ^{o}C min^{-1} and the melting point was taken to be 156.60 °C and the enthalpy of fusion of indium 28.45 Jg^{-1}. Tin was heated from 215 to 240 °C at 5 ^{o}C min^{-1} and the melting point taken to be 231.91 °C.

Between 5.0 and 7.0 mg of the 'as received' Co-PLA was cut from a pellet or moulded sheet and accurately weighed into an aluminium pan and sealed with a lid. This was used as the sample in all the DSC experiments. In order to remove its thermal history the sample was heated from 30 to 200 °C at various heating rates from 10 to 50 °C min^{-1}, held in the melt for 2 minutes at 200 °C before being cooled to 30 °C or the isothermal crystallization temperatures at various cooling rates, from 0.1 to 50 ^{o}C min^{-1}. This procedure was repeated in all the experiments to investigate the thermal behaviour of the sample.

In determining the glass transition temperature, Tg of Co-PLA the Richardson and Savill's method was adopted [96]. This method was applied in all cases of polymers exhibiting an endotherm superimposed on the step change in the heat flow response at Tg. Figure 2.4 is a schematic of the method and involves linear extrapolation of the heat capacity, $c_{p,}$ from 4 to 3 and from 1 to 2 and equating the sum of the areas of A and C to B i.e. A + C = B.

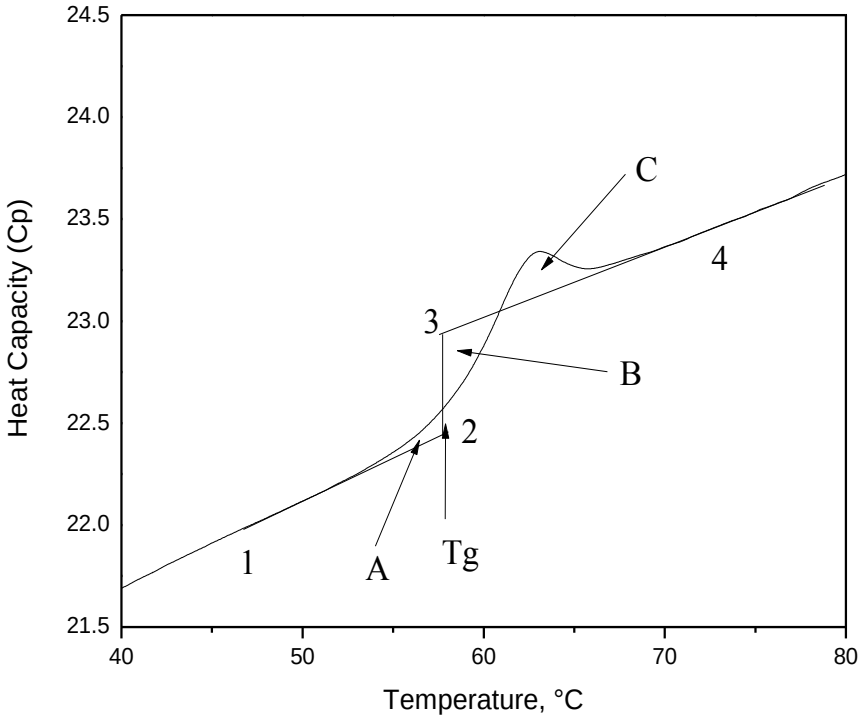

Figure 2.4. Schematic diagram to determine the Tg by using Richardson method

Since melting of the copolymer occurred over a wide range of temperatures, two melting points were measured by DSC, the peak of the endotherm, T_m (Peak), corresponding to the temperature at which most of the polymer melted and T_m (Max) when the endotherm returned to the baseline corresponding to the last trace of melting. Correction was made for thermal lag by extrapolating the observed melting points to zero heating rate.

The heat of fusion, ΔH_m, of the sample was determined from the area under the melting endotherm and a linear baseline drawn from the first onset of melting to the return to the thermal response of the melt, see Figure 2.5.

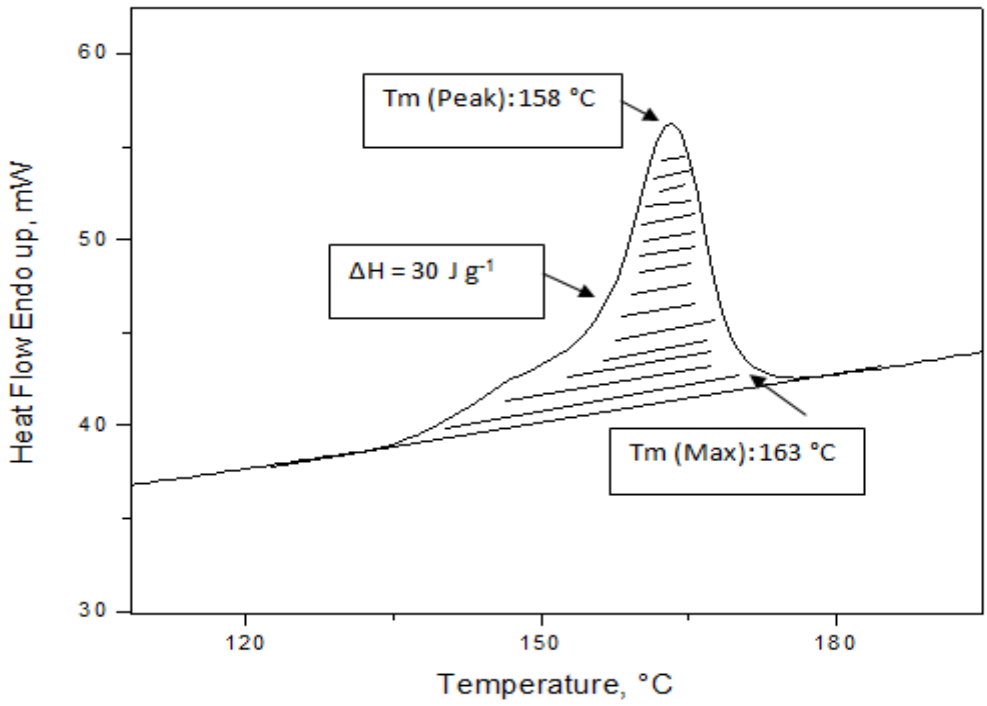

Figure 2.5. Determination of ΔH_m, T_{max} and T_m

The fractional crystallinity (*Xc*) was determined from

$$Xc = \frac{\Delta H_m}{\Delta H_m^o} \qquad (2.1)$$

where ΔH_m is the measured enthalpy of fusion of the sample and ΔH_m^o is the enthalpy of fusion of totally crystalline PLA. This was taken as 93.6 Jg^{-1} [11, 58].

2.5. Fourier Transform Infra-Red Spectroscopy (FTIR)

FTIR spectroscopy was the preferred method of analysis adopted since it has many advantages over other dispersive techniques. Measurements were achieved quickly since all frequencies and absorbances were measured instantaneously and sensitivity was good due to increased accuracy of the detectors by higher optical throughput (reducing noise), and signal averaging. The sensitivity and accuracy of the technique enables positive identification of a wide variety of materials, as well as improving the use for quantitative analysis.

IR spectroscopy is a powerful technique for analysing organic based materials especially polymers. It is a non-destructive characterisation technique and its basic concept is that when IR radiation passes through the sample certain wavelengths are absorbed by exciting vibrational and rotation modes in the molecules and the frequency of the absorbed wavelength depends on the energy differences between the vibration and rotational energy levels. These wavelengths are characteristic of the molecular bonds or groups and can be readily used to assign them, analyse their concentration and determine the molecular groups that make up a polymer.

The FTIR spectrometers used in this study relied on interferometers as beam-splitters to divide an incoming infrared beam into two separate beams. One of these beams is reflected by a stationary mirror, whilst the other is reflected off an oscillating mirror, causing the two beams to travel different distances. These are recombined at the beam-splitter, and the resulting signal is an interferogram since the two beams are in and out of phase. A frequency spectrum can be produced from the interferogram, which is the sum of sinusoidal waves containing information about wavenumber of a particular infrared peak and peak intensity at that wavenumber, and has to be decoded. This occurs via the mathematical technique of Fourier transformation, which calculates the spectra from summed sinusoidal waves in the interferogram.

By changing the experimental conditions, such as temperature or crystallinity, and by monitoring changes in absorbance and peak position within the IR spectrum on heating and cooling, it is possible to analyse conformational changes within the polymer. Polymer samples in the form of thin films can be used to study conformational changes and the crystallisation behaviour which provide information about the molecular arrangement within the polymer whilst it is amorphous or crystalline [11, 94].

2.5.1. Calibration of Temperature for Hot stage

A Linkam THM 600 hot stage cell and PR600 temperature controller was calibrated by attaching a thermocouple directly to the KBr disc to monitor the temperature which was maintained at a fixed value by a PR600 controller. The calibration was performed by heating from 35 to 200 °C and at each of 5 °C intervals; the KBr disc temperature was recorded. It was then subsequently cooled from 200 to 35 °C and again at each of 5 °C intervals; the KBr disc temperature was recorded. The temperature difference between reader and set from the PR600 controller was compared on heating and cooling.

2.5.2. Experimental Procedure

A Nicolet Spectrophotometers, model Magna IR 8700 equipped with a DTGS-KBr detector [97] and controlled by Omnic 8.1 software, was used to collect spectra of Co-PLA during transmission experiments, see Figure 2.6. For this technique, a Linkam THM 600 (Surrey, UK) hot-stage cell was placed within the spectrometer and the infra-red beam passed through the sample, mounted vertically between KBr discs. A Linkam PR600 thermometric stage was attached to the spectrometer to monitor temperature control.

A resolution of 1-4 cm^{-1} and total of a 100 scans were accumulated for each spectrum along with a background spectrum. Figure 2.7 shows the experimental set up in thermal analysis FTIR spectroscopy. Automatic smoothing and baseline corrections were made before analysing the spectra. In this study, the spectra were measured in transmission.

Potassium bromide (KBr) powder was prepared by grinded to a fine powder. It was then pre-dried in an oven for at least 12 hours to remove any moisture. Approximately 200 mg of KBr powder was weighed and compressed into a KBr disc of 16 mm diameter using a Specac compression mould, see Figure 2.8.

5.0 g of Co-PLA pellets were dissolved in the 100 cm^3 of chloroform. A few drops of the solution were deposited onto the KBr disc, allowed to evaporate in a fume cupboard until all solvent had evaporated and a thin film sample produced. Sufficient number of drops were added to produce a maximum absorbance in region of 0.5 – 1.0. A KBr disc was used as a reference sample (blank).

For dynamic experiments, thin Co-PLA films attached between two KBr discs were heated from 30 to 200 °C at 5 °C min^{-1} using the Linkam THM 600 hot-stage cell as shown in Figure 2.9. At 5 °C intervals the sample was scanned and recorded. The sample was subsequently cooled from the melt to 40 °C and the FTIR spectrum recorded at 5 °C intervals in order to investigate changes during heating and cooling.

In isothermal crystallization experiments, Co-PLA film samples were heated to melt (at 200 °C) at a heating rate of 50 °C min^{-1}. This temperature was maintained for 2 minutes to ensure the sample was completely melted and to erase the thermal history. It was then immediately cooled to the isothermal crystallisation temperature. In this study five temperatures were used to study the crystallisation i.e. 120, 124, 128, 132 and 136 °C. A series of spectra were collected at a constant time interval over the whole crystallization once the sample had reached the

isothermal crystallization temperature. By this means IR transmission spectra were readily measured every 2 minutes intervals for up to 1000 minutes over the temperature range studied.

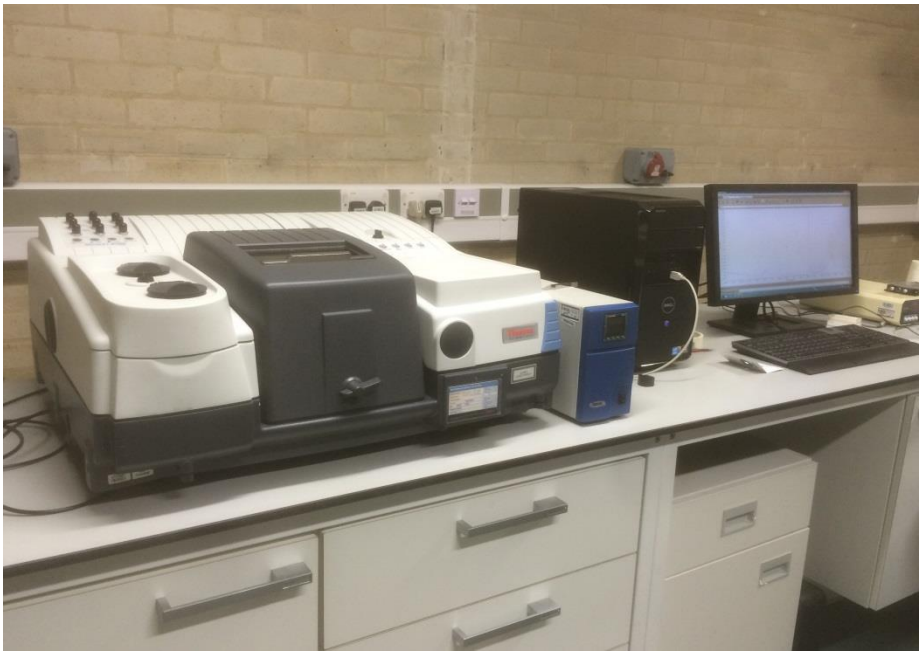

Figure 2.6. FTIR Nicolet Spectrophotometer.

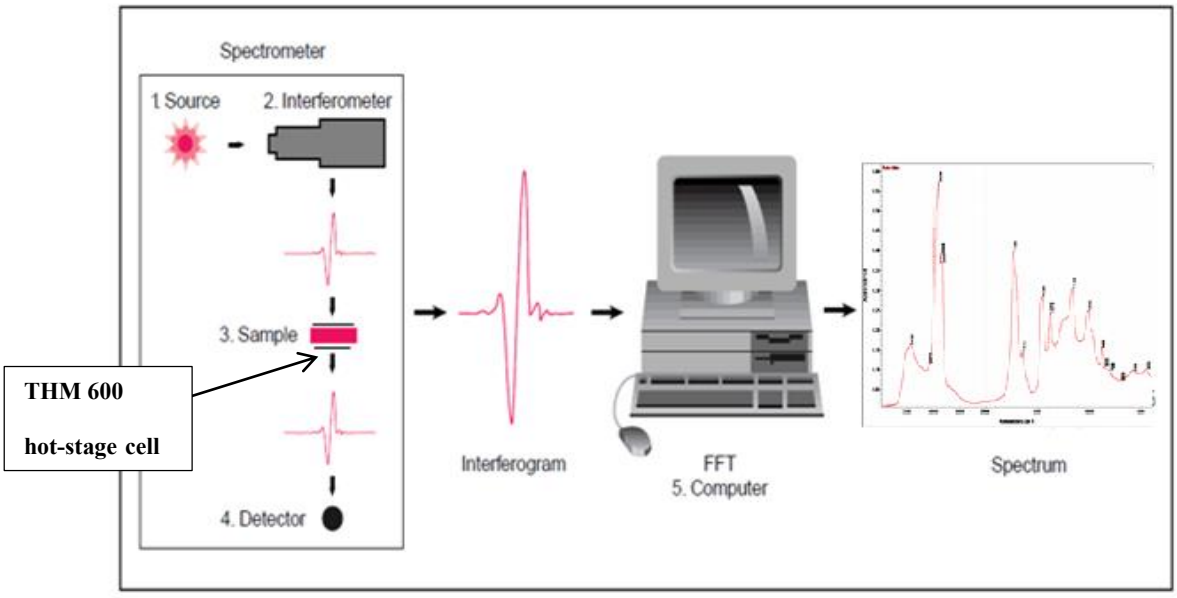

Figure 2.7. Experimental set-up used in Thermal Analysis FTIR Spectroscopy.

Figure 2.8. Specac Compression Mould

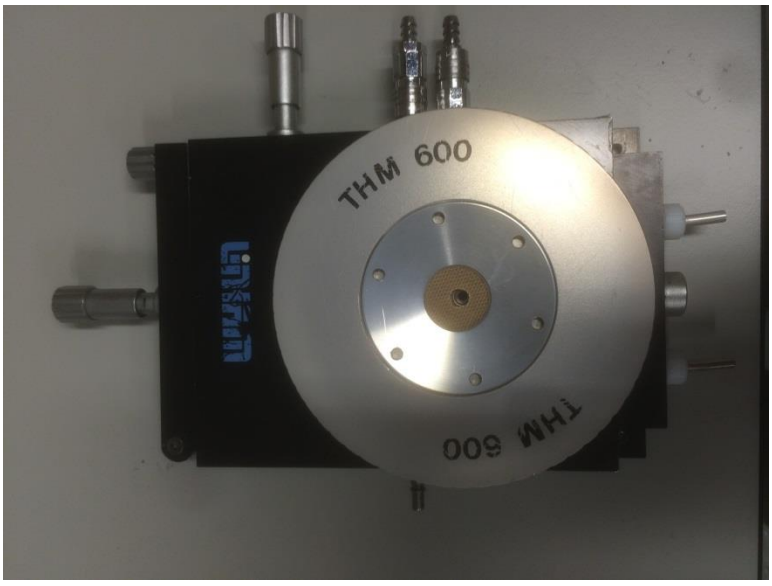

Figure 2.9. Linkam THM 600 hot-stage.

2.6. Hot Stage Microscopy

2.6.1. Optical Microscopy

Optical microscopy uses visible light to examine and magnify the image of small samples up to a limit of 500 to 1000 times by lenses. It is an old technique but simple in use. Modern developments have improved the resolution and contrast with the incorporation of digital and video cameras, charge-coupled devices (CCD) which allows capture of digitals images, along with software to measure the dimensions of the sample and store multiple images. By using CCD cameras, the images can be examined directly on the computer screen.

2.6.2. The Hot Stage Microscope

A Leitz Dialux-Pol polarising light binocular microscope with long distance working object lenses, x10, x32 and x50 magnification, and x10 eye-piece lens was used to examine a film specimens mounted between glass cover slips. These were clamped to a hot stage, Linkam THMS 600, securely mounted horizontally on the microscope platform, as shown in Figure 2.10. The hot stage was equipped with a thermal control unit, PR600 and the temperature controlled by PC thermal control software [98, 99]. This apparatus, as shown in Figure 2.10 and the hot-stage as shown in close-up in Figure 2.11, was used to investigate the visual changes in the sample on heating and cooling and during isothermal crystallization under polarised light using a quarter plate analyser which made non-polarised material red in colour rather than black and so enabled samples to be photographed.

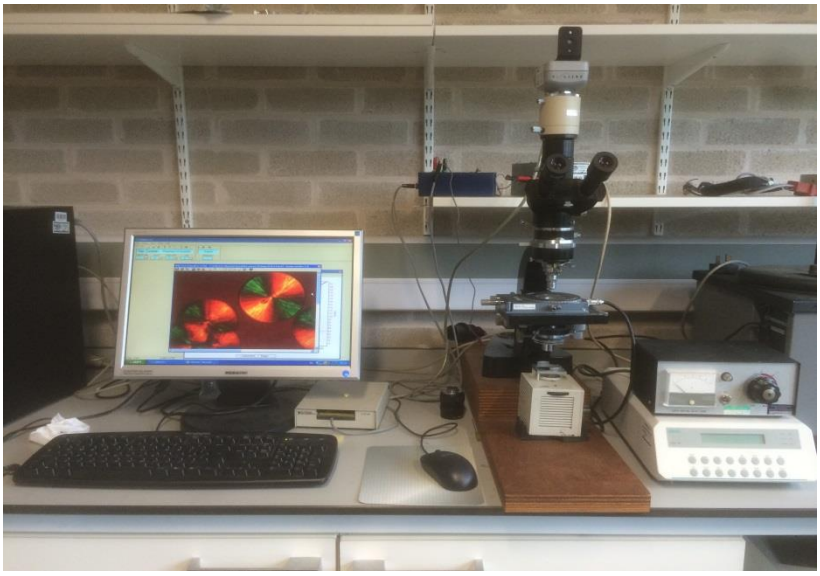

Figure 2.10. The Optical Microscope Apparatus.

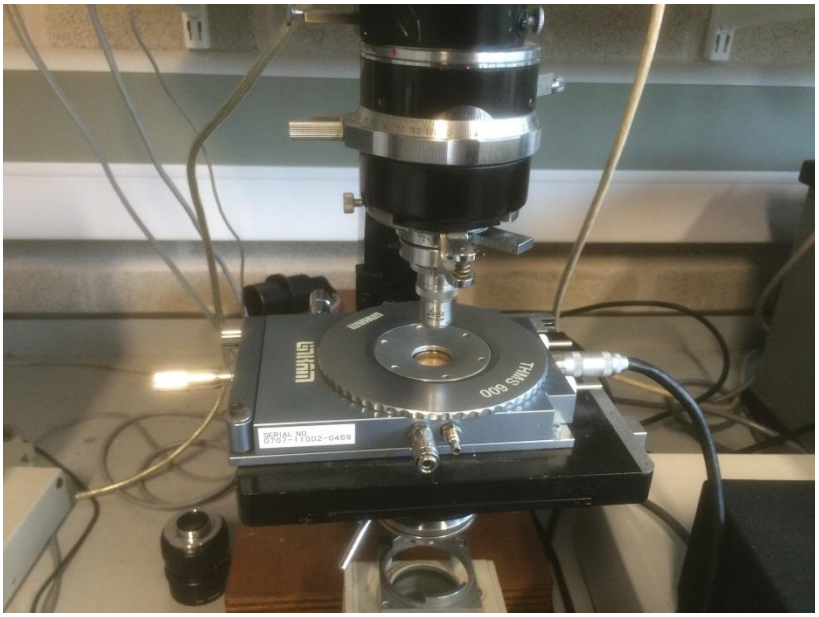

Figure 2.11. Close-up of the hot stage.

2.6.3. Method

Two types of experiments were conducted; dynamic and isothermal (by heating and cooling) and isothermal crystallization measurements observing spherulite growth and nucleation. In the dynamic runs the thin films (0.15-20 μm) were placed between glass cover slips and mounted horizontally in the hot stage of a polarized microscope under a ¼ quartz plate as shown in Figure 2.10. Micrographs were recorded as function of time and temperature to study any changes in the sample on heating and cooling.

The effect of crystallization temperature on spherulite growth and nucleation study were carried out on thin films prepared as described above in the dynamic studies but heated to the melt at 180 ^{o}C, held for 2 minutes before being cooled at 50 ^{o}C min^{-1} to the crystallization temperature for direct comparison with DSC measurements. The number of spherulites and their diameters were measured as a function of time to measure the nucleation densities and the radial growth rates as function of time and temperature.

Chapter 3. Glass transition and enthalpic relaxation of amorphous Co-poly (lactic acid).

3.0. Introduction

Differential Scanning Calorimetry (DSC) is commonly used to characterise polymers in that it readily measures the glass transition, crystallization temperature, melting points and crystallinity as well as enthalpic relaxation, crystallization kinetics, and thermal stability of the morphologies produced at different temperature [9, 11, 100, 101]. It was accordingly used to analyse the Co-PLA sample as-received and as-produced by various thermal treatments.

The focus of this chapter will be to study glass formation, and enthalpic relaxation at various temperatures below the glass transition since both have an effect on the material properties of polymers and determine the way material properties change on storage. These will determine the ultimate uses of the copolymer.

3.1. Results and Discussion

3.1.1. Initial Studies

Weighed samples of the Co-PLA, about 7.0 mg, were cut from moulded pellets and encased in aluminium pans. The samples were heated from 30 to 200 ^{o}C at a heating rate of 10 ^{o}C min^{-1}, held for 2 minutes and subsequently cooled to 30 ^{o}C before being reheated to 200 ^{o}C in a DSC. The DSC responses to heat, cool and reheat treatment are shown in Figure 3.1 as changes in heat flow against temperature. On first heating, a step change in heat flow with a slight endotherm was observed at about 60 ^{o}C characteristic of a glass transition with a small enthalpic relaxation or ageing peak. This was followed with a linear increase in heat flow and deviation from the linear increase in heat flow due to onset on melting occurred at 140 ^{o}C. Melting was complete at 160 ^{o}C when the heat flow returned to a linear increase with

temperature corresponding to the increase in specific heat of the liquid or mobile amorphous phase. On cooling at 10 ^{o}C min^{-1} the specific heat decreased with temperature with no deviation until the step change due to the glass transition at about 60 ^{o}C, Figure 3.2. The step at the glass transition was greater than on heating consistent with the initial sample being partially crystalline and the cooled sample amorphous. No change corresponding to the sample crystallizing was observed and on subsequent reheating the heat flow increased linearly with no detectable crystallization or melting.

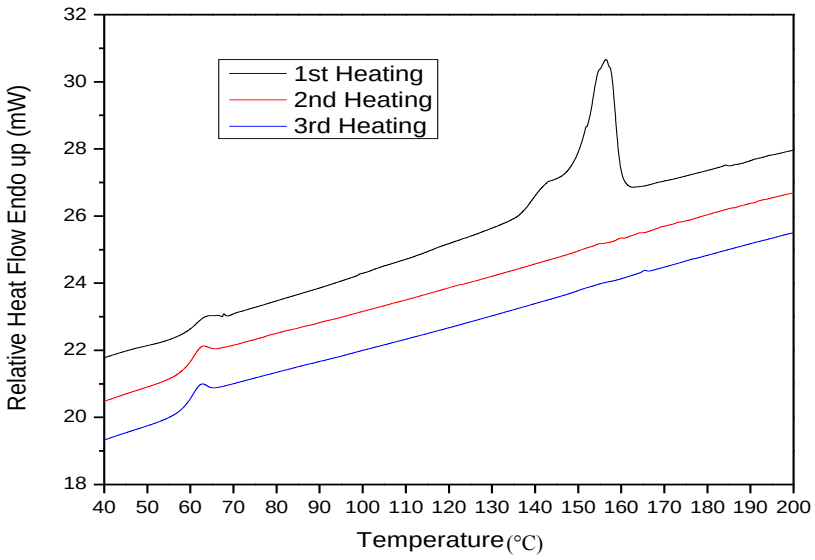

Figure 3.1. Dynamic DSC response of co-PLA on first, second and third heating.

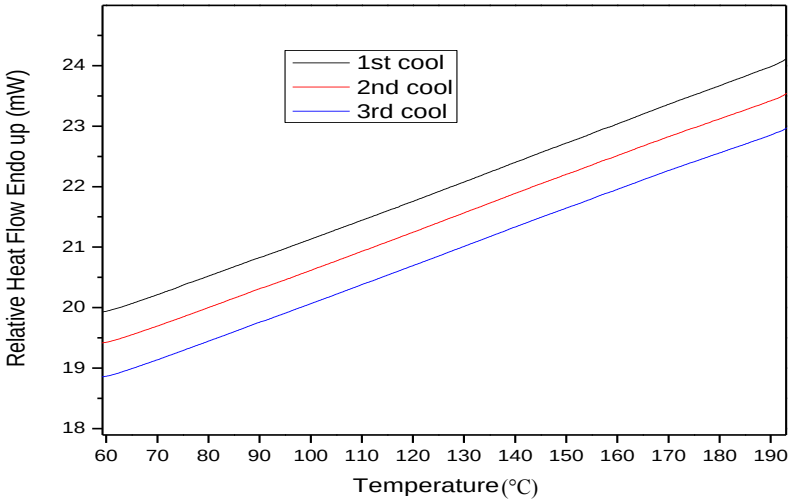

Figure 3.2. Dynamic DSC response of Co-PLA on first, second and third cooling.

The change in enthalpy, $H_T - H_o$, relative to a standard temperature, taken to be 30 ^oC was measured by integrating the heat flow response with time, in s, after correcting for the baseline with two aluminium pans, see Figure 3.3, since

$$H_T - H_o = \int_0^T c_p \, dT = \int_0^T (dH/dt)(dt/dT) \qquad (3.1)$$

where

(dH/dt)(dt/dT) = Heat Flow/ Heating Rate in s.

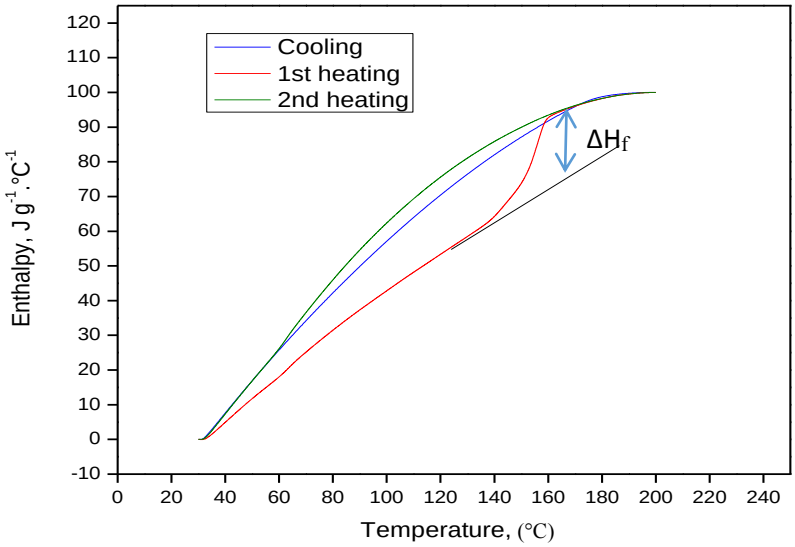

Figure 3.3. Enthalpy change of the as-received sample on heating and on subsequent cooling.

Melting is endothermic and the area under the melting curve above the linear response of the heat flow is a measure of the heat of fusion of the sample, ΔH_f, at the m.pt., see Figure 3.3,

i.e. $$\Delta H_f = \int_0^{\infty} (dH/dt).dt \qquad (3.2)$$

ΔH_f is a measure of the fractional crystallinity, X_c, of the as–received sample, since

$$X_c = \Delta H_f / \Delta H^o_f \qquad (3.3)$$

where ΔH^o_f is the heat of fusion of the totally crystalline sample. A value of 93.6 J g^{-1} was adopted for this [11, 58].

The heat of fusion, ΔH_f, was 26.3 J g^{-1} corresponding to 0.28 fractional crystallinity while the onset and the melting peak were observed at 148 and 155°C, respectively. Similar findings have been reported for PLA by Garlotta and De Santis [9, 102].

It is apparent from the first run that the Co-PLA sample was partially crystalline as-received but, however, as can be seen from Figure 3.2 it did not recrystallize on subsequent heat treatment, either on heating or cooling. There were no exotherms present and no subsequent melting endotherms on re-heating. This was also the case on subsequent heating and cooling; only a glass transition was apparent. The increase in heat capacity at the glass transition temperature, $\Delta c_p(T_g)$, on subsequent heating was consistent with the reheated sample being amorphous. The amorphous glass transition temperature was determined to be 58.5 ^oC as determined by Richardson's method [96] and as outlined in the experimental section. This method corrects for the small endothermic physical ageing peaks due to cooling and heating the specimen through the glass transition.

To conclude no exotherms were observed on cooling at 10 $^oC\ min^{-1}$ on the first, second or third cycles. Similar findings have been reported by Pantani and Tadakazu [103, 104] who reported that no exothermic peaks were observed on cooling but a small endothermic peak was present on heating for the second and third times.

Since the as-received samples were partially crystallined it is apparent that Co-PLA must crystallise but this was dependent on the correct thermal treatment or storage conditions. It was decided to explore the effect of different cooling rate on the degree of crystallinity which might develop and the effect on the glass transition temperature.

3.1.2. The effect of cooling rate on the development of crystallinity

As-received samples were melted in the DSC by holding them at 200 ^oC for 2 minutes before cooling at different rates from 0.1 to 50 $^oC\ min^{-1}$ and re-heating to 200 ^oC to determine the melting endotherm. Figure 3.4 shows the effect of cooling rate on the extent of crystallization of Co-PLA as measured by the melting endotherm on subsequent heating. It can be seen that at cooling rates of 5 $°C\ min^{-1}$ and above no endotherm was observed. Starting at

1°C min^{-1} and lower the endotherm progressively grew in size. Eventually at 0.1 °C min^{-1} the area of the endotherm obtained was similar to that of the original sample.

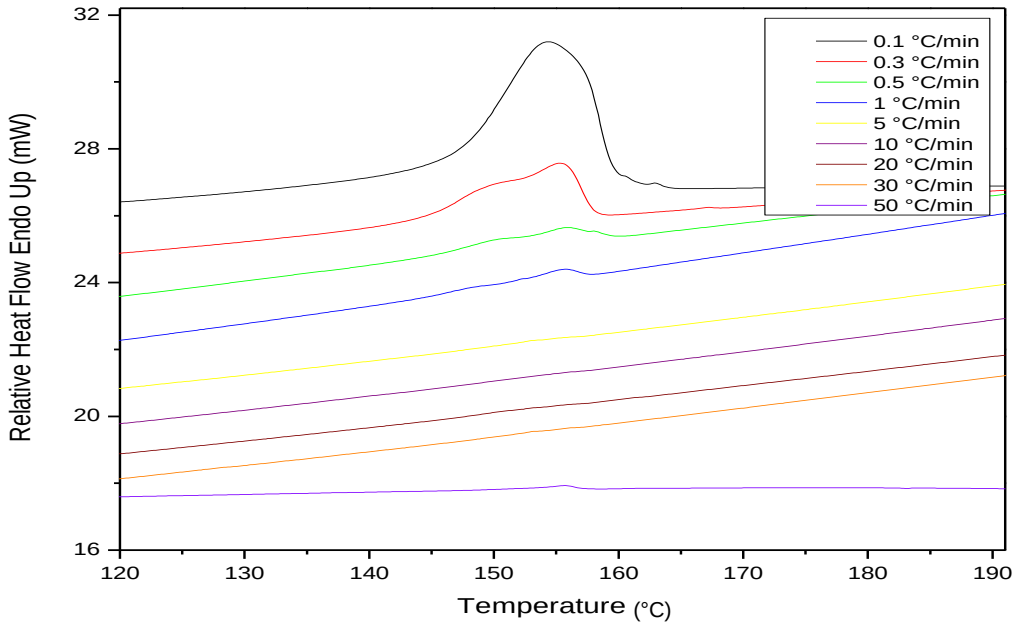

Figure 3.4. The effect of different cooling rates on the melting behaviour of Co-PLA.

This clearly shows that the higher cooling rates were too fast for crystallinity to develop within the time scale achieved at the cooling rate. At the lowest cooling rate adopted sufficient time had elapsed at each temperature for some crystallinity to develop, (see Figure 3.5). It also indicated that at cooling rates, above 5 °C min^{-1} amorphous samples could be prepared and by varying the rates below these value samples of different degree of crystallinity could be produced. It was interesting to note that no deviation from linearity in the heat flow-temperature response was observed by DSC on cooling at the slower cooling rates implying that although crystallization had occurred, as detected on subsequent heating, the crystallization rate was too low to be detected.

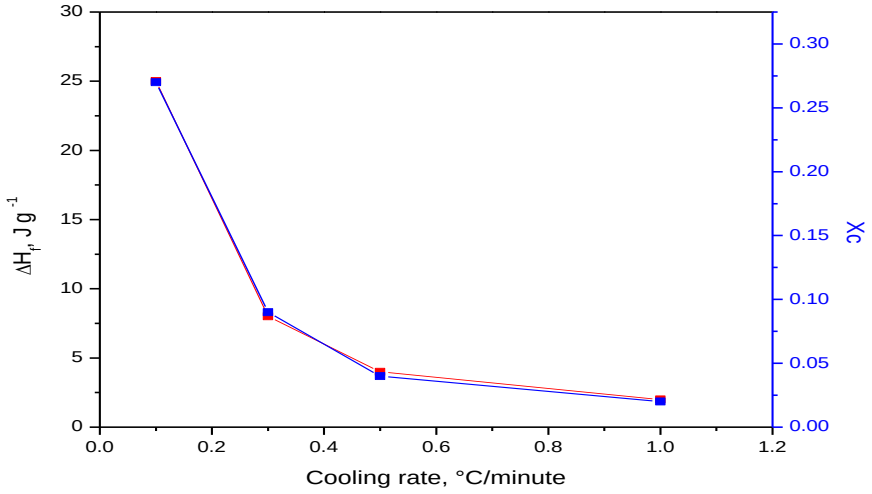

Figure 3.5. The effect of cooling rate on the heat of fusion and fractional crystallinity of Co-PLA.

3.1.3. The effect of cooling rate on the measured glass transition temperature

The effect of various cooling rates on the measured glass transition temperature, T_g, can be seen in Figure 3.6. The sample was cooled at different cooling rates from above the observed melting point to 30 ^oC, below the transition, such that different glasses were formed defined by the cooling rates and the value of the glass transition temperature, T_g, of each glass determined by reheating at 10 ^oC min $^{-1}$. The values of T_g were determined as before using Richardson's method [96].

Two well defined trends in the dependence of the T_g on cooling rate were observed; see Figure 3.7 in that for samples which were shown to be amorphous T_g decreased with slower cooling rates but for slow-cooled samples, considered to be partially crystalline, the opposite trend was observed and T_g increased with decreasing cooling rate. This later trend was attributed to the increased crystallinity as can be seen in Figure 3.8 where the T_g increased with the heat of fusion. The effect of the harder crystalline regions on the soft amorphous regions is to reduce

their segmental mobility and raise the Tg particularly in regions immediately adjacent to the crystalline domains.

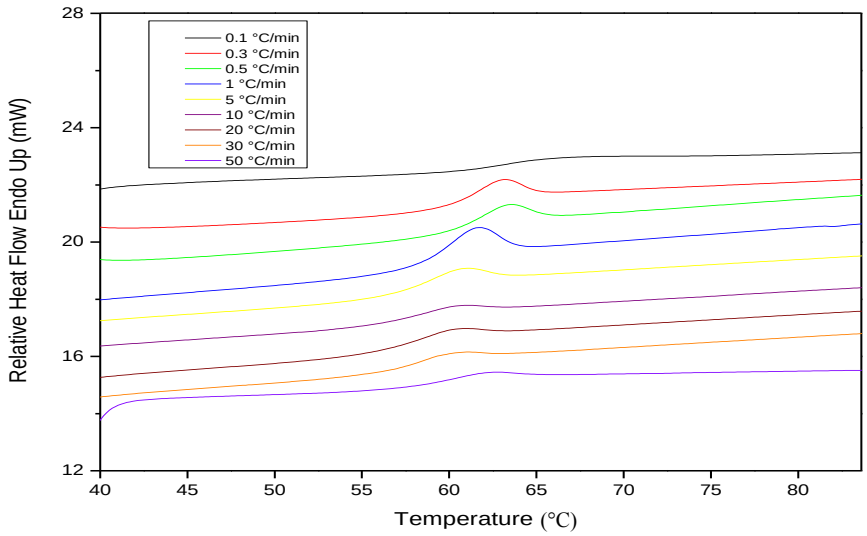

Figure 3.6. Measurement of the glass transition on heating at 10 ^{o}C min^{-1} after cooling through the transition at the different cooling rates listed.

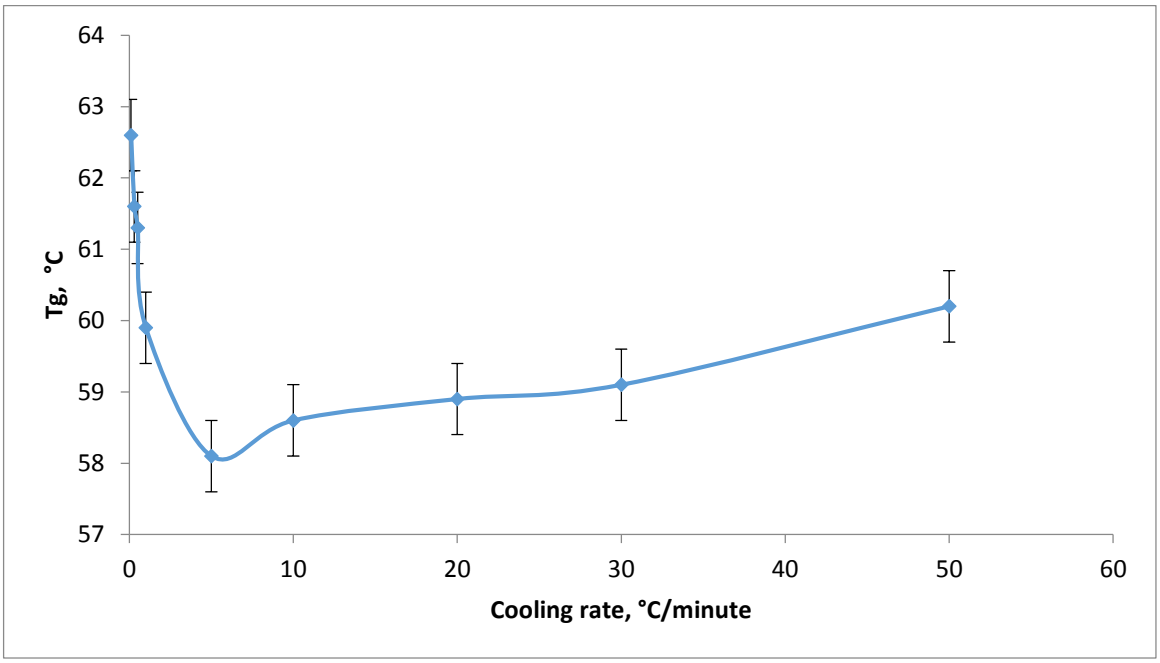

Figure 3.7. The dependence of observed T_g on cooling rate.

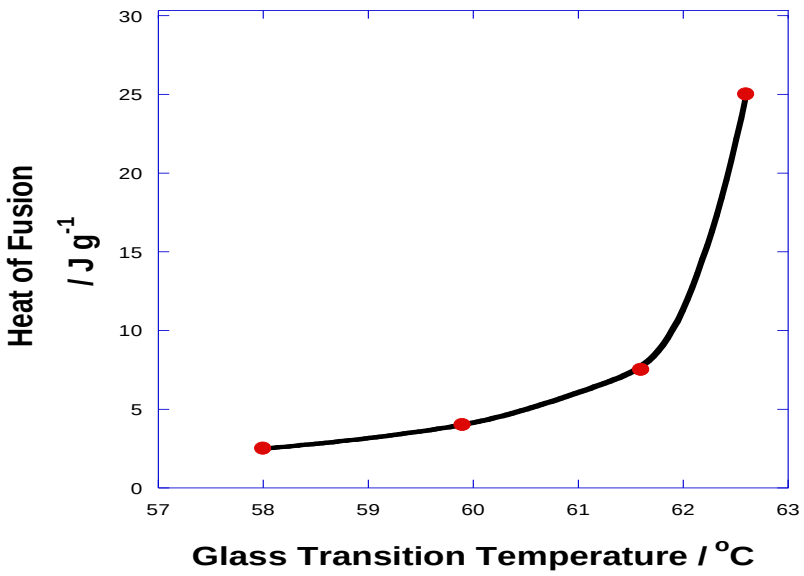

Figure 3.8. The dependence of the glass transition temperature on heat of fusion.

The glass transition is associated with amorphous (liquid-like) materials whose segmental mobility decreases with decreasing temperature until a temperature is reached, Tg, at which the time scale of the molecular groups rotating are of the order of the time scale of the change of the imposed constraint; in DSC, this constraint is temperature and in particular the rate at which temperature changes with time, i.e. the cooling rate. In DSC measurements the T_g is a function of the rate of cooling since this determines the temperature and structure at which molecular motions are frozen into the glass and consequently released on re-heating through this temperature. The glass transition is a thermally activated process and as such obeys an Arrhenius relationship, such that

$$R_C = A \exp(-\Delta E/RT_g) \qquad (3.4)$$

where R_C is the rate of the imposed constraint, i.e. rate of cooling, A a pre-exponential factor, ΔE the activation energy for molecular mobility, R the gas constant and T_g the glass transition

temperature (in K). An Arrhenius plot of log (rate of cooling) against reciprocal temperature is shown in Figure 3.9 for amorphous and crystalline samples. It is apparent that only amorphous samples exhibited the corrected dependence on reciprocal temperature, K^{-1}, with an activation energy of 0.98 ± 0.20 MJ mol^{-1}. This large value for the activation energy of segmental motion is consistent with the range of values observed with other polymers [105, 106] and is due to the number of monomer units involved in the molecular motion of glass forming systems [107].

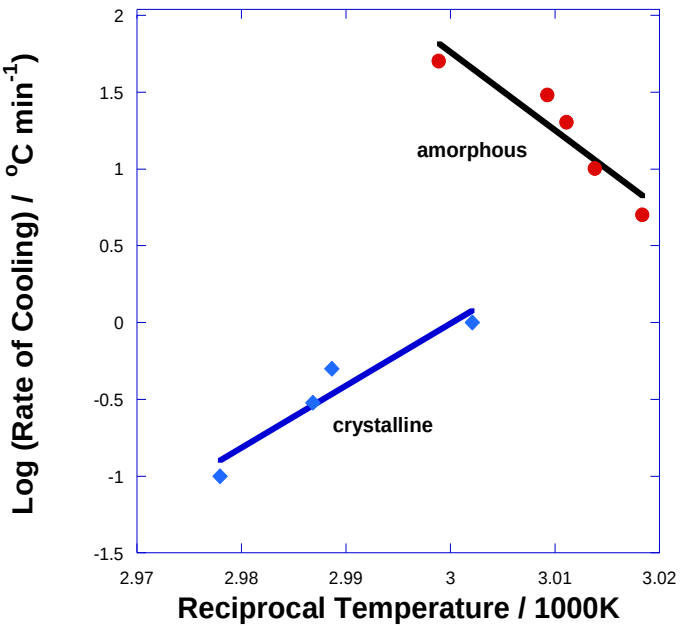

Figure 3.9. Arrhenius plot of log (cooling rate) against reciprocal temperature for amorphous and crystalline PLA samples.

The step change in specific heat which occurs at Tg was dependent on the fractional crystallinity due to the reduction in amorphous content and any reinforcement of the soft amorphous regions by the hard crystalline regions. The decrease in $\Delta c_p(Tg)$ was linearly proportional to the fractional crystallinity, see Figure 3.10.

This observation shows that cooling rate is the dominant factor in determining the value of Tg of amorphous Co-PLA provided Richardson's procedure is adopted to correct for any ageing which may occur with different heating and cooling rates. However, with partially crystalline samples the degree of crystallinity has a more pronounced effect and accounts for the increased in the observed T_g with decreasing cooling rate which is the reverse of what is observed with amorphous material. The dependence of the observed T_g of Co-PLA on cooling rate is complex since it depends on the fractional crystallinity which develops.

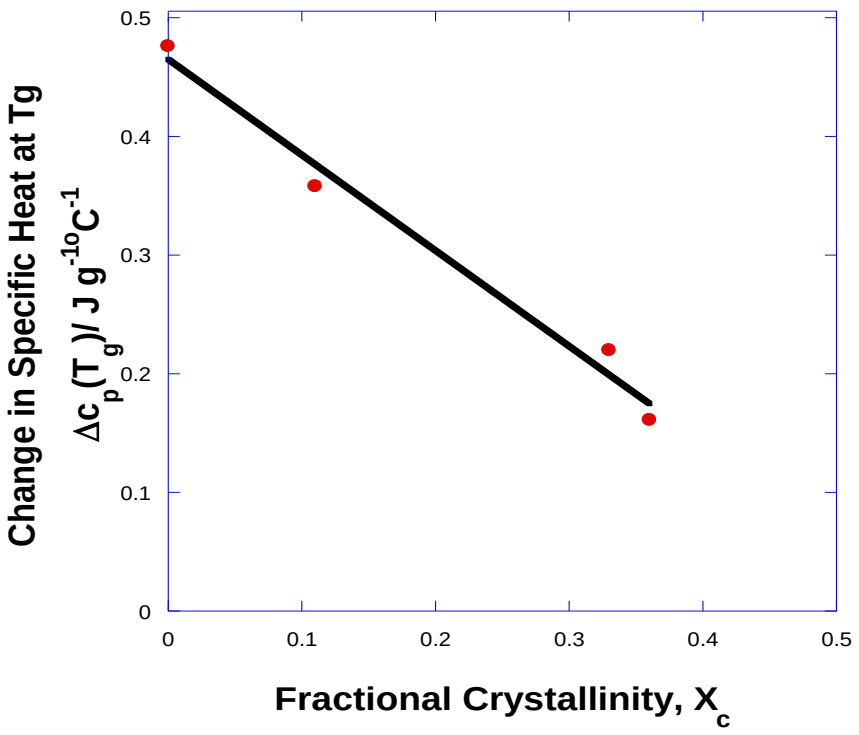

Figure 3.10. Dependence of the step change in specific heat at Tg, $\Delta c_p(Tg)$ with crystallinity.

3.1.4. Effect of cooling rates on the Tg of crystalline sample

In order to determine the effect of crystallinity on the response of the glass transition temperature to cooling rate on forming the glass the as-received Co-PLA was treated as described above but without heating to the melt to maintain the amount crystallinity. The effect of various cooling rates on the measured glass transition temperature, T_g, can be seen in Figure 3.11. The Tg on cooling through the glass transition was 7.5 ºC higher than that previously observed with the amorphous sample. The effect of cooling rate on Tg was measured as previously but without heating to the melting temperature and the results are shown in Figure 3.12.

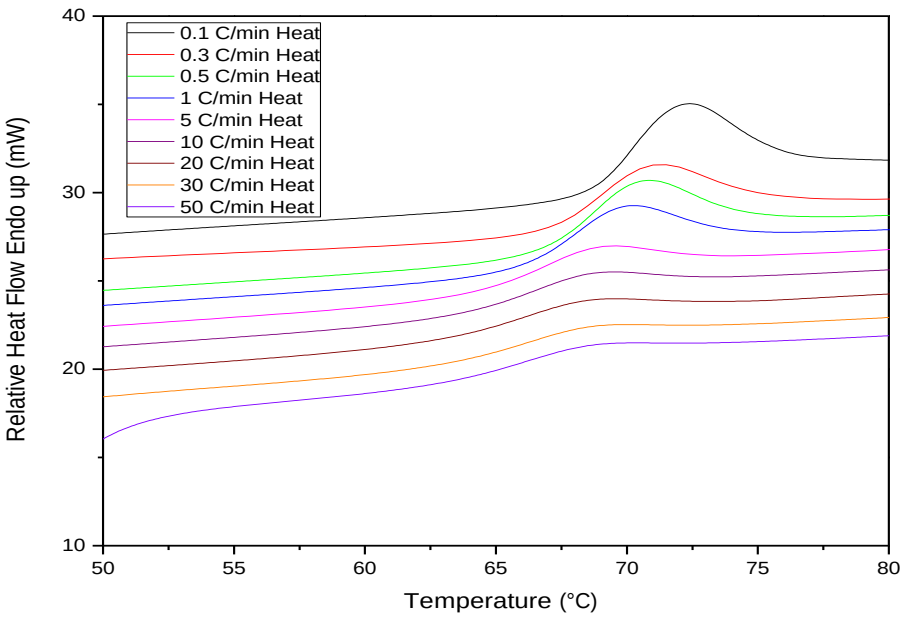

Figure 3.11. The effect of cooling rate on the measure T_g on the as-received sample at 0.33 fractional crystallinity without melting.

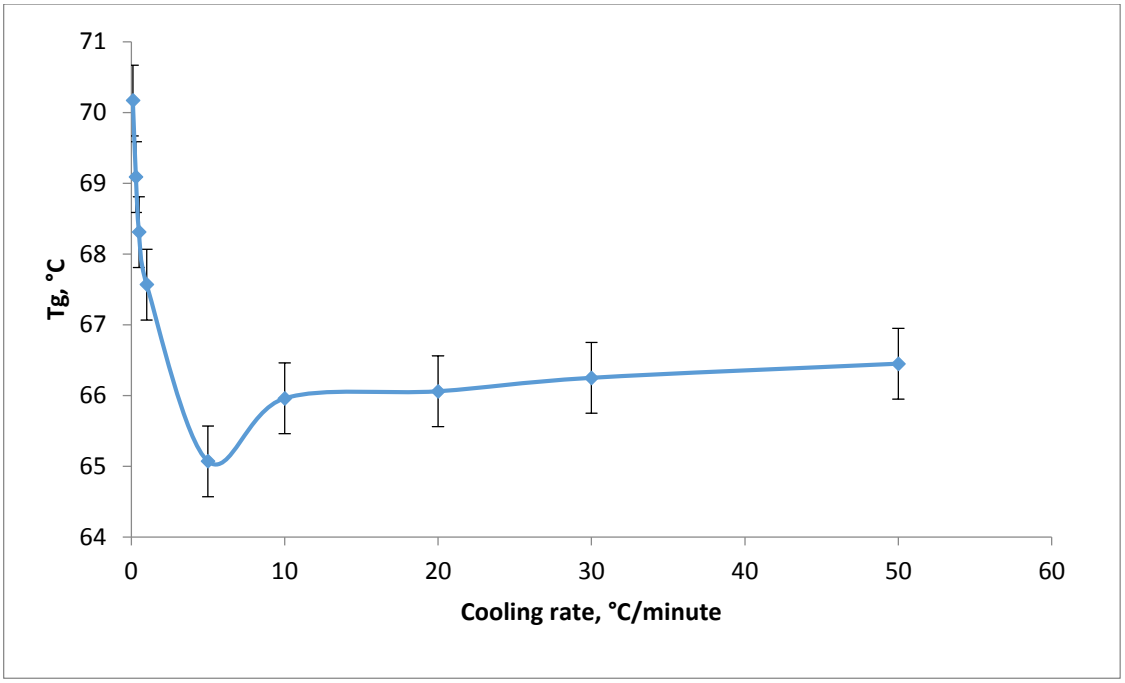

Figure 3.12. The variation of Tg of the as-received PLA sample with cooling rate.

Similar trends to that observed previously were obtained in that as the cooling rate decreases progressively larger ageing peaks were observed at Tg. Also two types of behaviour were observed; at high rates of cooling above 5 ^{o}C min^{-1} the Tg increased with increasing cooling rate although at a much lower dependence than previously observed and at low cooling rates, the Tg increased as the rate decreased, see Figure 3.12. We have previously attributed these to the glass forming process and to the development of further crystallinity on cooling respectively. For this to be the case, the dependence of Tg on rate should follow an Arrhenius relationship, see equation 3.4. The Arrhenius plot is shown in Figure 3.13 from which the activation energy was determined as 1.6 ± 0.3 MJ mol^{-1}. This is substantially greater than that obtained for amorphous Co-PLA and must reflect the restrictions to segmental motion imposed by the presence of crystalline regions. Based on these findings we conclude that further crystallization of the as-received sample occurred when the cooling rate was sufficiently slow and there was enough time for it to occur. If the rate is too rapid there is insufficient time.

Under fast cooling rate conditions Tg increased with increasing cooling rate and alternatively under slow cooling rate the Tg increases with decreasing cooling rate.

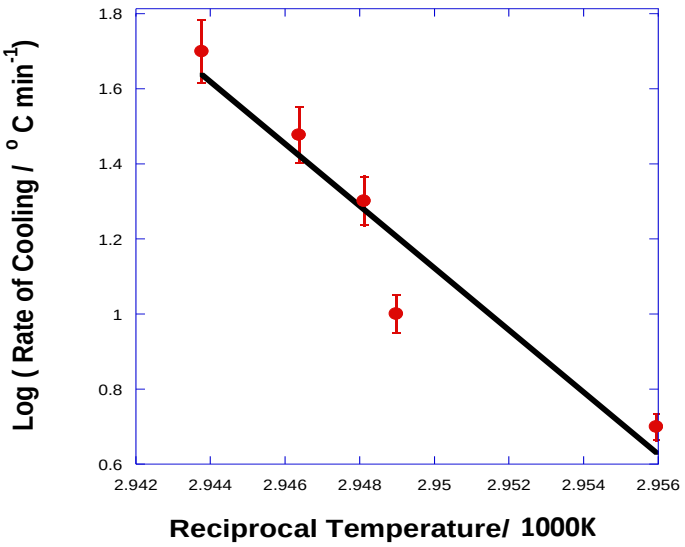

Figure 3.13. Arrhenius plot of dependence of Tg on the Rate of Cooling. (Crystalline sample)

3.2. Enthalpic Relaxation of Amorphous Co-PLA

Enthalpic relaxation and its relation to physical ageing have been discussed in Section 1.7 and how it relates to the non-equilibrium nature of amorphous glass. It is associated with the storage of glasses below but close to the glass transition and accounts for the observed change in material properties such as fracture toughness, elastic modulus and density with time. It is important in being able to predict the ultimate properties of commercial glasses.

Amorphous samples were prepared by cooling at 10 ^{o}C min^{-1} to room temperature which was well below the glass transition temperature. This produced a standard Co-PLA glass from which all others were compared. The glass transition was determined by immediately re-heating at 10 ^{o}C min^{-1} from room temperature through the glass transition to 80 ^{o}C and the Tg (58.5 ^{o}C) determined by the Richardson method [96]. At the same time the change in specific

heat at Tg, $\Delta c_p(Tg)$, for the amorphous sample was determined to be 0.48 ± 0.01 J $^oC^{-1}$ g^{-1}, see Figure 3.14. The sample was then cooled at 10 ^oC min^{-1} to the ageing temperature, T_A, and stored for various periods before the glass transition was re-determined on heating to 80 ^oC. In this case the ageing temperature, T_A, was an experimental variable and set to 5, 10, 15 and 20 °C below the measured glass transition. The development of the endothermic ageing peaks with storage time at several ageing temperatures is shown in Figures 3.15-18 and by comparing with the thermal response of the standard glass, the enthalpy change, ΔH_t at Tg was determined by direct subtraction of the standard glass.

The maximum enthalpy change has been shown in Section 1.7 to be

$$\Delta H_{max} = \Delta c_p.\Delta T \qquad (3.5)$$

where $\Delta T = (Tg-T_A)$ the undercooling from Tg and the degree of conversion towards equilibrium at time t, α_t, is $\alpha_t = \Delta H_t/\Delta c_p.\Delta T$ (3.6)

The progressive development of the physical ageing peak with time and at different degrees of supercooling can be seen in Figures 3.15-3.18 from the increase in size of the endotherms; from these the heat of physical ageing, the extent of conversion and the subsequent kinetics of ageing, see Table 3.1 to 3.4 were determined.

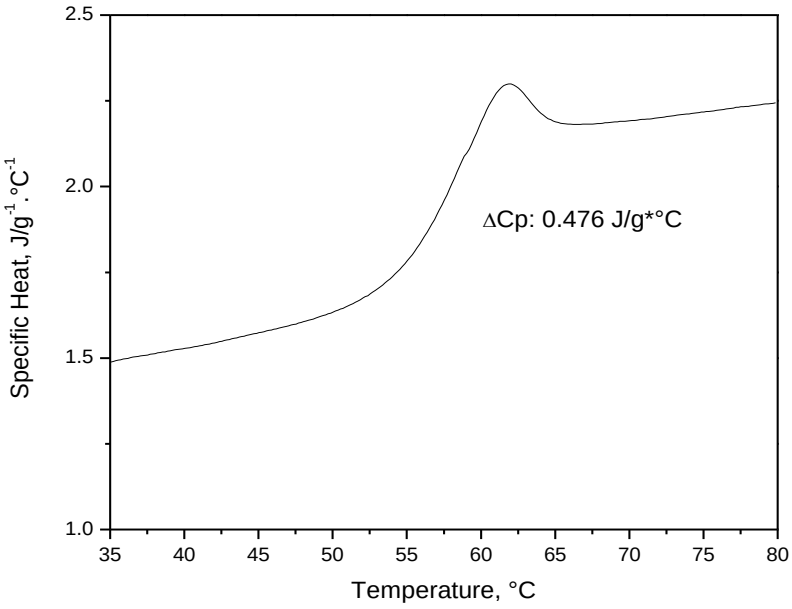

Figure 3.14. Change in specific heat of the amorphous glass on cooling at 10 ^{o}C min^{-1} at the glass transition.

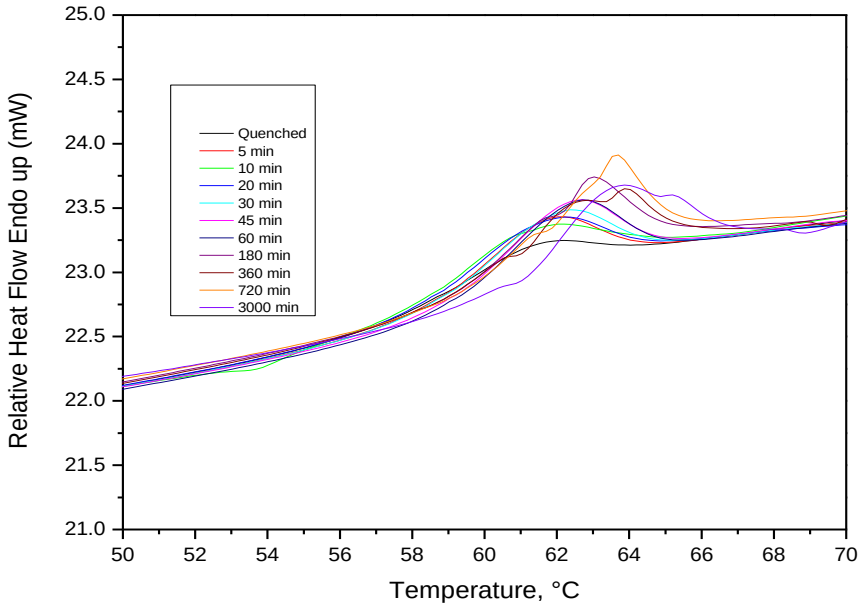

Figure 3.15. Development of the ageing endotherm at Tg with time at 53.5 ^{o}C.

Table 3.1. Change in Ageing endotherm with time at ΔT = 5 °C

Aging Time / min	ΔH / J g^{-1}	Conversion/ (α_t)
5	0.55	0.23
10	0.59	0.25
20	0.66	0.28
30	0.70	0.30
45	0.80	0.34
60	0.86	0.36
180	0.98	0.42
360	1.28	0.54
720	1.35	0.57
3000	1.56	0.66
∞	2.38	1.00

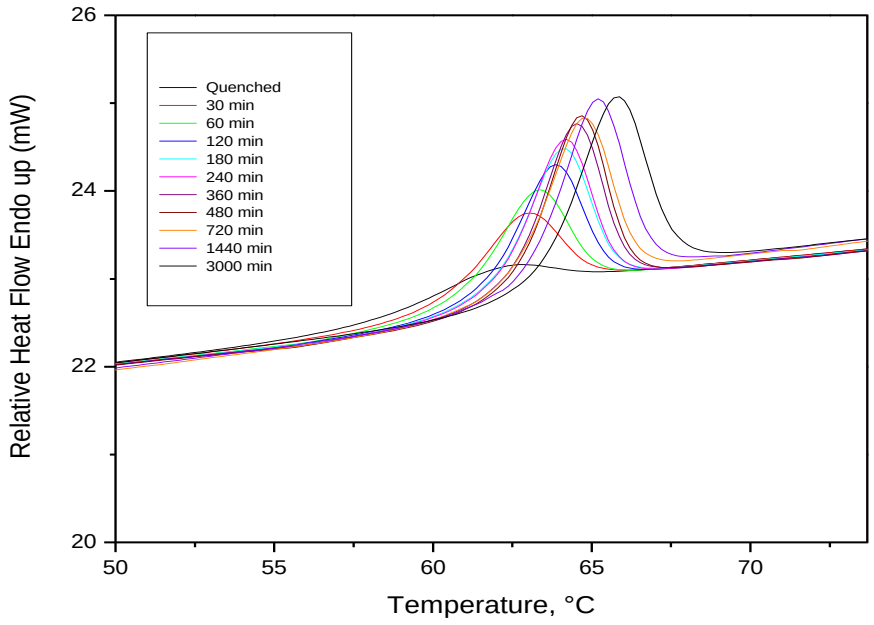

Figure 3.16. Development of the ageing endotherms at Tg with time at 48.5 °C.

Table 3.2. Change in Ageing endotherm with time at ΔT = 10 °C

Aging Time/ min	ΔH / J g^{-1}	Conversion/ (α_t)
30	1.18	0.25
60	1.57	0.33
120	1.86	0.39
180	2.07	0.43
240	2.20	0.46
360	2.27	0.48
480	2.29	0.49
720	3.20	0.67
1440	4.10	0.86
3000	4.19	0.88
∞	4.76	1.00

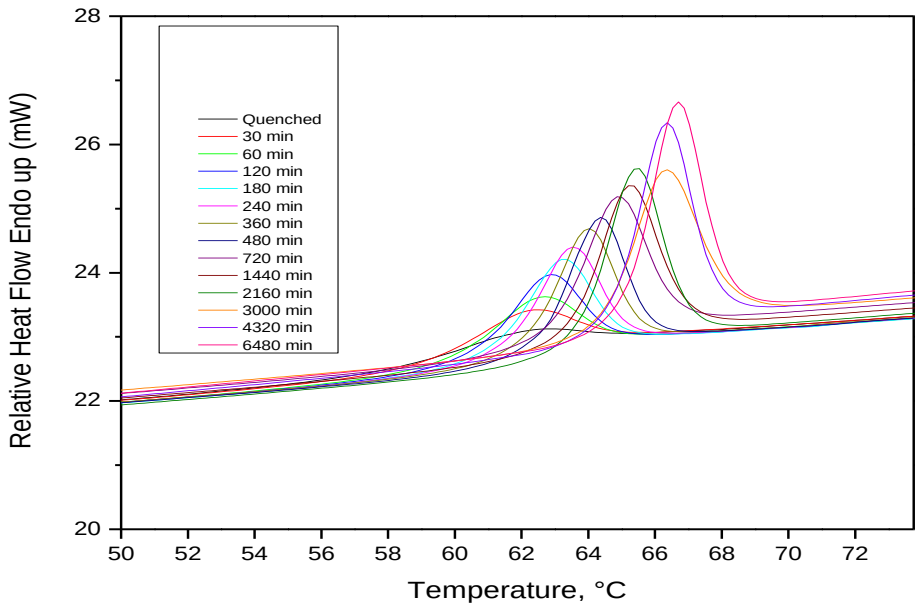

Figure 3.17. Development of the ageing endotherm at Tg with time at 43.5 °C.

Table 3.3. Change in Ageing endotherm with time at ΔT = 15 °C

Aging Time / min	ΔH / J g^{-1}	Conversion (α_t)
30	0.95	0.13
60	1.27	0.18
120	1.60	0.22
180	1.76	0.25
240	1.91	0.27
360	2.06	0.29
480	2.16	0.30
720	2.17	0.30
1440	2.77	0.39
2160	2.92	0.41
3000	3.30	0.46
4320	4.52	0.63
6480	5.48	0.77
∞	7.14	1.00

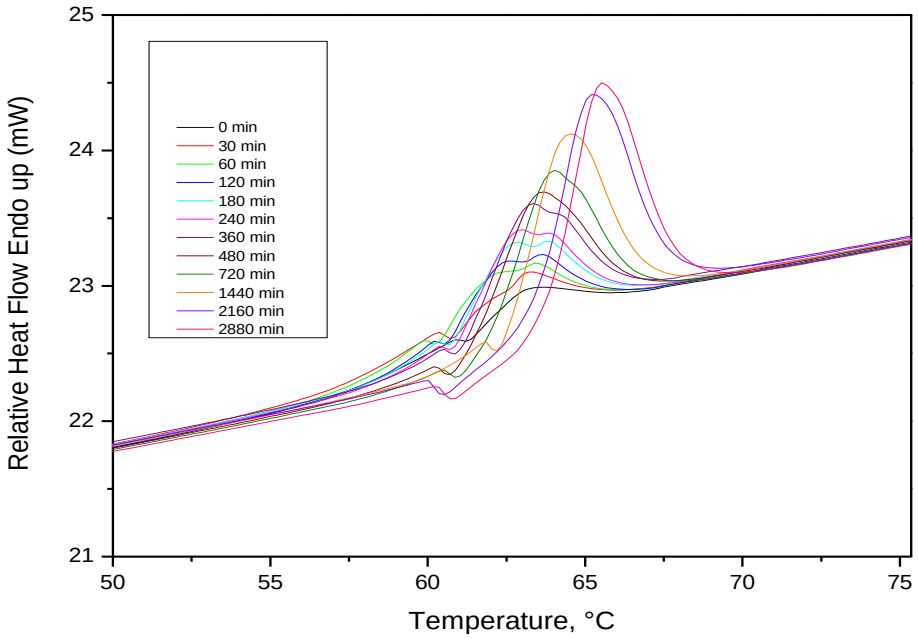

Figure 3.18. Development of the ageing endotherm at Tg with time at 38.5 ºC.

Table 3.4. Change in Ageing endotherm with time at ΔT = 20 °C

Aging Time/ min	ΔH/ J g^{-1}	Conversion/ (α_t)
30	0.44	0.046
60	0.76	0.080
120	1.05	0.11
180	1.26	0.13
240	1.62	0.17
360	1.71	0.18
480	1.78	0.19
720	1.87	0.20
1440	2.39	0.25
2160	2.57	0.28
2880	2.62	0.262
∞	9.52	1.00

The effect of changing the degree of supercooling on the development of the endothermic peak is quite pronounced as can be seen in Figures 3.19.

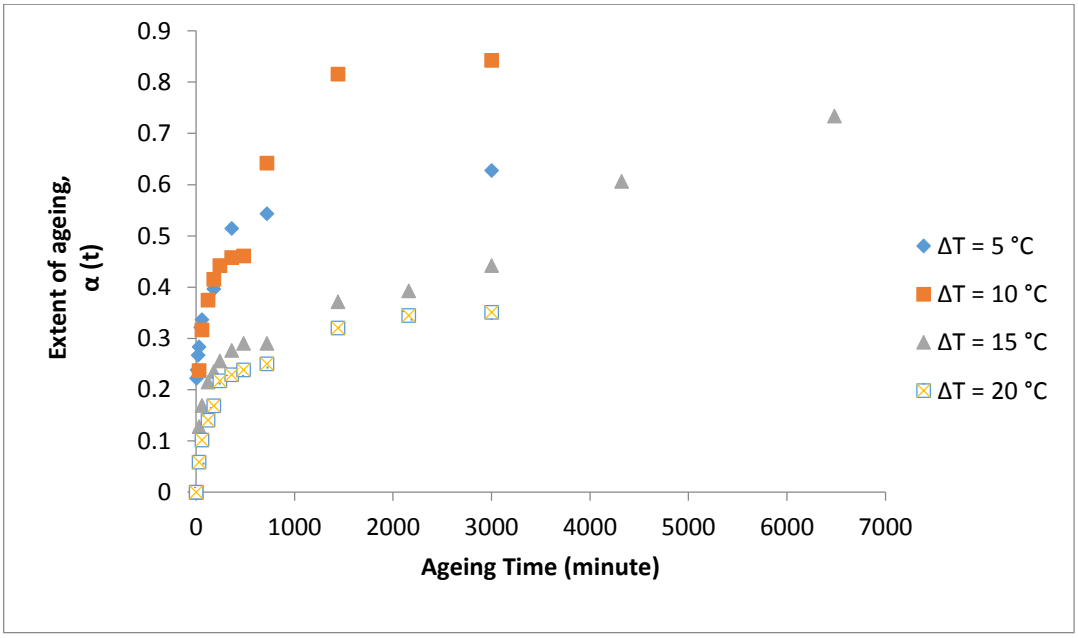

Figure 3.19. The development of enthalpic relaxation with time as a function of undercooling, ΔT, from Tg.

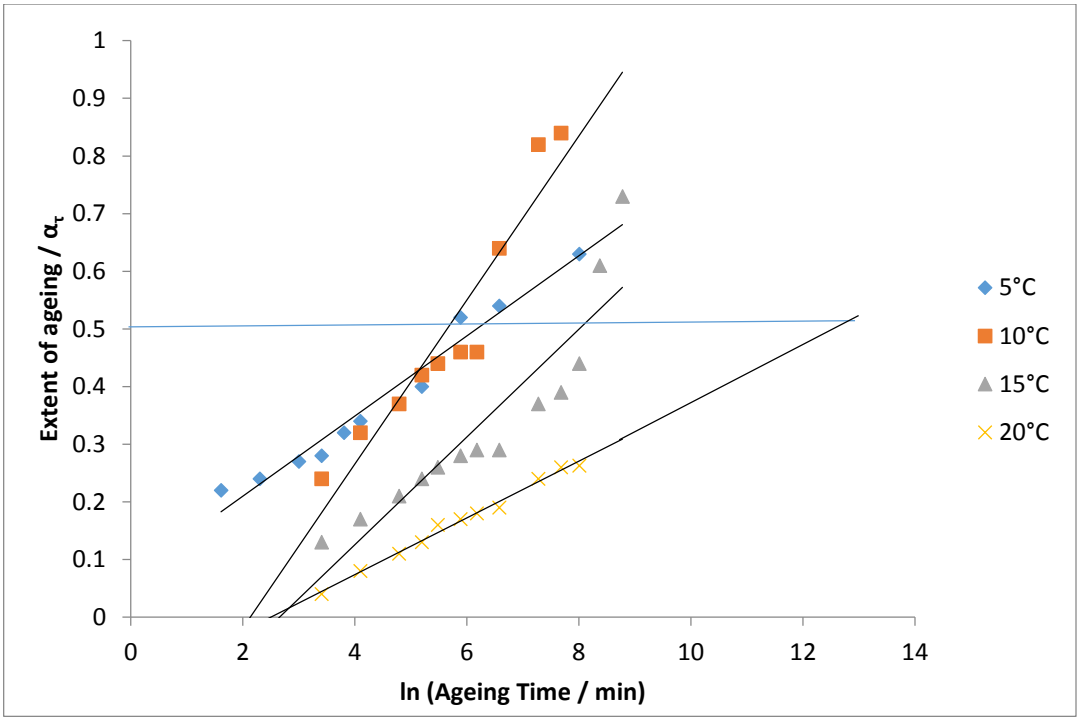

Figure 3.20. The dependence of enthalpic relaxation rate on degree of supercooling from Tg.

Since the measurements were limited in conversion, the time to 50% conversion, the half-life, $t_{1/2}$, was taken as a reciprocal measure of the rate of conversion at each value of ΔT, see Figure 3.20; $t_{1/2}$ was measured from the linear plots of the extent of ageing against logarithm of the ageing time and the best fit equation used to evaluate t at 0.5, see Figure 3.20. This value was used to measure the activation energy of enthalpic relaxation, ΔE_A, from a plot of ln ($t_{1/2}$) against T^{-1}, see Figure 3.21, since

$$t_{1/2} = A.\ \exp\left(\Delta E_A / RT\right) \qquad (3.7)$$

where A is a pre-exponential factor, and R the gas constant. An Activation energy of 0.50 ± 0.20 MJ mol^{-1} was obtained, which compares with 0.98 ± 0.10 MJ mol^{-1} for the dependence of Tg on cooling rate, implying that if the enthalpic relaxation is a continuation of the same

phenomenon to slower rates a different slower segmental motion of the polymer chain may be involved with a lower activation energy.

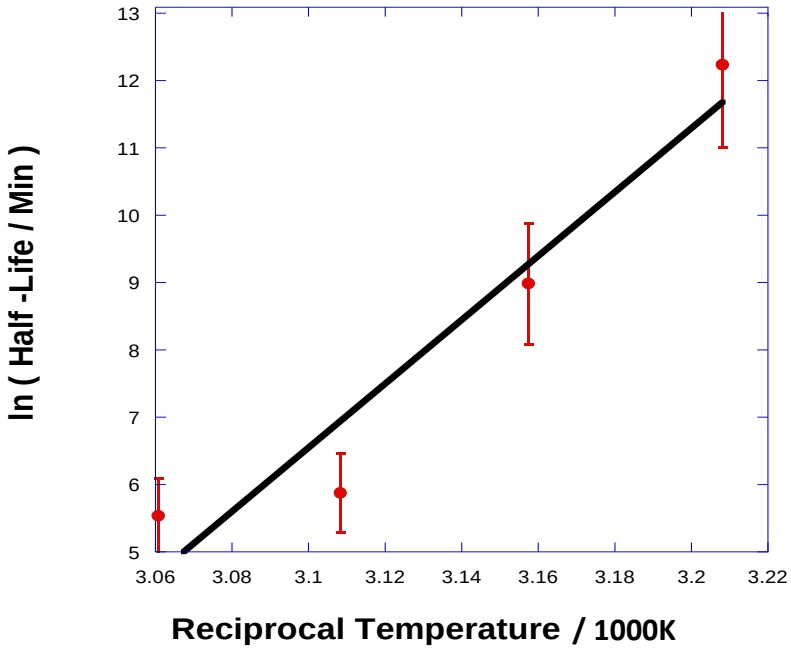

Figure 3.21. Arrhenius plot of dependence of the half-life of enthalpic relaxation on reciprocal temperature.

The extent of enthalpic relaxation, Φ(t), towards equilibrium with time is defined as

$$\Phi(t) = 1 - \Delta H_t/\Delta c_p(Tg).\Delta T \qquad (3.8)$$

The parameters, ΔH_t, $\Delta c_p(Tg)$ and ΔT are the same as defined above. The enthalpic relaxation is also related to an average relaxation time τ_o by the Williams-Watt stretched exponential function [108], such that

$$\Phi(t) = \exp (- t/ \tau_o)^{\beta} \qquad (3.9)$$

Where β is an inverse measure of the breadth of the relaxation spectrum [109] and is usually of the order 0.3-0.6 for many organic glasses and is determined from a plot of

$\ln(-\ln(1 - \Delta H_t/\Delta c_p(Tg).\Delta T))$ against $\ln(t)$ since from eqs. 3.8 and 3.9,

$$\ln(-\ln(1 - \Delta H_t/\Delta c_p(Tg).\Delta T)) = \beta \ln(t/t_o) \qquad (3.10)$$

In order to superimpose the data at different ageing temperatures and obtain an average β value for enthalpic relaxation, a reduced time, $t/t_{1/2}$, was adopted for t/t_o, see Figure 3.22. This analysis gave a value of 0.27±0.04 which is quite characteristic of the values obtained for the ageing of polymer glasses and indeed a value of 0.35 has been quoted for the physical ageing of poly (ethylene terephthalate) [109].

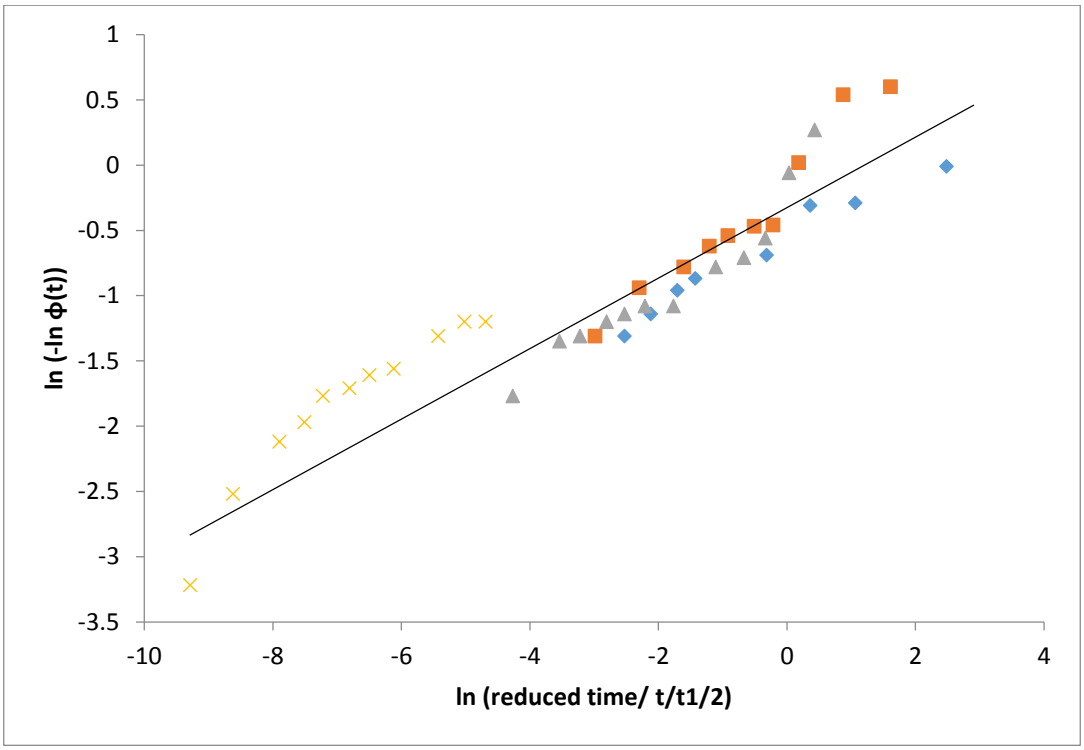

Figure 3.22. Williams-Watt fit of the extent of enthalpic relaxation against reduced time.

3.2.1. Enthalpic Relaxation of Partially Crystalline Co-PLA

In order to determine the effect of crystalline regions on the extent of enthalpic relaxation and the rate at the same degree of supercooling partially crystalline samples of Co-PLA were slow cooled in the DSC from above the melting point to produce different degrees of crystallinity, see Figure 3.23. Different cooling rate were used to create samples with different fractional crystallinities, see Table 3.5. A standard glass was produced by cooling the sample through Tg at 10 ^{o}C min^{-1} and this was aged at a ΔT of 15 ^{o}C, see Figures 3.24 and 3.25. As observed above only well-developed ageing endotherms developed with the 11% crystalline sample. While some ageing developed with the 36% crystalline sample it was small in line with the low value for $\Delta c_p(Tg)$ and increasing crystallinity had severely reduced the development of enthalpic relaxation, see Figure 3.24.

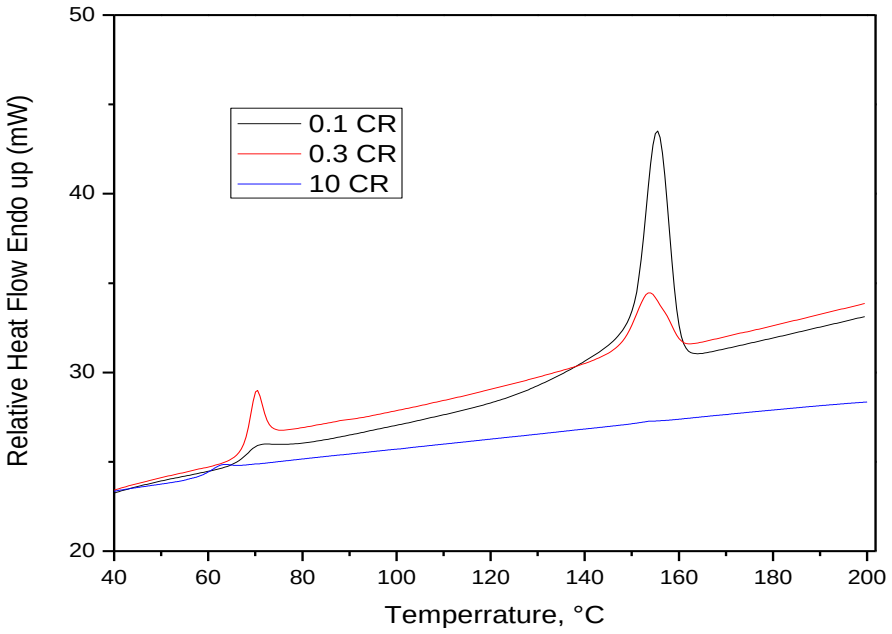

Figure 3.23. Effect of cooling rate on melting endotherm. (CR: Cooling rate)

Table 3.5. Cooling Rate used to prepare Crystalline Samples.

Cooling Rate / °C min^{1}	% Crystallinity	Glass Transition Temperature / ° C
0.1	36	63.5
0.3	11	61.5
10	0	58.5

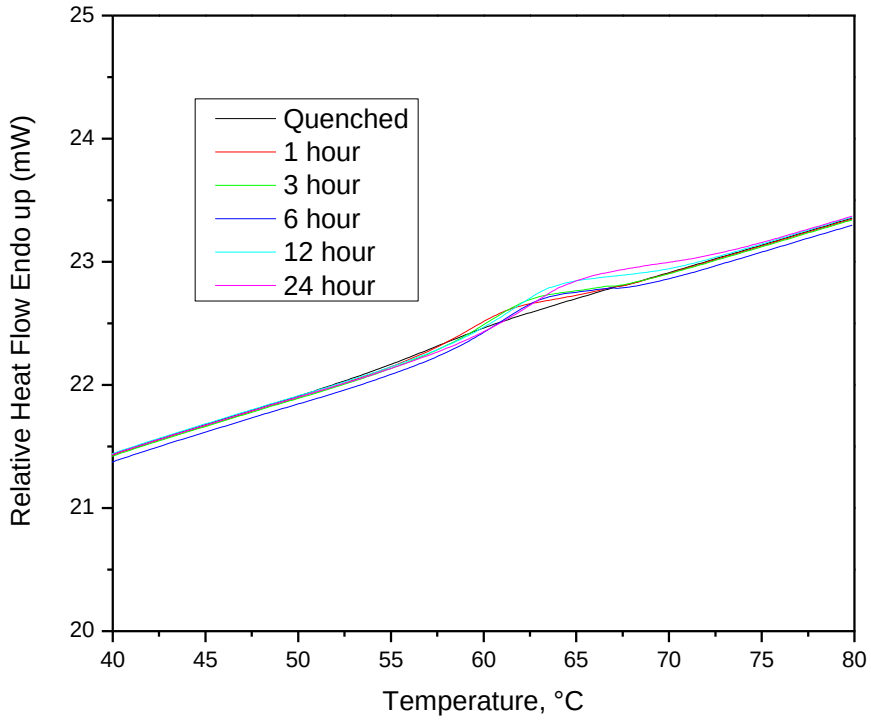

Figure 3.24. Ageing of 36% crystalline sample at ΔT =15 °C.

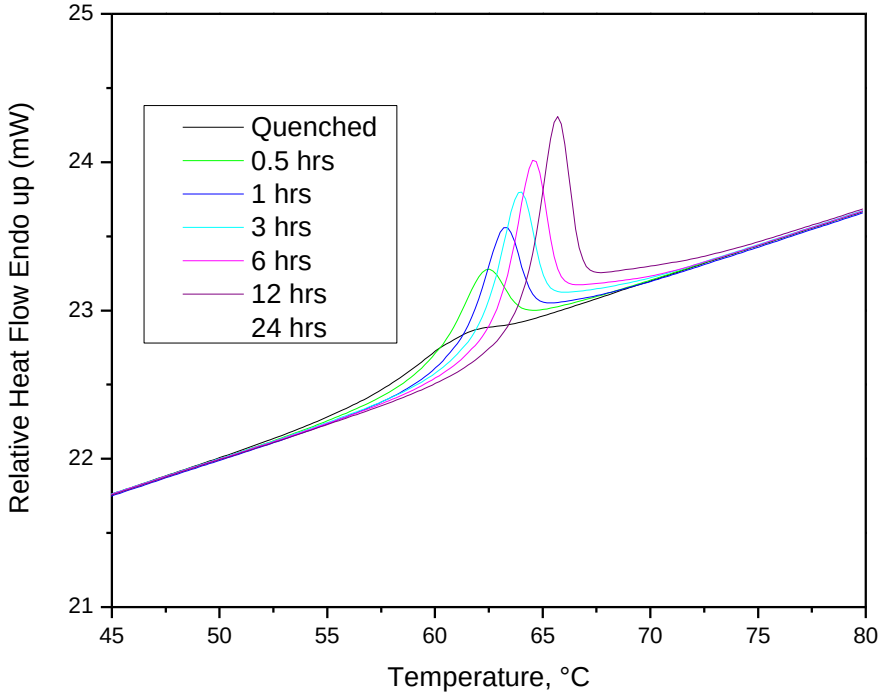

Figure 3.25. Ageing of 11% crystalline sample at ΔT = 15 °C.

Table 3.6. Ageing crystalline samples at ΔT= 15 °C.

A. 36% Crystallinity.

Ageing Time / min	ΔH_t / J g^{-1}	Enthalpic Relaxation $\Phi_t = 1 - \alpha_t$	Extent of Ageing (α_t) $\Delta H_t / \Delta H_\infty$
60	0.464	0.808	0.192
180	0.590	0.756	0.244
360	0.639	0.735	0.265
720	0.828	0.657	0.343
1440	1.084	0.551	0.449
∞	2.415	0.00	1.00

$\Delta c_p = 0.161$ $Jg^{-1}°C^{-1}$

B. 11% Crystallinity.

Ageing Time / min	ΔH_t / J g^{-1}	Enthalpic Relaxation $\Phi_t = 1 - \alpha_t$	Extent of Ageing (α_t) $\Delta H_t / \Delta H_\infty$
60	0.987	0.816	0.184
180	1.271	0.763	0.237
360	1.491	0.722	0.278
720	1.506	0.720	0.280
1440	1.797	0.666	0.334
∞	5.370	0.000	1.00

$\Delta c_p = 0.358$ $Jg^{-1}°C^{-1}$

The enthalpies of ageing with time for the crystalline samples are shown in Table 3.6 and Figure 3.26 for comparison with the amorphous material, the enthalpy developing with time decreased with increasing crystallinity. However, this decrease was in proportion to the drop in $\Delta c_p(Tg)$ since the extent of aging, $\Delta H_t / \Delta H_{max}$ were comparative for all three materials, see Figure 3.27.

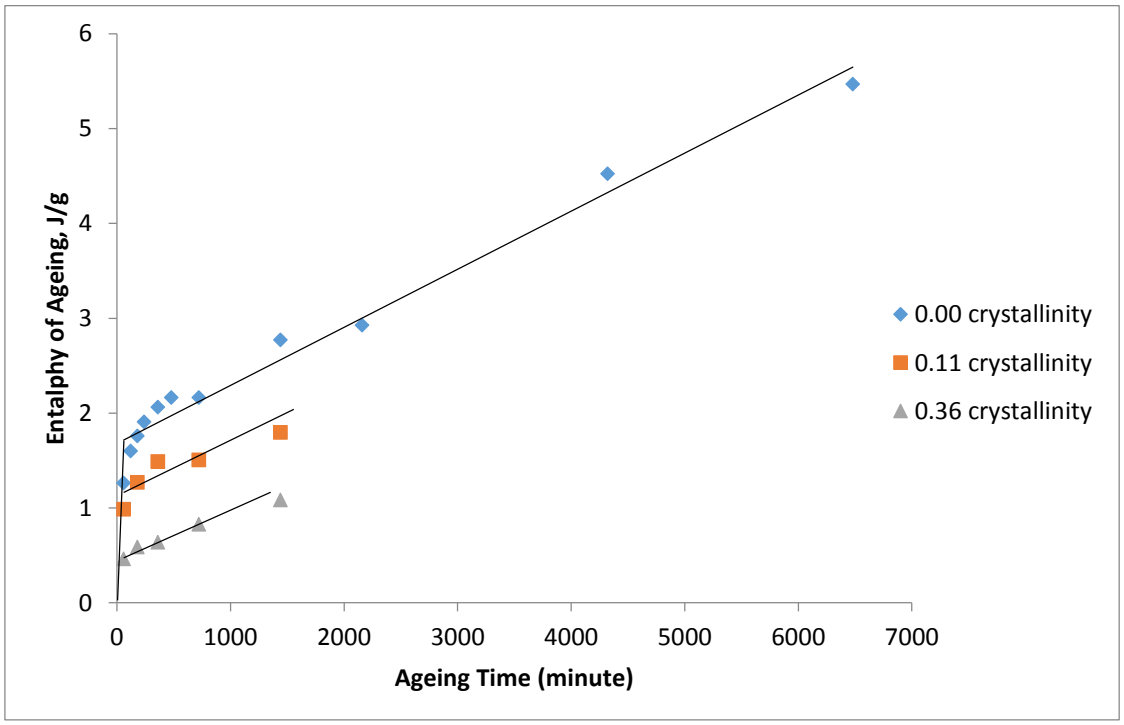

Figure 3.26. Development of enthalpy of ageing with time.

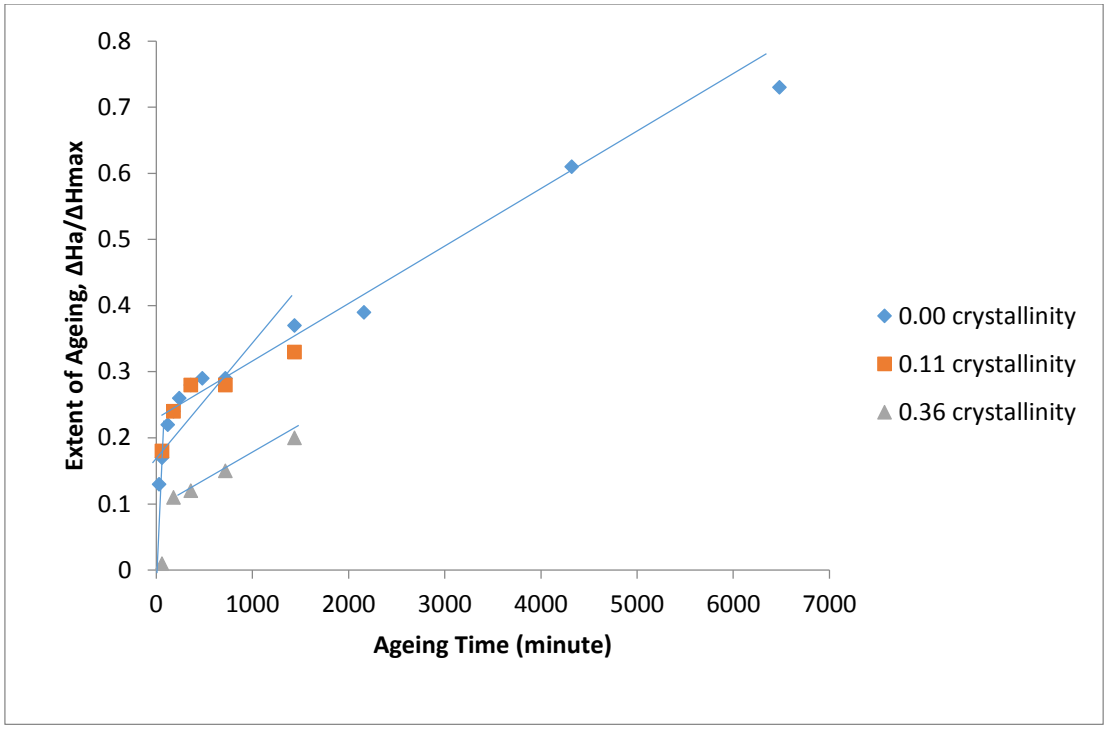

Figure 3.27. Development of ageing with time.

The extent of enthalpic relaxation towards equilibrium, Φ(t), with time is defined by the Williams-Watt equation, see eq. 3.9, and a plot of Φ(t) against $\ln(t/t_{0.2})$ was used to compare the effect of crystallinity on the kinetics of ageing. Time to reach 20% conversion, $t_{0.2}$, was adopted in defining the reduced time since it was in the range of experimental measurements. The 0 and 11 % crystallinity samples aged following similar kinetics, rate constant ($1/t_{02}$) and β value 0.27±0.3 while the more crystalline material had a lower rate but similar β value, as indicated by the slope of Williams-Watt plot in Figure 3.28.

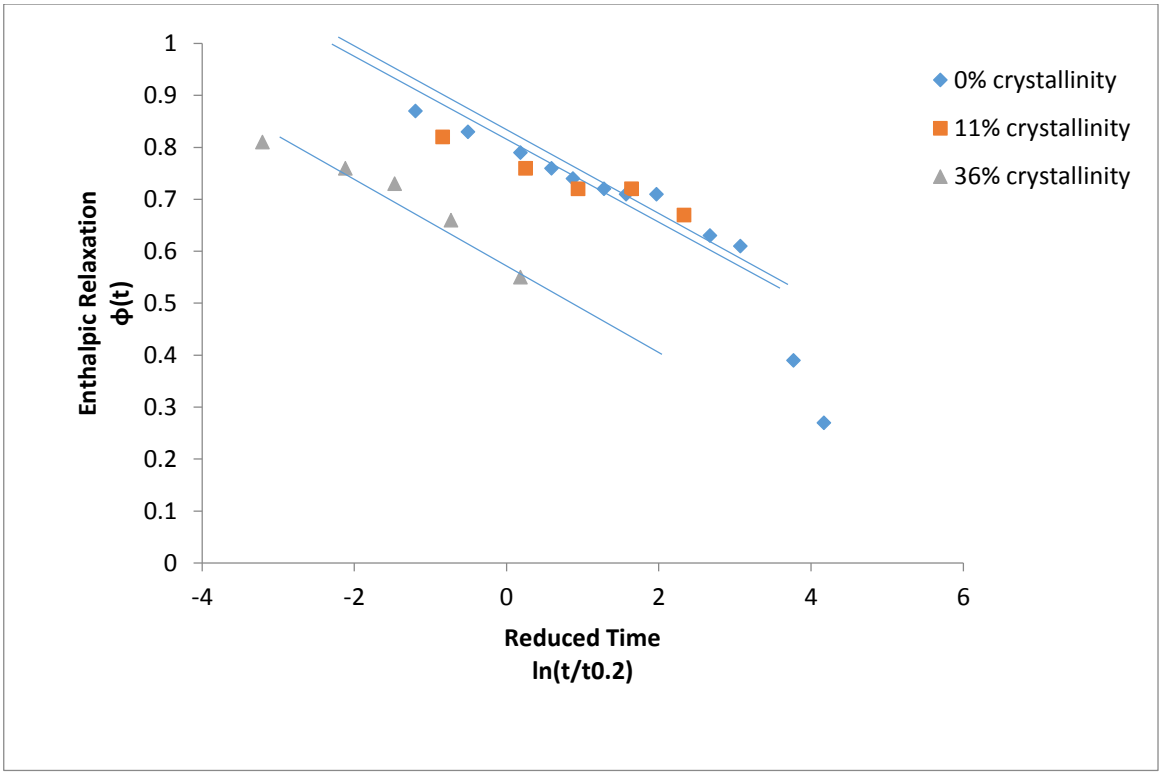

Figure 3.28. Williams-Watt fit of the extent of enthalpic relaxation against reduced time.

3.3. Conclusions

Samples of Co-PLA were slow to crystallize and this allowed them to be crystallized by controlled cooling from the melting point. This enabled amorphous samples and samples with controlled fractional crystallinity to be produced in order to compare enthalpic relaxation rates. The glass transition of Co-PLA, produce with cooling rate at 10 ^{o}C min^{-1} was 58.5 ^{o}C but it was raised to higher values on crystallization and a greatly reduced step in the specific heat, $\Delta c_p(Tg)$, with crystallinity.

Ageing at temperatures close to but below Tg was accompanied with an endotherm at Tg on reheating and this increased with logarithm of the storage time in agreement with the Williams-Watt equation with a β value of 0.27. Crystallization appears to inhibit ageing in that the reduction in $\Delta c_p(Tg)$ reduces the heat of enthalpic relaxation and the rate of ageing. This is

attributed to the hard crystalline phase reducing the mobility of the segmental motion in the amorphous regions, which is not in proportion to the crystallinity present.

4.0. Introduction

From the previous chapter on the effect of cooling rate on Co-PLA it was concluded that the crystallization rates were too slow to be measured directly by isothermal calorimetry and alternative procedures, A to D, were adopted to determine the development of crystallinity with time over the range of temperatures.

4.1. Crystallization of Co-PLA in DSC by Procedure A

This procedure involved heating samples of weight 5-7 mg encased in aluminium pans, from 30 to 200 ^{o}C at 10 ^{o}C min^{-1} in a DSC, holding it at 200 ^{o}C for 2 min, and cooling at 10 ^{o}C min^{-1} to room temperature to produce an amorphous sample. The samples were removed from the DSC and placed in a thermostated oven at various temperatures from 70 to 145 ^{o}C corresponding to the region of maximum rate of crystallization (half way between T_g and the melting point). The samples were held for various periods up to 120 min before being removed from the oven and cooled to room temperature. The fractional crystallinity, X_t, which had developed was determined by subsequently melting the polymer at 10 ^{o}C min^{-1} and measuring the heat of fusion, ΔH_f, from the area under the melting endotherm. This was divided by the heat of fusion of totally crystallized PLLA, taken to be 93.6 Jg^{-1} [11, 58], to determine the fractional crystallinity, X_t, since

$$X_t = \Delta H_f / \Delta H^{o}_f \qquad (4.1)$$

The melting endotherms are reproduced in Figure 4.1a-h.

On crystallizing at 70^{o}C, see Figure 4.1a, the crystallization rate was too slow to be measured with any accuracy since only after 60-120 min was an ill-defined melting endotherm observed, equivalent to a fractional crystallinity of about 0.01. The measured crystallinities

were not reproducible and the melting point, T_m, was also difficult to determine precisely but was in the region of 155 ^oC.

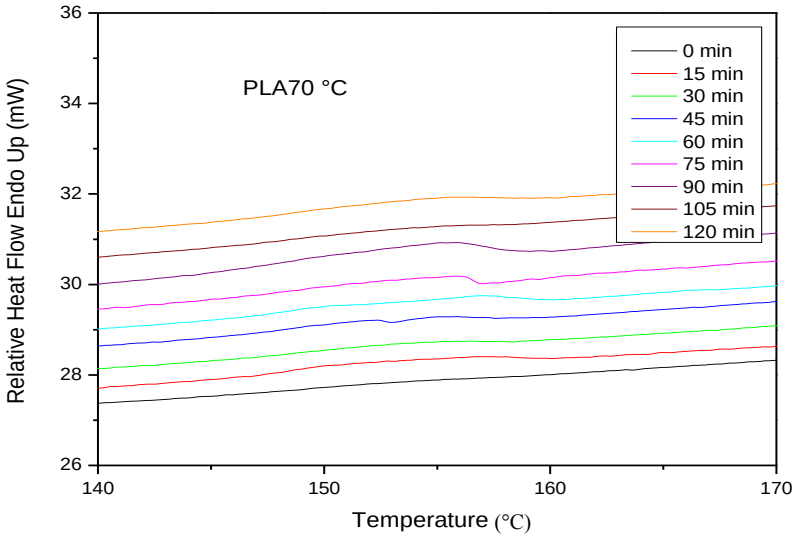

Figure 4.1a. Endotherms produced by crystallizing at 70 °C.

On crystallizing at 85 ^oC the rate of crystallization had increased slightly and the measured crystallinities were more reproducible. However, the fractional crystallinity which developed within 2 h was only 0.02. The endotherms occurred at higher temperatures than at 70 ^oC and drifted higher with increasing time; melting occurred over 10-20 ^oC and was associated with the melting of lamellae with a range of thermal stabilities. Two m.pts. were accordingly defined corresponding to the maximum in the endotherm, T_m (Peak) and to the melting of the maximum number of lamellae, and corresponding to the last trace of crystallinity, T_m (Max). This was the melting point of the most stable lamellae in the distribution.

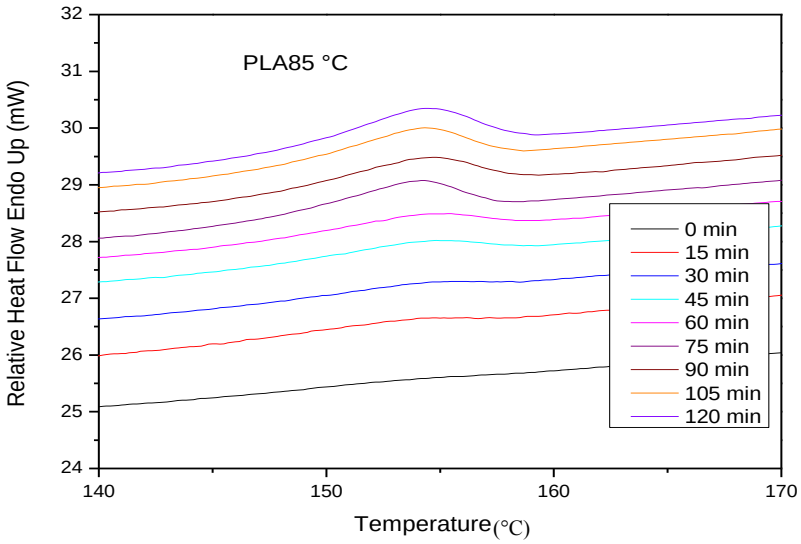

Figure 4.1b. Endotherms produced by crystallizing at 85 °C.

The crystallization was still faster at 95 °C and an endotherm was detectable after 15 min corresponding to the development of 0.015 fractional crystallinity but it was obvious that crystallization was not complete after 2 hours (Figure 4.1c). The melting endotherm exhibited a double distribution with two maxima, T_m (Peak 1) and T_m (Peak 2) both of which appeared to increase with increasing time, although the last traces of crystallinity, T'_m, did not appeared to increase with time. The presence of a higher m.pt. in a double melting endotherm has in the past [110, 111] been attributed to presence of lamellae which develop at the crystallization temperature and thicken on heating. Nevertheless the presence of the double distribution endotherm is consistent with two separate distributions of lamellae thickness.

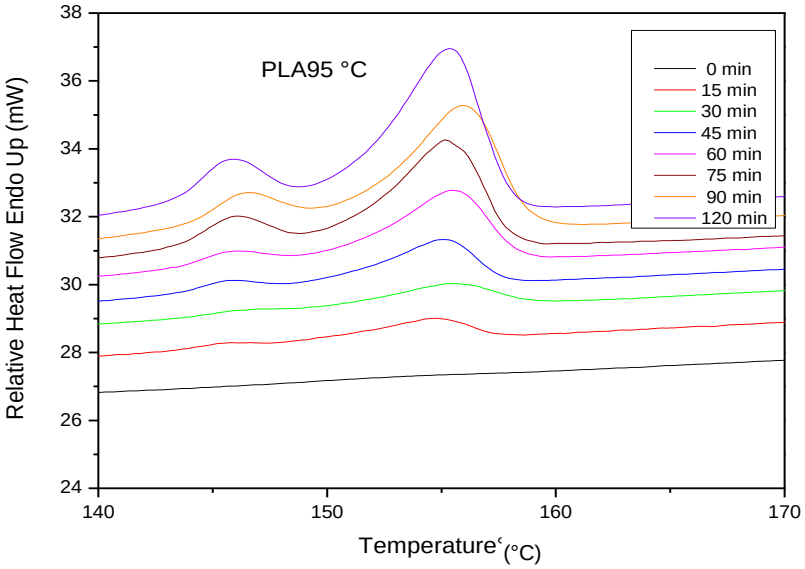

Figure 4.1c. Endotherms produced by crystallizing at 95 °C.

At 105 °C, the crystallization rate continued to increase with temperature since after 90 min the fractional crystallinity was 0.28 and the crystallization was nearing completion in that the fractional crystallinity changed less between 90 and 120 min. than before (Figure 4.1d). A double distribution melting endotherm was again observed with the lower one more dominant implying that more of the lamellae crystallized at 105 °C had not thickened on heating to the melting point (m.pt.) as they were more stable than those crystallised at 95 °C and lower.

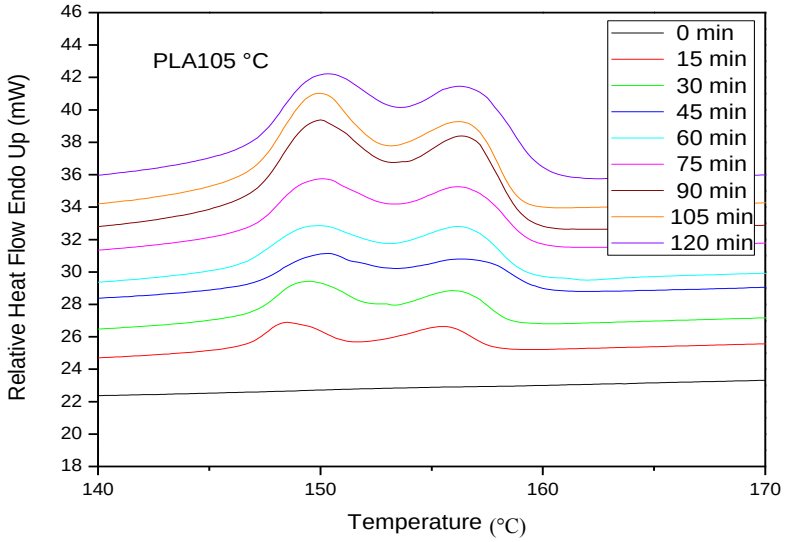

Figure 4.1d. Endotherms produced by crystallizing at 105 °C.

The crystallization rate was higher at 118 than 95 °C as the crystallinity developed to 0.38 after 2 hours compared with the previous one of 0.28 (Figure 4.1e). However, the melting endotherms exhibited a single melt distribution with the absence of the higher melting endotherm produced on thickening. Melting now occurred above 150 °C. The endotherms broadened with time and shifted to higher temperatures, such that both T_m and T'_m increased progressively with time.

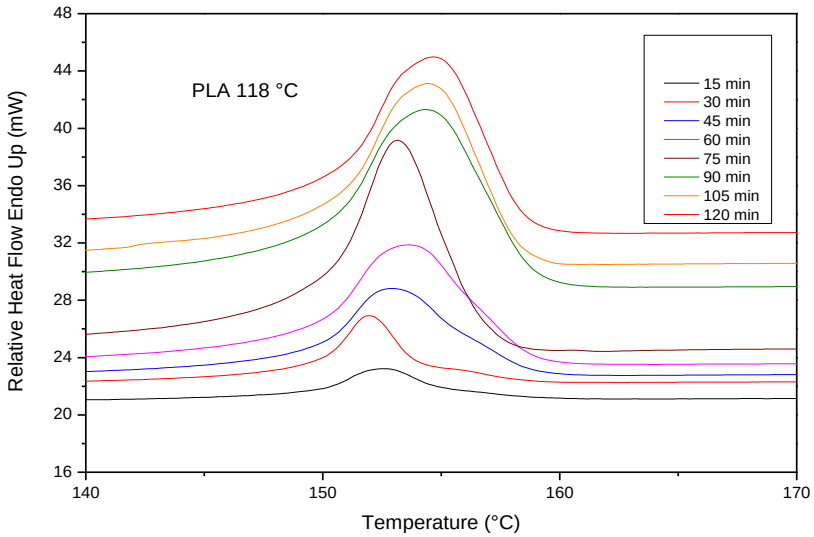

Figure 4.1e. Endotherms produced by crystallizing at 118 °C.

The crystallization at 125 °C occurred at a similar rate to that at 118 °C and the crystallinity appeared to have reached a limit after 2 hours of 0.40 (Figure 4.1f). The melting endotherms were more regular than previous and occurred at higher temperatures with a single distribution which moved to higher temperatures with time.

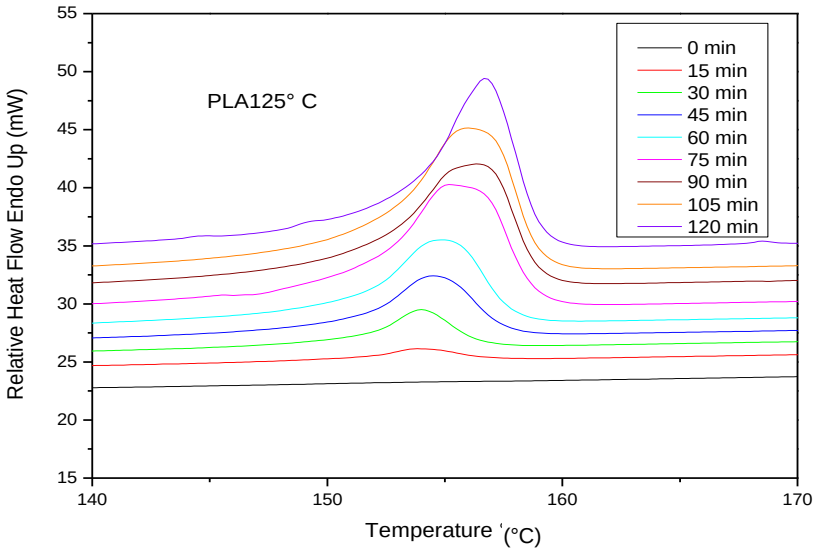

Figure 4.1f. Endotherms produced by crystallizing at 125 °C.

The trends observed at 125 continued at 135 °C with higher m.pts. and a progressive increase in T_m with time. The crystallinity appeared to be constant after 90 mins.

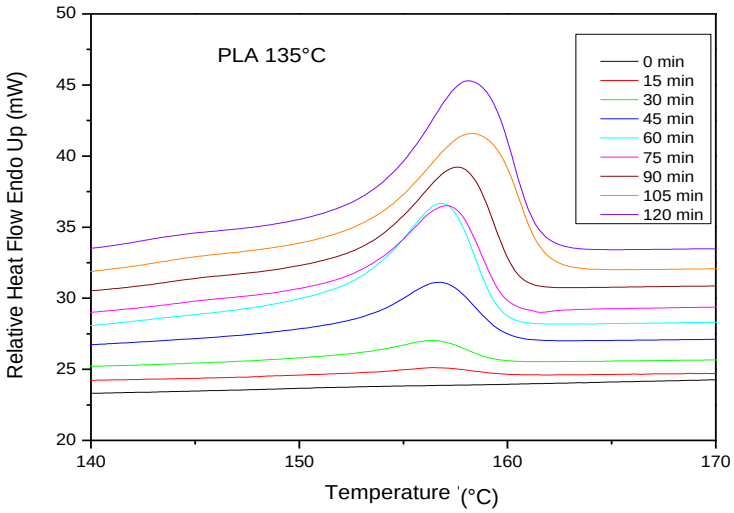

Figure 4.1g. Endotherms produced by crystallizing at 135 °C.

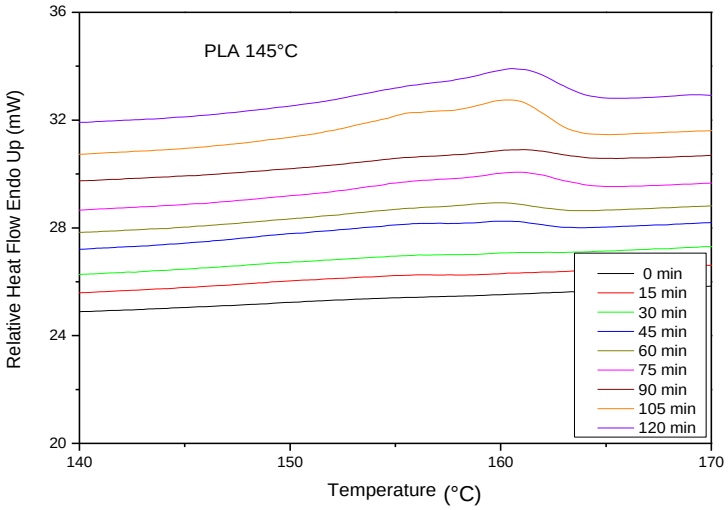

Figure 4.1h. Endotherms produced by crystallizing at 145 °C.

Figure 4.1. The development of the melting endotherms with time at various isothermal crystallization temperatures.

At 145 ºC well developed melting endotherms did not appear until after 60 min and the rate of crystallization was clearly slower than observed at the previous temperatures. The rate was slowing as the crystallization temperature increased closer to the m.pt. This is

characteristic of nucleation control as the crystallization rate, R_c, is dependent on the reciprocal degree of super-cooling, i.e.

$$R_c \sim 1/(T_m - T_c) \qquad (4.2)$$

Despite the reduction in rate the m.pt. continued to increase, to 165 °C, with crystallization temperature.

From Figure 4.2 it can be seen that the crystallization developed over a wide range of temperature and although the rates were slow initially it increased to a maximum between 118 to 125 °C and then decreased again to an extremely low rate at 145 °C. This bell-shaped dependence of rate on temperature is characteristic of polymer crystallization and in the case of Co-PLA the rate decreased at low temperatures due to viscosity control of the crystallization and at high temperature the rate decreased with increasing temperature due to the dependence on supercooling characteristic of nucleation control.

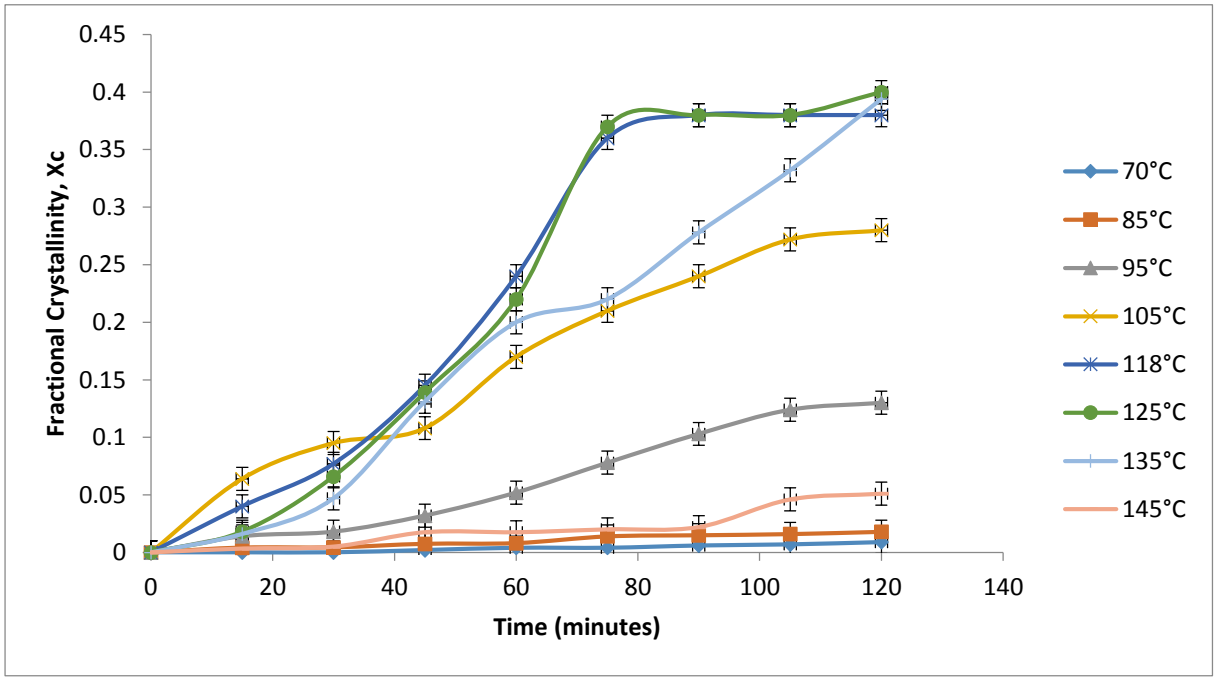

Figure 4.2. The development in fractional crystallinity, X_c with time over the temperature range 70–135 °C.

4.2. Crystallization of Co-PLA by Procedure B

Procedure B is a partial repeat of procedure A except that since the rate of crystallization of Co–PLA was slow it was decided to extend the time up to 16 h, repeat some of the crystallizations to check the reproducibility of the method and use an increased rate of heating to eliminate melting and recrystallization on heating to the melt. This was used to explain the presence of some of the double distribution melting endotherms. As previously 5-7 mg samples were encapsulated in aluminium pans, melted at 200 ^{o}C, held for 2 min before cooling at 10 ^{o}C min^{-1} to 30 ^{o}C in the DSC. This ensured that the samples were amorphous and would crystallize at the temperature of the oven, within the range 95 to 135 ^{o}C. The crystallinity of the samples were determined by measuring the heats of fusion within the DSC under the conditions adopted previously except that the rate of heating was 50 ^{o} C min^{-1} to reduce the amount of melting and recrystallization which occurred on re-heating to the melting point. Some of the crystallizations were repeated to check the reproducibility of the method and samples were removed after 2, 4, 6 and 16 h only. These results are shown in Figure 4.3a-e.

On crystallizing at 95 ^{o}C after 2 h the crystallinity was 0.15 and T_m was 160 ^{o}C which compares with 0.25 and 155 ^{o}C on crystallizing by procedure A. Heating at a faster rate had considerable effect in reducing the measured fractional crystallinity as additional material had crystallized at a lower temperature; consequently melting at a lower temperature. However, the greatest difference between the two procedures was the absence of the bimodal melting endotherm. A barely discernible lower endotherm was present which was very different from that observed previously in section 4.1; the absence is attributed to heating the sample at 50 rather than 10 ^{o}C min^{-1} since it reduced the time for the lamellae to thicken on heating to the melting point. The crystallinity of the sample continued to increase with time and the melting endotherm broadened moving to higher temperatures with time.

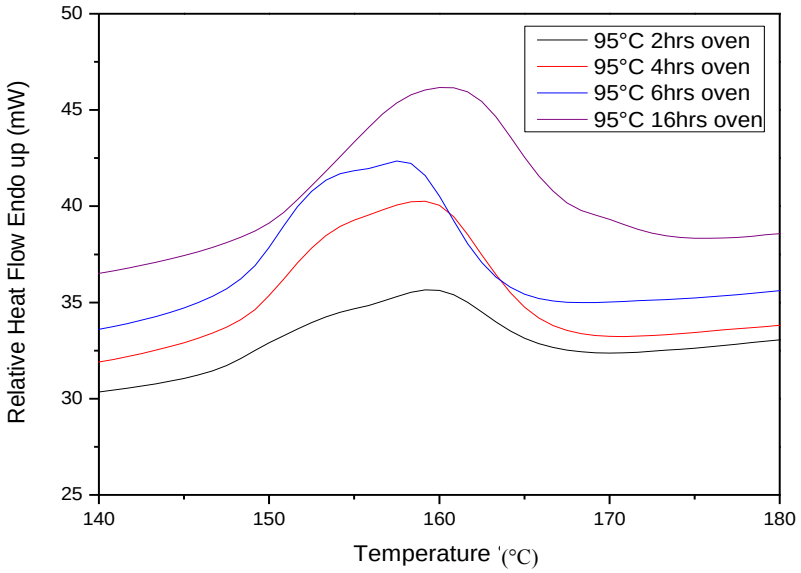

Figure 4.3a. Endotherms produced by crystallizing at 95 °C.

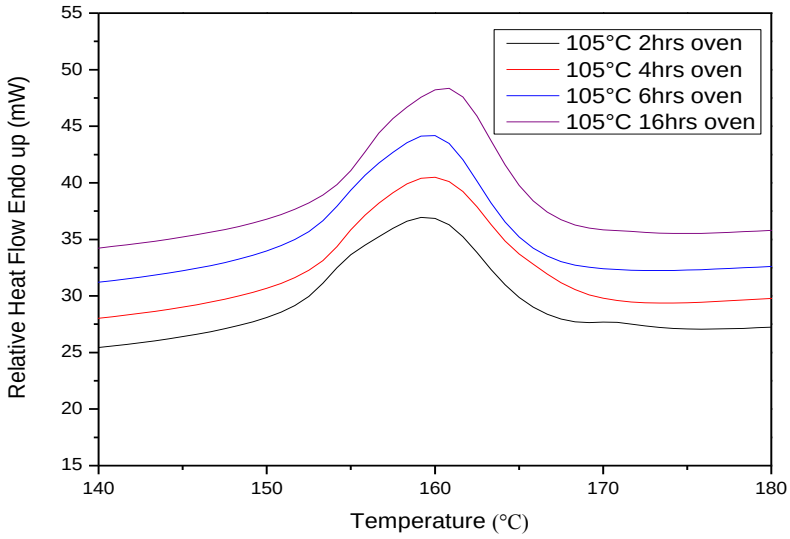

Figure 4.3b. Endotherms produced by crystallizing at 105 °C.

Again the greatest difference between samples produced by methods A and B was the absence of the bimodal melting endotherms and in particular the absence of the lower temperature endotherm. This is attributed to the higher heating rate adopted, as discussed

above. The crystallization, however, continued to develop with time, from 0.3 to 0.4 fractional crystallinity. These trends were continued at higher temperatures as can be seen in Figures 4.3c-e.

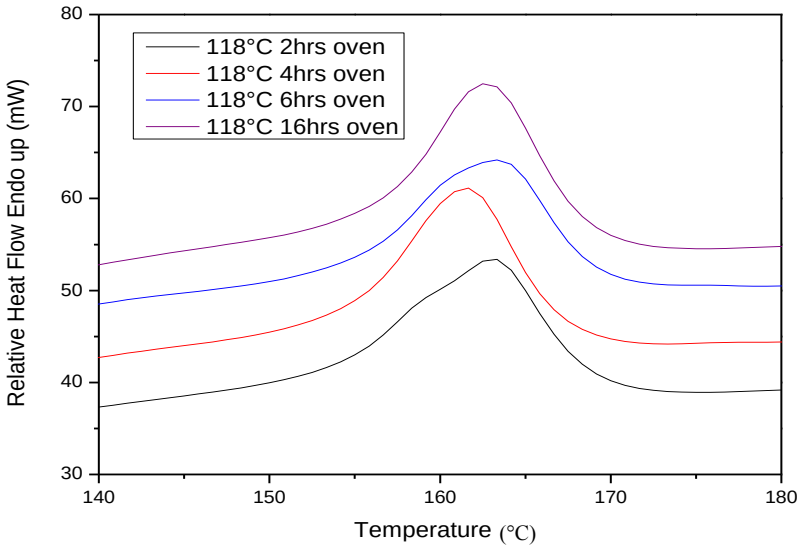

Figure 4.3c. Endotherms produced by crystallizing at 118 °C.

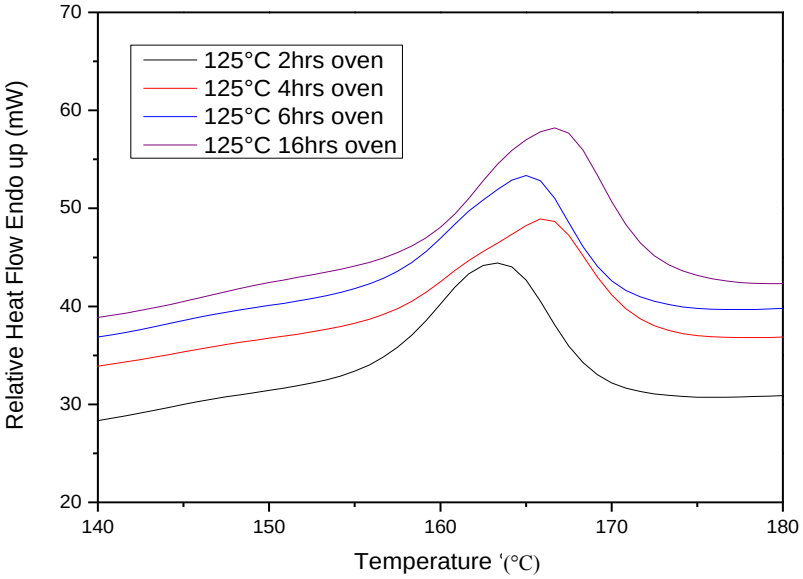

Figure 4.3d. Endotherms produced by crystallizing at 125 °C.

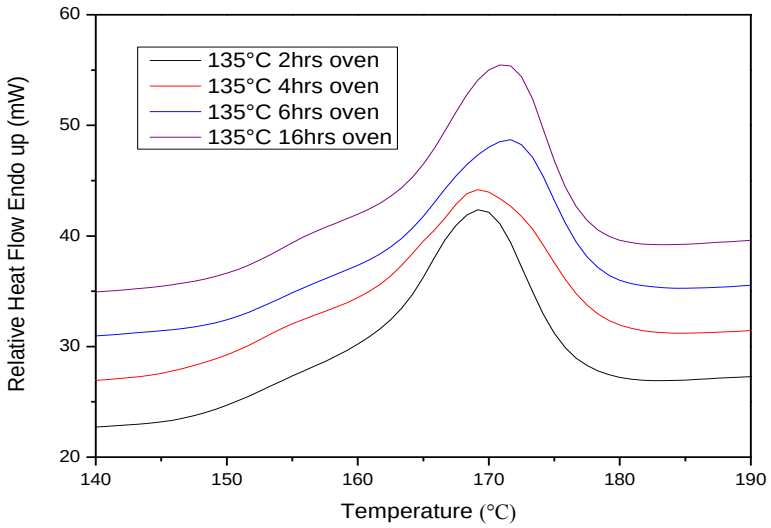

Figure 4.3e. Endotherms produced by crystallizing at 135 °C.

Figure 4.3. PLA sample crystallized various temperatures by procedure B.

From these observations it was apparent that by using a faster heating rate (50 °C min^{-1}) there is less time for the crystalline material to reorganise and develop thicker lamellae. It is accompanied by the disappearance of the double melting endotherms in the crystallization temperature range 95 to 105 °C and replaced by a single one centred at the lower m.pt. previously observed on heating at a slower rate. Accordingly Tm_2 is attributed to the melting of material crystallized at the crystallization temperature and Tm_1 to material structurally re-organised on heating. Similar findings have been observed by He et al [74]; they attributed the increased thermal stability of the lamellae to their crystallizing at higher temperature. The DSC traces all exhibited a single melting endotherm whose T_{m1} increased with increasing crystallization temperature due to an increase in the lamellae thickness.

The development of crystallinity with time at the various crystallization temperatures is shown in Figure 4.4. At all the temperatures, there is a rapid increase in crystallinity with

time; this is attributed to the presence of a primary crystallization process which appears to complete within 2-4 h and is followed by a much slower secondary process which has a different time dependence. The fractional crystallinity at the end of the primary process, $X_{p,\infty}$, did not exceed 0.40.

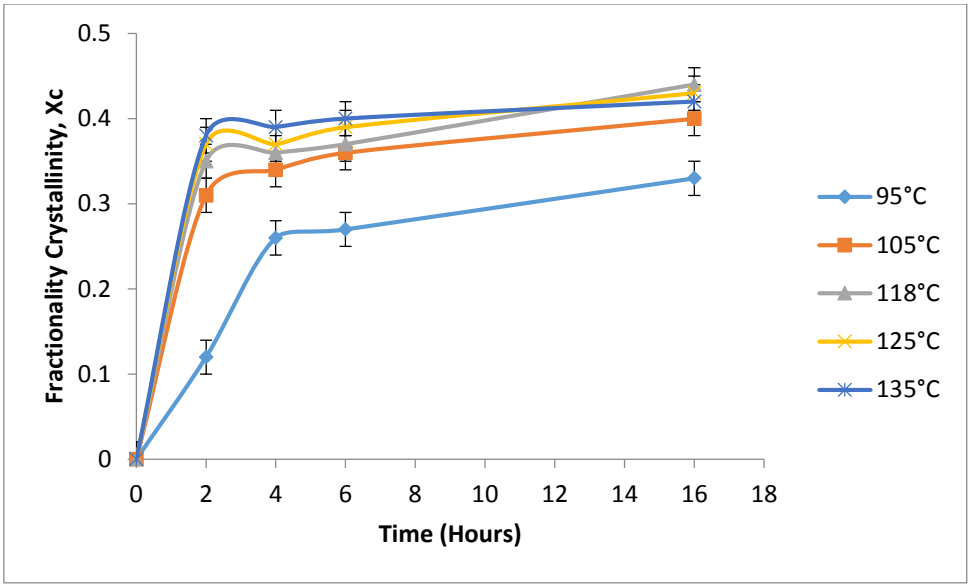

Figure 4.4. The development of crystallinity with time by procedure B. The effect of melting at 50 ^{o}C min^{-1}.

4.3. Crystallization of Co-PLA in the DSC by Procedure C

In this procedure the samples were heated to the melt and cooled directly to the crystallization temperature, held for 2, 4, 6 and 16 h before being heated to melt again to determine the endotherms shown in Figure 4.5a-e. All this was carried out in the DSC.

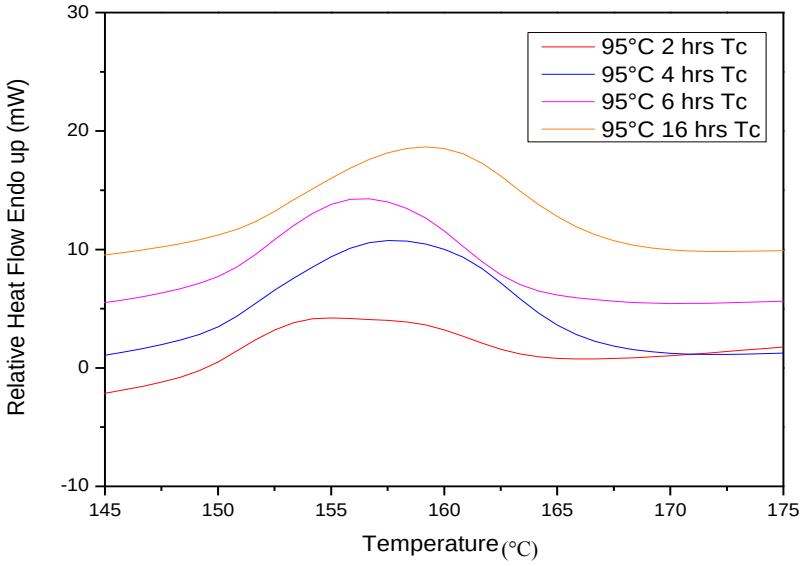

Figure 4.5a. Endotherms produced by crystallizing at 95 °C in DSC.

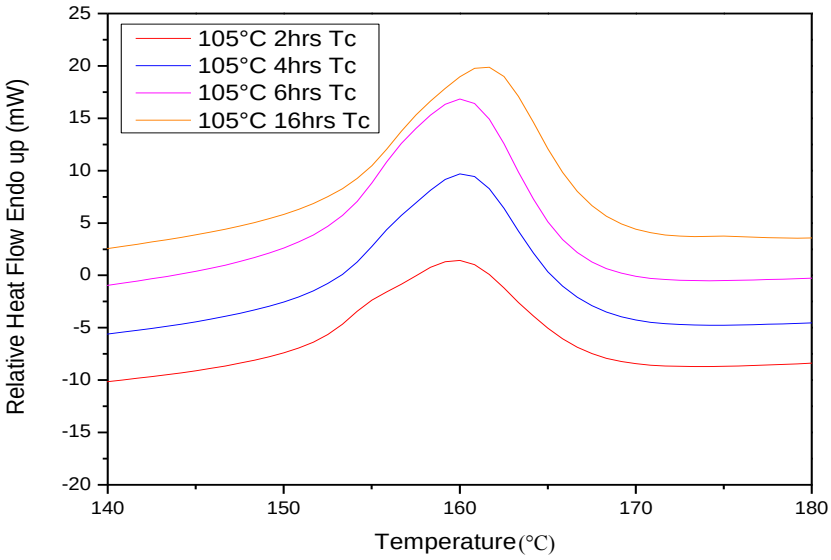

Figure 4.5b. Endotherms produced by crystallizing at 105 °C.

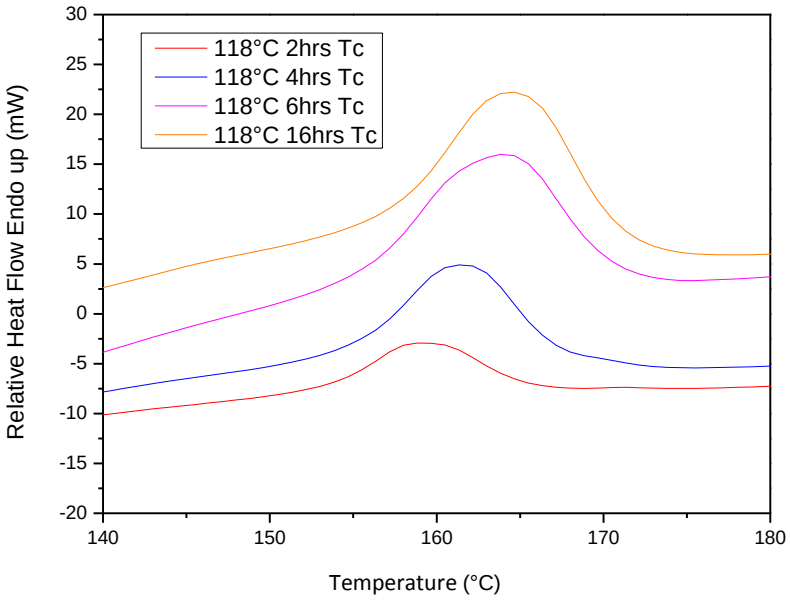

Figure 4.5c. Endotherms produced by Crystallizing at 118 °C.

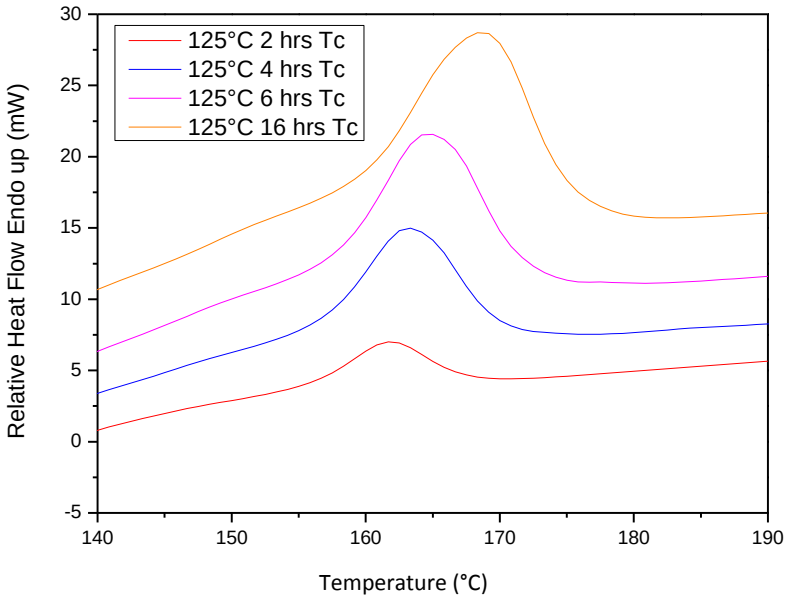

Figure 4.5d. Endotherms produced by crystallizing at 125 °C.

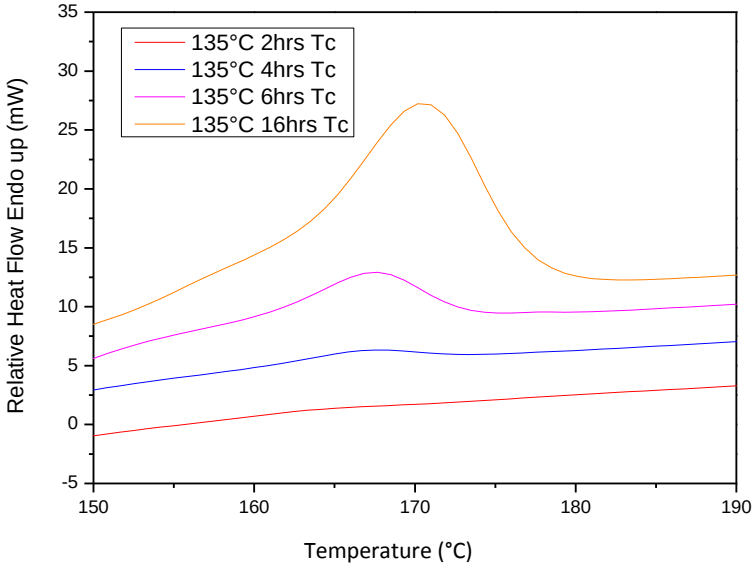

Figure 4.5e. Endotherms produced by crystallizing at 135 °C.

Figure 4.5. Crystallizing amorphous PLA samples in DSC at various temperatures.

The development of crystallinity with time at each crystallization temperature is shown in Figure 4.6. The behaviour is substantially the same as from that observed in Figure 4.3 in that the development of crystallinity with time shows an initial primary followed by a secondary process with different time dependence.

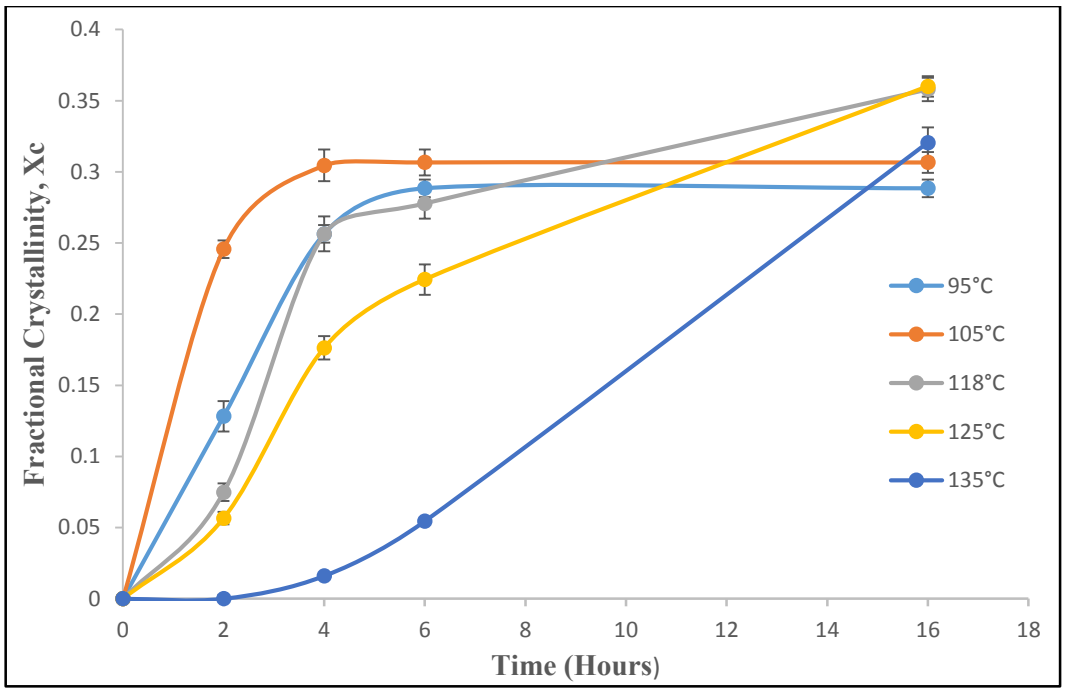

Figure 4.6. The development of crystallinity with time by procedure C.

4.4. Crystallization of Co-PLA by Procedure D

In order to determine the effect of cooling the sample to room temperature and re-heating to the melt, which is inevitable in the use of the oven to crystallize samples for a long period, samples were heated to 200 ºC in the DSC, for 2 min and cooled to the crystallization temperature. They were held there for up to 16 h and then cooled to 30 ºC before re-heating to melt and determining the endotherms shown in Figure 4.7a-e

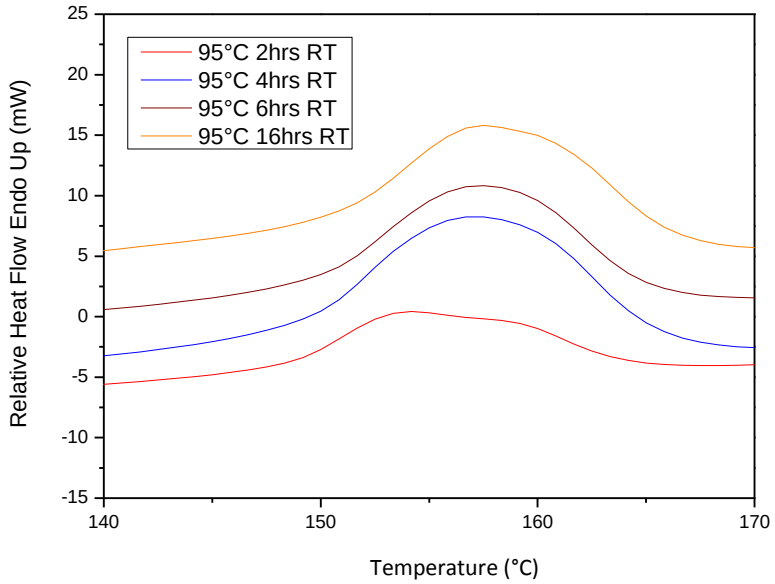

Figure 4.7a. Endotherms produced by crystallizing at 95 °C in DSC.

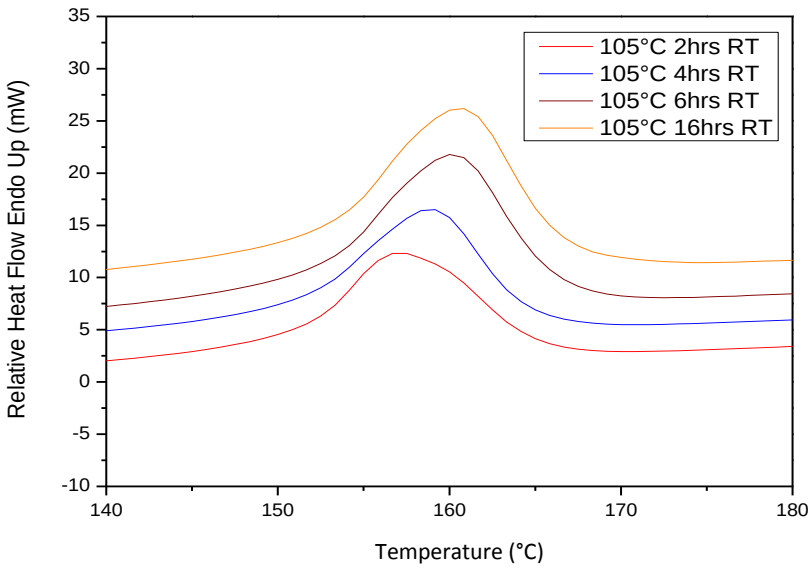

Figure 4.7b. Endotherms produced by crystallizing at 105 °C in DSC.

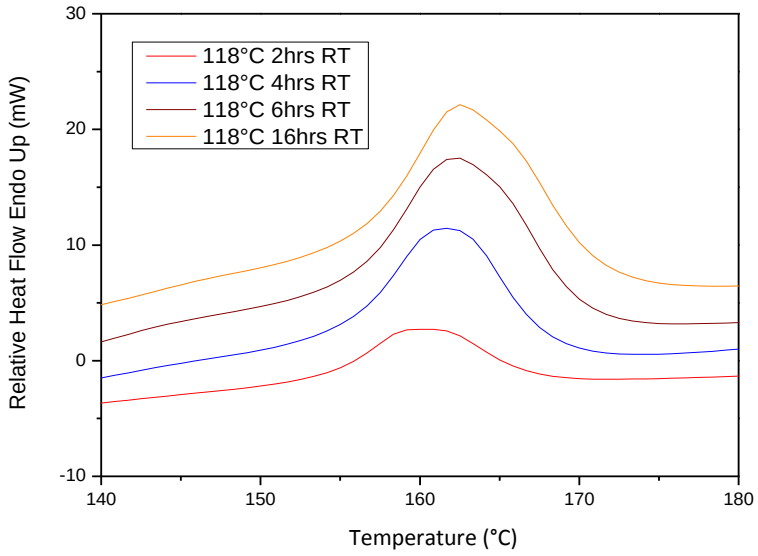

Figure 4.7c. Endotherms produced by crystallizing at 118 °C in DSC.

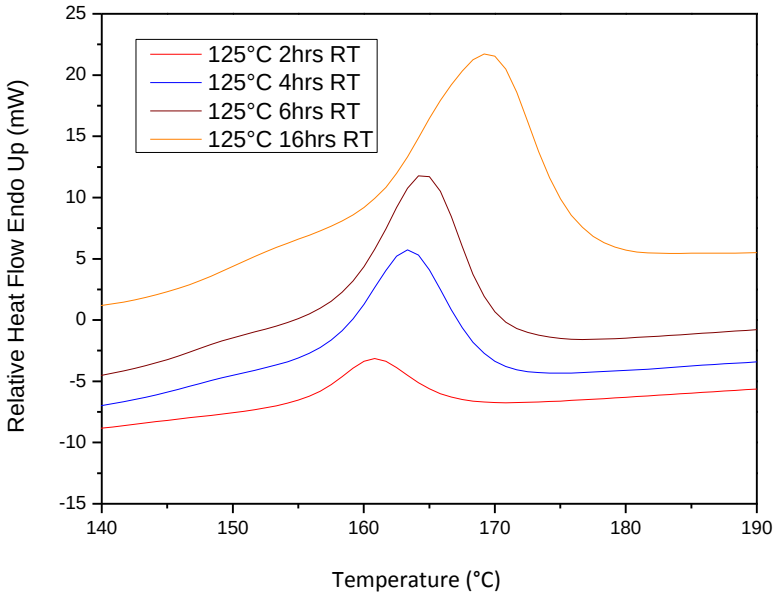

Figure 4.7d. Endotherms produced by crystallizing at 125 °C in DSC.

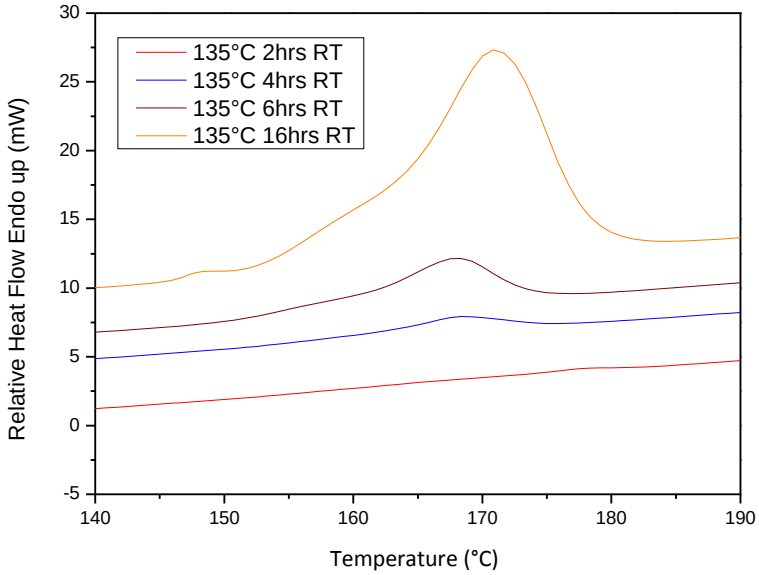

Figure 4.7e. Endotherms produced by crystallizing at135 °C in DSC.

Figure 4.7. Crystallizing amorphous Co-PLA samples in the DSC at various temperatures by procedure D.

The development of crystallinity with time at the various isothermal temperatures are shown in Figure 4.8; there is a considerable difference between this and Figure 4.6 in that the final crystallinities achieved are greatly reduced from 0.30-0.45 to 0.25-0.35 and the faster rates do not seem to exhibit any secondary crystallization component. Clearly cooling to and re-heating from room temperature substantially increases the crystallinity measured and procedures A, B and D cannot be used to determine the kinetics of crystallization at each isothermal temperature.

The times taken to crystallize Co-PLA to 0.30 crystallinity at various temperatures are shown in Figure 4.9 for all the procedures. It can be seen that procedures A, B, C and D are all different and variable results were obtained depending on conditions. It is, however, apparent that crystallizing within the DSC gave more consistent results and eliminated cooling to room temperature and reheating from there which is inevitable in using the oven gave

inconsistencies, greater final crystallinity and lower m.pts. Also using high heating rates and correcting for thermal lags was better than using slower rates with less thermal lags due to the additional crystallinity created on cooling and reheating from 30 ºC in that recrystallization and crystal perfecting was substantially reduced. These conditions must be adopted in measuring isothermal crystallization kinetics by DSC, since it does not have the sensitivity to measure the kinetics directly. However, the procedure is time consuming, determining the crystallinity one point at a time and limited by the number of determinations adopted. The final accuracy in determining the degree of crystallinity is low, frequently ± 0.05, and not sufficient for kinetic analysis of the crystallization.

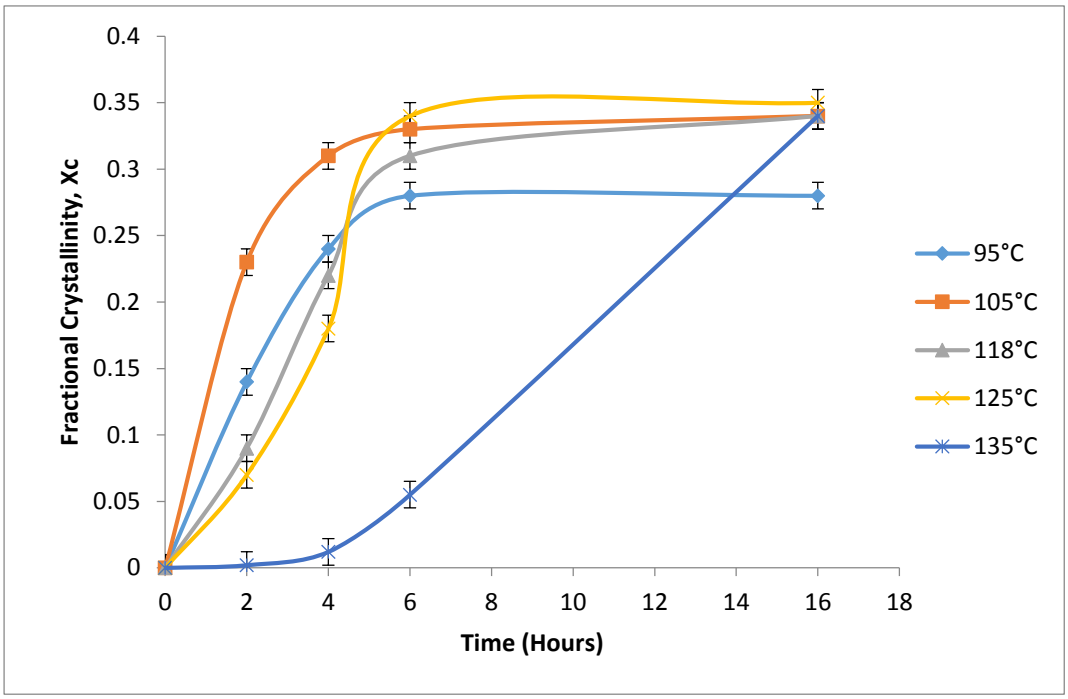

Figure 4.8. The development of crystallinity with time heating directly from the crystallization temperature following procedure D.

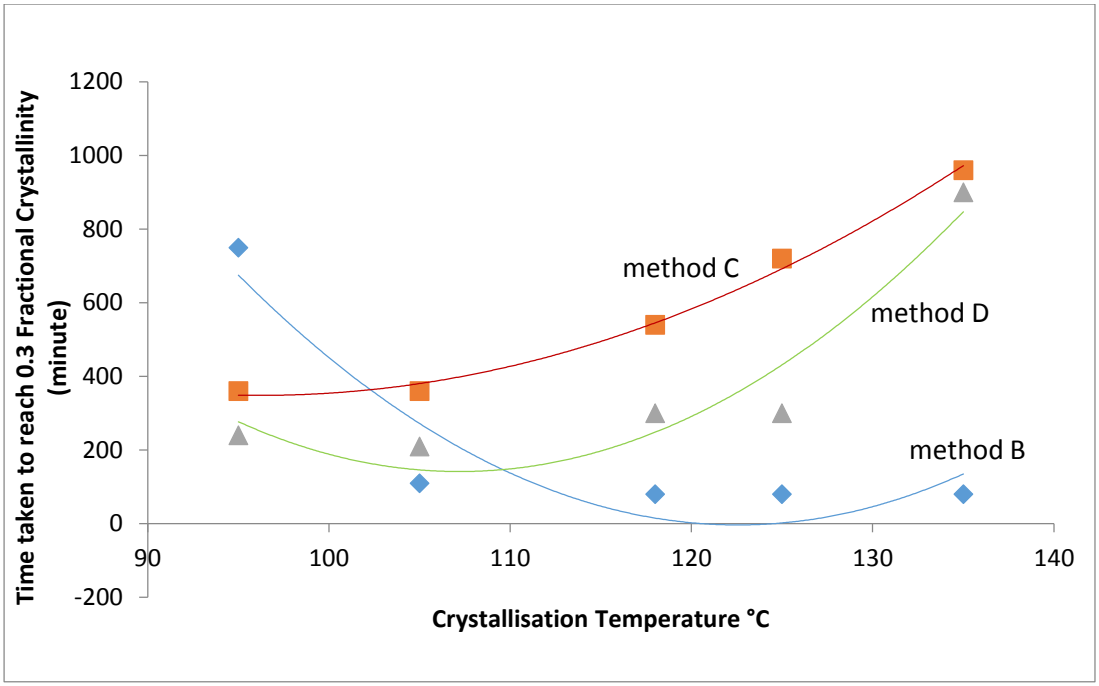

Figure 4.9. Time taken to reach 0.30 fractional crystallinity using Methods B, C and D.

4.5. The Melting and the equilibrium melting point, T_m^o of Co-PLA

The melting of polymers is different from that of low molar mass materials in that melting generally occurs over a wider temperature range and is dependent on thermal history [11]. The presence of multiple melting endotherms, as observed previously, is very common and has been observed with many semi-crystalline polymers, copolymers and blends. The phenomenon has been extensively studied but conflicting interpretations have been made. A variety of effects have been invoked to explain the phenomenon, i.e. to the presence of more than one crystallographic forms (polymorphism); to the presence of melting/re-crystallisation and re-melting; to changes in morphology, such as lamellar thickening and crystal perfecting; to changes in orientation; and to the effect of molecular weight distribution [110]. It is more than likely that one of these mechanisms alone cannot explain the observation of multiple endotherms.

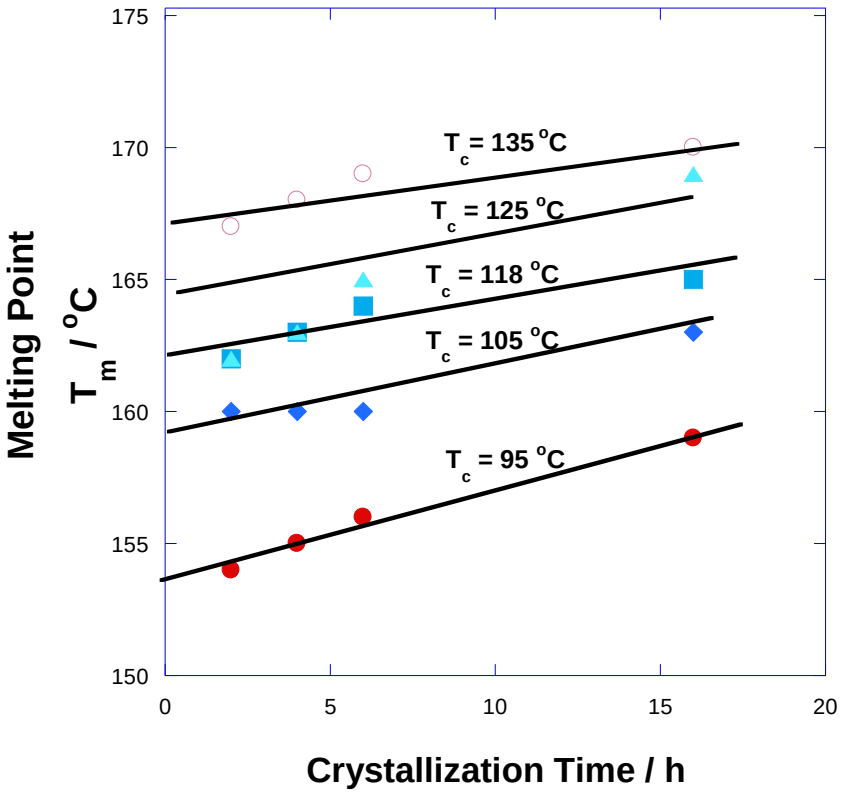

Figure 4.10. Dependence of melting point on crystallization time and temperature.

Co-PLA crystallises over a wide temperature range and samples crystallised for different times and at different temperatures, see Figure 4.10, some with the same degree of crystallinity, have different melting points. These clearly depend on experimental conditions. As we have seen two endotherms are present in a limited number of samples in which the lower one represented the melting of lamellae produced by crystallizing isothermally. Only m.pt. determined by crystallizing under well-defined conditions, namely by method C, were analysed in any detail. Measured values of T_m are shown in Figure 4.10 as a function of crystallization temperature and time. In every case the higher value of T_m was adopted as a measure of the melting point of the lamellae produced under these conditions. The value of T_m increased with increasing crystallization temperature and with time at each temperature. Similar findings have

been reported by Farrow [112] where the increase in the melting temperature was attributed to crystal perfecting and lamellae thickening as the crystallisation temperature increases.

If T_m reflects the original crystalline lamella thickness, the equilibrium melting temperature, T_m^o, can be determined using the Hoffman-Week's relationship [56] in which the observed melting point T_m is related to T_c by,

$$T_m = T_m^o (1- 1/\gamma) + T_c/2\gamma \qquad (4.3)$$

And $\gamma = (\sigma_e \xi /\sigma\xi_e)$

Where σ and σ_e are the surface free energy of the of the fold surface of the lamellae as crystallized and under equilibrium conditions, and ξ and ξ_e are the stem lengths (thickness) of the lamellae as crystallized and under equilibrium conditions.

A linear plot of T_m *vs.* T_c was observed but only for the higher crystallization temperatures, as shown in Figure 4.11 from which the value of lamella thickening coefficient, γ, was determined to be 1.0 indicating that the maximum lamella thickness was close to the critical size of the primary nucleus and the measurement of T_m was carried out under equilibrium conditions. No re-crystallisation or crystal perfection had occurred during heating.

The extrapolated value of T_m^o was 205 ^oC which was in good agreement with literature values [11, 61, 69, 113]. The lower m.pt. have a γ value of ½ indicating that their thickness was half the equilibrium value as the surface free energy terms are unlikely to change significantly.

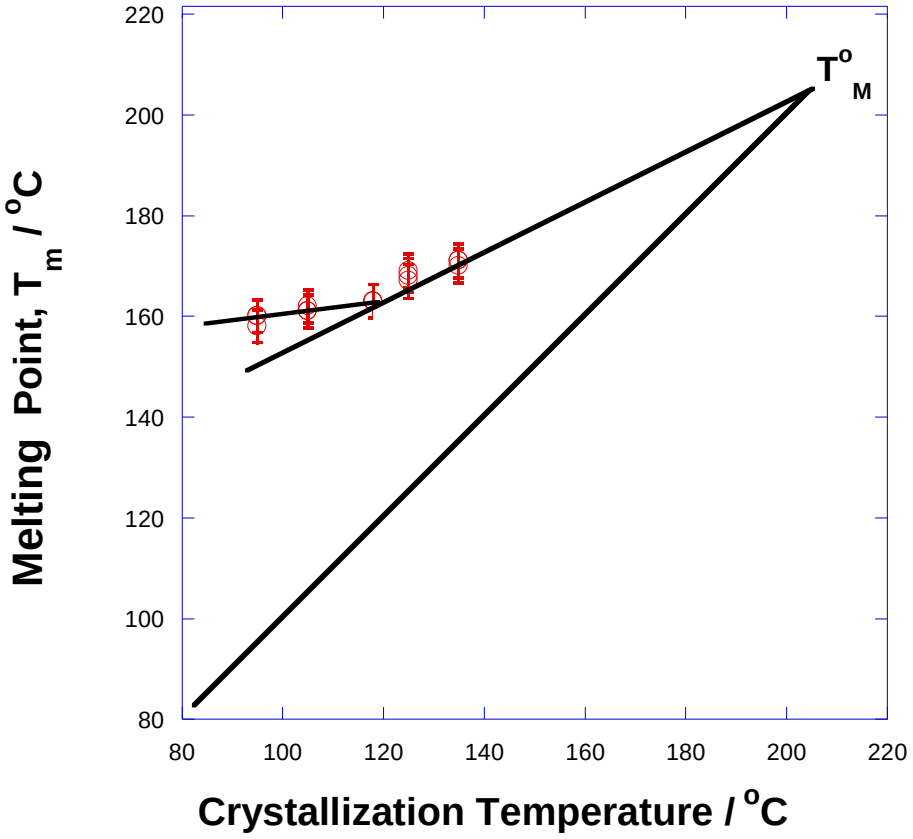

Figure 4.11. Hoffman-Weeks plot of m.pt against crystallization temperature.

According to a model proposed by Flory and Vrij [114-116] and extended by Hay to lamellar crystals [117, 118] the m.pt. of oligomers with degree of polymerization, n , is,

$$T_m = T_m^o \{1- 2RT_m \ln (n)/n\Delta h - \ldots . \} \qquad (4.4)$$

The higher terms involving heat capacity for the temperature dependence of Δh are minor corrections

And $$\ln (n)/n = 2RT_m . T_m^o / \Delta h (T_m^o - T_n) \qquad (4.5)$$

where T_m is the m.pt. of the oligomer, T_m^o the equilibrium m.pt. , R the gas constant and Δh the heat of fusion per monomer mole. This equation was used to determine the value of n, the

number of monomer units in the lamellae thickness as a function of crystallization time from the value of ln (n)/ n. A table of ln (n)/n against n enabled the number of monomer units to be determined at each crystallization temperature and lapsed time. The stem length increased with time throughout the crystallization and was attributed to secondary crystallization as discussed above. The stem lengths were plotted as a function of the square root of the crystallization time in accordance with equation 4.5 and a linear dependence observed, see Figure 4.12. The slopes of the lines are a measure of the increase in crystallinity due to an increase in stem length and are a measure of the secondary rate constant, k_s, in monomer moles per $h^{-1/2}$. These values are listed in Table 4.3, and although there is considerable scatter in the values there is an overall increase with temperature. This is consistent with a thermally activated process such as diffusion control and is inconsistent with a nucleation controlled process.

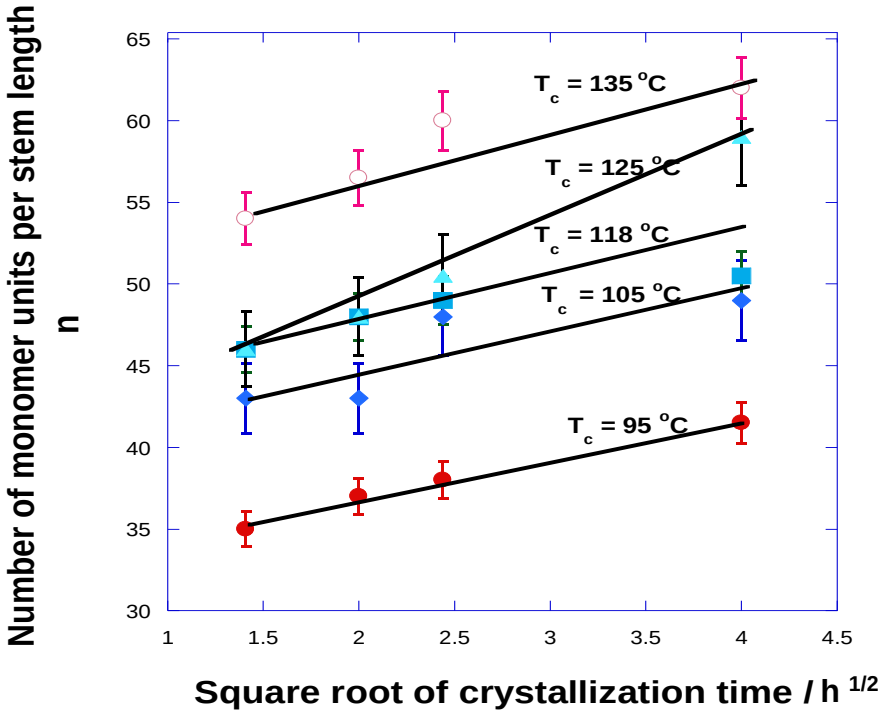

Figure 4.12 Dependence of the lamellae stem length on square root of the crystallization time.

Table 4.3. Secondary Crystallization Rates.

Crystallization Temperature/ ^{o}C	95	105	118	125	135
Rate Constant k_s $h^{-1/2}$	2.6	2.3	3.0	4.1	3.0

4.6 Conclusions

The PLA samples were observed to crystallize slowly and even at the fastest rate the half-life was 50 min and isothermal calorimetry was an inappropriate technique to study isothermal crystallization directly. Accordingly modifications were made to the conventional method used to study polymer crystallization by DSC. Crystallizing in a thermostated oven was also inappropriate since it involved cooling the sample and reheating from room temperature. This gave false results in increased the crystallinity and lowered the m.pt. of the samples. Accordingly, the samples were crystallized within a DSC for different periods at different temperatures and the crystallinities measured from the heat of fusion at the m.pt. However, a further refinement was required in that the sample was observed to melt and recrystallize on heating to the m.pt. and it was necessary to increase the heating rate from 10 to 50 ^{o}C min^{-1} to minimise the effect. The increased heating rate required a thermal lag correction to be made to the melting temperature.

The m.pt. of the lamellae increased with crystallization temperature in line with Hoffman and Weeks' nucleation theory of crystal growth and was consistent with an equilibrium melting point for PLA of 205±2.0 ^{o}C. The m.pt. at constant crystallization

temperature increased with time from the beginning of the crystallization; this was consistent with lamellae thickening occurring from the time they were produced and primary and secondary crystallization co-existing together during the primary stage of crystallization. The increase in stem length of the lamellae with the square root of crystallisation time was evidence for the mechanism of secondary crystallization and the increase in rate constant with temperature that it was a thermally activated process and not nucleation controlled.

5.0. Introduction

FTIR spectroscopy – thermal analysis has been widely used to characterise polymers since it enables the intensities of functional groups to be measured with temperature and time. It is particularly useful in characterising the phase transitions in crystallizable polymers [94, 119, 120], in following the crystallization kinetics with temperature [121-123], and measuring the kinetics of degradation and side group reactions in polymers from the change in intensity of functional groups [124-126]. It can measure the relative importance of competing reactions as well as the build-up of transient species involved in decomposition reactions. FTIR-TA has been used widely to characterise Co-PLA as a function of temperature and time and establish its crystallization and melting temperatures (11, 127-131].

In polymers the position and intensities of the absorption bands can be sensitive to the stereochemistry which in PLA is determined by the monomer used in its production. D or L-monomers give rise to isotactic polymers while the D, L-lactide produce alternating D, L sequences or syndiotactic polymers. A random mixture of D or L-monomer would give rise to atactic polymer with a disordered D, L sequence. These changes are attributed to the configuration of the polymer chain and are due its chemical structure and in particular to the asymmetric centre but do not change on heating, cooling, crystallization or melting unless the main chain bonds are broken. They will give rise to different bands in the infra-red spectrum of the polymer but require samples of different stereoregularity in order to assign the bands to a stereochemical structure.

Further complications exist, in the amorphous state, in that rotation occurs about the C-C bonds in the chain. In amorphous regions above the glass transition chain segments are mobile and rotate freely about each chain bond. In a single rotation there are 3 minimum energy positions,

corresponding to positions where adjacent groups on the C atoms are close together and the chain adopts a staggered conformation; there are two of these designated (±) gauche, i.e. ± g. There is a further position in which adjacent groups on the C atoms are furthest apart which corresponds to the lowest energy and is called trans i.e. t. Different gauche and trans sequences, such as gtg, tgt etc. persists in thermal equilibrium with one another and change with temperature which can be detected by changes to the IR spectrum. On crystallization the polymer chain in PLA adopts a 10_3 helix at the expense of the random conformation of the melt and there is a change in that the random conformations disappear as the helical ones develop. This is reversed on melting; heating and cooling a polymer can be useful in assigning crystalline and amorphous infra-red bands as well as conformation sequences.

5.1. The FTIR Spectrum of Co-poly (lactic acid)

The spectrum of partially crystalline Co-PLA is shown in Figure 5.1. It is characteristic of a linear aliphatic ester polymer consistent with its formula, i.e.

$$(- CH_2 – CH (-CH_3) – CO – O -)_n$$

with degree of polymerization n.

Group frequencies, as listed in Table 5.1, were assigned using reference standard tables [11].

The absorption bands at 2800-3000 cm^{-1} were attributed to aliphatic bond stretching of the C-H, $–CH_2–$, and $–CH_3$ groups, 1740-80 cm^{-1} to the ester carbonyl bond stretching and the bands below 1500 cm^{-1} to the chain conformation and configuration associated with $C-CH_3$, ester and C-C groups.

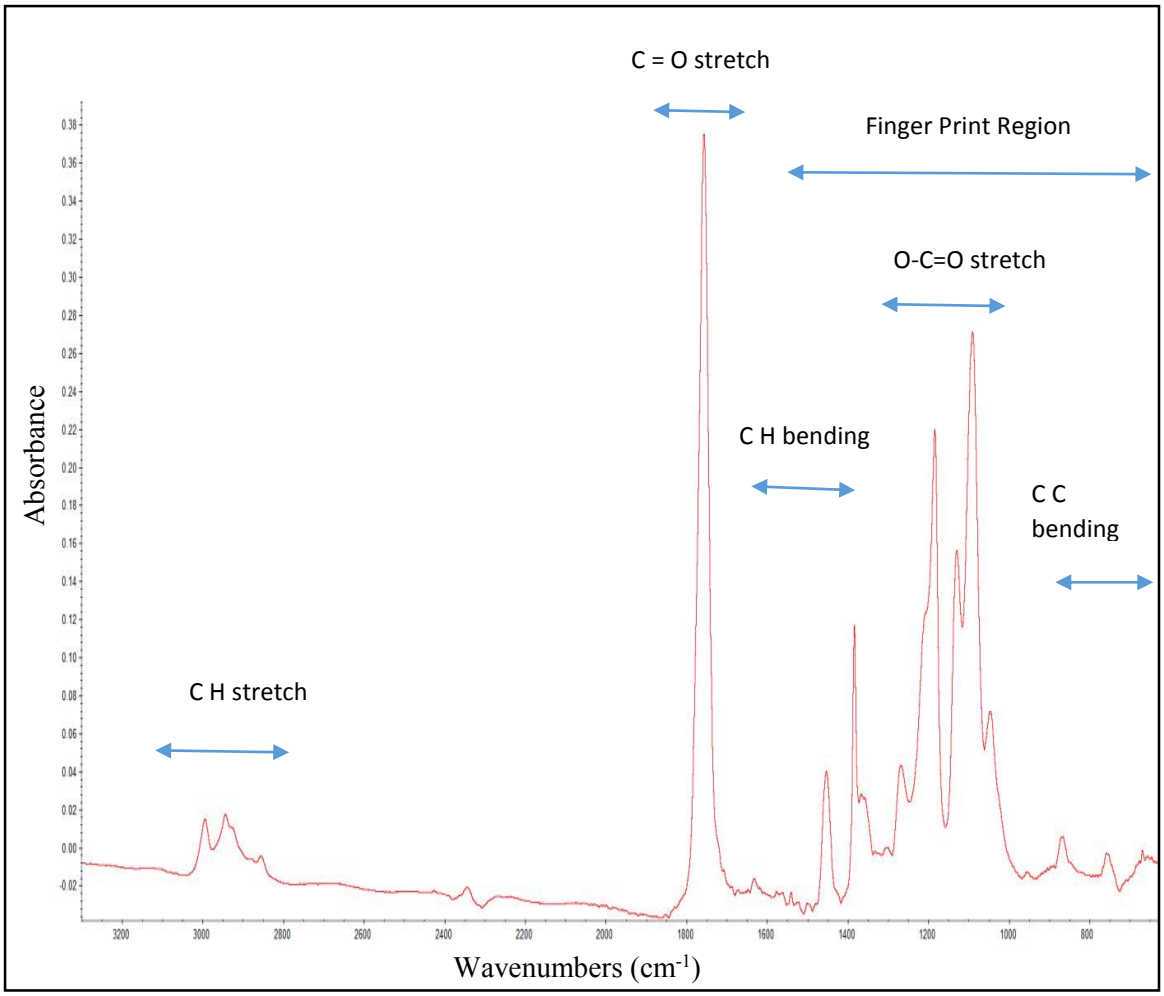

Figure 5.1. Thin film FTIR Spectrum of crystalline Co-PLA at room temperature.

Table 5.1. Molecular Group Assignment [132]

Wavenumber cm^{-1}	Absorbance	Group Assignment
2800-3050	weak	Aliphatic -C-H stretching, C-H, CH_2, CH_3
1740-1780	very strong	>C=O stretching
1300-1450	strong	-C-H bending
1000-1300	strong	C – O ester group stretching
1130 1044	weak weak	CH_3 C-CH_3 vibration
800-900	weak	-C-C- bending

Many of the bands alter on crystallization due to the difference in force fields between amorphous and crystalline regions, and the difference in chain configurations - gauche and trans isomers in equilibrium in the mobile amorphous regions, and 10_3 helical structure of the crystalline phase. In order to assign which bands were associated with each conformer samples were heated and cooled through the glass transition, through crystallization and to the melting temperature.

5.2. Changes in the IR spectrum on heating and cooling

Figures 5.2 a-b show that the temperature dependence of the IR spectrum of Co-PLA in the range 4000 to 800 cm^{-1} is reversible on heating and cooling and changes occur on heating and cooling associated with melting and crystallization. There are five regions of the spectrum,

as listed in Table 5.1, which are sensitive to structural changes taking place during crystallization and melting; these are the C-H stretching region 2800-3050 cm^{-1}, the >C=O stretching at 1740-1780 cm^{-1}, the CH_3 and CH bending at 1044 to 1130 cm^{-1}, C-O-C stretching band at 1000 to 1500 cm^{-1} and -C- C- bending from 800 to 900 cm^{-1}.

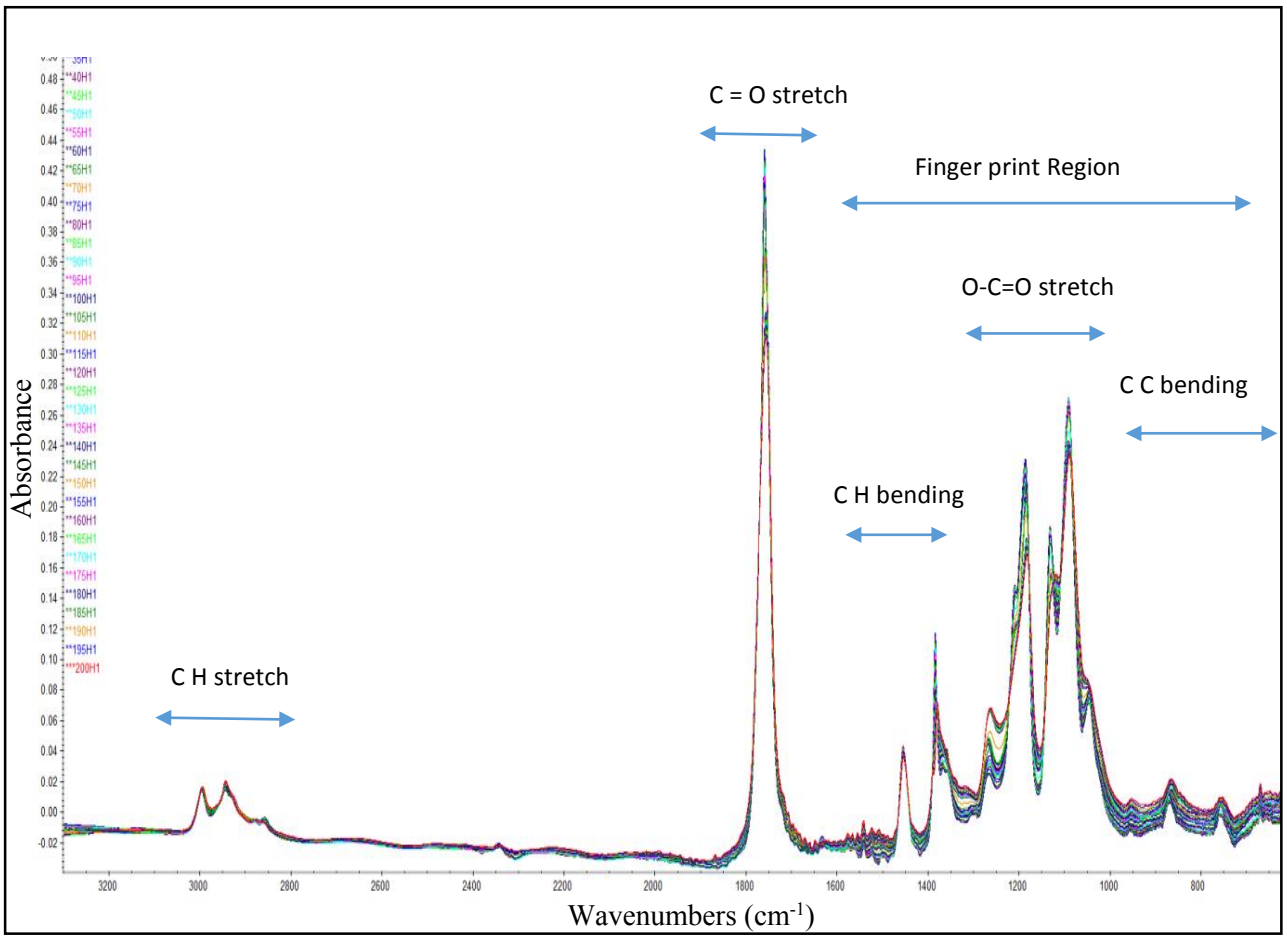

Figure 5.2a. Dynamic Run – IR Spectra on heating from 35 to 200°C at 5 °C min^{-1}

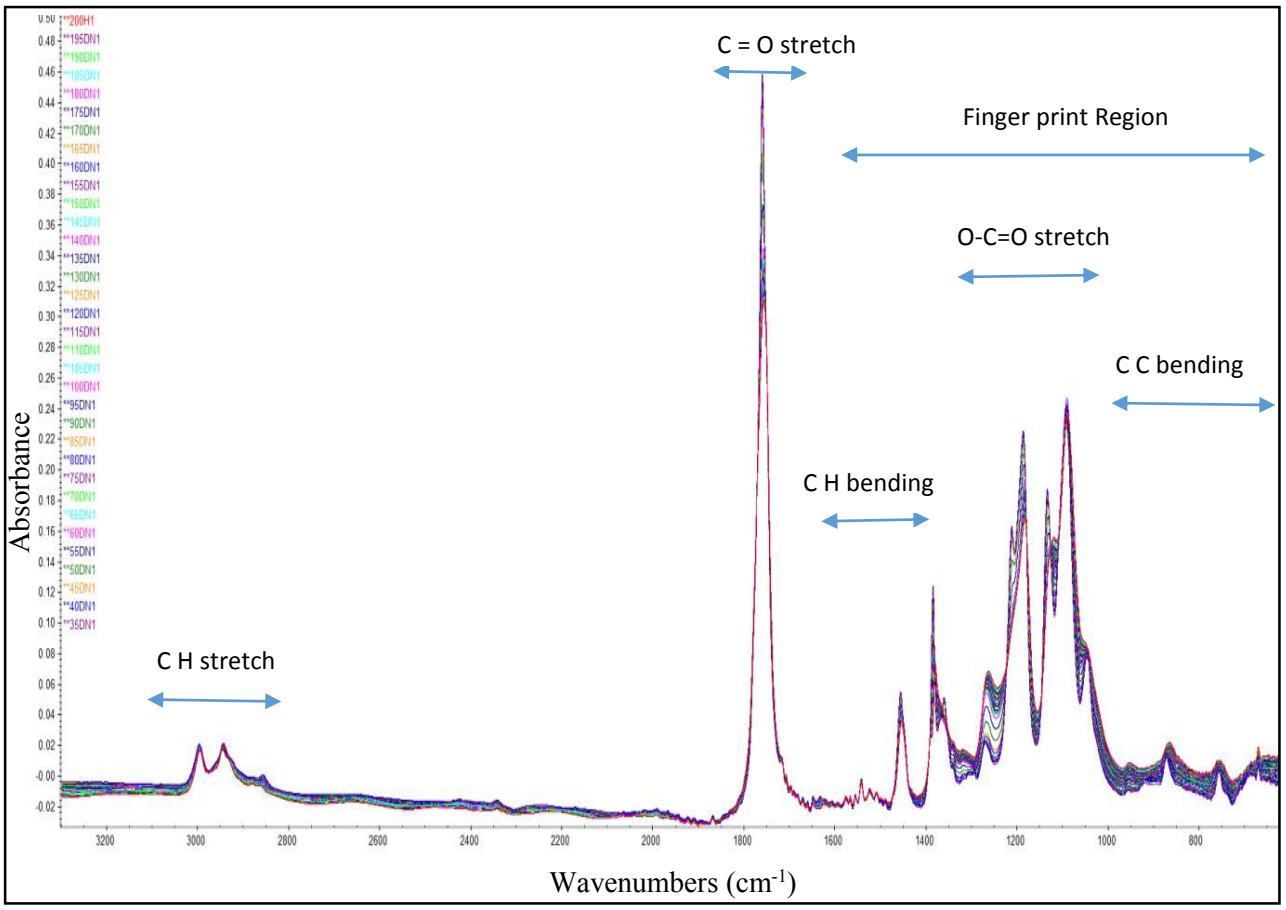

Figure 5.2b. Dynamic Run – IR Spectra on cooling from 200 to 35°C at 5 °C min^{-1}

Since the absorbances of the bands are, however, very variable, the carbonyl is intense and the C-H is weak, detailed analyses of the changes on crystallization and melting were carried out separately on individual band within these regions.

5.2.1. Changes in the region 2800-3050 cm^{-1} on heating and cooling

There are five bands of low intensities in this region assigned to CH_3- asymmetric stretching, CH_2< asymmetric and -> C-H antisymmetric stretching, see Figure 5.3a-b. Small changes in intensities and position of the bands occur on heating and cooling, crystallization and melting. Most changes were observed in the intensities of the bands at 2995 and

2944 cm^{-1} initially in that they were observed to move to a higher wavenumber on crystallization at about 100 ^{o}C, and back on melting at 160 ^{o}C. The reverse is observed on cooling below 100 ^{o}C. The trend was observed in the peak intensities which were sensitive to temperature and crystallinity, see Figures 5.4–5. On heating the absorbance of the 2944 cm^{-1} band increases with temperature but there is a step down at 70 ^{o}C, due to the glass transition. At 85 ^{o}C there is a sharp drop followed by an increase from 95 to 140 ^{o}C. Above 140 ^{o}C, there is a rapid rise from 140 to 155 ^{o}C until it reached a value close to what it would have reached if the initial rise had continued to increase linearly with temperature. On cooling the intensity decreased linearly with temperature until 100 ^{o}C when it decreased sharply. At lower temperatures it continues to decrease. These sharp step changes in intensity on heating are attributed to crystallization at 95 ^{o}C followed by melting from 140 to 155 ^{o}C and on cooling to onset of crystallization at 100 ^{o}C. Similar changes were observed with the 2995 cm^{-1} although the noise level tended to confuse the trends. There is a decrease in intensity on heating and on crystallization although the trend is masked by the accuracy in measuring the intensity, ±0.001, These changes in intensities of the peaks and the shift in wavenumbers are attributed to differences between crystalline, at 2995 and 2944 cm^{-1}, and amorphous bands, at 2992 and 2942 cm^{-1}.

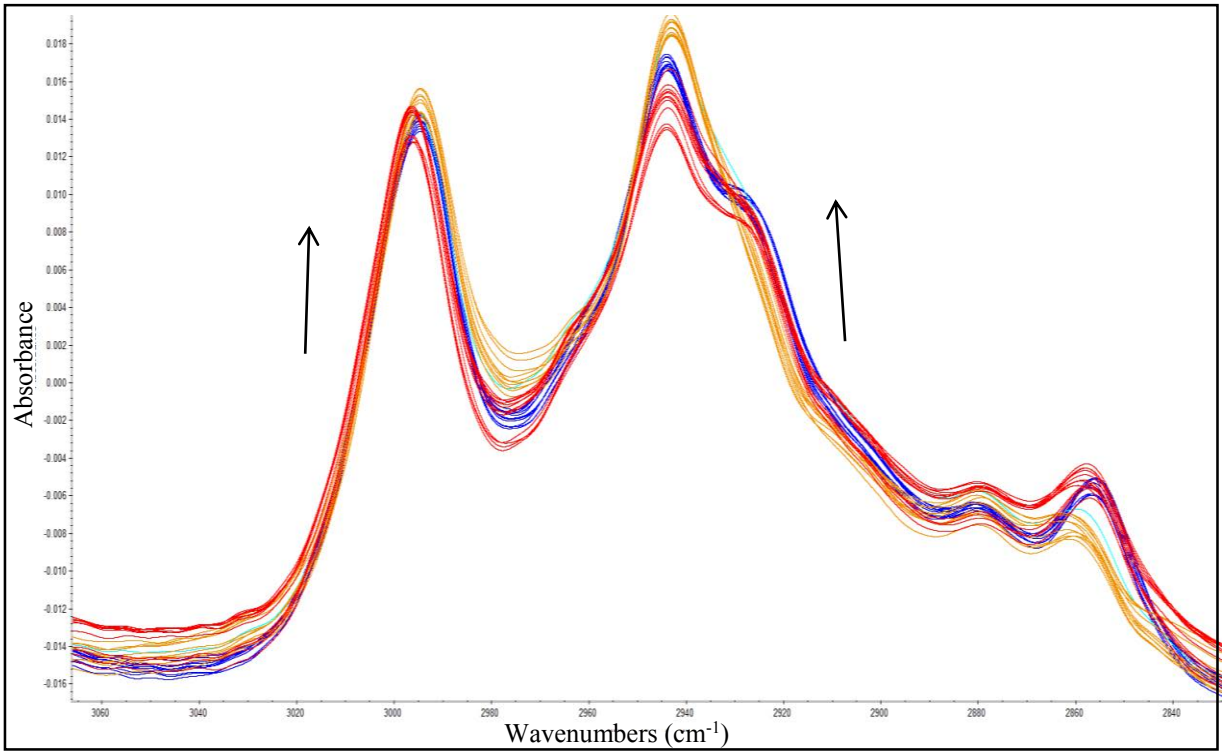

Figure 5.3a. Dynamic Run – IR Spectra on heating from 35 to 200°C at 5 °C min^{-1}.

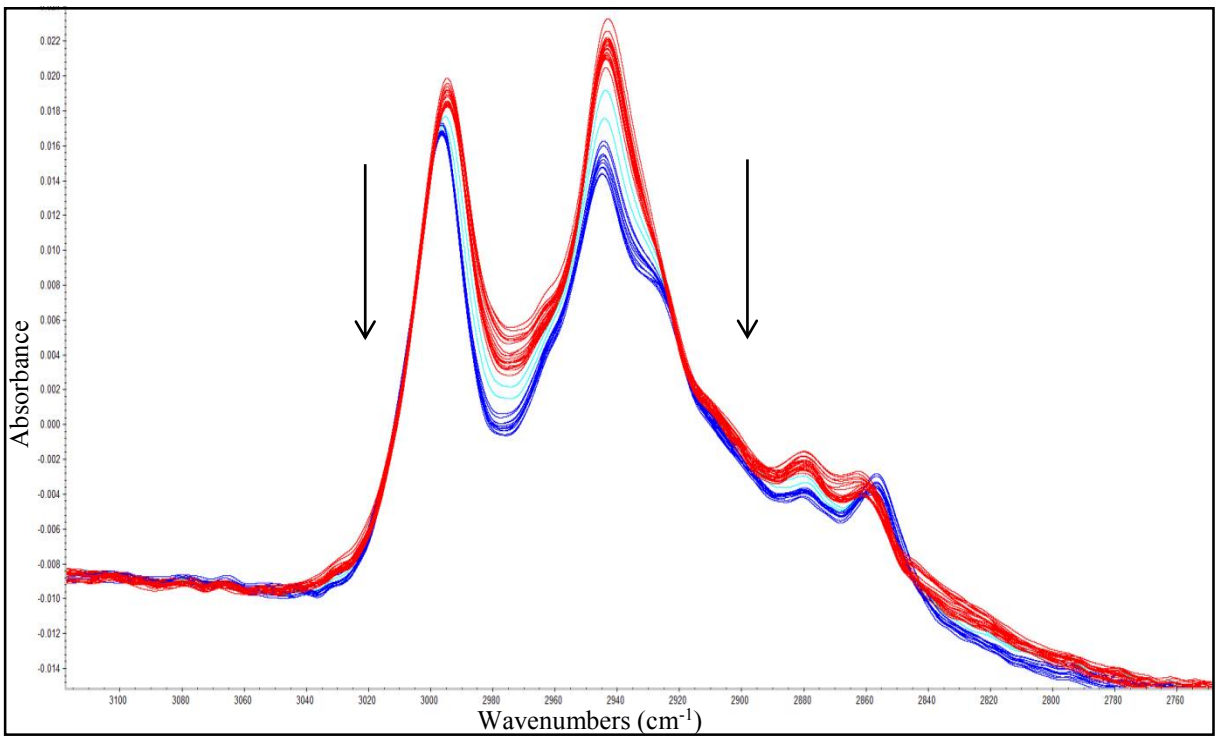

Figure 5.3b. Dynamic Run – IR Spectra on cooling from 200 to 35°C at 5 °C min^{-1}.

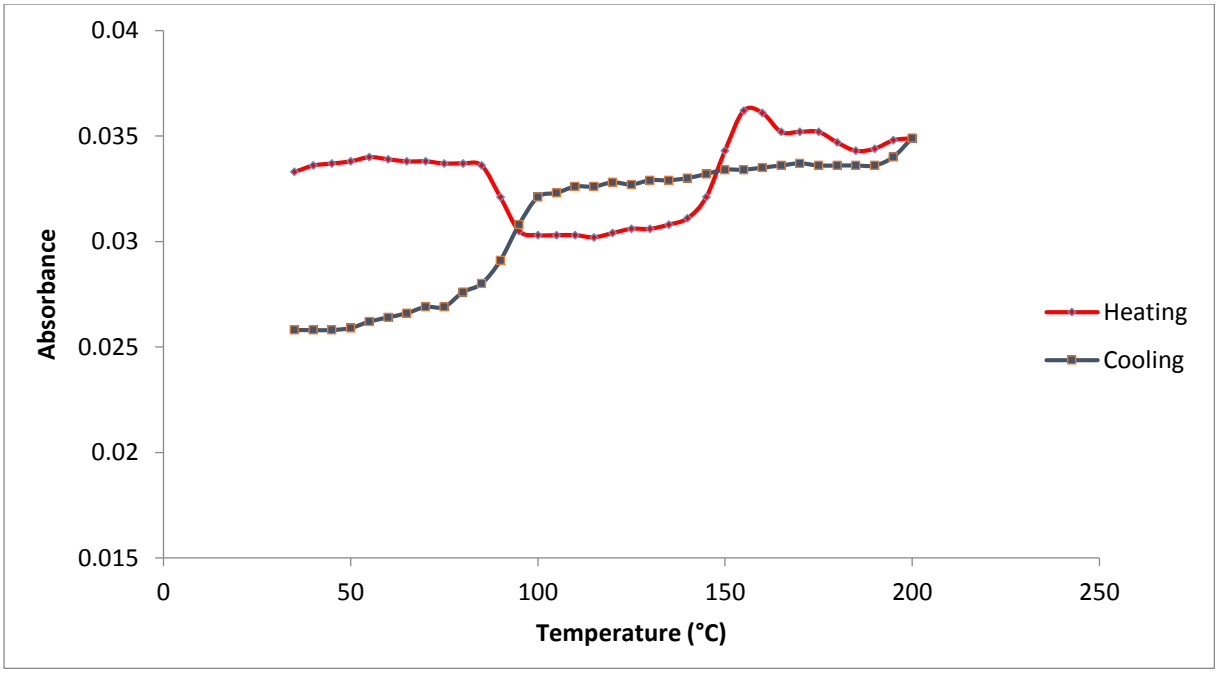

Figure 5.4. Change in intensity of the 2944 cm^{-1} band with temperature on heating and cooling.

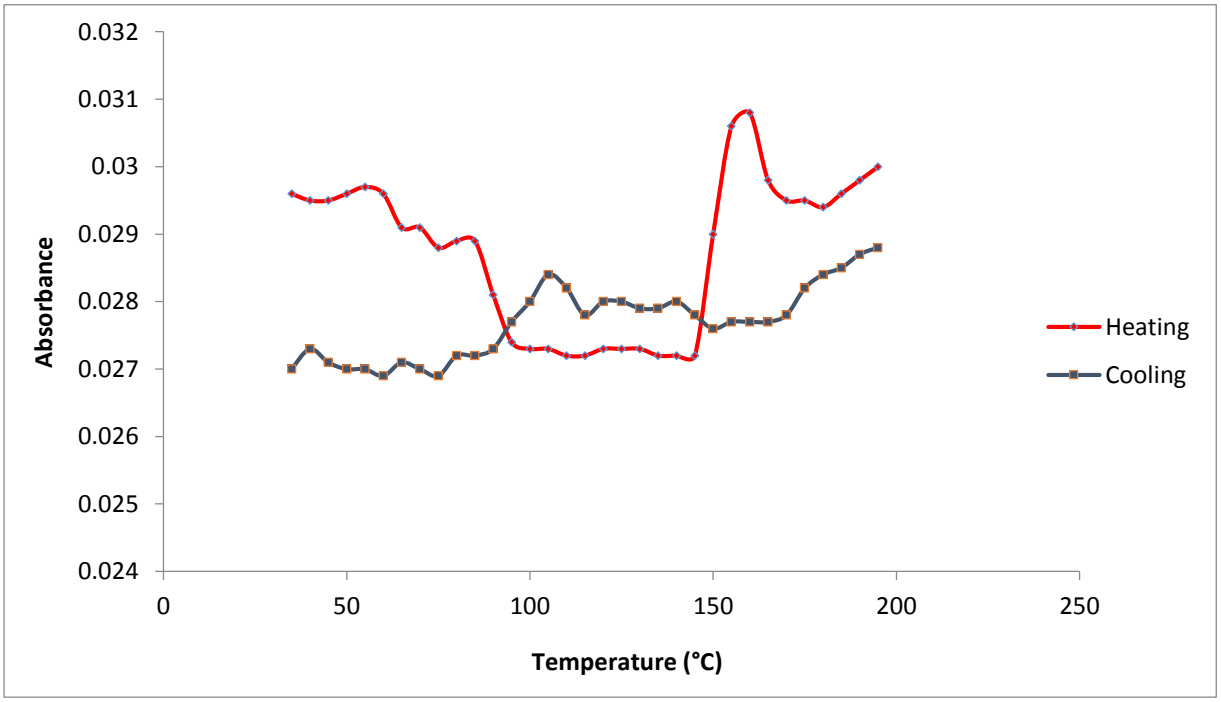

Figure 5.5. Change in intensity of the 2995 cm^{-1} band with temperature on heating and cooling.

5.2.2. Changes in the carbonyl region 1740 to1780 cm^{-1} on heating and cooling

The ester carbonyl stretching band was intense and broad. Its shape changed with temperature on melting and crystallization, see Figure 5.6. On heating crystallization was observed to start at 85 °C and develop up to 95 ^{o}C and the onset of melting occurred at 140 ^{o}C. Crystallization was followed by an increase in absorption at 1759 cm^{-1}, see Figure 5.6a, and the progressive narrowing of the band and the development of a sharper peak at 1759 cm^{-1}. On melting this sharp peak decreased in intensity with a broadening of the overall band and an increase in intensity at 1780 and 1740 cm^{-1}. These changes were reversible on cooling with the onset of crystallization at 95 ^{o}C, see Figure 5.6b.

The change in intensity at 1759 cm^{-1} followed the phase changes with a step increase in intensity on crystallization at 85 to 95 ^{o}C and a step decrease from 140 to 155 ^{o}C on melting. At intermediate temperatures the intensities increased with temperature and on amorphous intensities could be extrapolated to the linear increase above the final trace of melting. On cooling the intensities decreased with temperature following the same trend of the amorphous material on heating until the onset of crystallization at 100 ^{o}C when it increased to values observed for the crystalline material after linear extrapolation to correct for the temperature difference, see Figure 5.7.

The intensity of the band decreased with increasing temperature, increased following the onset of crystallization and decreased following the extent of melting. It would appear that the crystalline band which developed at 1759 cm^{-1} was sensitive to the extent of crystallization and amorphous content but decreased with increasing temperature.

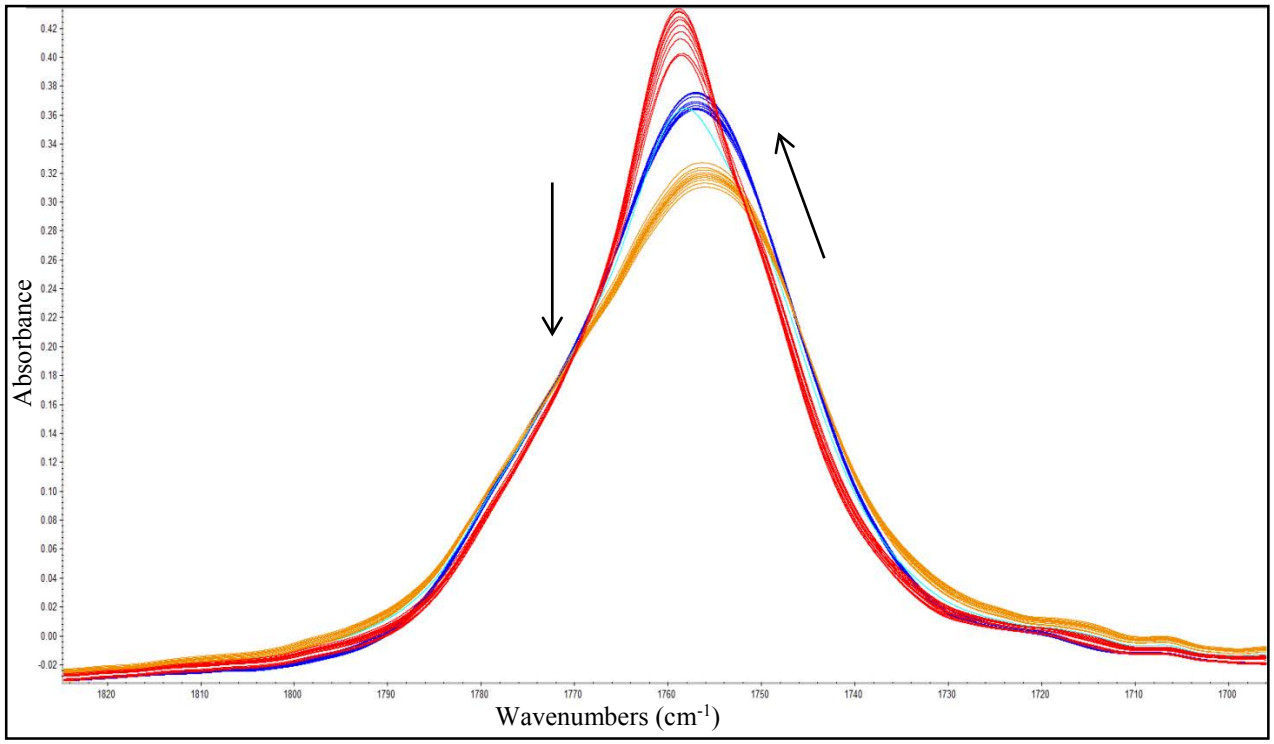

Figure 5.6a. Change in the carbonyl absorption, 1740-1790 cm^{-1}, with temperature on heating

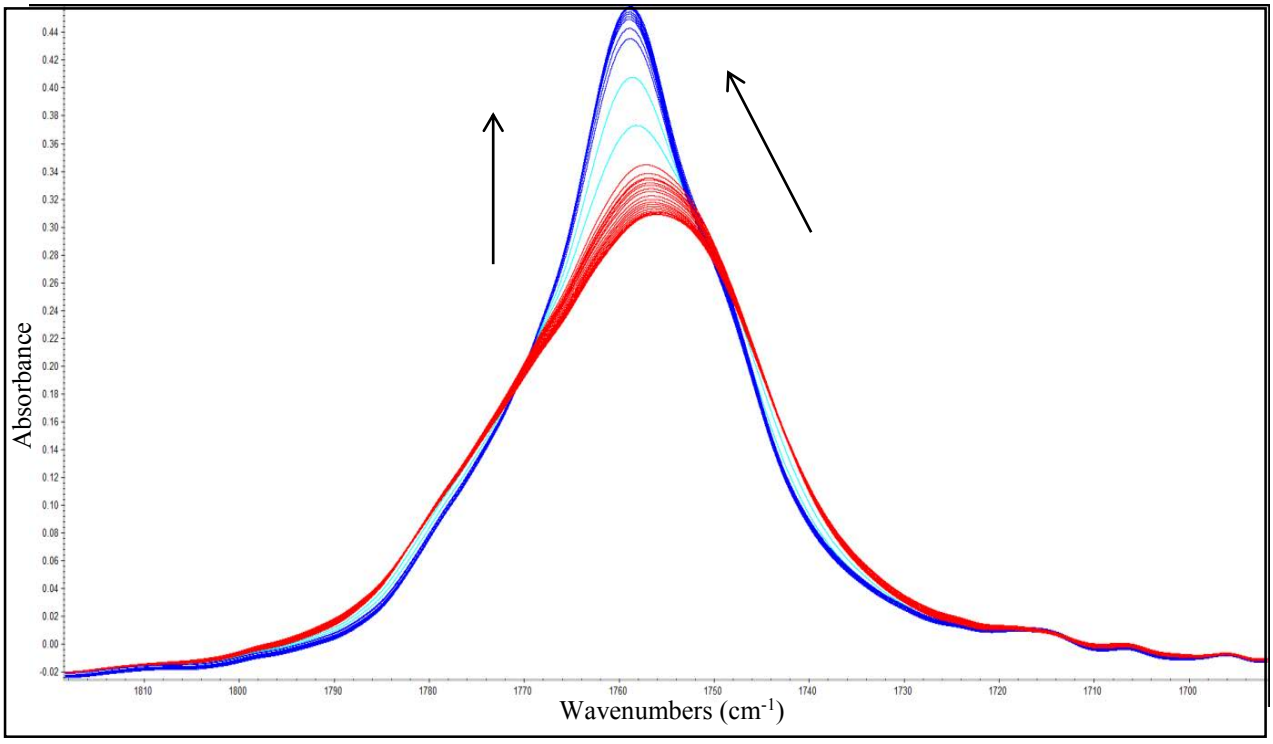

Figure 5.6b. Change in the carbonyl absorption, 1740-1790 cm^{-1}, with temperature on cooling.

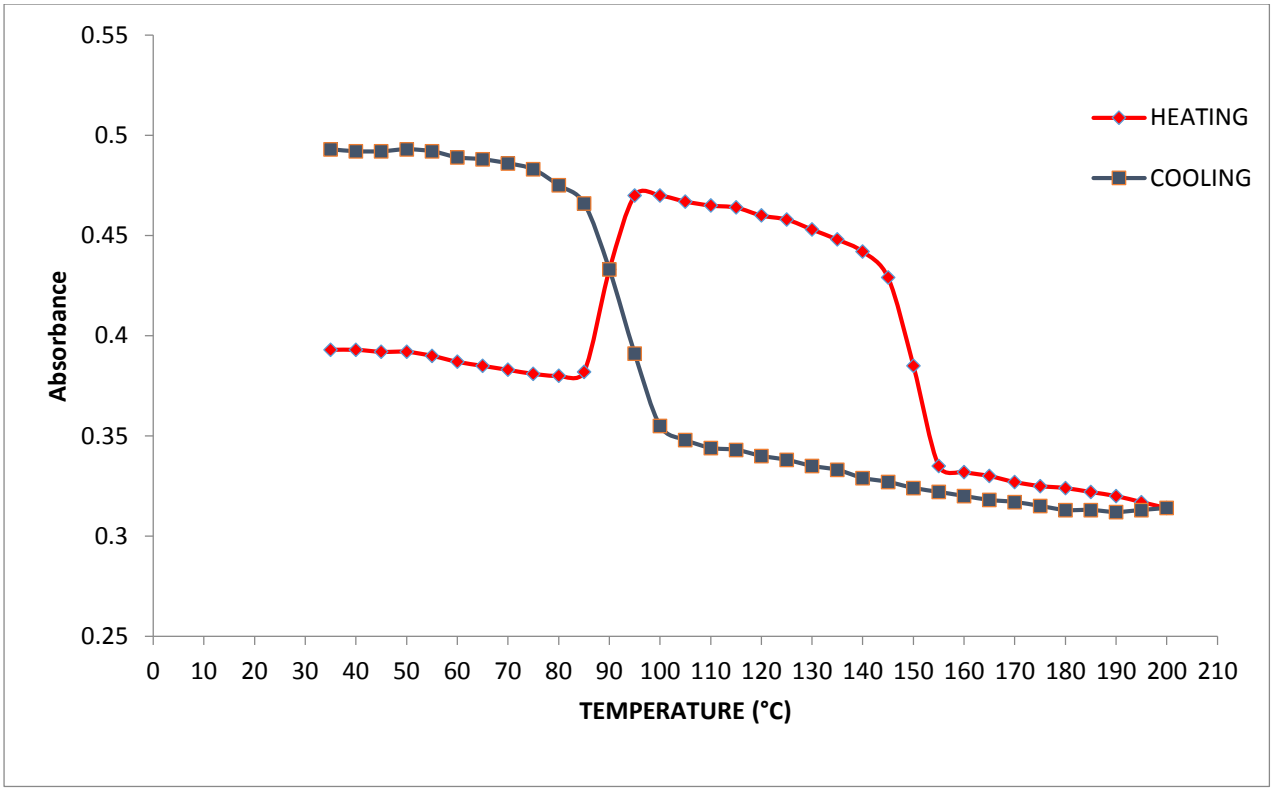

Figure 5.7. Change in intensity at 1759 cm^{-1} band with temperature on heating and cooling.

The carbonyl stretching band, centred at 1755 cm^{-1} was considered to be very broad. It changed significantly in shape on crystallization, see Figure 5.8, narrowing by increasing in intensity at 1759 cm^{-1} and loosing intensity between1740-1750 and 1765-1780 cm^{-1}. These changes are reversed on melting and this was attributed to the presence of several overlapping peaks due to conformer isomers as well as crystalline and amorphous bands. Accordingly the bands obtained from amorphous and partially crystalline samples were analysed in order to assign components present. The resolved bands are shown in Figures 5.9 for amorphous sample and 5.10 for a sample crystallized at 120 ºC.

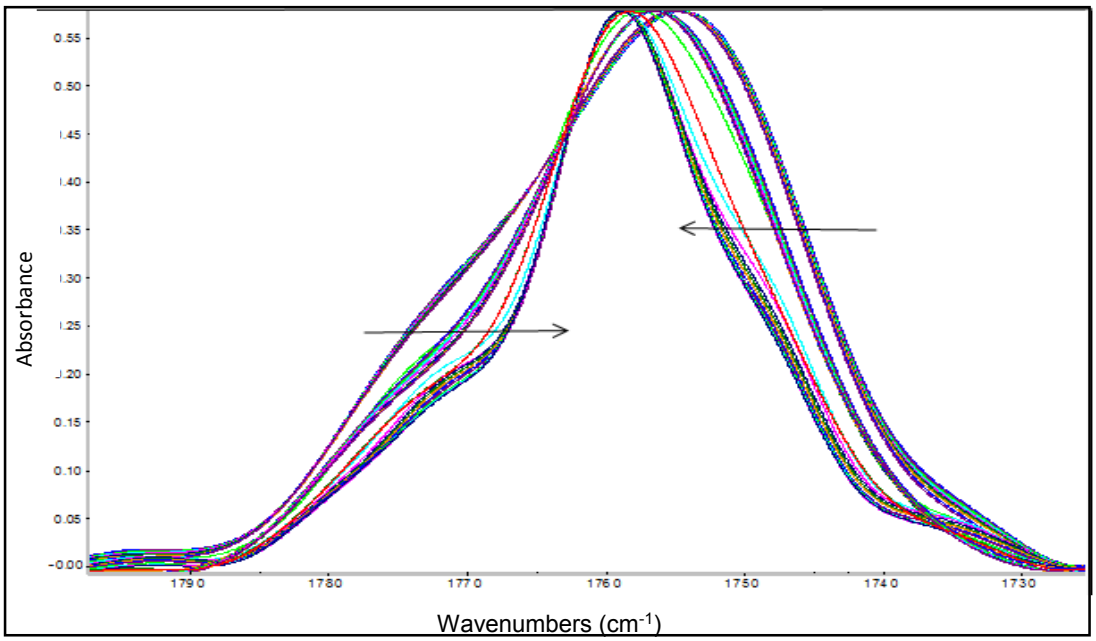

Figure 5.8. Change on shape of carbonyl band on Crystallization at 120 ºC.

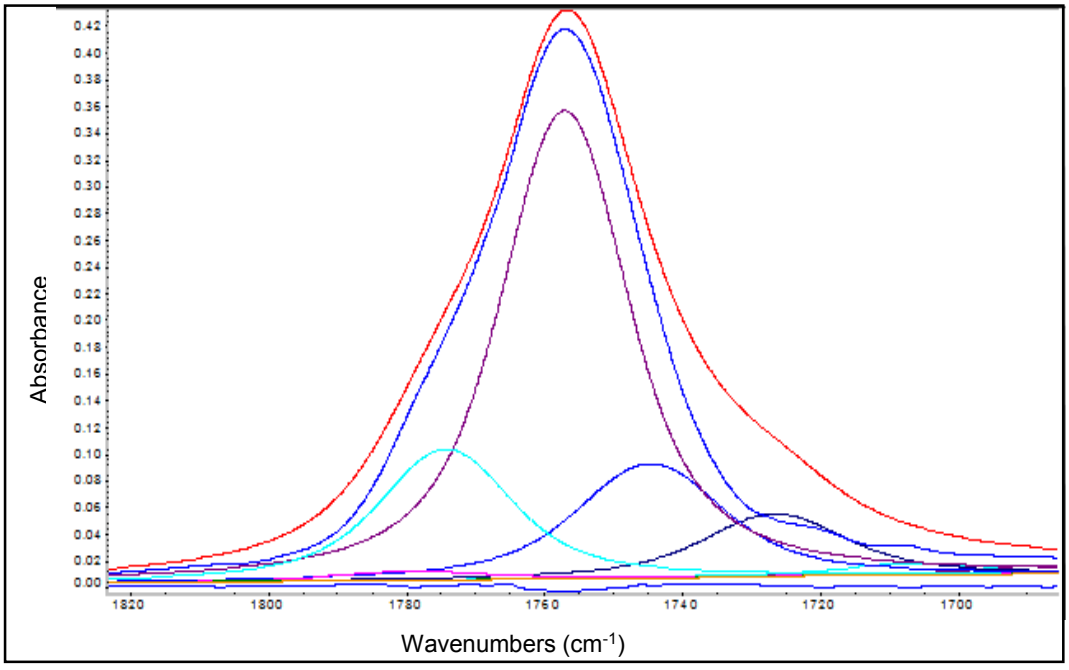

Figure 5.9. The components of the amorphous carbonyl band.

{The outside (red line) is the original, the inner (blue) is the sum of the intensities of the components and shows how closely the analysis fits the original. The other 4 are due to the 4 conformers. The biggest being the crystalline band at 1759 cm-1}

The amorphous band exhibited four components at 1759, 1749, 1745 and 1725 cm^{-1}, the two highest of which have been attributed by Meaurio et al [129] to gt, and tt conformers. The two lower bands were not observed although they decreased in intensity on crystallization. In contrast, the crystalline absorption band exhibited three componnts at 1767, 1759, and 1749 cm^{-1} while there is an overall increased in intensity at 1759 cm^{-1}. The 1767 cm^{-1} has been attributed to gg conformer [129]. The increase in the component at 1759 and the decrease at 1749 cm^{-1} indicates that these components are a measure of the crystalline and amorphous content during crystallization.

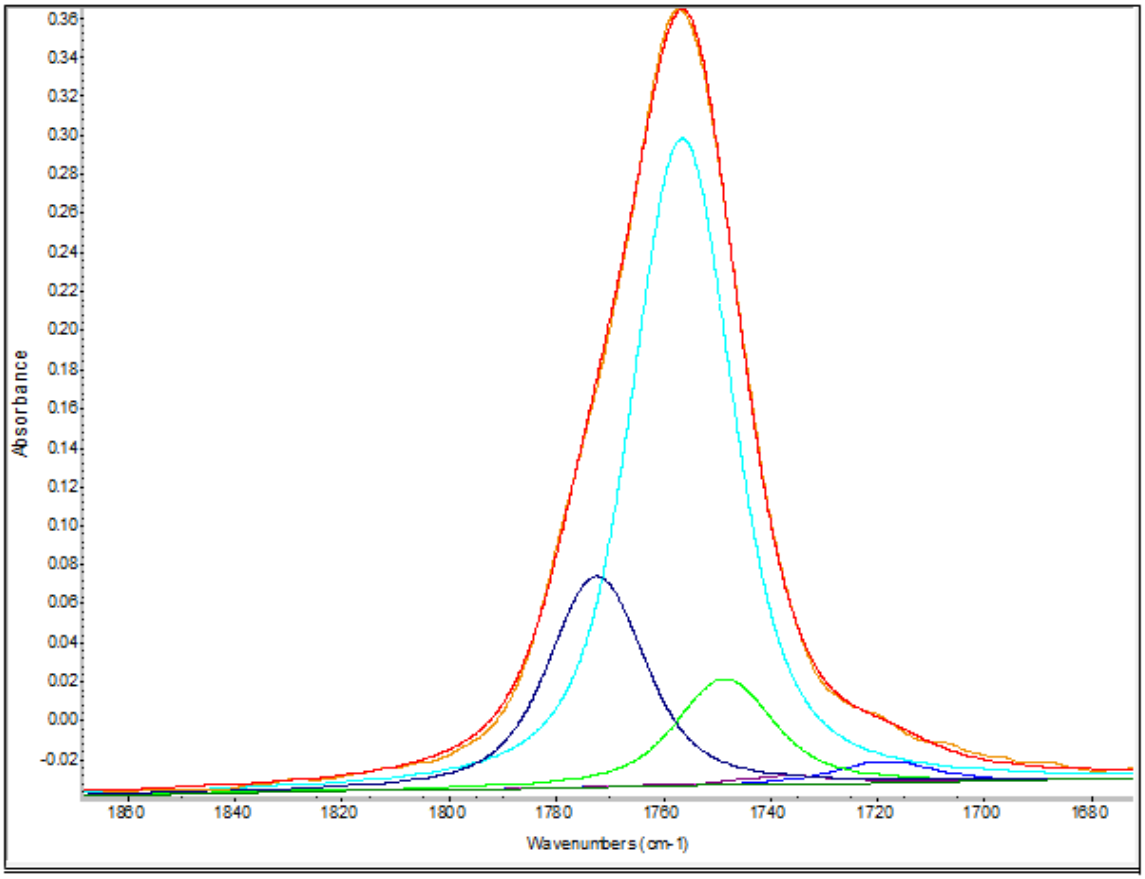

Figure 5.10. The components of the crystalline carbonyl band.

5.2.3. Changes in C-H stretching band at 1300-1500 cm^{-1} on heating and cooling

The CH_3 bending and at 1384 cm^{-1} did not alter position or change in intensity with crystallization or melting but it was sensitive to temperature, on heating or cooling. It appears to be an excellent internal standard against which all other bands can be ratioed to correct for any change in sample dimensions. By comparison the asymmetric C-H band at 1382 and shoulder at 1390 cm^{-1} shifted to a single band at 1384 cm^{-1} on crystallization and this reversed on melting but the intensity decreased linearly with temperature and was insensitive to changes in crystallinity, see Figure 5.11a-b and 5.12.

The intensity of the band at 1360 cm^{-1} is fairly typical in that it is sensitive to crystallinity, see Figure 5.13. It exhibits a step down at the glass transition temperature, 70 ^{o}C, and a rapid increase as the sample crystallizes between 80 and 105 ^{o}C. The intensity decreases as the temperature increases until it drops on melting. On cooling it continues at a low value until it crystallizes below 105 ^{o}C.

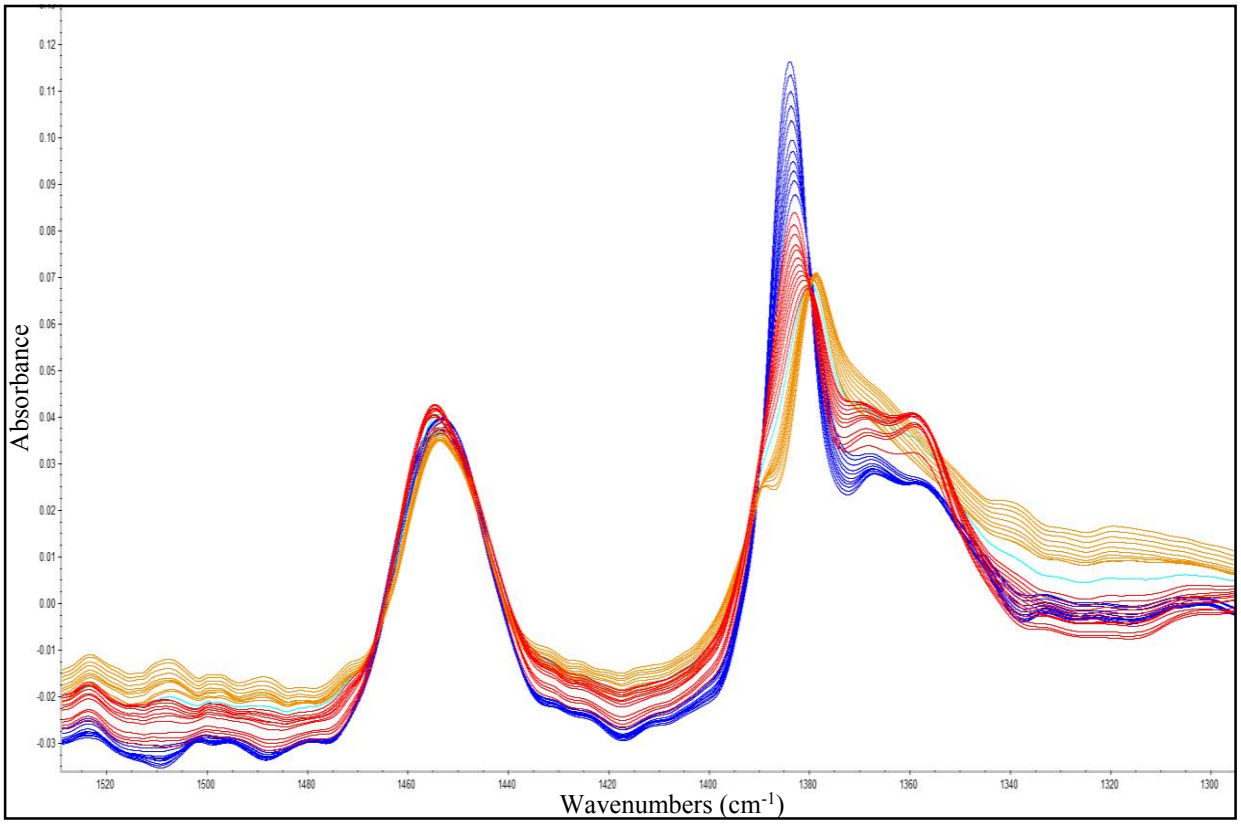

Figure 5.11a. Change in intensity of the band in the region 1500 to 1300 cm^{-1} on heating.

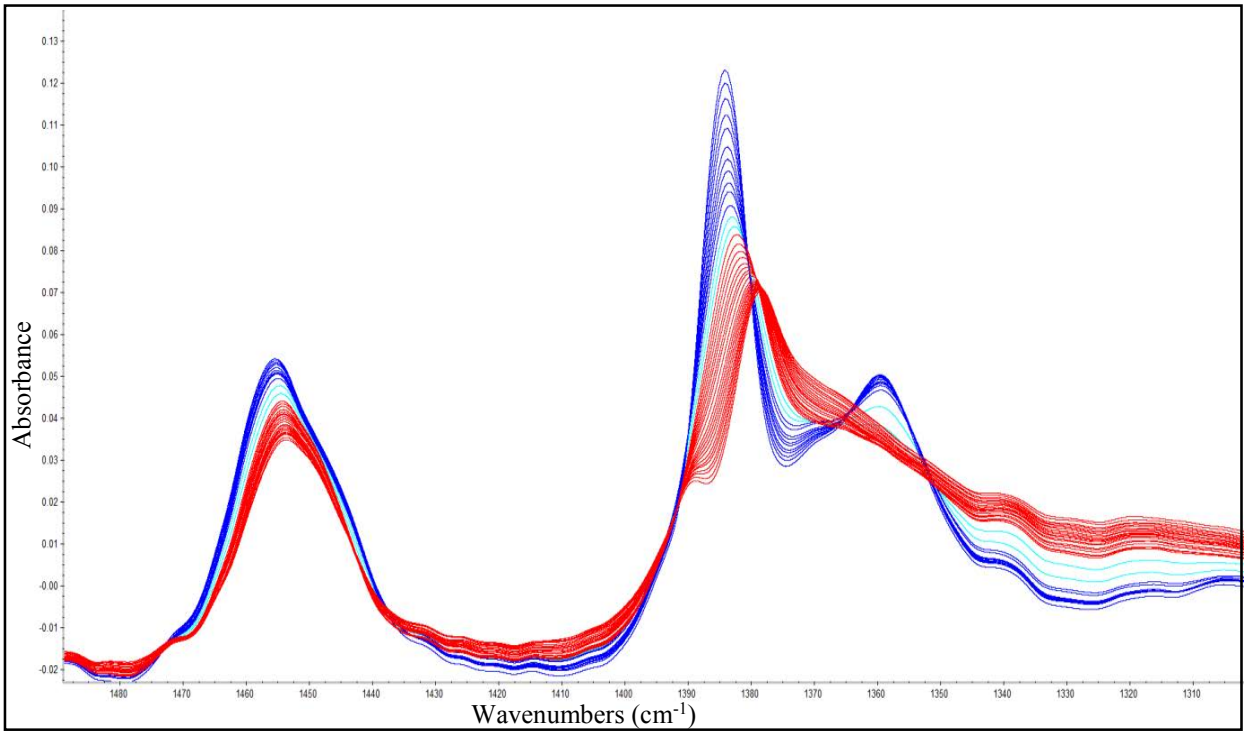

Figure 5.11b. Change in intensity of the band in the region 1500 to 1300 cm^{-1} on cooling

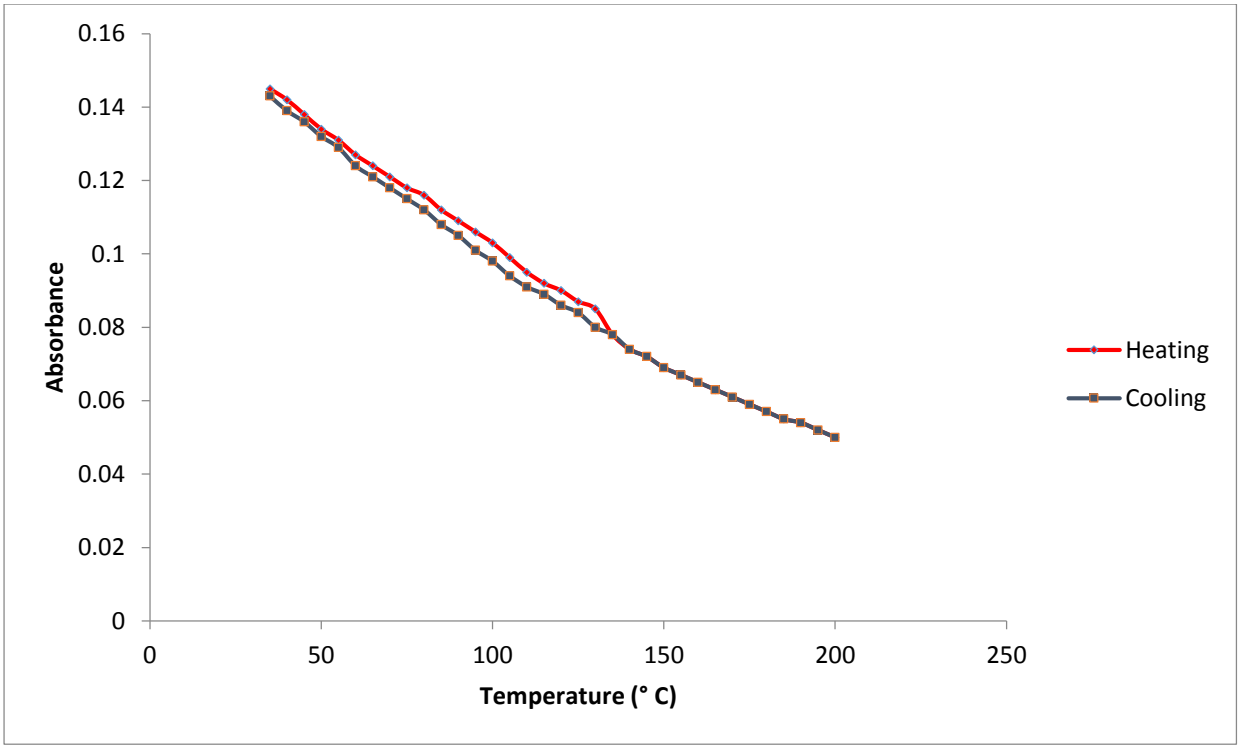

Figure 5.12. Change in intensity of the band at 1384 cm^{-1} on heating and cooling.

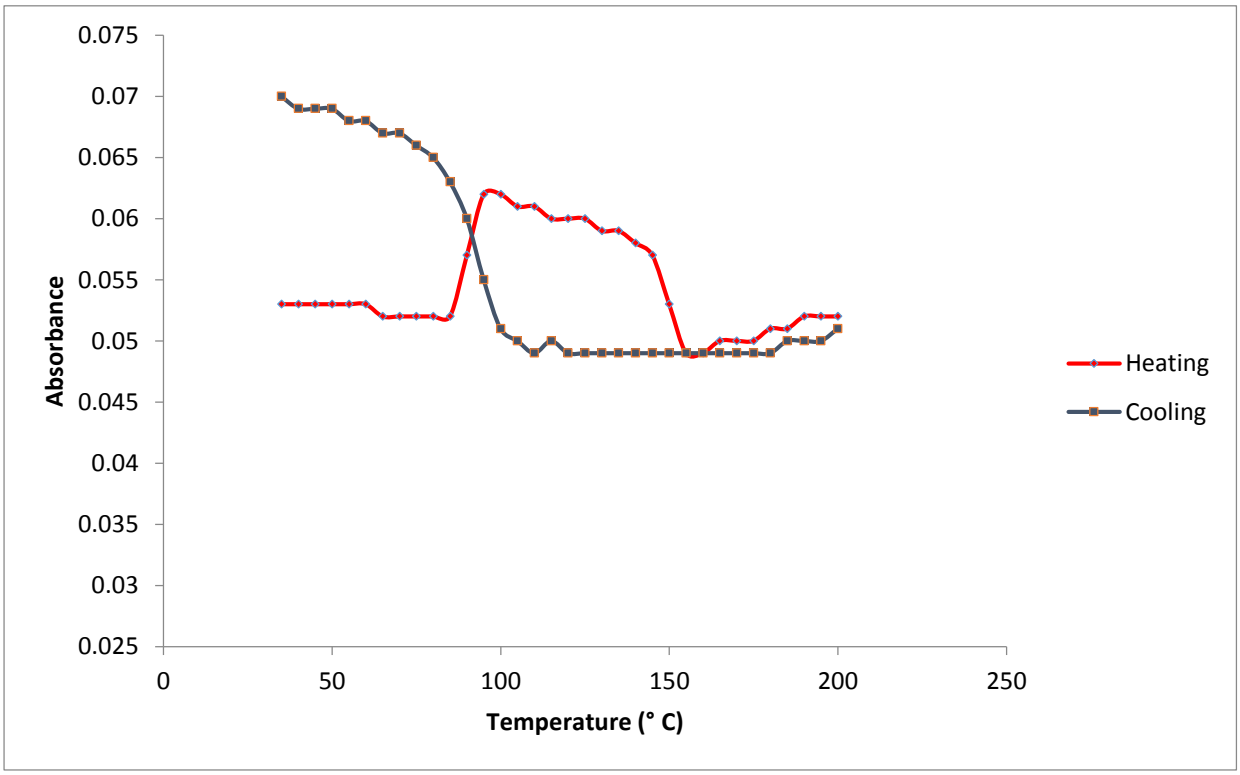

Figure 5.13. Changes in intensity of band at 1360 cm^{-1} on heating and cooling.

5.2.4. Changes in the C-O-C region 1350-1150 cm^{-1} on heating and cooling

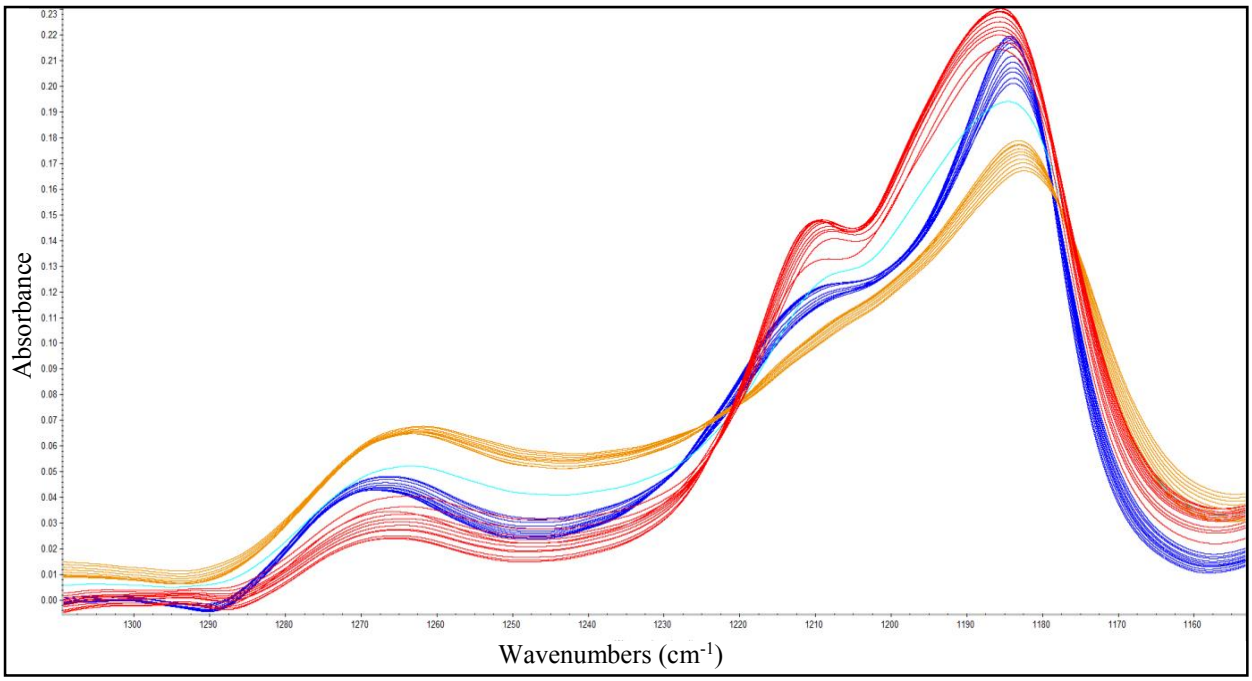

Figure 5.14a. Changes in the region C-O-C stretching band at 1350 to 1150 cm^{-1} on heating

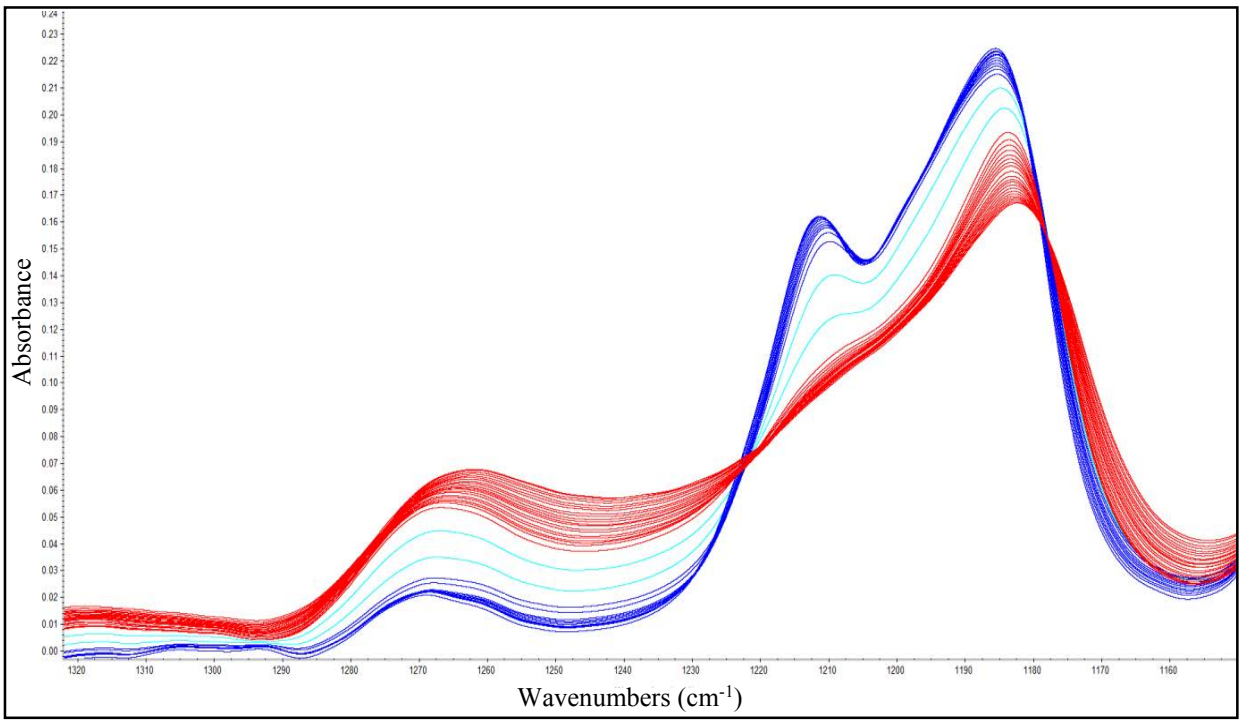

Figure 5.14b. Changes in the region C-O-C stretching band at 1350 to 1150 cm^{-1} on cooling.

The bands in the region 1350 to 1150 are associated with the ester group and its configuration and the intensities are closely linked with one another in that as one increase others decrease, on crystallization and melting, see Figure 5.14. The band at 1270 cm^{-1} initially increases in intensity on crystallization and shifts to 1265 cm^{-1} on crystallization and reverses on melting, see Figure 5.15. While the bands at 1212 and 1184 cm^{-1}, see Figure 5.16-17 show the opposite trend as a result there are two isobiestic points at 1250 and 1175 cm^{-1}, showing that the intensities are linked.

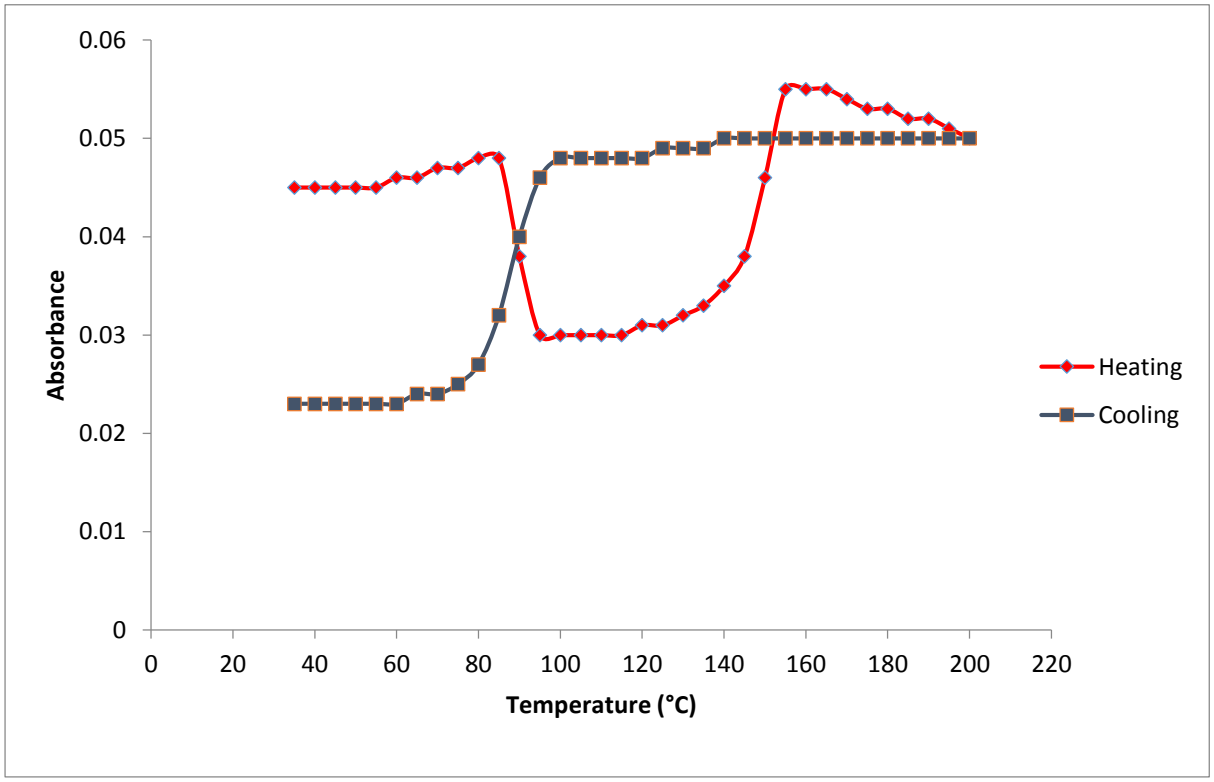

Figure 5.15. Changes in the intensity of 1270 cm^{-1} band on heating and cooling.

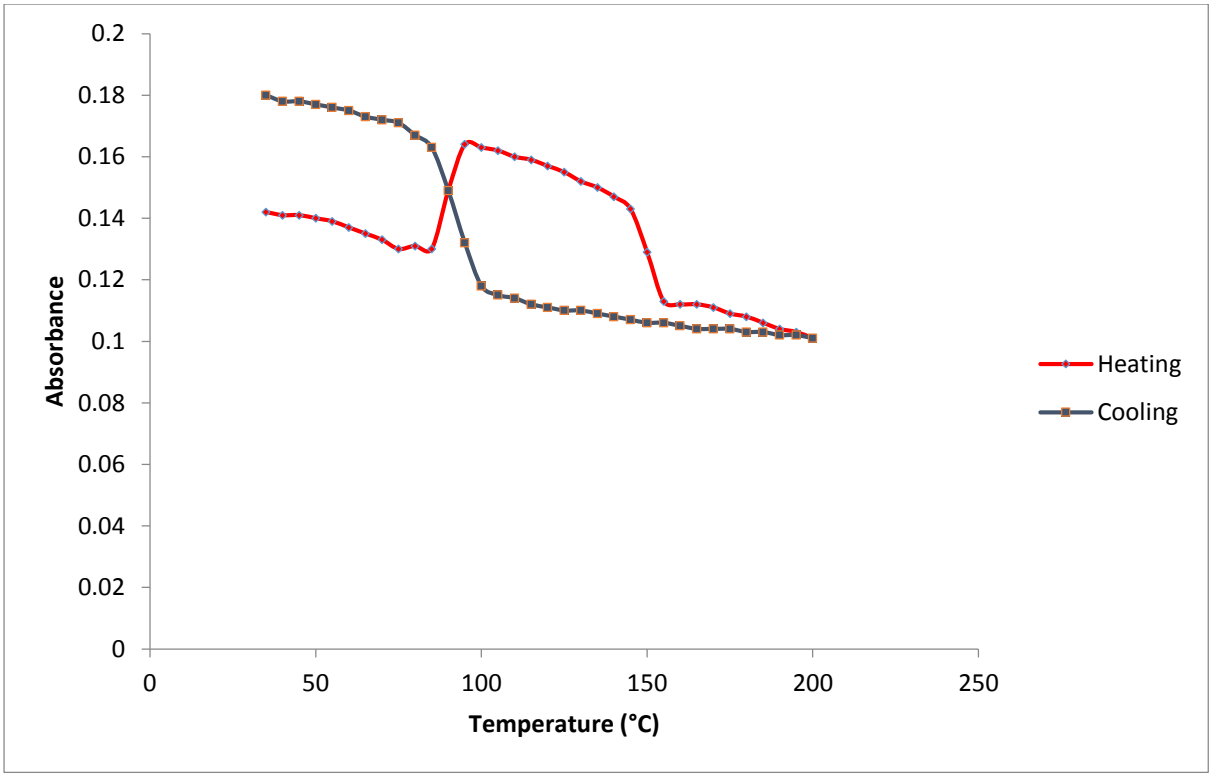

Figure 5.16. Changes in the intensity of 1212 cm^{-1} band on heating and cooling.

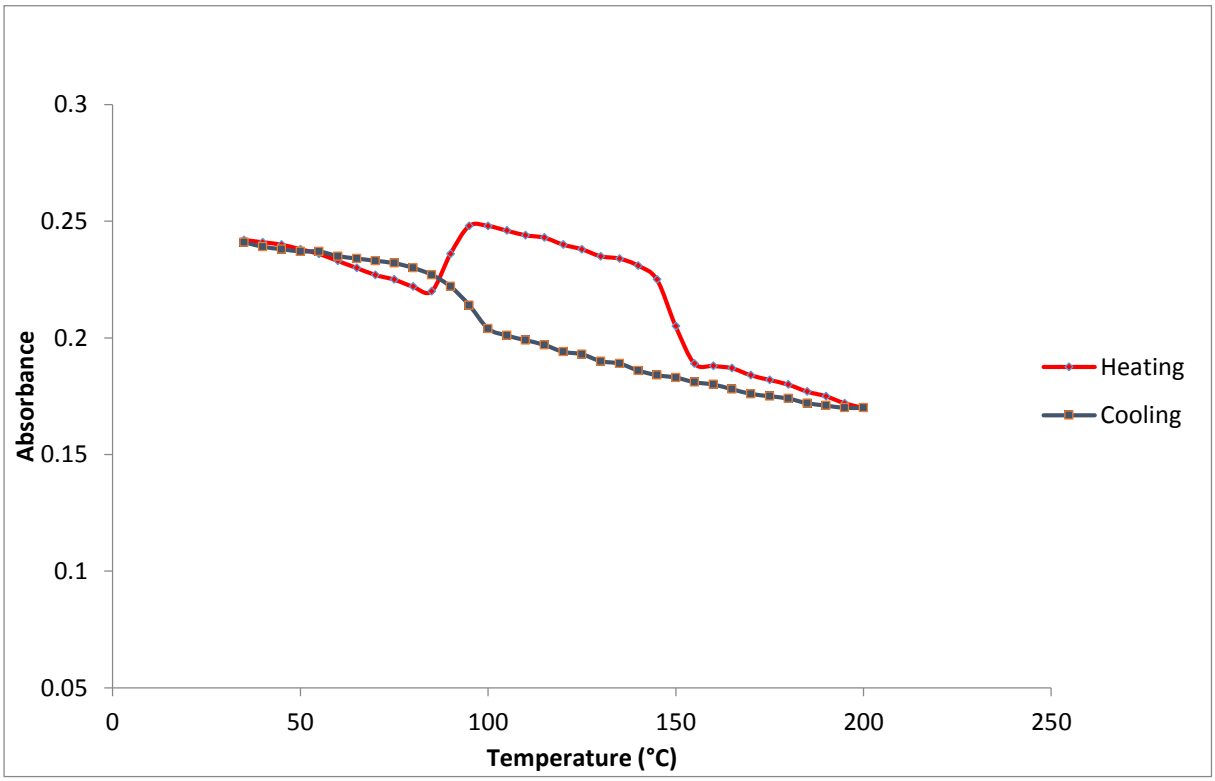

Figure 5.17. Changes in the intensity of 1184 cm^{-1} band on heating and cooling

5.2.5. Changes in the C-H region 1150-1000 cm^{-1} on heating and cooling.

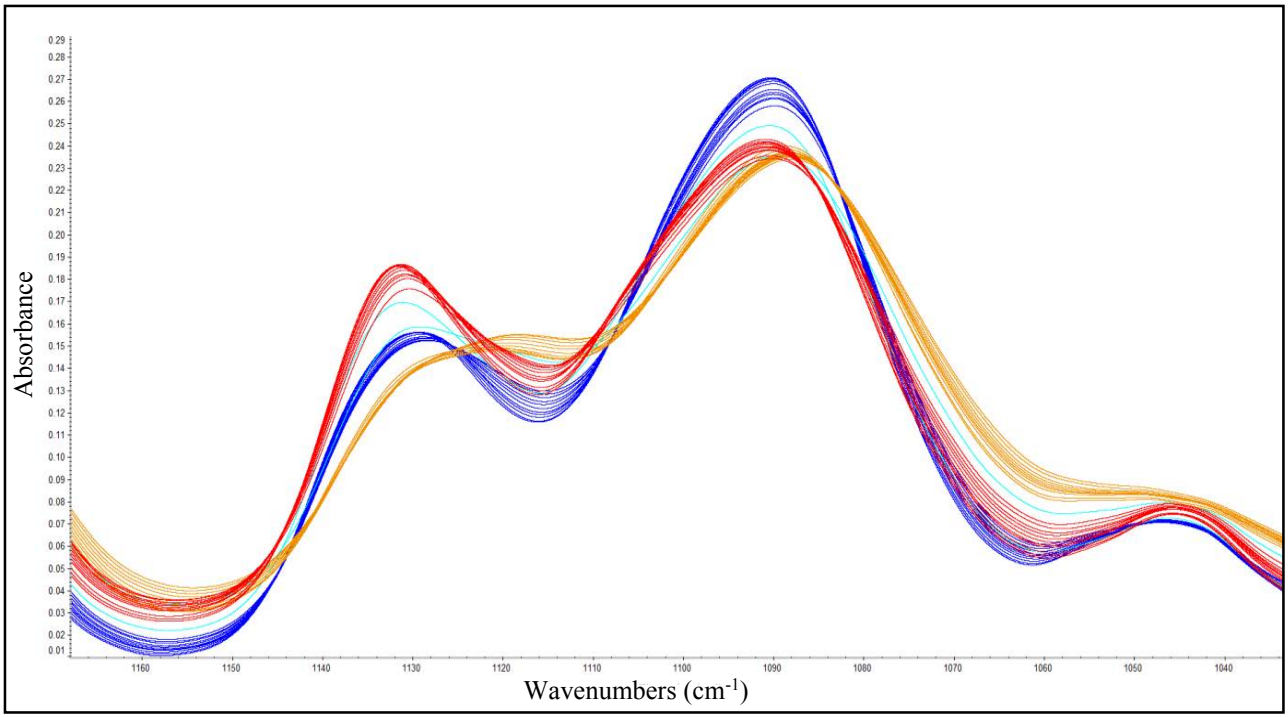

Figure 5.18a. Changes in the region 1150 to 1000 cm^{-1} on heating.

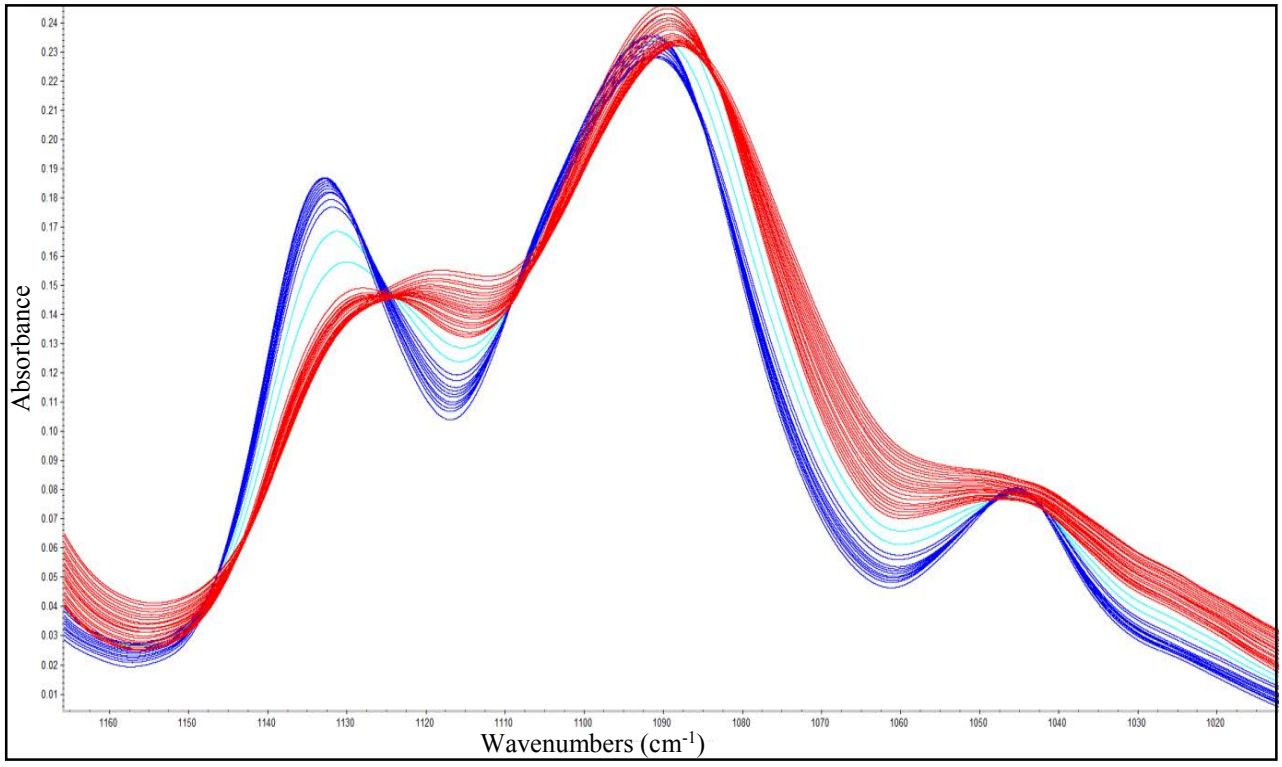

Figure 5.18b. Changes in the region 1150 to 1000 cm^{-1} on cooling.

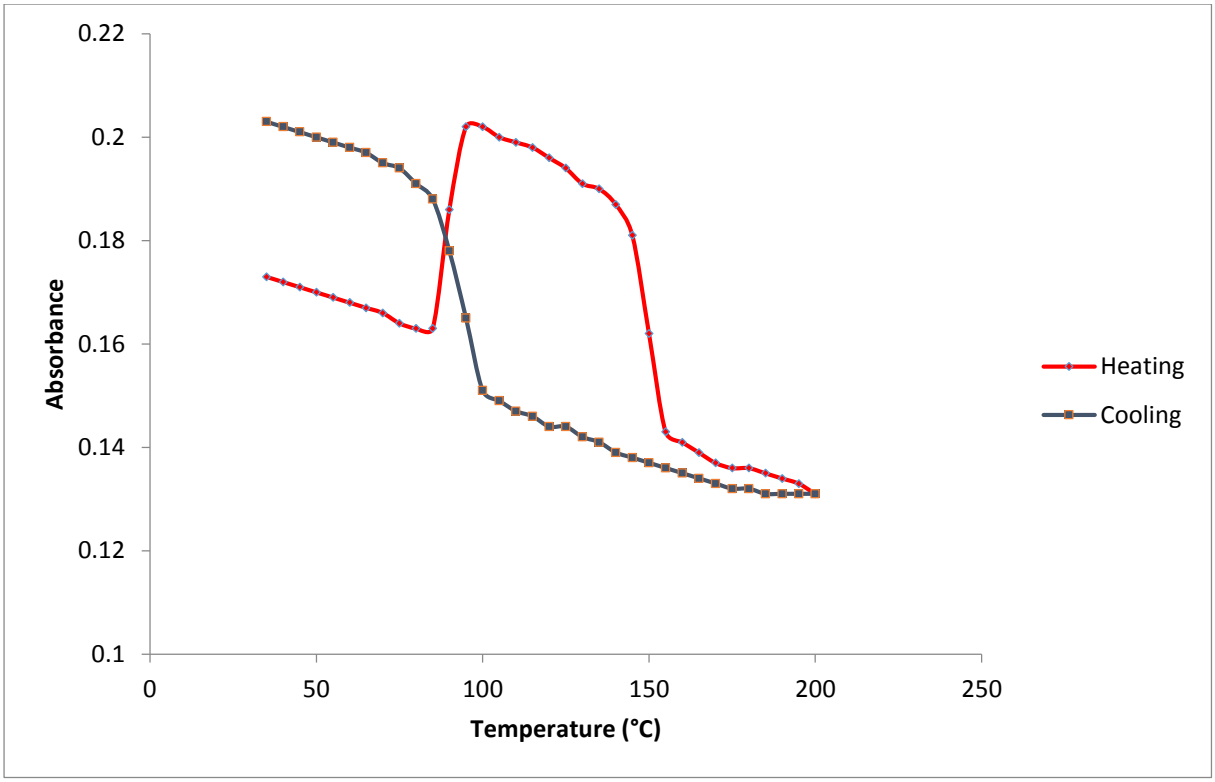

Figure 5.19. Changes in C-H deformation band at 1132 cm^{-1}on heating and cooling.

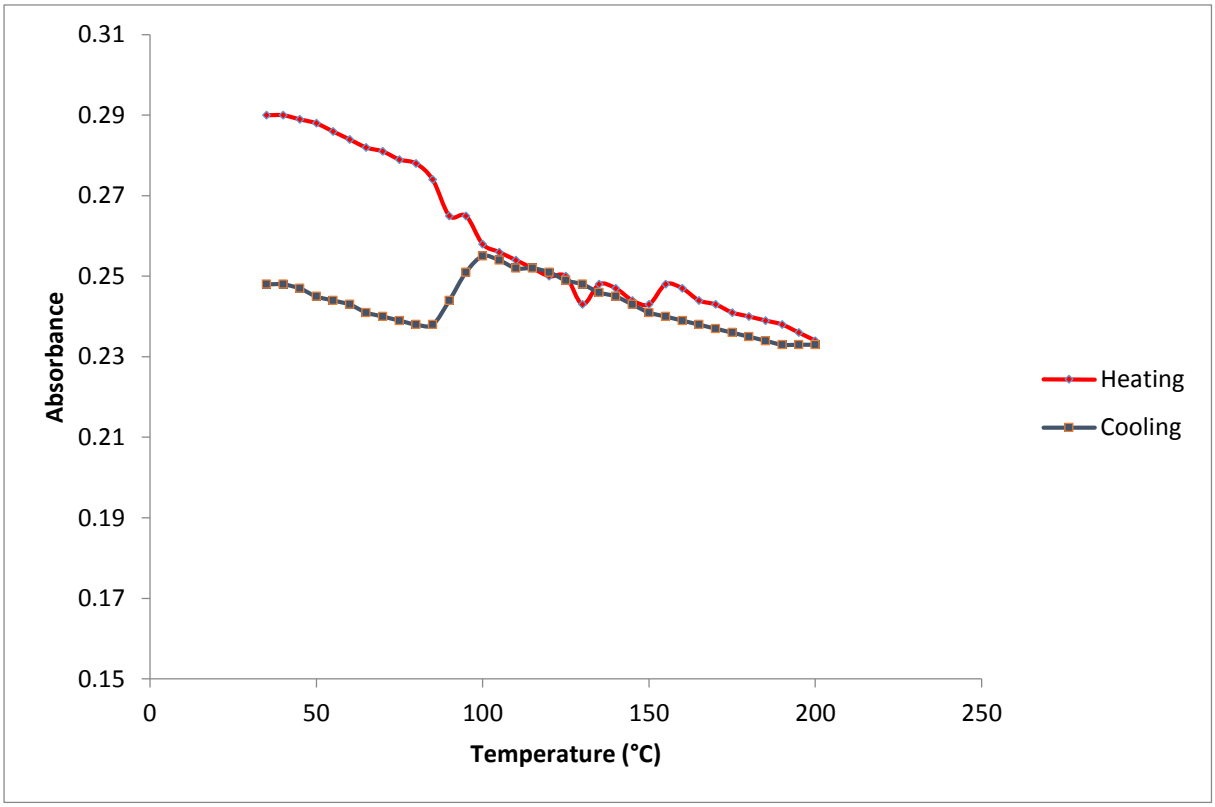

Figure 5.20. Changes in C-H deformation band at 1090 cm^{-1}on heating and cooling.

Similar changes were observed in the intensities of the C-H bands in this region on melting and crystallization due to the appearance and disappearance of the bands on phase change which enables the bands to be assigned to crystalline or amorphous regions, see Figure 5.18a-b. The presence of an isobiestic point at 1130 cm^{-1} also indicates that the appearance of the band at 1135 cm^{-1} is associated with the disappearance of another at 1150 cm^{-1}. All the other bands change in intensity with temperature and on phase change. The changes in intensity for both 1132 and 1090 cm^{-1} were shown in Figure 5.19-20. Table 5.2 shows the change of peaks on crystallization.

Table 5.2 Change of Peaks on Crystallization.

Wavenumber cm^{-1} Amorphous	Wavenumber cm^{-1} Crystalline	Temperature Dependence of the Absorbance	Change in intensity on Crystallization	Relative Intensity
2999	2997	+ ve	-ve	m
2946	2944	+ve	-ve	m
2828	2828	+ve	-ve	w
1755	1759	-ve + ve	-ve +ve	vs
1381	1384	-ve -ve		sh
1360	1360	-ve	+ve	s
1310	1300	-ve	-ve	w
1210	1212	-ve	+ve	m
1266	1266			sh
1185	1188			s
1125	1132	-ve -ve	+ve +ve.	sh
1090	1190	-ve	-ve	s
1045	1045			sh

W weak; m medium; s strong ; vs very strong; sh shoulder. +ve increase; -ve decrease.

5.3. Conclusion

A somewhat complicated picture has emerged from the study on the change in the spectra of Co-PLA on heating and cooling in that many of the absorption bands change their position and intensities with temperature. This is usually linear with temperature and is undoubtedly due to equilibrium between the gauche and trans conformers. Crystallization and melting also results in configurational changes to the molecules and this is accompanied by a step change in intensity. Only one band appears not to change on crystallization and to exhibit only a linear change with temperature, such that it could be used as an internal standard. This is the band at 1384 cm^{-1} but measurements must be made at a fixed temperature.

All further measurements on the FTIR spectrum of Co-PLA were made at constant temperature in order to eliminate the change in intensity due to temperature differences.

Although the carbonyl band is complex due to the presence of 4 rotational isomer it is clear that the one at 1759 cm^{-1} precisely follows the development of crystallinity and melting. It is also the most intense band in the spectrum of Co-PLA. It was used in further isothermal experiments to follow the development of crystallinity with time and derive the kinetic and rate parameters.

6.0. Introduction

Hot stage polarised light microscopy has been widely used to examine the development of crystallization of polymers. Generally bulk polymers crystallize by the development of spherical particles, called spherulites which have a characteristic Maltese cross birefringent pattern in polarised light due to the spherical symmetry of the spherulites. This symmetry is created by the growth of lamellar crystals which grow linearly with time along their length and by regular branching into multiple lamellae produce spherical contours. The radii of the spherulites grow linearly with time.

The variation of the radial growth rate of the spherulite and the nucleation density with temperature, i.e. the number of spherulites per unit volume, are the two characteristic crystallization parameters which are measure by light microscopy. These in turn can be related to the Avrami crystallization rate parameter, Z as discussed before.

6.1. Dynamic runs on Co-PLA

The crystallization of Co-PLA was examined as thin films, 15-20 μm thick, placed between glass cover slips and mounted horizontally in the hot stage of a polarized microscope under a ¼ quartz plate. A partially crystalline sample was prepared by heating the sample from 30 °C to 180 °C at 30 °C min^{-1}, cooled to 118 °C, held for 1 hour and then cooled to room temperature. The sample then was heated to the melt and cooled to study any changes on heating and cooling.

The micrographs are shown as a function of temperature in Micrographs 6.1. They are typical of impinged multiple spherulites with a distinction Maltese cross birefringence but variable nucleation density across the sample

A. On heating

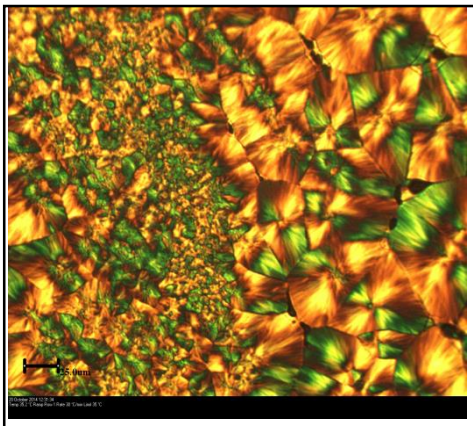

35 °C

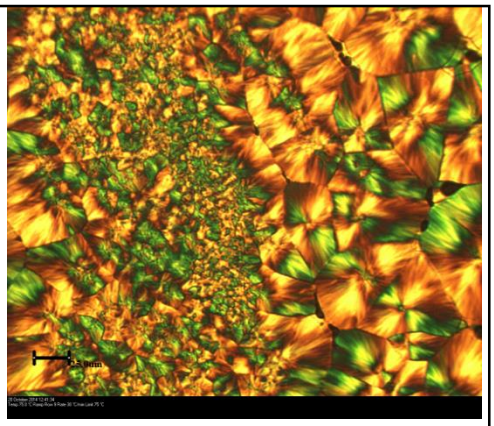

75 °C

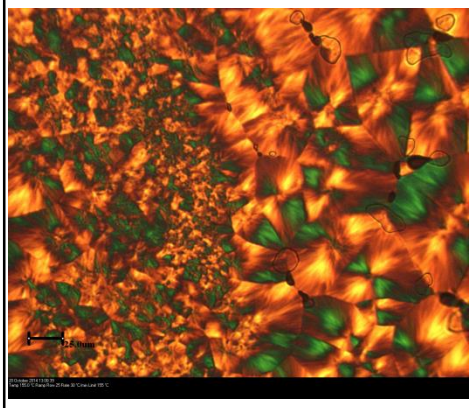

155 °C

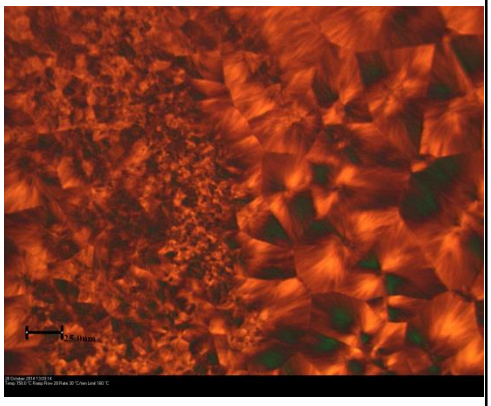

158 °C

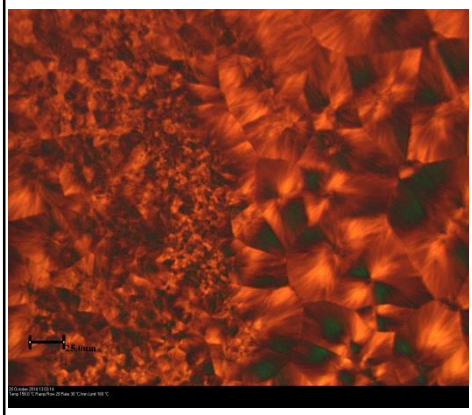

160°C

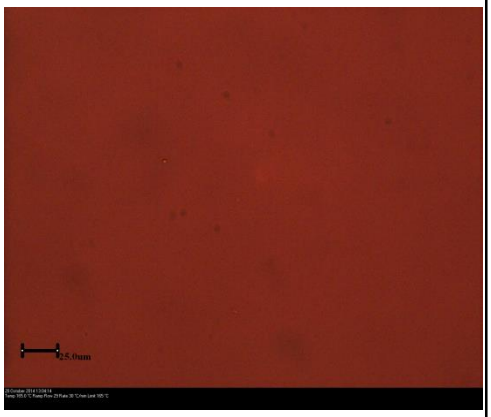

165 °C

Scale used: 25 µm

B. On cooling

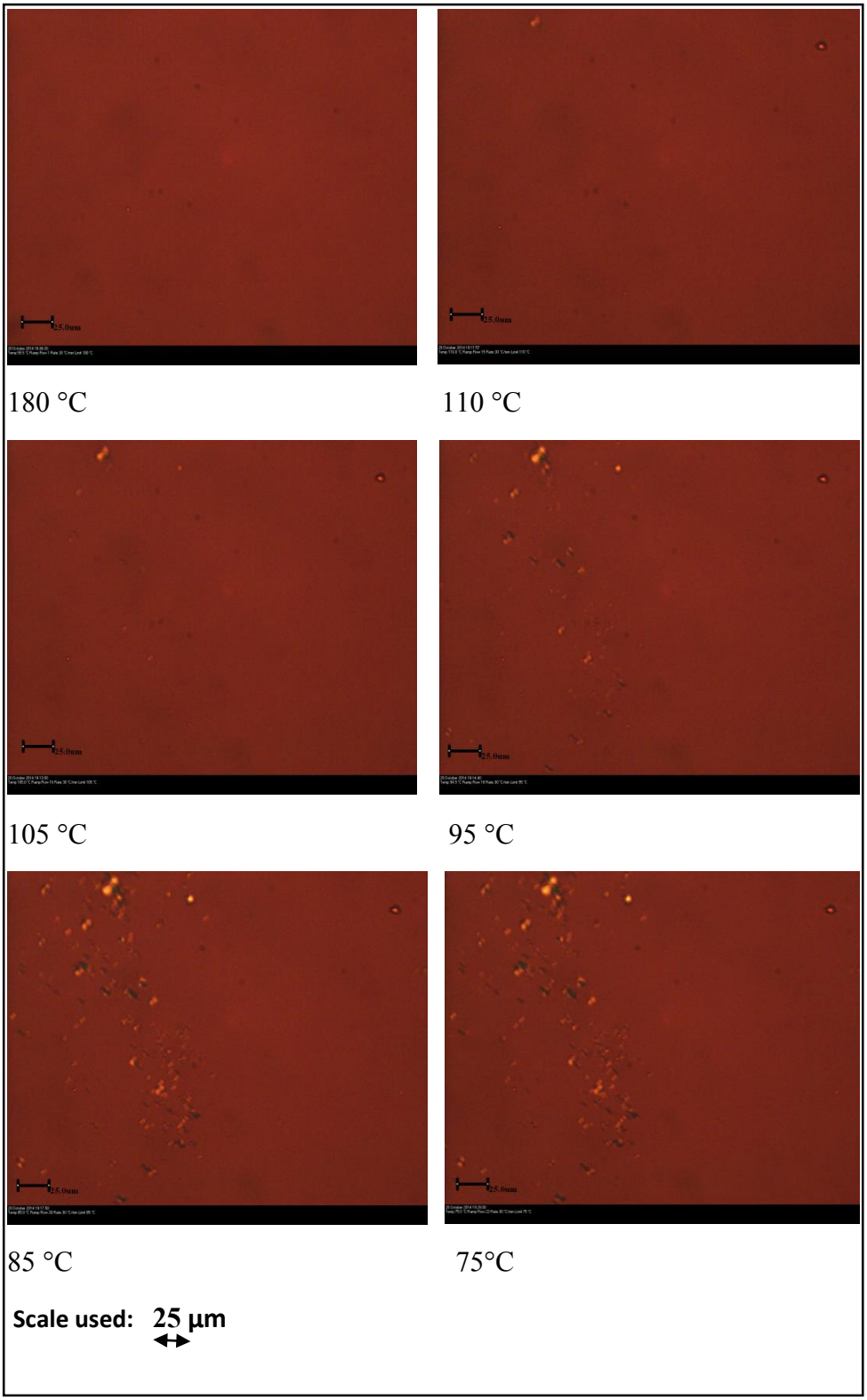

Micrographs 6.1. Birefringence changes on heating and cooling Co-PLA at 50 $^{o}min^{-1}$ from 30 to 180 ^{o}C.

No changes were observed in the birefringence on heating until above 150 ^{o}C and melting appeared to occur between 160 and 165 ^{o}C from the disappearance of the spherulite. On cooling at 50 ^{o}C min^{-1} crystallization did not occur but localised birefringent spherical particles were observed from 110 ^{o}C down. Limited growth of these occurred and the original birefringent pattern of multiple spherulites did not return at room temperature. Undoubtedly the cooling rate was too high to allow crystallization to develop to any extent.

6.2. Effect of crystallization temperature on spherulite growth and nucleation

6.2.1. At 95 °C

The sample was melted at 180 ^{o}C, held for 2 minutes before being cooled at 50 ^{o}C min^{-1} to the crystallization temperature. The number of spherulites and their diameters were measured with time and the nucleation density and radial growth rate determined. The micrographs 6.2 show the development of spherulites and their impingement with one another.

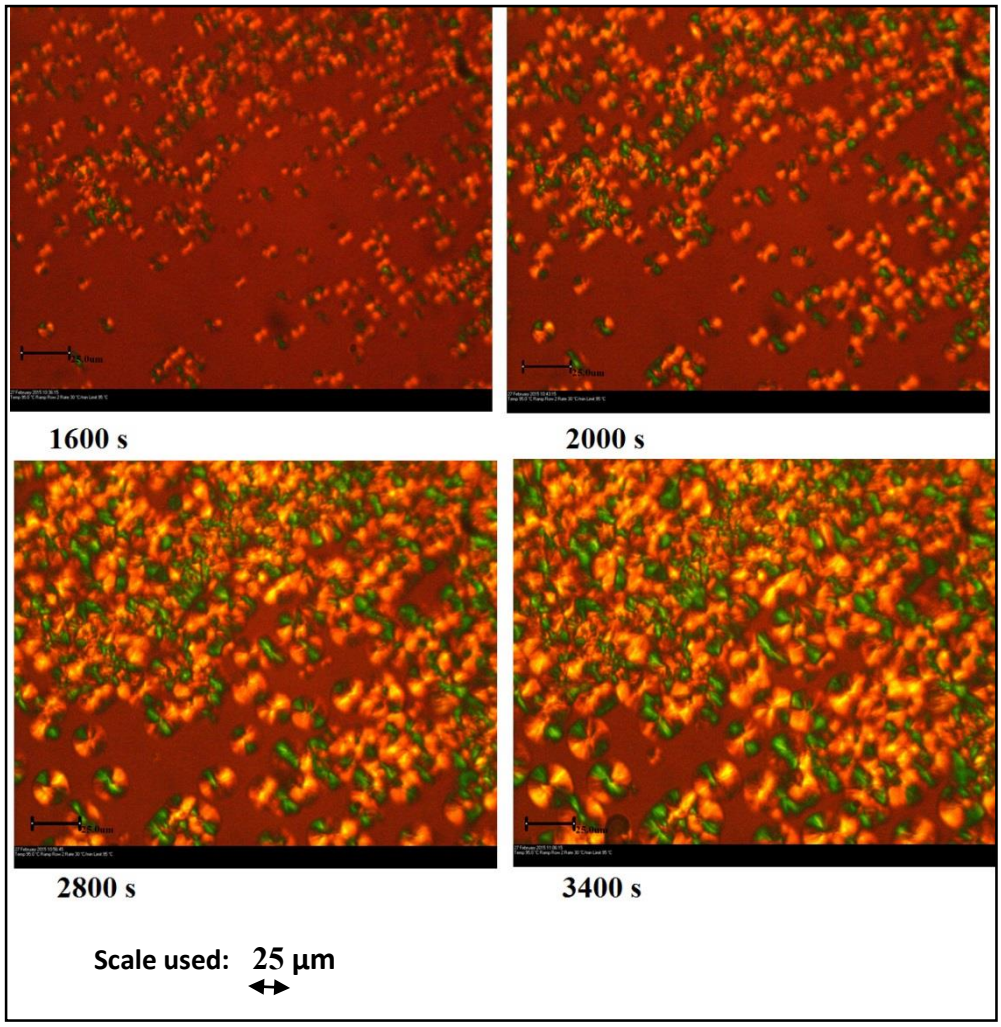

Micrographs 6.2. Growth of the spherulite with time at 95 °C. (objective lens X32 eyepiece lens X10 320X)

Nucleation Density = Number of spherulite / Volume

$= 35 / (80\mu \text{ X } 120\mu \text{ X } 15\mu) = 35 / 144000 = 2.4 \times 10^{-4}\ \mu m^{-3}$

$= 240 \times 10^{-6}\ \mu m^{-3}$

Table 6.1. Growth of Spherulites (95 °C).

Time (s)	Diameter (µm)
1600	9.0
2000	13.8
2800	20.4
3400	24.6

6.2.2. At 105 °C

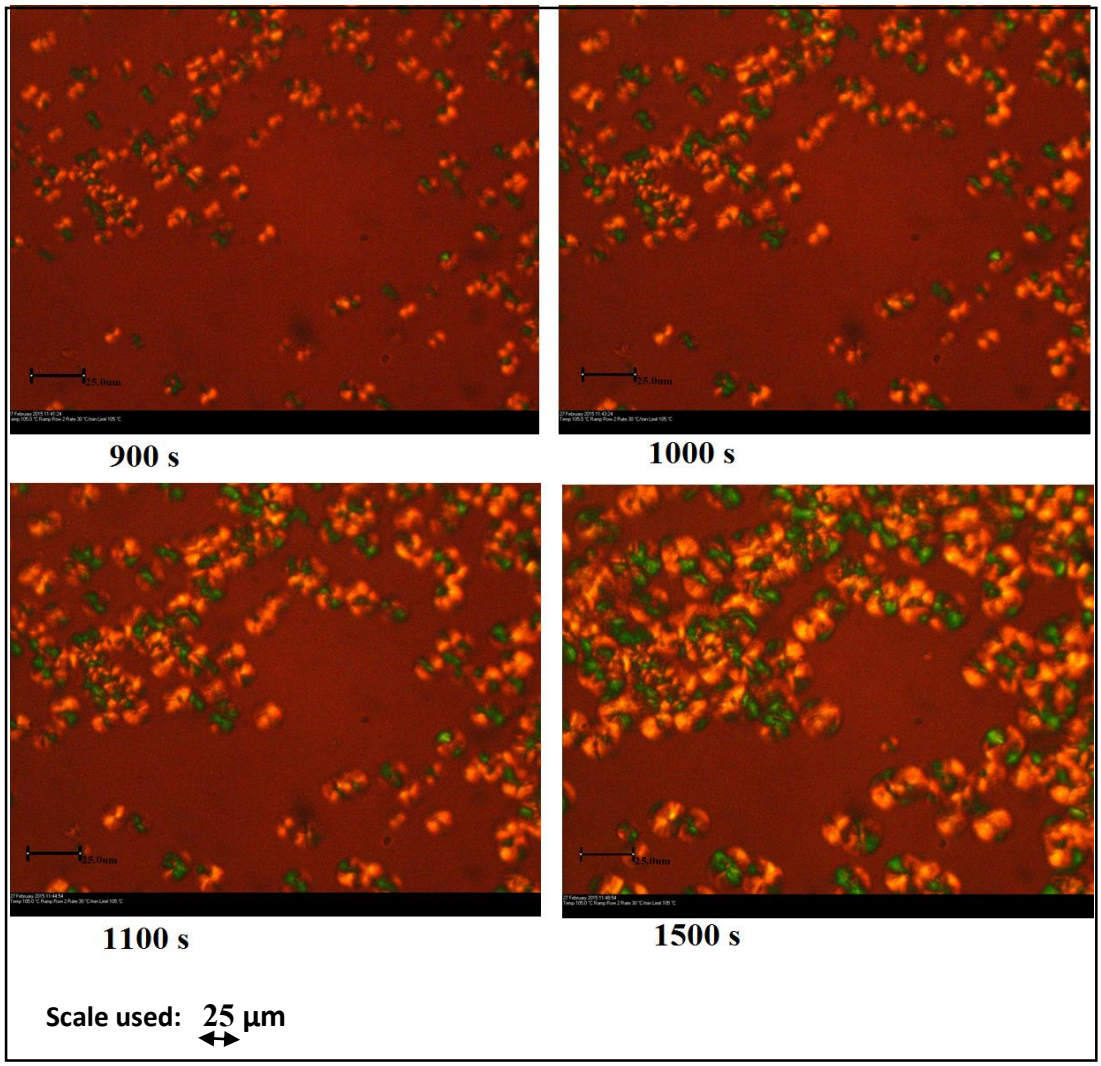

Micrographs 6.3. Growth of the spherulite with time at 105 °C.
(objective lens X32 eyepiece lens X10
320X)

Nucleation Density = Number of spherulite / Volume

$= 16 / (80\mu \text{ X } 120\mu \text{ X } 15\mu = 16/ 144000 = 1.1 \text{ x } 10^{-4} \mu m^{-3}$

$= 110 \text{ x } 10^{-6} \mu m^{-3}$

Table 6.2. Growth of Spherulites (105 °C).

Time (s)	Diameter (µm)
900	10.6
1000	16.9
1100	18.9
1500	20.5

6.2.3. At 118 °C

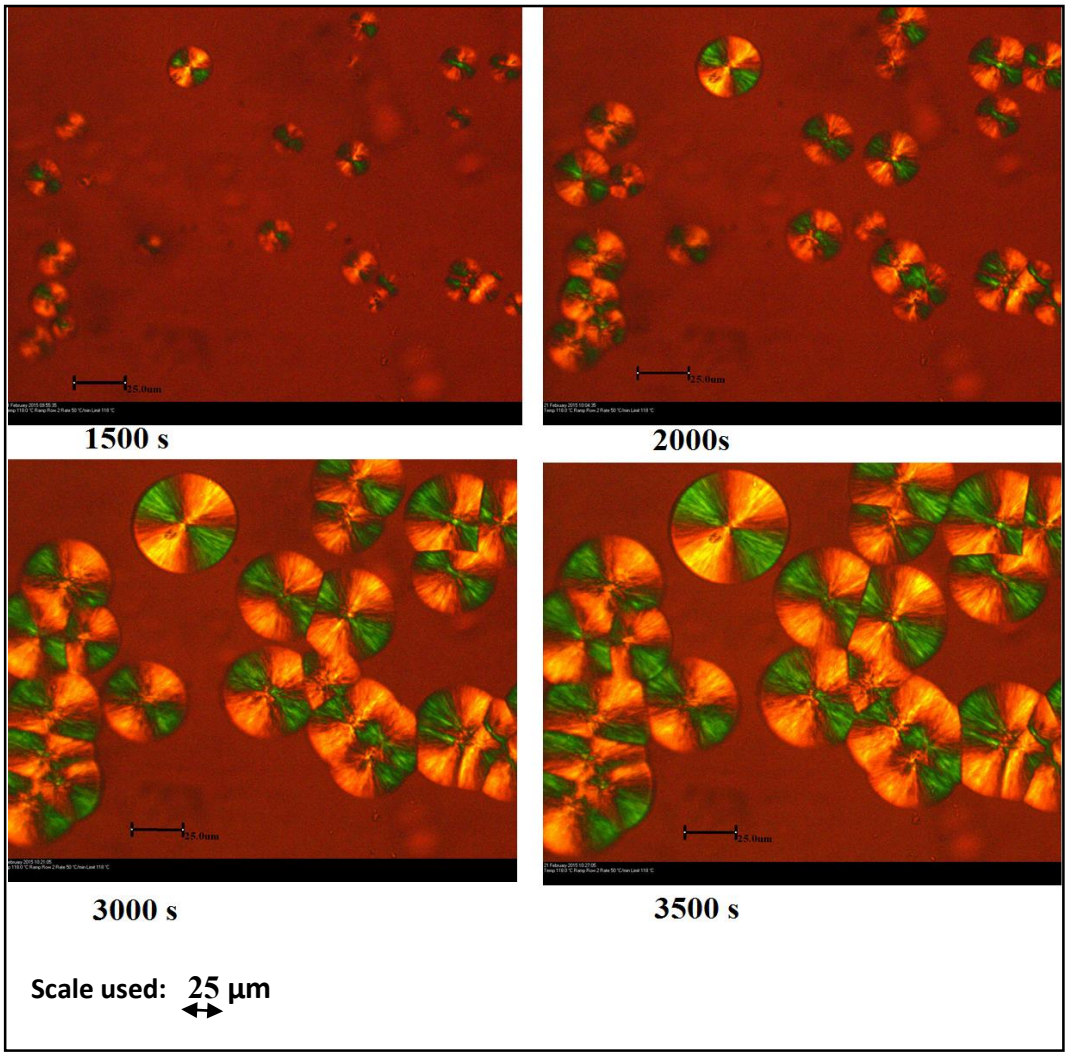

Micrographs 6.4. Growth of the spherulite with time at 118 °C.
(objective lens X32 eyepiece lens X10
320X)

Nucleation Density = Number of spherulite / Volume

= 6 / (80µ X 120µ X 15µ) = 6/ 144000 = 4.2 x 10^{-5} μm^{-3}

= 42 x 10^{-6} μm^{-3}

Table 6.3. Growth of Spherulite (118 °C).

Time (s)	Diameter (µm)
1500	23.2
2000	32.6
3000	50.9
3500	60.3

6.2.4. At 125 °C

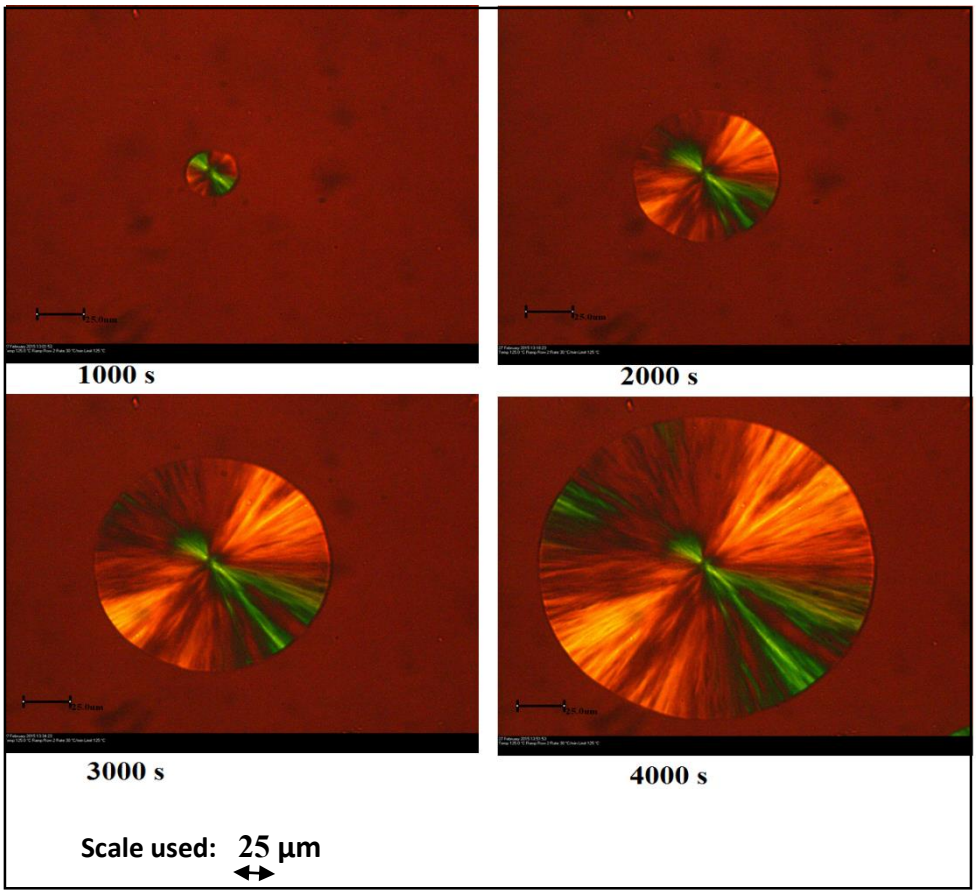

Micrographs 6.5. Growth of the spherulite with time at 125 °C. (objective lens X32 eyepiece lens X10 320X)

Nucleation Density = Number of spherulite / Volume

$= 1 / (80\mu \text{ X } 120\mu \text{ X } 15\mu) = 1/ 144000 = 6.9 \times 10^{-6}\ \mu m^{-3}$

$= 6.9 \times 10^{-6}\ \mu m^{-3}$

Since only one spherulite is in the field this is a minimum value and not representative of the nucleation density.

Table 6.4. Growth of spherulite (125 °C).

Time (s)	Diameter (µm)
1000	28.1
2000	76.5
3000	126.6
4000	174.6

6.2.5. At 135 °C

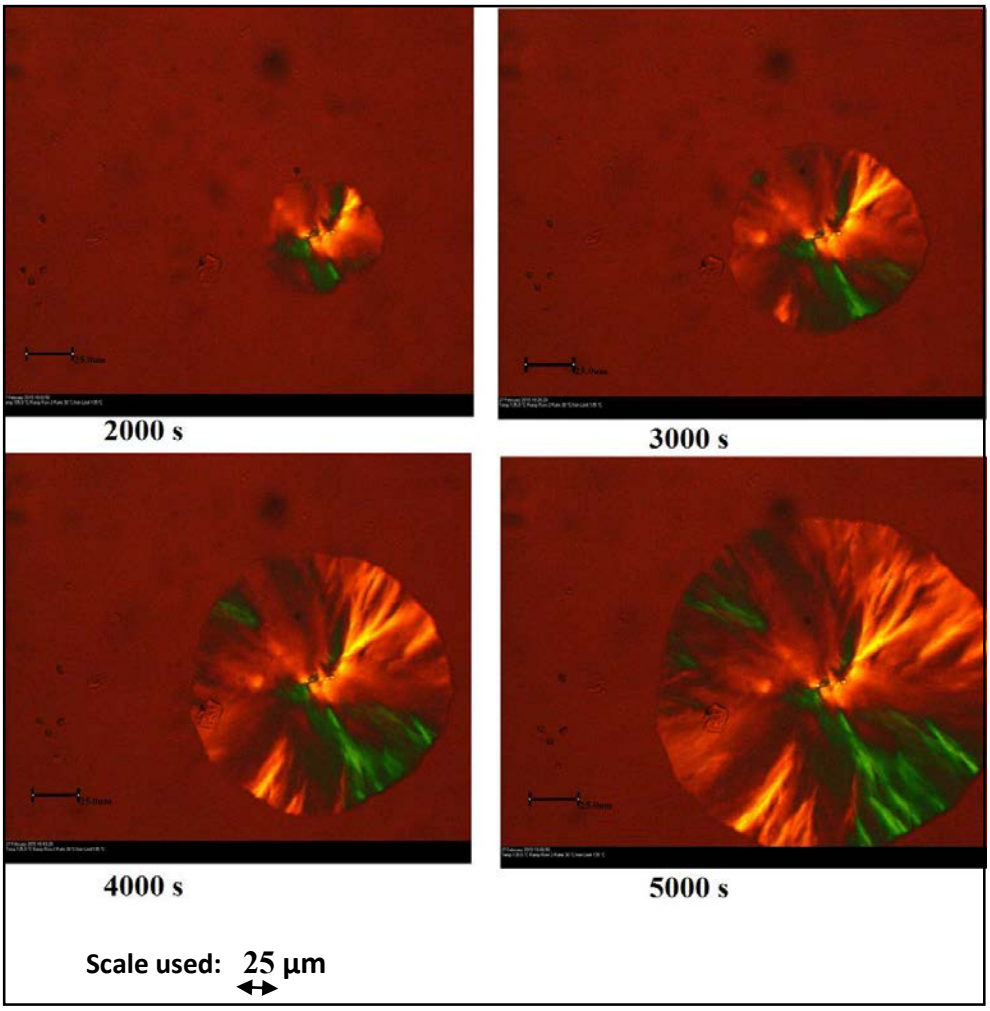

Micrographs 6.6. Growth of the spherulite with time at 135 °C.
(objective lens X32 eyepiece lens X10
320X)

Nucleation Density = Number of spherulite / Volume

= 1 / (80µ X 120µ X 15µ) = 1/ 144000

= 6.9 x 10^{-6} μm^{-3}

Table 6.5. Growth of Spherulite (135 °C).

Time (s)	Diameter (µm)
2000	65.8
3000	98.9
4000	141
5000	175.4

6.2.6. At 140 °C

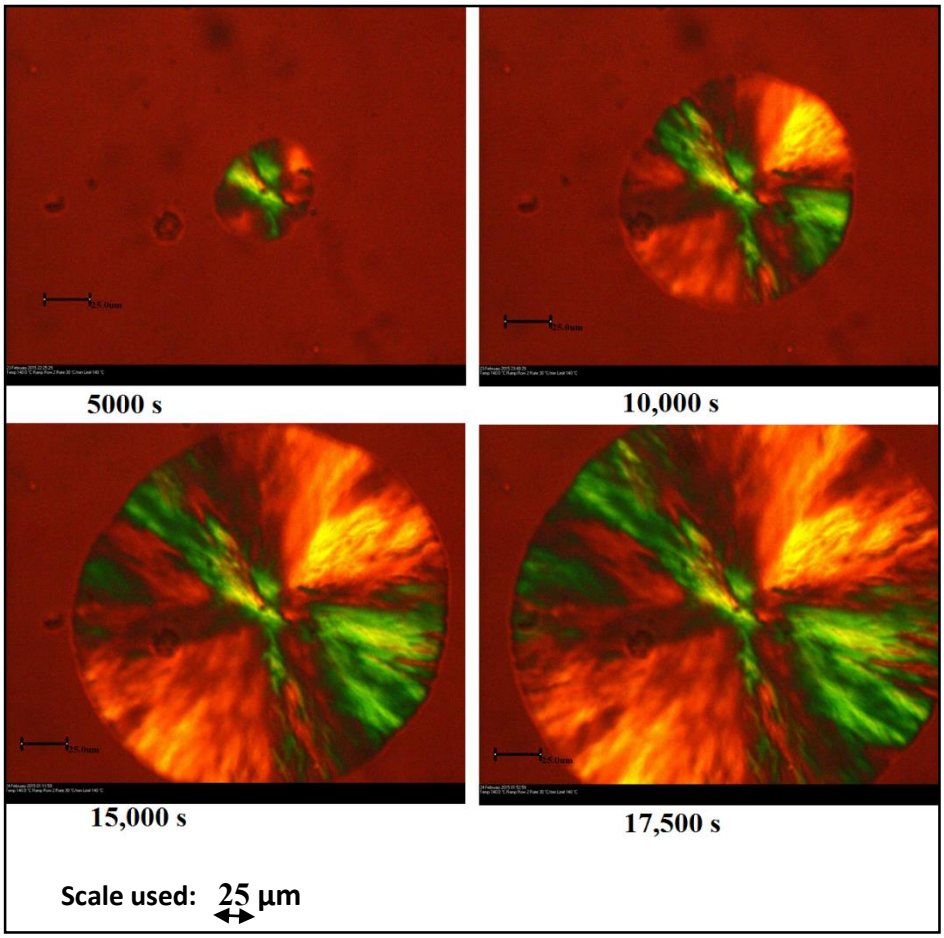

Micrographs 6.7 Growth of the spherulite with time at 140 °C.
(objective lens X32 eyepiece lens X10
320X)

Nucleation Density = Number of spherulite / Volume

= 1 / (80µ X 120µ X 15µ)

= 1/ 144000

= 6.9 x 10^{-6} μm^{-3}

Table 6.6. Growth of spherulite (140 °C).

Time (s)	Diameter (µm)
5000	56.6
10,000	127.4
15,000	208.8
17,500	252

6.2.7. At 145 °C

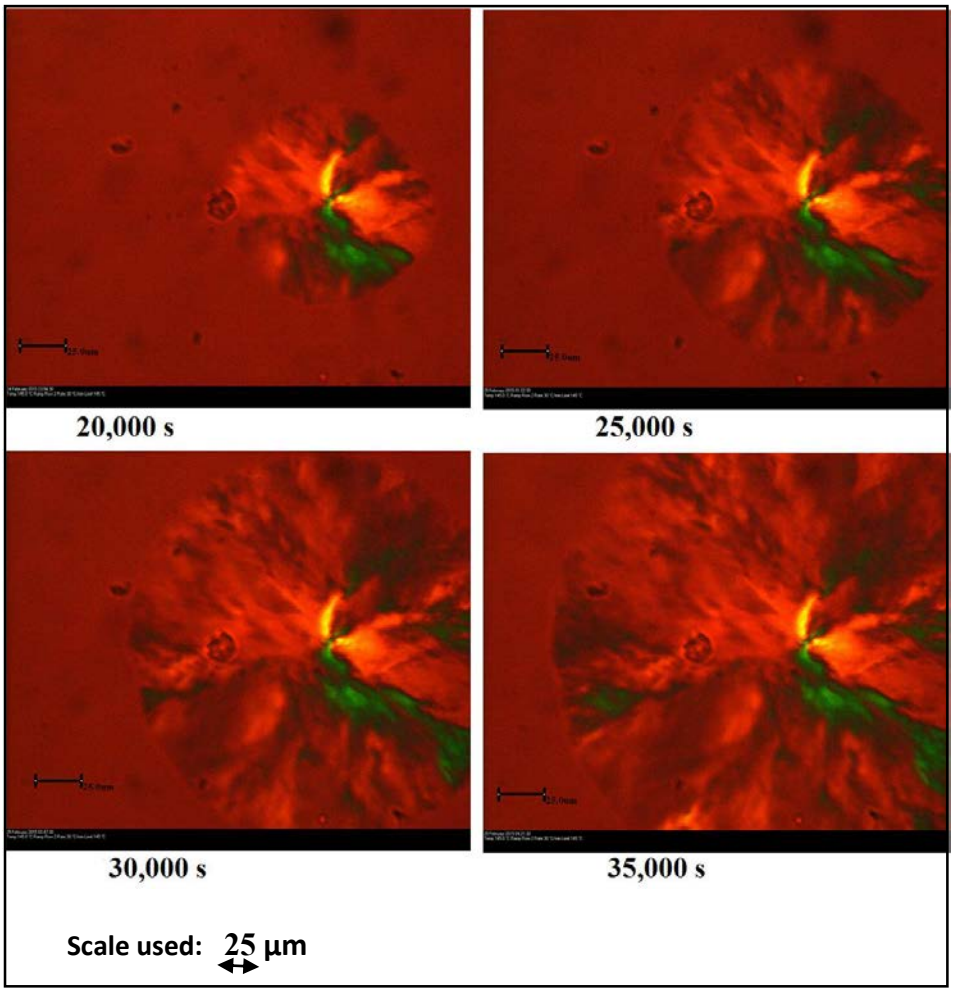

Micrographs 6.8. Growth of the spherulite with time at 145 °C. (objective lens X32 eyepiece lens X10 320X)

Nucleation Density = Number of spherulite / Volume

= 1/ (80µ X 120µ X 15µ)

= 1/ 144000

= 6.9 x 10^{-6} μm^{-3}

Table 6.7. Growth of Spherulite (145 °C).

Time (s)	Diameter (µm)
20,000	108
25,000	153.4
30,000	216.2
35,000	254

6.3. Discussion

As can be seen from Micrographs 6.2 to 6.4 the numbers of spherulites did not increase with time at constant temperature and on average the spherulites at any crystallization temperature and at the same time had very similar diameters, in that there are no very large or very small ones present. This indicates that they were all nucleated at the same time and grew to similar sizes. Nucleation was heterogeneous, perhaps on dust particles but there was an induction time which increased with crystallization temperature, see Table 6.8. The heterogeneous nucleation density, see Table 6.8 and Figure 6.9, also increased exponentially with decreasing temperature – increasing with the degree of supercooling from the melting point. This is consistent with the size of the critical size nucleus, or nucleating heterogeneous particle, decreasing in size with decreasing temperature. This produced a larger number of smaller spherulites at lower crystallization temperatures, compare Micrographs 6.2 to 6.5 with 6.6 to 6.8.

Table 6.8. Nucleation Characteristics.

Crystallisation Temperature (°C)	Nucleation Density (μm)$^{-3}$ x 10^6	Induction Time s
95	240	20
105	110	95
118	42	110
125	6.9	420
135	6.9	260
140	6.9	1500
145	6.9	8400

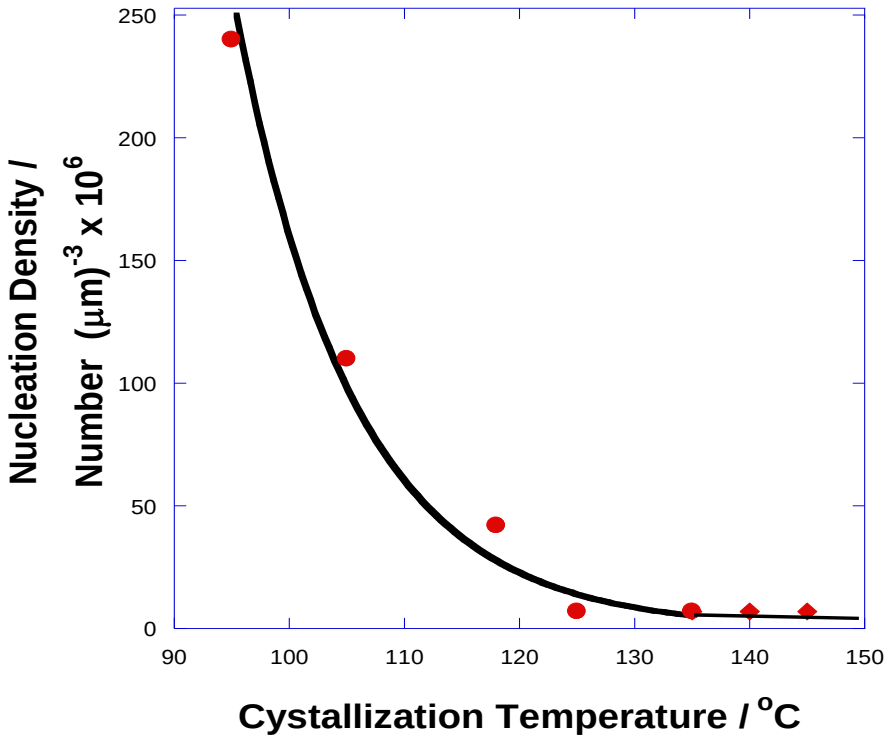

Figure 6.9. The decrease in nucleation density with temperature.

The nucleation density increased continuously with decreasing crystallization temperature, see Figure 6.9 but was constant with time at each temperature, see Micrographs. There was no decrease in nucleation density at low temperature due to increased viscosity as observed with the growth rate, see Figure 6.9, such that no maximum nucleation density was observed but instead it decreased continuously depending on the degree of supercooling from the equilibrium melting point, ΔT, consistent with nucleation on heterogeneous particles which decrease in size with decreasing crystallization temperature and increasing supercooling.

The diameters of the spherulites increased linearly with time from nucleation to impinging with adjacent spherulites, see Figure 6.10 and the growth rates increased with temperature up to a maximum at about 125 - 130 ^{o}C before decreasing to zero at the melting point. Table 6.9 and

and Figure 6.11 show the temperature dependence of the radial growth rate. This characteristic bell shaped curve is due to two effects, viscousity control at low temperature due to the onset of glass transition at 58.5 ^{o}C, and nucleation control at high temperature as the melting point is approached and has been expressed by Hoffman and Lauritzen in the relationship [33-40].

$$v = v^{o} \exp(-U/R(T_c-T_2)) \exp(-K/T_c \Delta T f) \quad (6.1)$$

where v is the radial growth rate, v^{o} a pre-exponential factor, U the activation energy of viscous flow, T_c the crystallization temperature, T_2 the thermodynamic glass transition temperature, ΔT the degree of supercooling, R the gas constant and K the nucleation constant.

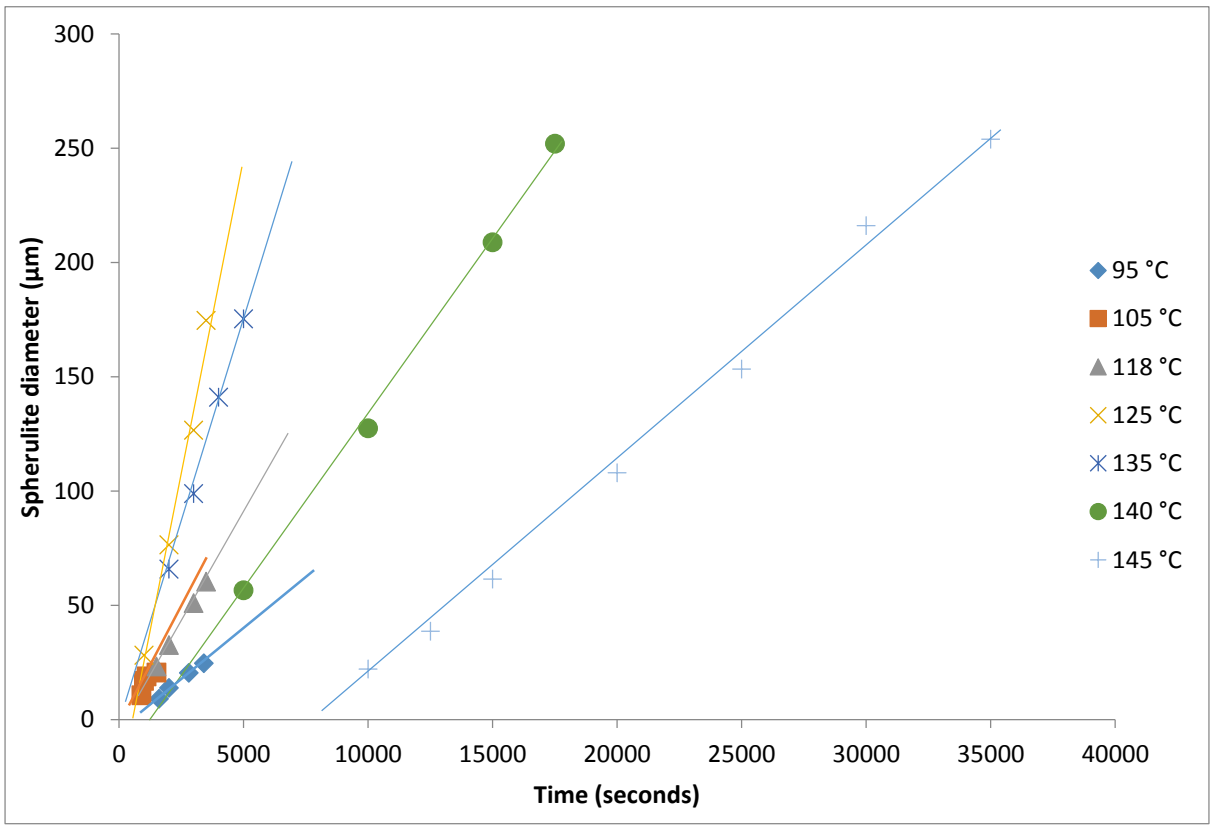

Figure 6.10. The increase in spherulite diameter with time at each crystallisation temperature.

Table 6.9. The temperature dependence of the radial growth rate.

Crystallisation Temperature °C	Radial Growth rate / μm min^{-1}
95	0.52
105	0.99
118	1.11
125	2.93
135	2.19
140	0.96
145	0.58

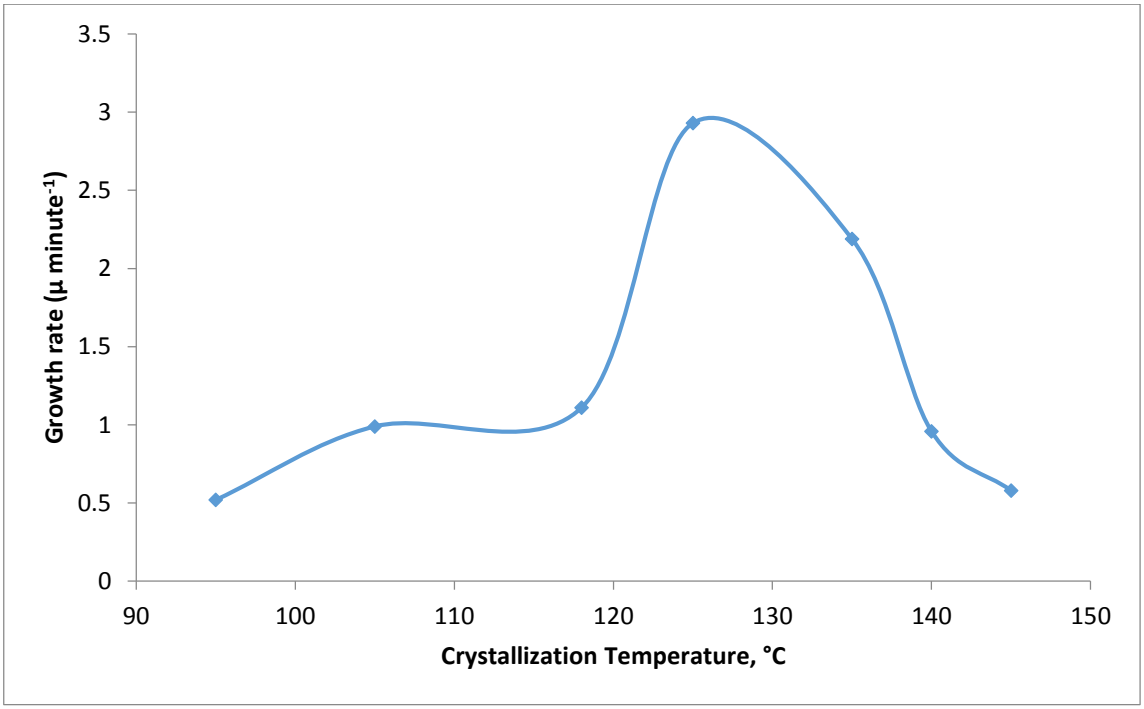

Figure 6.11. Temperature dependence of radial growth rate.

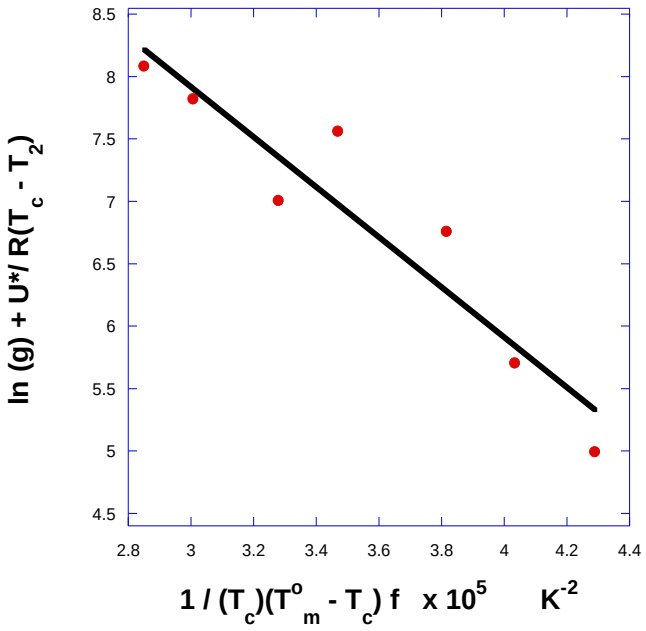

Figure 6.12. The dependence of the radial growth rate on the degree of supercooling.

From the plot of ln(g) +U/R(T_c-T_2) against 1/T_c(T_m^o-T_c), see Figure 6.12, K the nucleation constant was determined to be 2.03 ± 0.50 x10^5 K^2. Since this covers the temperature range 95 to 145 ^oC which corresponds to a very high degree of supercooling, 60 to 120 ^oC, it must be assumed that nucleation occurs in regime ll (see Chapter 7) and

$$K_{ll} = 4b\sigma\sigma_e T_m^o / k\Delta H_v \qquad (6.2)$$

Where b is the monomolecular layer thickness, σ and σ_e the side and fold surfaces free energies, T_m^o the equilibrium melting point, k Boltzmann constant and ΔH_v the enthalpy of fusion per unit volume. From the value of K determined from the slope of the linear relationship shown in Figure 6.12 and the value for b and ΔH_v listed by Garlotta [9] $\sigma\sigma_e$ was 617 erg^2 cm^{-4} and σ_e 51.0 erg cm^{-2}. This compares with 60.9 erg cm^{-2} adopted by using σ Garlotta for L-PLA.

6.4 Conclusion

Examination of the development of the spherulite diameters with time shows that only in the initial stages of crystallization and with the lowest temperatures studied were the diameters less than the film thickness of the film sample, 15-20 μm. Accordingly for most of the crystallizations studied the spherulites grew as constant thickness discs and in terms of heterogeneously nucleated discs the corresponding Avrami equation would have a n constant value of 2.0.

Chapter 7. The Kinetics of Crystallization of Co-poly (lactic acid) measured by FTIR-TA spectroscopy.

7.0. Introduction

It was concluded in Chapter 4 that DSC did not have the necessary sensitivity to measure the heat flow from isothermal calorimetry to measure the kinetics of crystallization of Co-PLA. However, since FTIR spectroscopy measures the crystallinity directly from the absorbance of a crystalline band and not the rate of crystallization it has the potential to measure the kinetics directly from the change in absorbance. It only requires that sufficient time elapses for a measurable change in the absorbance to have developed. Because absorbance is a direct measure of the fractional crystallinity it has the potential to measure it over extended time periods and in particular to measure the slower secondary crystallization, which has been observed to develop with the logarithm of time.

Analysis of the IR spectrum of Co-PLA has shown that the carbonyl stretching band at 1759 cm^{-1} is the best vibrational band to study the kinetics of crystallization isothermally over a range of temperature. At constant temperature any variation in absorbance is attributed to changes due crystallinity.

This chapter is devoted to a study of the kinetics of crystallization of Co-PLA solution cast films on to KBr discs.

7.1. Analysis of the crystallization data

Measurements of the absorbance of the 1759 cm^{-1} band were made on thin films of Co-PLA cast from solution and mounted vertically in a hot-stage in the optical path of the spectrometer. The samples were melted for 2 min at 200 ^{o} C before being cooled to the crystallization temperature at 50 $^{o}C\ min^{-1}$. Measurements of absorbance were made over an extended period

up to 1000 minute in the temperature range 120-136 ^{o}C. The change in relative absorbance, defined as $(A_t - A_o)/(A_\infty - A_o)$ where A_o, A_t and A_∞ are the absorbances initially, at time t and at the end of the crystallization, with time at each temperature is shown in Figure 7.1.

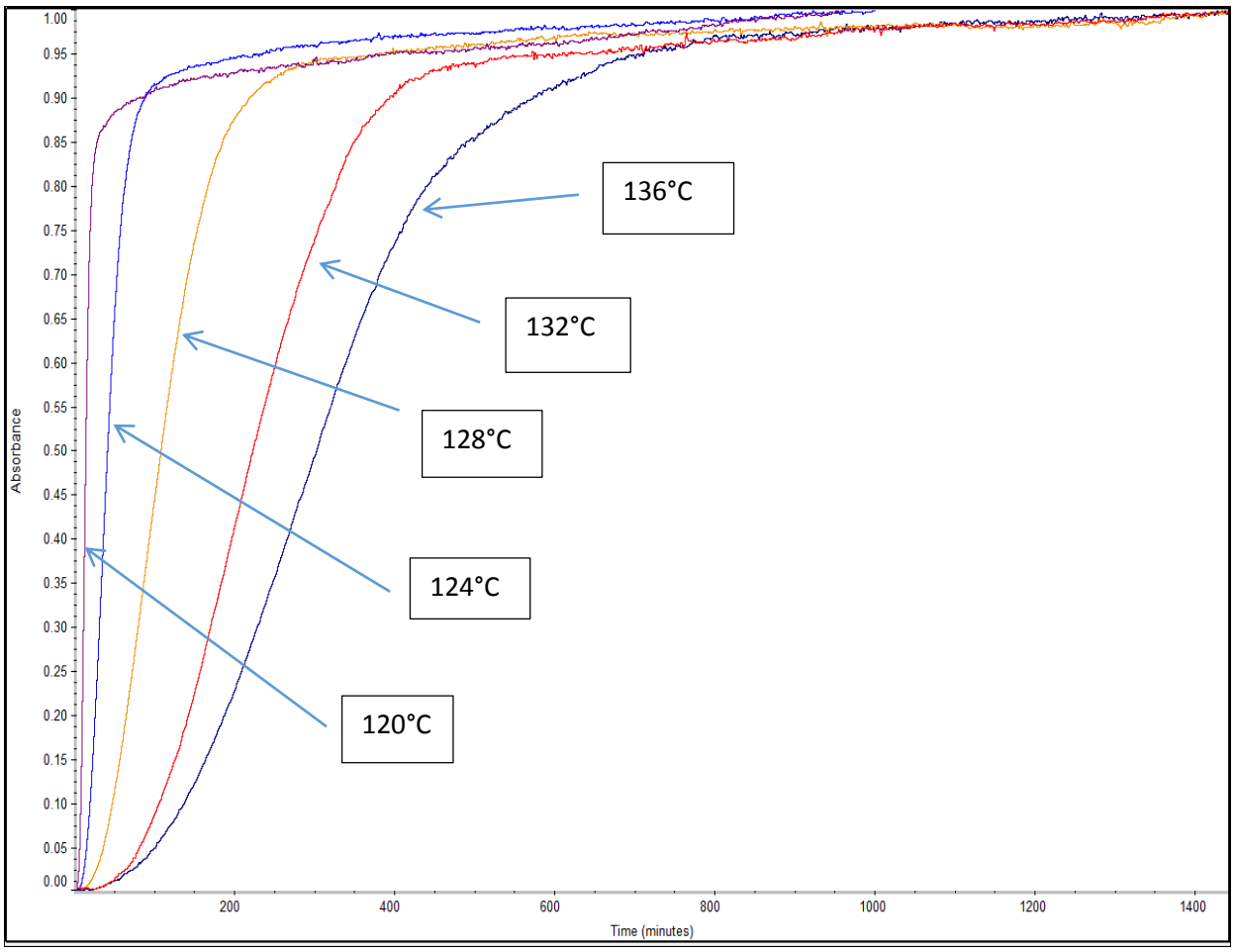

Figure 7.1. Relative change in absorbance at 1749 cm^{-1} with time on crystallization.

The change in absorbance on crystallization, 0.25-0.30, was relatively constant; the difference being due to different degrees crystallinity achieved. This is shown in Figure 7.2a. The change in absorbance due to crystallization was analysed as follows;-

The absorbance observed initially, A_o, before crystallization had started, was constant and attributed to an overlap of the broad amorphous band at 1750 cm^{-1} which decreased on crystallization due to the reduction of the amorphous regions. Assuming a two component

system for the partially crystalline copolymer, the absorbance at time t, A_t, will have an amorphous and crystalline component. If the fractional crystallinity is X_t then,

$$A_t = (1-X_t)\, A_o + X_t A_c \qquad (7.1)$$

Where A_c is the absorbance of a totally crystalline sample of the same thickness and the fractional crystallinity is

$$X_t = (A_t - A_o) / (A_c - A_o) \qquad (7.2)$$

Since A_o is unknown we adopt a relative crystallinity, X, relative to that achieved after the end of the measurements, i.e. t_∞ minute, defined as

$$X = X_t / X_\infty = (A_t - A_o) / (A_\infty - A_o) \qquad (7.3)$$

Figure 7.2b shows the increase in relative crystallinity, X, with time.

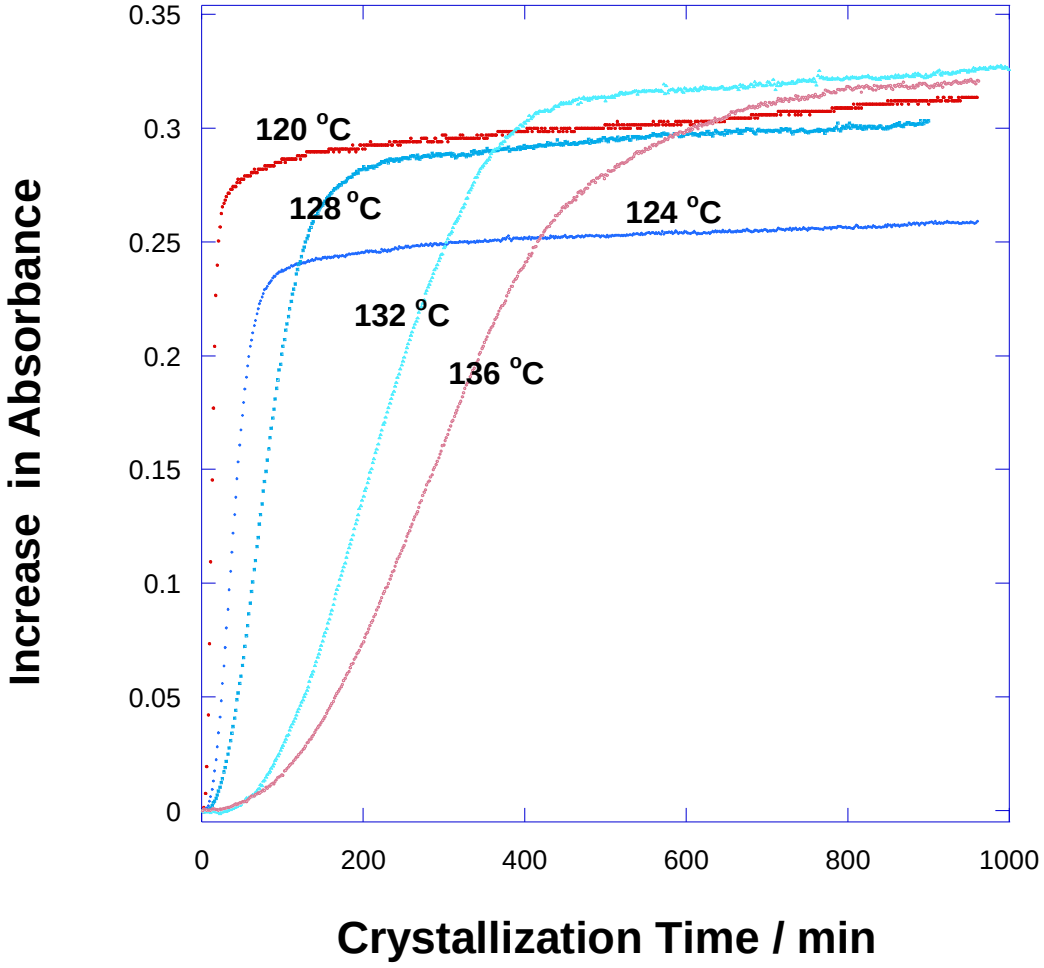

Figure 7.2a. The increase in absorbance with time on crystallization.

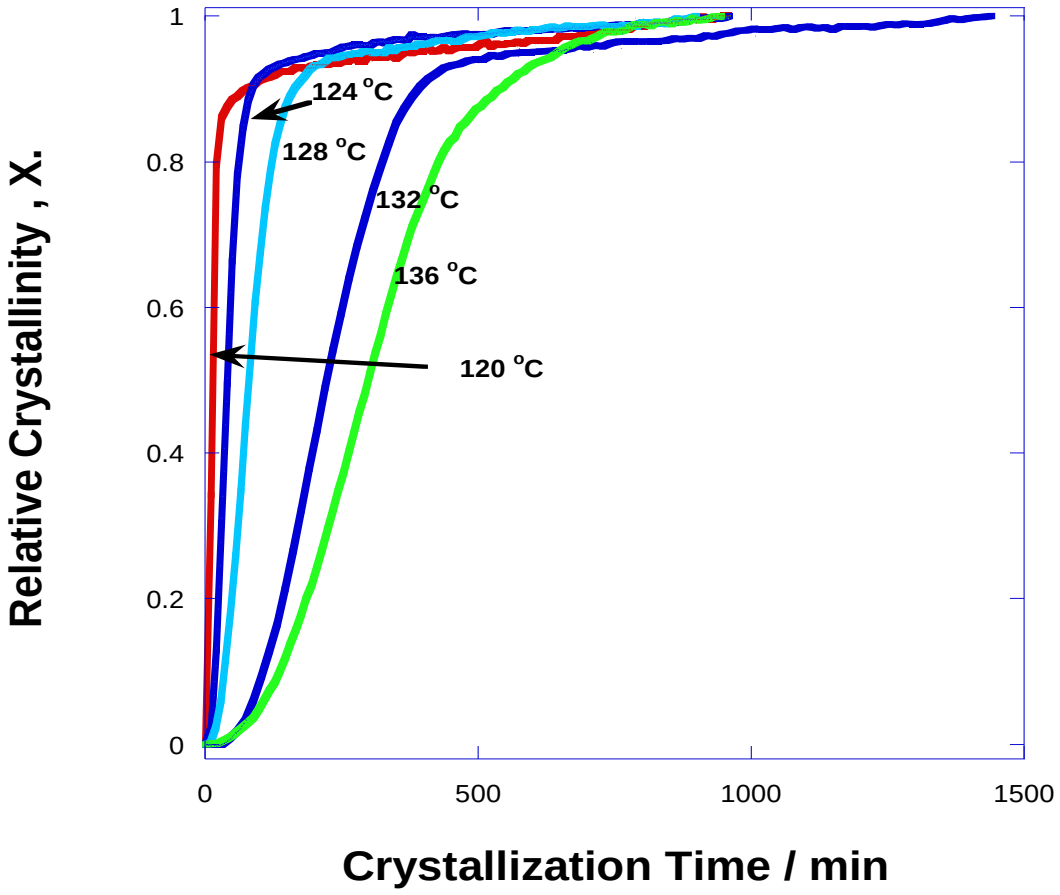

Figure 7.2b. The increase in relative crystallinity, X, with time.

7.2. Analysis of the kinetics of the primary process

The relative crystallinity-time dependence over the initial part of the crystallization, the primary process, was analysed using the Avrami equation, assuming that it ended at $X_{p,\infty}$

$$X_p = X_{p,\infty}(1- \exp(-Zt^n)) \qquad (7.4)$$

where X_p is the relative crystallinity developed within the primary process, Z is a composite rate constant incorporating nucleation characteristics and growth rate, t is time and n an integer constant characteristic of the crystallization mechanism.

It follows that

$$\log(-\ln(1-(X_p/X_{p,\infty}))) = n \log(t) + \log(Z) \qquad (7.5)$$

and plots of $\log(-\ln(1-(X_p/X_{p,\infty})))$ against log (t) were linear with intercept of log (Z) and slope n, see Figure 7.3. $X_{p,\infty}$ was used as an adjustable parameter and a value chosen which gave the best linear fit to the data as determined by R^2, see 7.4. Figure 7.5 and 7.6 show the plots of $\log(-\ln(1-(X_p/X_{p,\infty})))$ against log (t) for different temperature i.e 124 and 128 ^oC. The analysis of time dependence of the primary crystallization is summarised in Figure 7.7 and the Avrami rate parameters are listed in Table 7.1.

Using the best fit value of $X_{p,\infty}$ the n values were fractional, about 2.5 ± 0.4, and as such were inconsistent with the growth of disc for which a value of 2.0 or 3.0 was expected, depending on nucleation being heterogeneous or homogeneous respectively. The inconsistency was considered to lie in the assumption that secondary crystallization occurred towards the end of the primary process and made no contribution to the relative crystallinity which developed during the primary process.

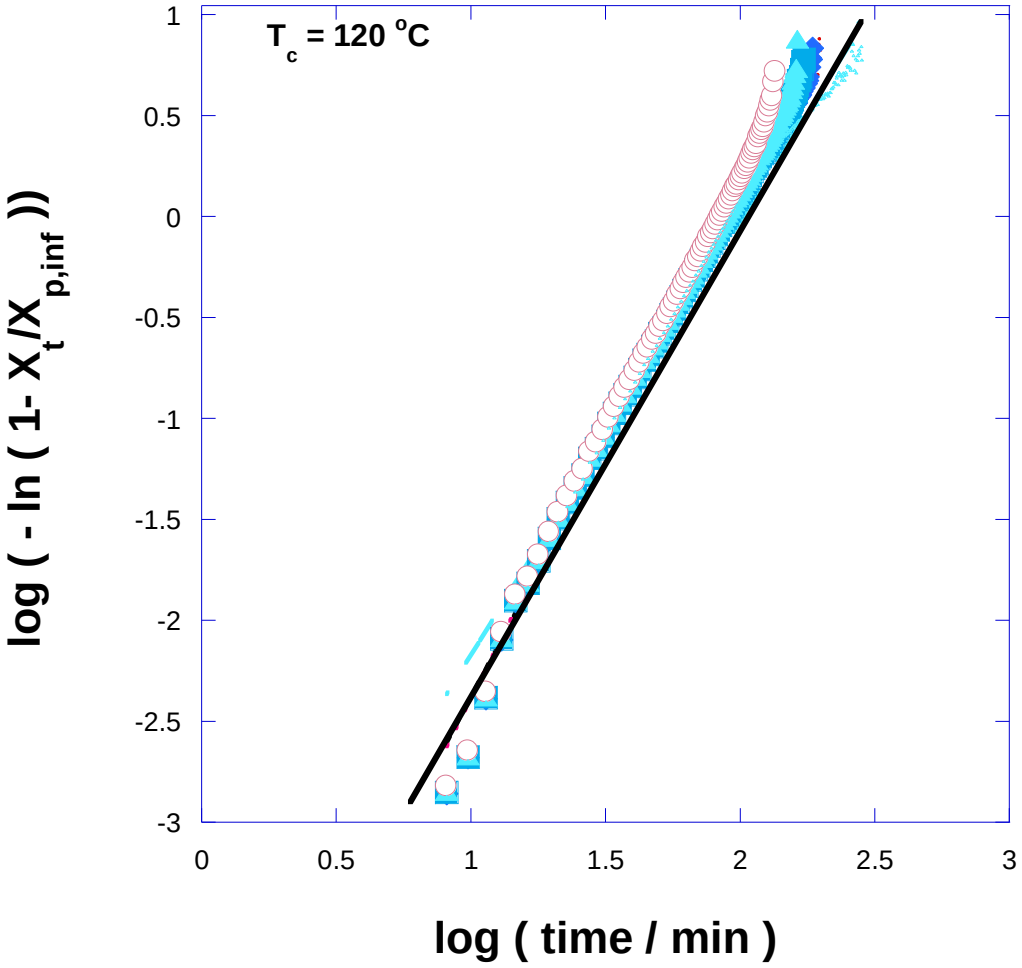

Figure 7.3. Double log plot of log(-ln(1-(X_p/$X_{p,\infty}$))) against log (t) at 120 °C. The effect of changing $X_{p,\infty}$.

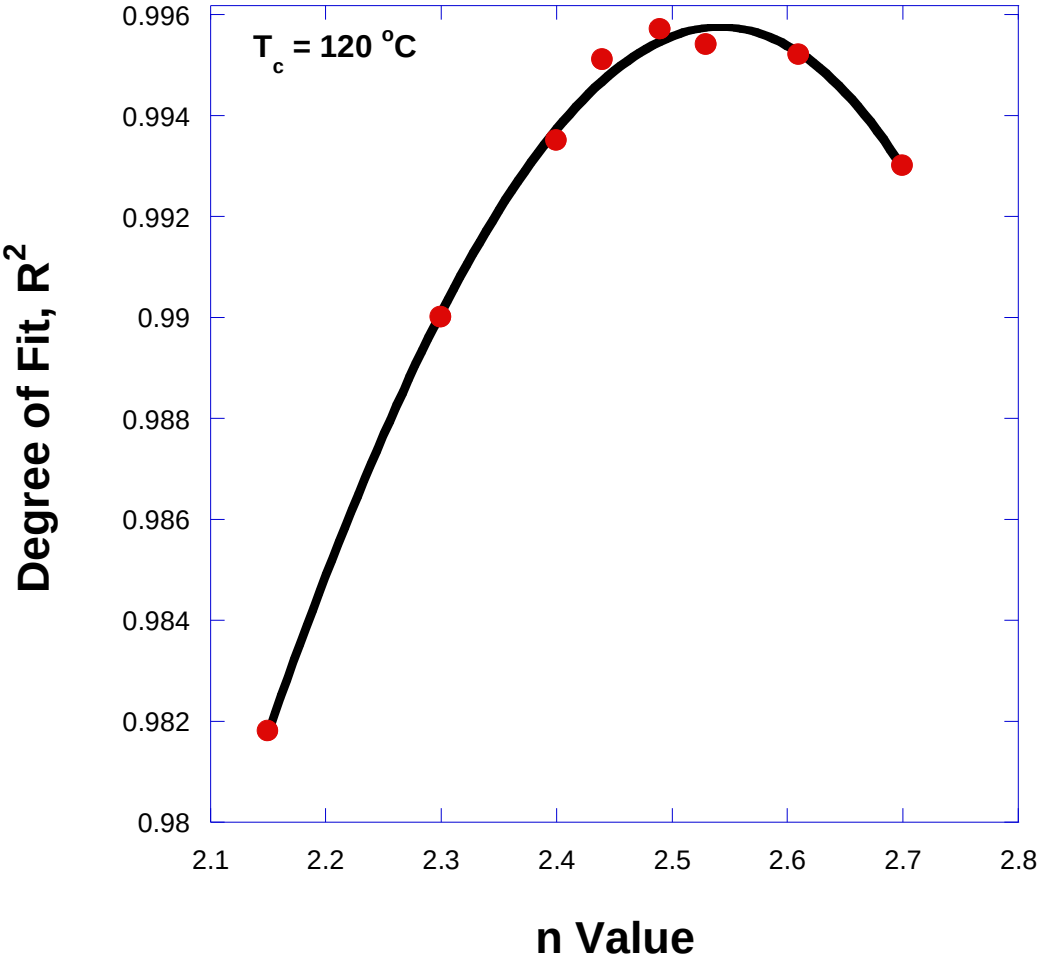

Figure 7.4. The effect of changing $X_{p,\infty}$. On the degree of fit.

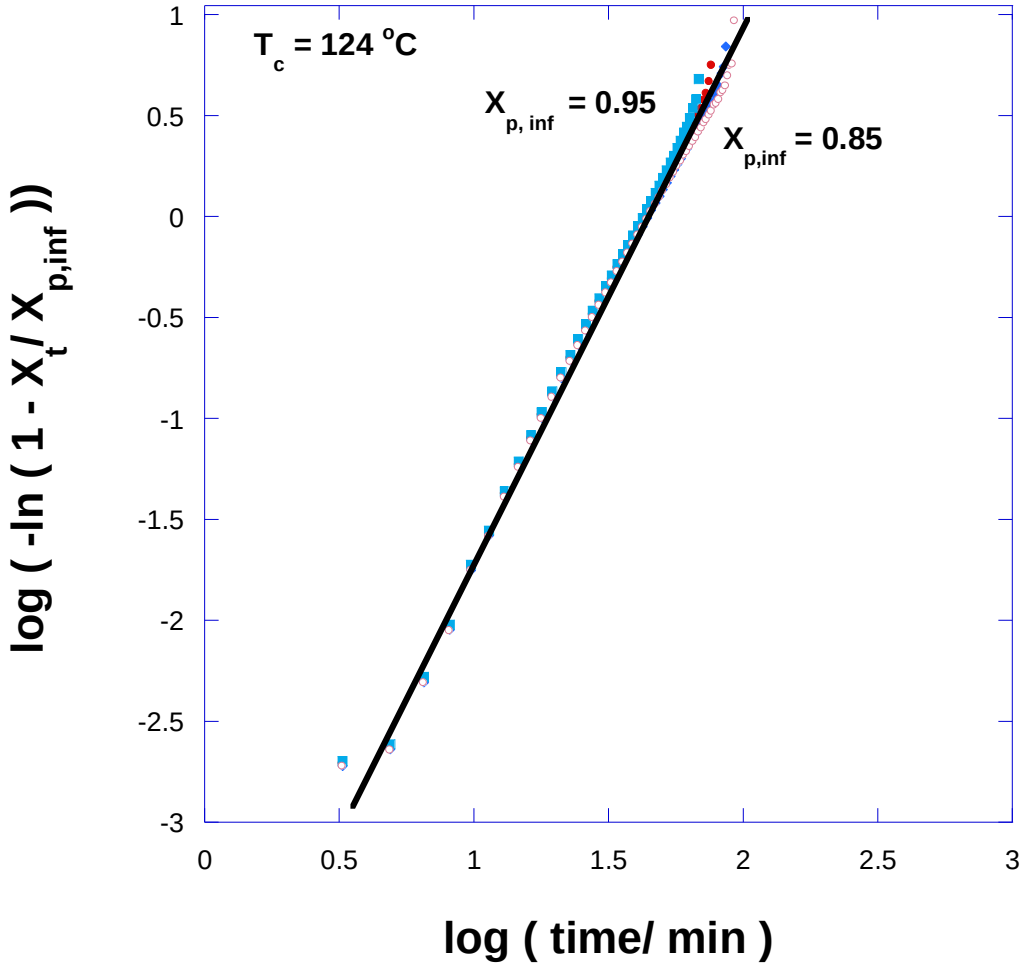

Figure 7.5. Double log plot of log(-ln(1-(X_p/$X_{p,\infty}$))) against log (t) at 124 °C. The effect of changing $X_{p,\infty}$.

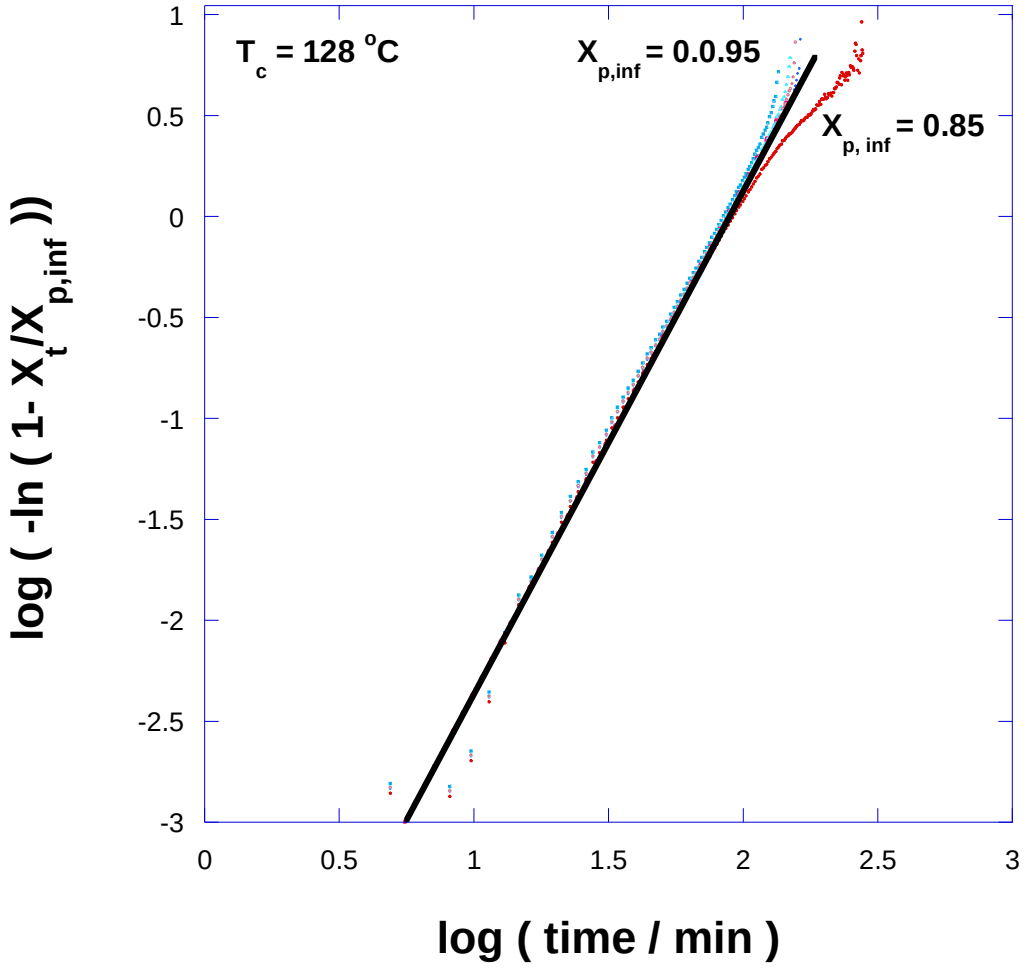

Figure 7.6. Double log plot of log(-ln(1-($X_p/X_{p,\infty}$))) against log (t) at 128 °C. The effect of changing $X_{p,\infty}$..

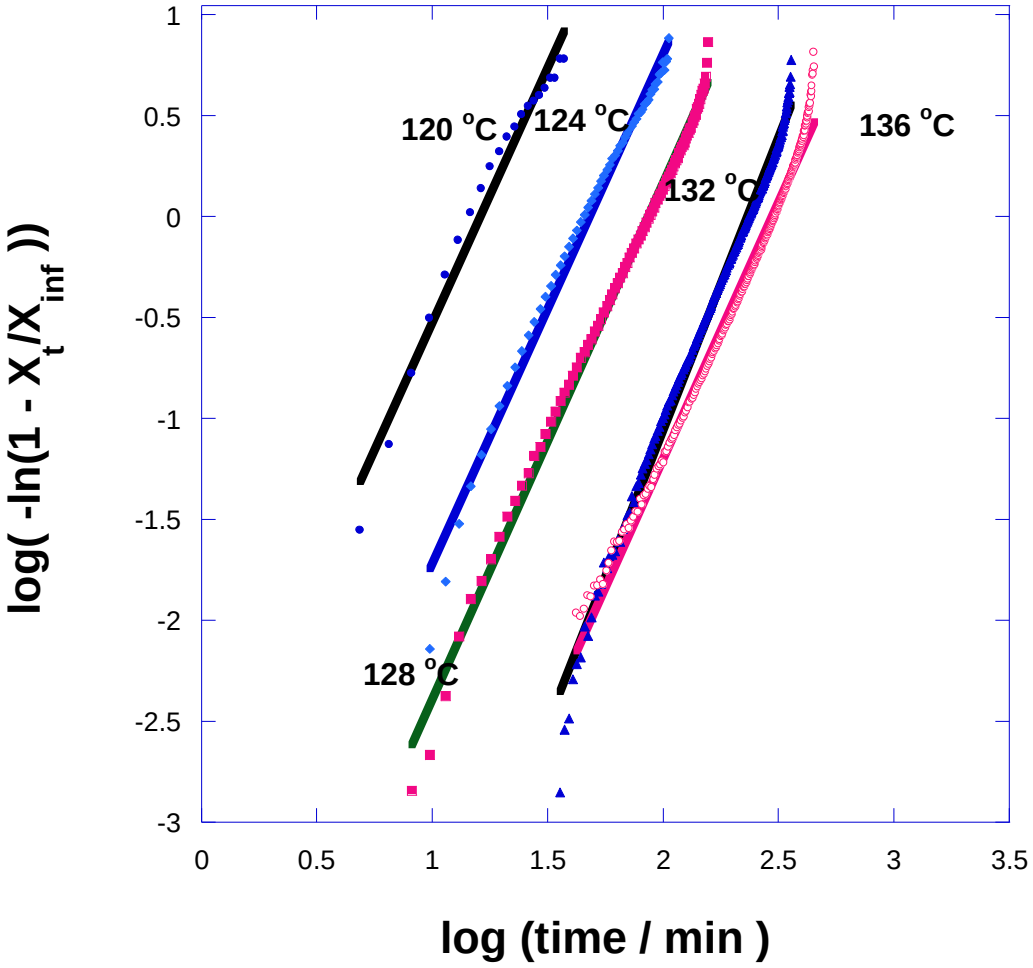

Figure 7.7. A summary of the Avrami analysis over temperature range studied.

Table 7.1. Avrami Rate Parameters for primary crystallization

Crystallization Temperature/ ^{o}C	120	124	128	132	136
n Value ± 0.2	2.5	2.5	2.5	2.8	2.1
-log (Z / min^{-n})	3.06	4.24	4.87	6.87	6.30
Crystallinity $X_{p,\infty}$	0.91	0.92	0.89	0.94	0.83
Variance R^2	0.996	0.986	0.994	0.993	0.983

7.3. Kinetic analysis of the secondary process

Evidence has recently been produced that the secondary crystallization process [133] was diffusion controlled, exhibited a dependence on the square root of the lapsed time and that it occurred as soon as crystalline material formed. Accordingly the relative crystallinity was the sum of both primary and secondary processes, i.e.

$$X_t = X_{p,t} + X_{s,t} \qquad (7.6)$$

where $X_{p,t}$ and $X_{s,t}$ are the contribution from primary and secondary crystallization at time t.

The amount of secondary is limited by the amount of primary crystallization but continue beyond it and so, $X_{s,t} = X_{p,t} k_s t^{1/2}$ (7.7)

This leads to $X_t = X_{p,\infty}(1 - \exp(-Zt^n)(1 + k_s t^{1/2})$ (7.8)

for the dependence of the crystallinity with time.

Once the primary process is complete, and $X_t > X_{p,\infty}$ then X_t is a linear function of $t^{1/2}$ with slope k_s and intercept $X_{,\infty}$ since

$$X_t = X_{p,\infty}(1 + k_s t^{1/2}) \quad (7.9)$$

This plot is shown in Figure 7.8 and rate parameters determined from it are listed in Table 7.2. The values determined for $X_{p,\infty}$ agree closely with those determined by the fit of the Avrami equation and listed in Table 7.1 and although the rate constants do not vary much they tend to increase with temperature which is inconsistent with a nucleation controlled process but consistent with diffusion control.

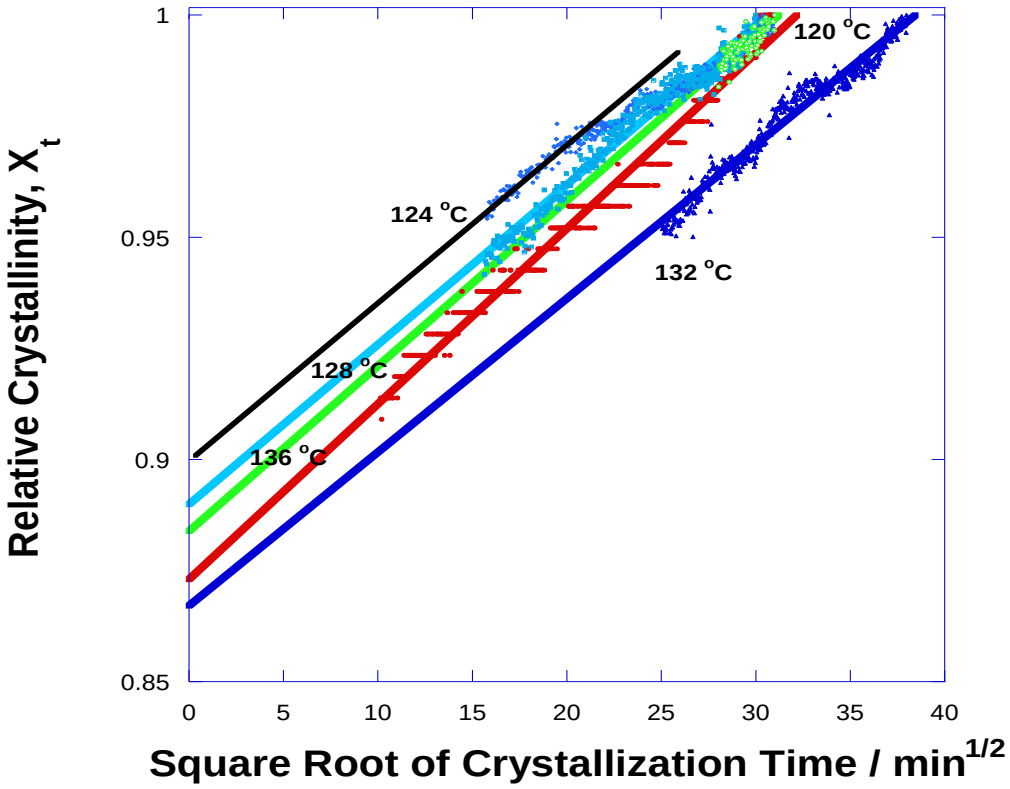

Figure 7.8. The dependence of the extent of secondary crystallization on the square root of the lapsed time.

Table 7.2. Rate parameters for secondary crystallization.

Crystallization Temperature / °C	120	124	128	132	136
Secondary Rate Constant, ks / $min^{-1/2}$	0.0031	0.0030	0.0041	0.0040	0.0042
$X_{p,\infty}$	0.87	0.92	0.89	0.87	0.83

7.4. Fit of Crystallization data to equation 7.8

Equation 7.8 was derived assuming that primary and secondary crystallization occur concurrently and the observed relative crystallinity at time t would not be expected to obey an Avrami rate equation. Only the primary process follows such a dependence, since

$$X_t = X_{p,\infty}(1 - \exp(-Zt^n)(1 + k_s t^{1/2}) \qquad (7.8)$$

The relative crystallinity due to the primary process which follows an Avrami equation is then,

$$X_{p,t} = X_{p,\infty}(1 - \exp(-Zt^n) = X_t /(1 + k_s t^{1/2}) \qquad (7.10)$$

And a plot of log $(-\ln(X_t /(1+ k_s t^{1/2})))$ against log (t) will be linear with a slope of n and intercept at t=1 of log(Z) if the primary process follows the time dependence of the Avrami equation. Figure 7.9 shows such a plot for the crystallization at 136 ^{o}C, for which n was 1.99 ± 0.10. The Avrami Rate parameters for the primary crystallization determined by this method are shown in Table 7.3. In every case n was 2.0 ± 0.2 which is consistent with the growth of discs confined to the thickness of the thin films and nucleated by heterogeneous nuclei as observed previously by hot stage microscopy.

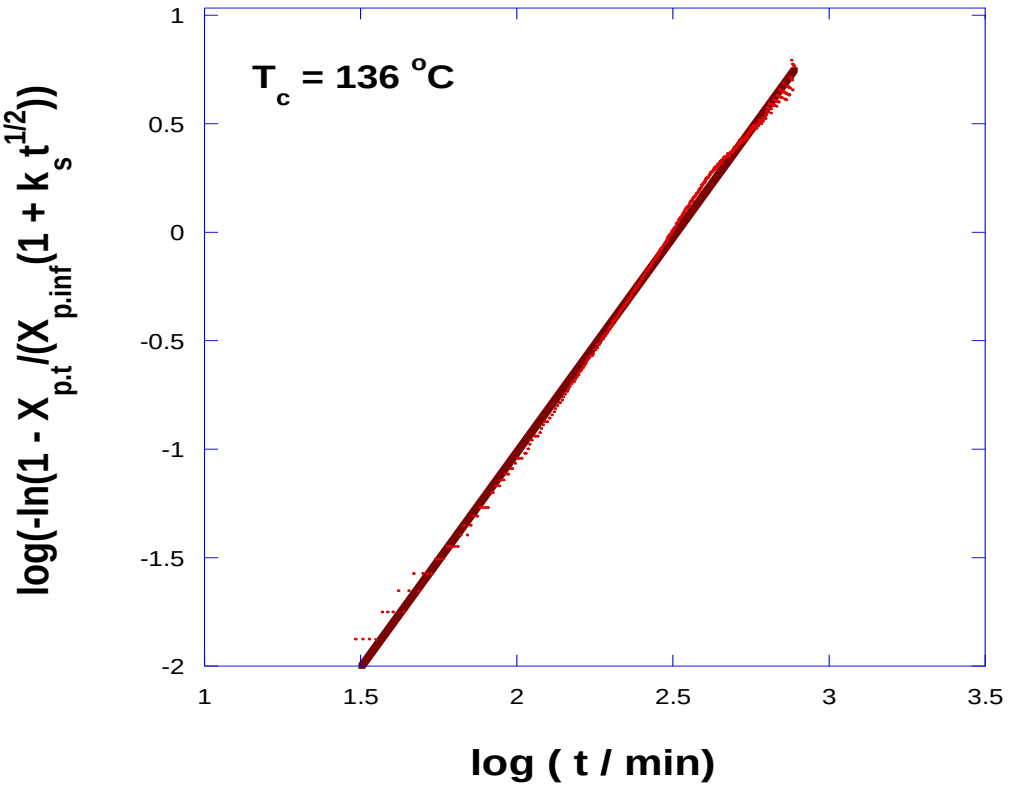

Figure 7.9. Analysis of the primary crystallization by Avrami equation.

Table 7.3. The Avrami Crystallization Rate Parameters.

Crystallization Temperature / ^{o}C	120	124	128	132	136
$\mathbf{X_{p,\infty}}$	0.87	0.92	0.89	0.87	0.83
Half-life / min	12	38	75	205	280
n Value	2.0	2.0	2.0	2.2	1.99
Z / min^{-2} x 10^{6}	4440	479	123	15.7	8.84

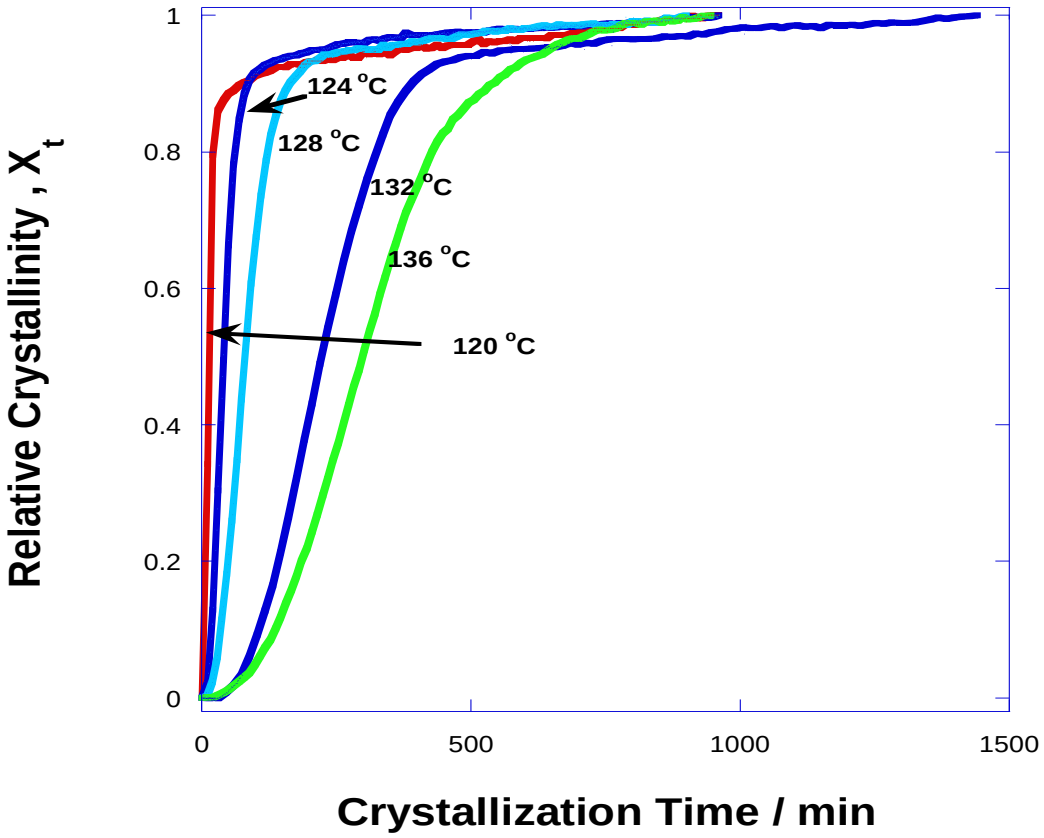

Figure 7.10. Calculated (dots) and experimental (lines) relative crystallinity against time.

In order to confirm that eq. 7.8 was a valid description of the crystallization-time dependence the relative crystallinity was calculated for each temperature using the rate parameters listed in Tables 7.2 and 7.3. A comparison was made between the experimental and calculated data to show that the equation was a reasonable fit to the overall time dependence of the crystallizations in Figure 7.10. Good fits of the experimental data was obtained with little or no variations observed between them. However, to highlight the differences between the two curves, the calculated crystallinity was subtracted from the experimental and the difference was

plotted against time in Figure 7.11. The maximum difference was about 0.02 and represented no more than the accuracy in measuring the absorbance i..e. 0.005 in the difference of 0.200.

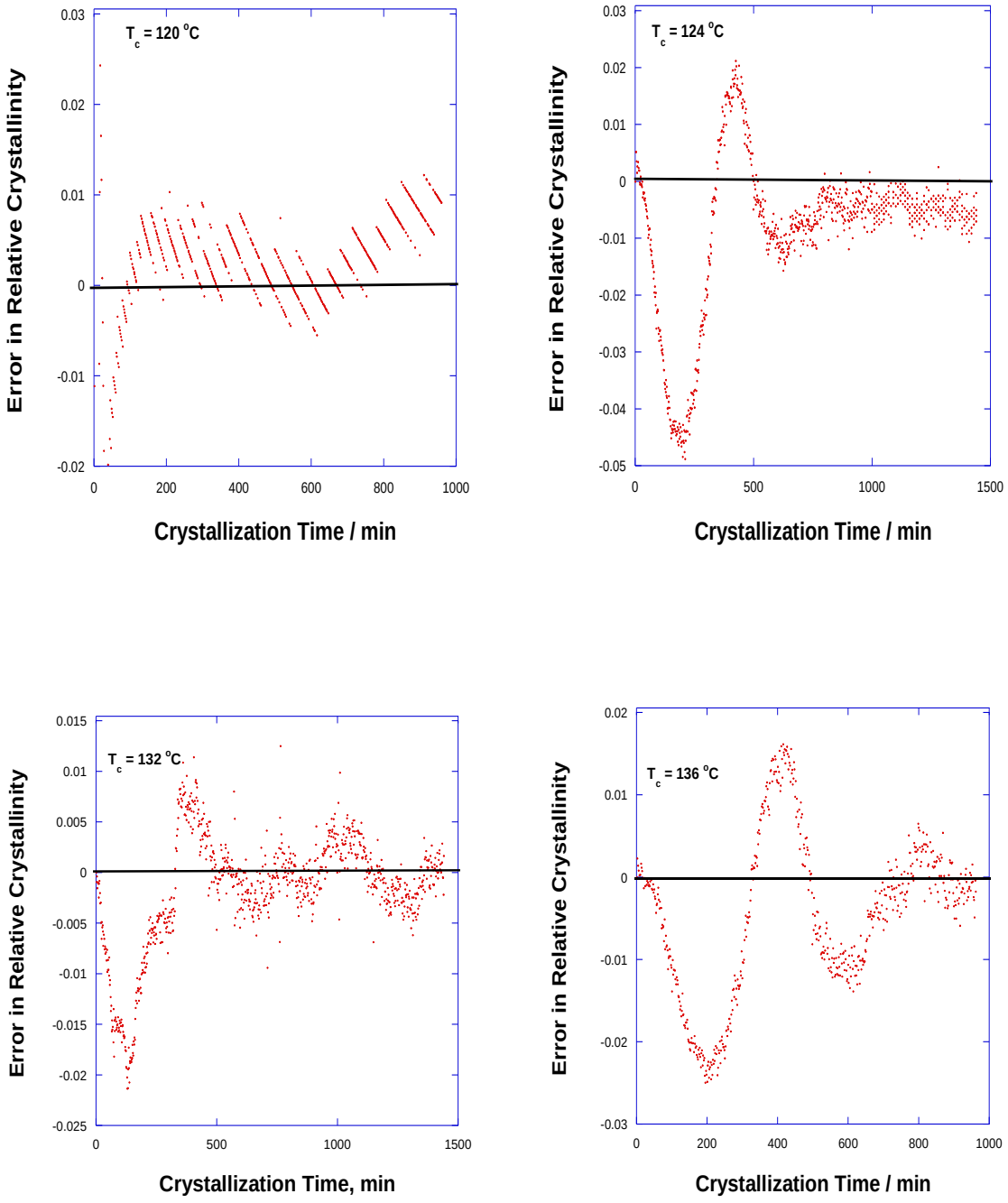

Figure 7.11. The Error in fitting equation 7.8 to experimental data at various crystallization temperatures.

The relative amount that the individual components of primary and secondary crystallizations make to the overall relative crystallinity was also calculated from the rate parameters listed in Tables 7.2 and 7.3 are shown in Figures 7.12 and 7.13. By comparison of the two figures it can be seen that secondary crystallization makes a substantial contribution to the overall crystallinity even in the initial stages of the crystallization, of the order of 10%, and this must account for the increased n value observed on assuming the initial stages was due to primary crystallization.

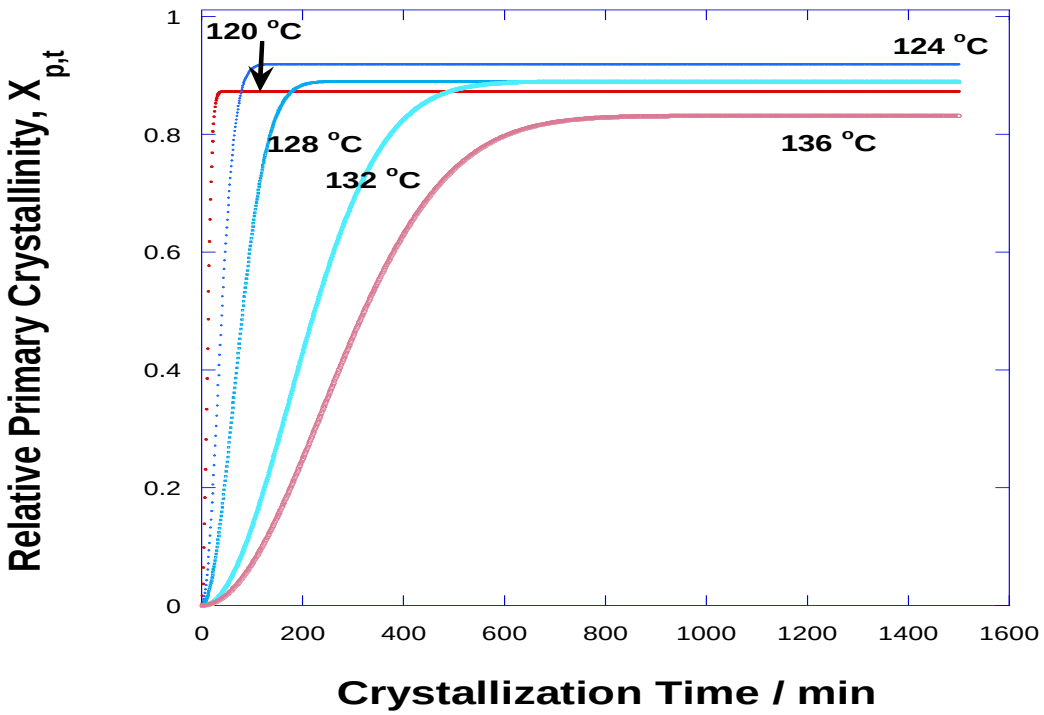

Figure 7.12. The contribution of primary crystallization to the overall relative crystallinity

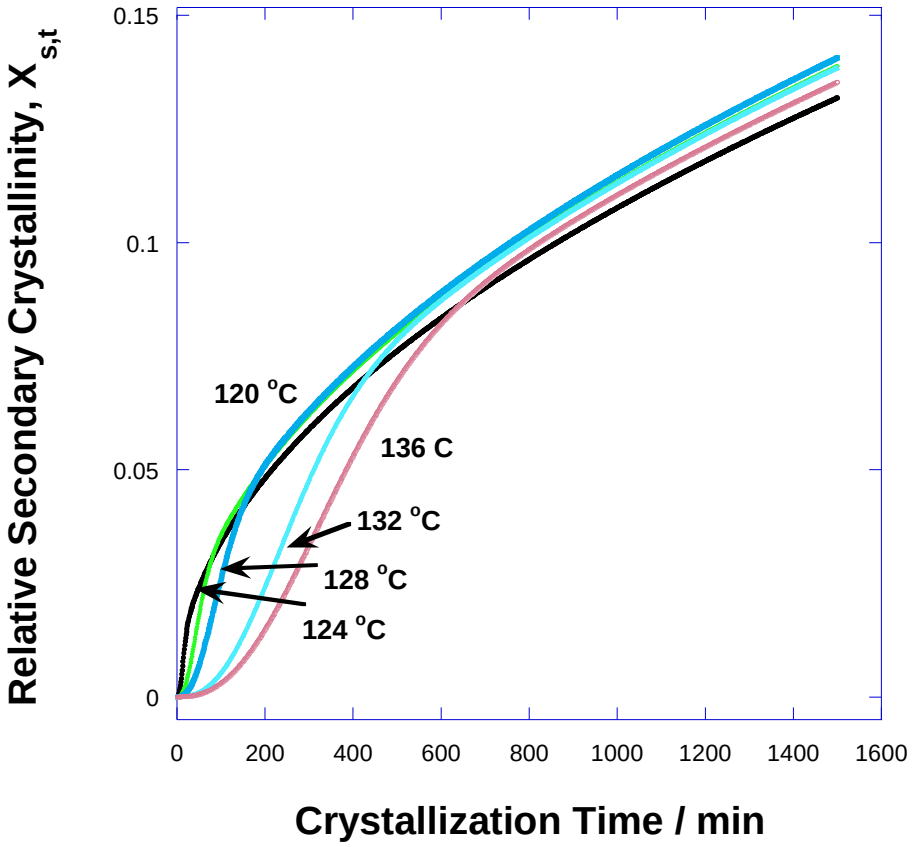

Figure 7.13. The contribution of secondary crystallization to the overall relative crystallinity.

7.5. The temperature dependence of primary crystallization

Unlike secondary crystallization primary crystallization slowed with increasing temperature resulting in the half-lives increasing with temperature, see Figure 7.14. This is consistent with nucleation control of the process and not diffusion as postulated for secondary crystallization. Accordingly, Hoffman and Lauritzen's theory of nucleation of polymer crystallization was adopted to explain the temperature dependence,

$$v = v^o \exp(-U^*/R(T-T_2).\exp(-K/T_c(\Delta T\, f)) \qquad (7.11)$$

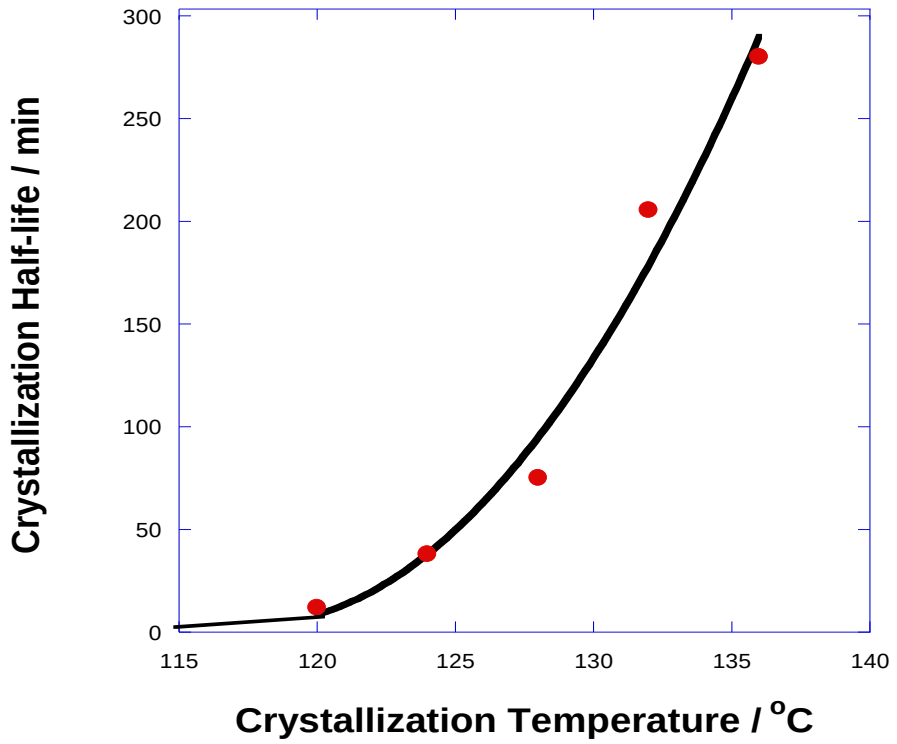

Figure 7.14. Dependence of primary crystallization half-lives on crystallization temperature.

and following Chan and Isayey ($1/t_{1/2}$) [134] values were substituted for the crystal growth rates, g and g_0, respectively and the dependence of the crystallization half-life given by

$$(1/t_{1/2}) = (1/ t^{o}_{1/2,0}) \exp(-U^*/R(T-T_2).\exp(-K^*/T_c(\Delta T\, f)) \qquad (7.12)$$

where U* is the activation energy of viscous flow, taken to be 6284 J $mol.^{-1}$, T_2 is the thermodynamic glass transition temperature, K* the nucleation constant, T_c the crystallization temperature, and ΔT the super-cooling from the equilibrium melting point, T_m^o. f is a correction for the temperature dependence of heat of fusion and is equal to 2Tc/{Tom +Tc). Plots of $\ln(1/t_{1/2})+U^*/R(T-T_2)$ against $1/(T\Delta T\, f)$ are show in Figure 7.15 for primary crystallization and the linear relationships gave a K* value of 4.09 $\pm$ 0.20 x 10^5 K^2 which compared with

$2.03 \pm 0.50 \times 10^5 K^2$ determined previously from the temperature dependence of the spherulitic growth rates see chapter 6. Since the nucleation constant in regime l is exactly twice that in regime ll we deduce that the measurements differ in being measured in the two different regimes; the high temperature measurements in Regime l and lower in Regime ll

For the crystallization to occur in Regime 1 then

$$K_l = 2K_{ll} = 4b\sigma\sigma_e T_m^o / k \Delta H_v \qquad (7.13)$$

Where b is the monomolecular layer thickness determined from the crystallographic dimensions of the unit cell, σ the surface free energy of the side of the lamellae, σ_e the fold surface free energy, k the Boltzmann constant and ΔH_v the enthalpy of fusion per unit volume. T_m^o is the equilibrium melting point of Co-PLA.

Using the values for these constants listed by Garlotta, [9] $\sigma.\sigma_e$ was determined to be 630 ± 30 $erg^2\ cm^{-4}$, which compares with values of 700 to 750 $erg^2\ cm^{-4}$ for PLA, [9]. Using the accepted value for σ of 12.0 erg cm^{-2} the fold surface energy was 52.5 ± 2.6 erg cm^{-2} and this compares with values for similar polymers of 54.9 erg cm^{-2} for poly (ϵ –caprolactone) and 76.0 erg cm^{-2} for PET [135].

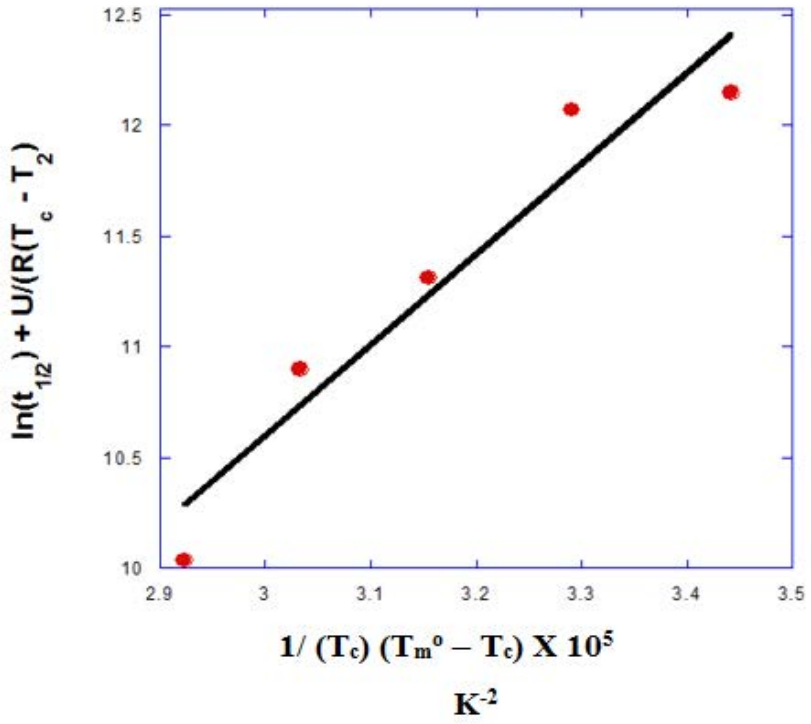

Figure 7.15. Nucleation control of primary crystallization after Hoffman and Lauritzen.

7.6. Conclusions

The absorbance of the carbonyl stretching band at 1759 cm^{-1} is a relative measure of the crystallinity of Co-PLA and is sufficiently accurate to measure the kinetics of the conversion for extended periods. However, because of the breadth of the amorphous band it was not possible to separately determine the amorphous and crystalline bands and the fractional crystallinity could not be determined without measuring it by some other means, e.g. from the heat of fusion. Both primary and secondary crystallizations have been measured over 1000 min which allowed detailed analyses of their time dependence over an extended period.

Primary crystallization exhibited an exponential dependence on time following an Avrami equation while secondary crystallization increased in crystallinity with the square root of the lapsed time. The rate constant increased with increasing temperature and so the process was considered to be diffusion controlled.

Assuming that secondary crystallization occurred towards the end of the primary gave Avrami exponents with constant fraction n values which have no significance in terms of Avrami's adopted crystallization models but assuming that it occurred as soon as crystallization started gave n values of 2.0 ± 0.2 which was consistent with growth of predetermined discs, as observed by examination of the samples by light microscopy. Although primary crystallization dominates the crystallization in the early stages secondary crystallization increases the overall crystallinity sufficiently to increase the n value determined above that expected for the model. The half-lives of the primary crystallization increased with increasing temperature consistent with a nucleation controlled process. Analysing with Hoffman and Lauritzen's model of nucleation growth allowed a value of $\sigma\sigma_e$ to be determined, which compared favourably with the literature values for PLA. This enabled the free energy of the fold surface, σ_e, to be estimated for future consideration.

Chapter 8. A Summary of the Experimental Results.

8.1 Outcomes and Discussions.

In Chapters 3 to 7 different aspects of the behaviour of the copolymer of poly (L-lactic acid) with 4% D-isomer have been studied and in this penultimate chapter an attempt has been made to draw the various conclusion together in some sensible order.

In chapter 3 experimental procedures were developed to follow the time dependence of crystallinity over extended periods of time using DSC but the isothermal crystallization rates were too slow for direct measurements. Use of a laboratory oven to develop samples with a range of crystallinity proved ineffective because of the problems in transferring samples from the oven to the DSC to measure the degree of crystallinity. An indirect method of measuring the development of crystallinity in the DSC by measuring the heat of fusion was less than satisfactory as the experimental accuracy was not acceptable, ± 5%. As a result other experimental methods to explore the kinetics of crystallization were explored.

However, melting studies showed that the m.pt. increased with time from the onset of isothermal crystallization and also with temperature. This was in-line with Hoffman and Week's nucleation theory of crystal growth and consistent with the lamellar crystals increasing in thickness with increasing temperature. Analyses of the dependence of the m.pt. on crystallization temperature gave a value of 205 ± 2 ^{o}C for the equilibrium melting point of Co-PLA of 207±2.0 °C in good agreement with the finding of others on PLLA. It was also been observed that the melting point at constant temperature increased throughout the crystallization, from the beginning to the end, in line with the secondary crystallization co-existing together with the primary process.

However, by controlling the cooling rate of the sample from the melt it was possible to study the effect of the degree of crystallinity on the glass transition temperature, and by forming standard glasses measure their enthalpic relaxation using DSC. The subject of Chapter 4 is accordingly the glass transition of the copolymer and its enthalpic relaxation using well developed procedures adopted for DSC. Two types of behaviour were observed in which at high cooling rates above 10^{o} C min^{-1} the Tg increased with increasing cooling while at very low rates of cooling 5^{o} C min^{-1} and below the Tg increased with decreasing cooling rates. Cooling rate was the dominant factor in determining the value of Tg of amorphous, but at the slower rates crystallinity determined the Tg, and the degree of crystallinity had a pronounced effect. With amorphous samples enthalpic relaxation on standard glasses developed following the Williams-Watt kinetics with a β value of 0.27±0.04 in good agreement with the literature on the copolymers in that the value decreased with the D-isomer content. Since β is a measure of the inverse breadth of the relaxation spectrum the comonomer content is increasing the breadth of the spectrum by producing more rotational modes in the relaxation spectrum.

Due to the failings of DSC in not having sufficient sensitivity to measure the crystallization kinetics of Co-PLA and FTIR-TA was used. In Chapter 5 the change in the spectrum of Co-PLA on heating and cooling to determine the phase changes occurring with temperature; in this way it was shown that the carbonyl band was sensitive to chain configuration and a crystalline band could be separately measured.

The isothermal crystallization kinetics of Co-PLA was measured in the temperature range from 120 to 136 °C from the change in absorbance of the carbonyl band at 1759 cm^{-1} and the change in relative crystallinity determined over 1000-2000 min which enabled the secondary to be separated from the primary process, in Chapter 7. The relative crystallinity-time data was analysed using modified Avrami equations assuming firstly that the primary and secondary crystallizations could be separated by their different time dependences, and secondly assuming

that the two co-existed together from the start of the crystallization but at the end the secondary process continued in the absence of the primary following a dependence on the square root of the lapsed time. Analysis of the data by the first method gave fractional n values which had no meaning in terms of the models adopted by Avrami. The second method fitted the kinetic data well and enabled the rate parameters of the two processes to be separately determined.

The study also shows that although the primary crystallization dominated the crystallization in the early stage, the secondary crystallization increased the overall crystallinity and this was sufficient to account for the increased fractional values of n. The analysis correcting for the increased crystallinity due to the secondary process could be fitted to an Avrami equation with n value equal to 2.00, consistent with the growth of disc spherulites in thin films as observed by hot-stage microscopy.

Hot stage polarised light microscopy was used to measure the radial growth rates and nucleation densities of thin films of co-PLA from 95 to 145 ^{o}C, in Chapter 6. The number of spherulites in the field of view did not increase with time at any temperature and since the spherulites had very similar diameters it was concluded that nucleation was heterogeneous. The nucleation density increased with increasing degree of supercooling but the growth rates increased with decreasing temperature, reached a maximum at about 120 ^{o}C and then decreased to zero at the glass Transition. The growth rates observed the characteristics bell shaped curve that has accounts for by Hoffman and Lauritzen relationship in terms of viscosity control at low temperature due to onset of glass transition and nucleation control at temperatures close to the melting point. Hoffman and Lauritzen's model for secondary nucleation of growth gave a value for the nucleation constant value of $2.03 \pm 0.50 \times 10^{5} K^{2}$. This enabled $\sigma\sigma_{e}$ to be measured, which compared favourably with the literature value for PLLA.

9.1 Conclusions.

● Co-PLA is slow to crystallize. The equilibrium melting point was 205 ^{o}C.

● Glass transition temperature varied with the cooling rate; faster cooling increased Tg and produced amorphous glasses; slower cooling increased Tg and produced more crystalline material.

● Amorphous glasses underwent enthalpic relaxation obeying the Williams-Watt relationship with a β value of 0.27 and activation energy of 0.4 ± 0.2 MJ mol^{-1}.

● The enthalpic relaxation of partially crystalline glasses confined to the amorphous regions was reduced in line with the change in $\Delta c_p(Tg)$,

● Infra-red spectrum of Co-PLA was sensitive to chain configuration and conformation and changed on heating or cooling and on crystallization and melting

● Intensity of the carbonyl band at 1759 cm^{-1} followed the degree of crystallinity and could be used over extended periods to measure crystallization kinetics.

● Crystallization occurred by the growth of heterogeneously nucleated spherulites whose radii grew linearly with time until they impinged with neighbouring ones. The spherical particles became discs early in the crystallization as the diameters approached the film thickness.

● Deviations in the crystallization kinetics were attributed to presence of secondary crystallization, such that the development of crystallinity with time followed the equation,

$$X_t = X_{p,\infty}(1 - \exp(-Zt^n) (1 + k_s t^{1/2})$$

● Crystallization mechanism was interpreted as growth of heterogeneous disc spherulites which grew obeying an Avrami equation with n=2.0 along with a secondary process by which the lamellae thickened with a rate proportional to the square root of time.

9.2. Future Work

FTIR-TA has been successfully applied to a study of the crystallization kinetics of a polyester over extended time periods with sufficient accuracy to test the validity of the Avrami equation, and in particular eliminate the embarrassment of fractional constant n values. This has been attributed to the presence of a secondary process which develops from the initial onset of crystallization and increases the crystallinity over that predicted by the Avrami equation. It would be interesting to extend this study to other polymer systems which have previously been shown to exhibit fractional n values to determine if this is a general solution of the problem or is it specific to this system alone.

It would be interesting to extend this approach to other polymer system, such as PEEK and PEK which contain carbonyl groups, and other polymers which do not contain carbonyl group to see if it is more generally applicable, e.g. polyethylene, polyethylene oxide etc. All these systems have been observed to exhibit fractional n values when their crystallization data has been analysed by the Avrami equation. It would confirm or otherwise that the conclusions on the secondary crystallization process was more generally applicable to the crystallization of polymers.

Similar rate measurements should also be carried out on D and L-PLA and their copolymers with the D:L lactide in order to determine the effect of chain irregularities on crystallization behaviour. This will confirm the effect of rejection of chain irregularities on these properties.

It would also be useful to measure the mechanism of secondary crystallization by direct observation of the thickening mechanism and measurement of the time dependence of the thickness in order to confirm the square root dependence on time. Hot stage ATM or Environmental SEM on thin polymer films would appear to be an obvious technique for such a study. Direct measurements of the growth rate will enable the nucleation constant to be

determined and directly measure the lateral surface energy term, σ, which has previously been determined indirectly.

References

[1] Mirinae K, Cheol L. S and Jeong Y. G, Influences of physical aging on enthalpy relaxation behaviour, gas permeability, and dynamic mechanical property of Polylactide films with various D-isomer contents, Macromol. Res., 8(4), 2010, p 346-351.

[2] Lunt. J, Large-scale production, properties and commercial applications of polylactic polymers, Polym. Degrad. Stabil., 59(1-3), 1998, p 145-152.

[3] Drumright R. E, Gruber P. R and Henton D. E, Polylactic Acid Technology, Adv. Mater., 12(23), 2000, p 1841-1846.

[4] Tsuji H, in Polyesters III Applications and Commercial Products, Doi Y and Steinbuchel A, Eds., Wiley-VCH, Weinheim, 4, 2002, p.129-177.

[5] Jung H. J, Ahn K. D, Han D. K, and Ahn D. J, Surface characteristics and fibroblast adhesion behavior of RGD-immobilized biodegradable PLLA films, Macromol. Res., 13(5), 2005, p 446-452.

[6] Park H. M, Lee K. Y, Lee S. J, Park K. E and Park W. H, Macromol. Res., Plasma-treated poly(lactic-***co***-glycolic acid) nanofibers for tissue engineering, 15(3), 2007, pp 238-243.

[7] Soppimath K. S, Aminabhavi T. M, Kulkarni A. R, and Rudzinski W. E, "Biodegradable polymeric nanoparticles as drug delivery devices," Journal of Controlled Release, 70(1-2), 2001, p 1-20.

[8] Guarino V, Causa F, Taddei P, Di Foggia M, Ciapetti G, Martini D, "Polylactic acid fibre reinforced polycaprolactone scaffolds for bone tissue engineering," Biomaterials, 29(27), 2008, p 3662-3670.

[9] Garlotta D, "A Literature Review of Poly(Lactic Acid)," Journal of Polymers and The Environment, 9(2), 2001, p 63-84.

[10] NatureWorksLLC. (2013). How Ingeo Is Made. Available: http://www.natureworksllc.com/TheNIngeoNJourney/EcoNProfileNandNLCA/HowNIngeo is Made.

[11] Groot W, Krieken J. V, Sliekers O and De Vos S, "Production and Purification of Lactic Acid and Lactide," in Poly(lactic acid) Synthesis, Structures, Properties, Processing, and Applications, R. Auras, L.-T Lim, S. E. M Selke, and H. Tsuji, Eds, Ed New Jersey: Wiley, 2010.

[12] Todo M, Park S. D, Takayama T, and Arakawa K, "Fracture micromechanisms of bioabsorbable PLLA/PCL polymer blends," Engineering Fracture Mechanics, 74(12), 2007, p 1872-1883.

[13] Ahmed J, Zhang J. N. X, Song Z and Varshnet S. K, "Thermal Properites of Polylactides: Effect of molecular mass and nature of lactide isomer,"Journal of Thermal Analysis and Calorimetry, 95(3), 2009, p 957-964.

[14] Lim L. T, Auras R and Rubino M, "Processing technologies for poly(lactic acid)," Progress in Polymer Science, 33(8), 2008, p 820-852.

[15] Mihai M, Huneault M. A and Favis B. D, "Crystallinity development in cellular poly(lactic acid) in the presence of supercritical carbon dioxide,"Journal of Applied Polymer Science", 113(5), 2009, p 2920-2932.

[16] Baratian S, Hall E. S, Lin J. S, Xu R and Runt J, "Crystallization and Solid-State Structure of Random Polylactide Copolymers, A Poly(l-lactide-co-d-lactide)s," Macromolecules, 34(14), 2001, p 4857-4864.

[17] Kolstad J. J "Crystallization kinetics of poly(L-lactide-co-meso-lactide),"Journal of Applied Polymer Science, 62(7), 1996, p 1079-109.

[18] Averous L and Pollet E, "Biodegradable Polymers," in Environmental Silicate Nano-Biocomposites, Averous L and Pollet E, Eds., ed, London: Springer, 2012.

[19] Martin O and Averous L, "Poly(lactic acid): plasticization and properties of Biodegradable multiphase systems," Polymer, 42(14), 2001, p 6209-6219.

[20] MacDonald R. T, McCarthy S. P and Gross R. A, "Enzymatic Degradability of Poly(lactide): Effects of Chain Stereochemistry and Material Crystallinity," Macromolecules, vol. 29(23), 1996, p 7356-7361.

[21] Wentao Z, Yoorim K, Wenli Z, Anson W and Chul B. Park, A Study of the Crystallization, Melting, and Foaming Behaviors of Polylactic Acid in Compressed CO_2, Int. J. Mol. Sci., 10(12), 2009, p 5381-5397.

[22] Dyson R. W, Specialty Polymers (1998), 2nd ed. London: Blackie Academic & Professional.

[23] http://plc.cwry.edu/tutorial/enhanced/files/polymers/orient/orient.htm, (polymer Marphology).

[24] Linda C. Sawyer, David T. Grubb, Gregory F. Meyers, Polymer microscopy, 2008.

[25] Cowie J. M. G, Polymers: chemistry and physics of modern materials. 2nd ed. London, 1991: Blackie Academic & Professional.

[26] Day M, Deslandes-Y, Roovers, J and Suprunchuk, Effect of molecular weight on the crystallization behaviour of poly(aryl ether ether ketone): a differential scanning calorimetry study. Polymer, 32(7), 1991, p 1258-1266.

[27] Cheng S. Z. D, Cao M. Y and Wunderlich, B, Glass Transition and melting behaviour of Poly (oxy-1,4-phenyleneoxy-1,4-phenylenecarbonyl-1,4-phenylene). Macromolecules, 19(7), 1986, p 1868-1876.

[28] Cebe P and Hong S. -D, Crystallisation behaviour of poly(ether-ether-ketone), Polymer, 27, 1986, p 1183-1192.

[29] Blundell D. J and Osborn B. N, The morphology of poly(aryl-ether-ether-ketone). Polymer, 24, 1983, p 953-958.

[30] Lauritzen J. I and Hoffman J. D, Extension of Theory of Growth of Chain-Folded Polymer Crystals to Large Undercoolings, Journal of Applied Physics, 1973, 44(10): p 4340-4352.

[31] Di Lorenzo M. L and Silvestre C, Non-isothermal crystallisation of polymers, Progress in Polymer Science, 24(6), 1999, p 917-950.

[32] Turnbull D and Fisher J. C, Rate of Nucleation in Condensed Systems, Journal of Chemical Physics, 1949, 17(1), p 71-73.

[33] Wunderlich B, Macromolecular Physics, Volume 2, Crystal Nucleation, Growth. 1976, London: Anealing Academic Press

[34] Jenkins M. J, Crystallisation in miscible blends of PEEK and PEI, Polymer, 2001. 42(5), p 1981-1986.

[35] Al Lafi A. G, James N. Hay, and Parker D. J, The effect of proton irradiation on The melting and isothermal crystallization of poly (ether-ether-ketone), Journal of Polymer Science Part B-Polymer Physics, 2008, 46(11), p 1094-1103.

[36] Guttman C. M, Hoffman J. D, and Dimarzio E. A, Monte-Carlo Calculation of Sans for Various Models of Semi-Crystalline Polyethylene, Faraday Discussions, 68, 1979, p 297-309.

[37] Hoffman J. D, Guttman C. M, and Dimarzio E. A, On the Problem of Crystallization of Polymers from the Melt with Chain Folding. Faraday Discussions, 68, 1979, p 177-197.

[38] Hoffman J. D, Regime-Iii Crystallization in Melt-Crystallized Polymers – the Variable Cluster Model of Chain Folding, Polymer, 24(1), 1983, p 3-26.

[39] Hoffman J. D, Role of Reptation in the Rate of Crystallization of Polyethylene Fractions from the Melt, Polymer, 23(5), 1982, p 656-670.

[40] Hoffman J. D, et al., Growth-Rate of Spherulites and Axialites from Melt in Polyethylene Fractions - Regime-1 and Regime-2 Crystallization, Journal of Research of the National Bureau of Standards Section a-Physics and Chemistry, 79(6), 1975, p 671-699.

[41] Lauritzen, J. I and Hoffman J. D, Theory of Formation of Polymer Crystals with Folded Chains in Dilute Solution, Journal of Research of the National Bureau of Standards Section a-Physics and Chemistry, 64(1), 1960, p 73-102.

[42] Muthukumar M, Nucleation in Polymer Crystallization, Advances in Chemical Physics, 128, 2004, 128: p 1-63.

[43] Avrami M, Kinetics of Phase Change II Transformation-Time Relations for Random Distribution of Nuclei, Journal of Chemical Physics, 8, 1940, p 212-224.

[44] Avrami M, Kinetics of Phase Change and Microstructure Kinetics of Phase Change III Journal of Chemical Physics, Journal of Chemical Physics, 8: 1940, 212-224, 9, 1941, p 177-184.

[45] Evans U. R, The Laws of Expanding Circles and Spheres in Relation to the Lateral Growth of Surface Films and the Grain-Size of Metals, Transactions of the Faraday Society, 1945, 41(7): p 365-374.

[46] Velisaris C. N and Seferis J. C, Crystallization Kinetics of Polyetheretherketone (Peek) Matrices, Polymer Engineering and Science, 26(22), 1986, p 1574-1581.

[47] Banks W, Gordon M, Roe R. J and Sharples A, The Crystallization of Polyethylene, Polymer, 4(1), 1963, p 61-74.

[48] James N. Hay and Sabir M, Crystallization Kinetics of High Polymers, Polyethylene Oxide .2, Polymer, 10(3), 1969, p 203-&.

[49] James N. Hay and Mills P. J, The Use of Differential Scanning Calorimetry to Study Polymer Crystallization Kinetics, Polymer, 23(9), 1982, p 1380-1384.

[50] Hillier I. H, Modified Avrami Equation for Bulk Crystallization Kinetics of Spherulitic Polymers, Journal of Polymer Science Part a-General Papers, 3(9pa), 1965, p 3067-&.

[51] Price F. P, A Phenomenological Theory of Spherulitic Crystallization - Primary and Secondary Crystallization Processes, Journal of Polymer Science Part a-General Papers, 3(9pa), 1965, p 3079-&.

[52] Banks W, Sharples A, and James N. Hay, The effect of simultaneously occurring processes on the course of polymer crystallization, Journal of Polymer Science Part a-1-Polymer Chemistry, 2(9), 1964, p 4059–4067.

[53] Verhoyen O, Dupret F, and Legras R, Isothermal and non-isothermal crystallization kinetics of polyethylene terephthalate: Mathematical modelling and experimental measurement, Polymer Engineering and Science, 38(9), 1998, p 1594-1610.

[54] James N. Hay, Application of modified Avrami equations to polymer crystallization kinetics, British Polymer Journal, 3, 1973, p 74-82.

[55] Qin, J. L, Guo S. Q, and Li Z. T, Melting behavior and isothermal crystallization kinetics of PP/mLLDPE blends, Journal of Polymer Research, 15(5), 2008, p 413-420.

[56] Hoffman J. D and J. J, Weeks, Melting Process and Equilibrium Melting Temperature of Polychlorotrifluoroethylene, Journal of Research of the National Bureau of Standards Section a-Physics and Chemistry, 66(Jan-F), 1962, p 13-&.

[57] Lim J. S, Noda I, and Im S. S, Effects of metal ion-carbonyl interaction on miscibility and crystallization kinetic of poly(3-hydroxybutyrate-co-3-hydroxyhexanoate)/lightly ionized PBS, European Polymer Journal, 44(5), 2008, p 1428-1440.

[58] Fisher E. W, Sterzel H. J, Wegner G, Kolloid Z. Z, Polym., Investigation of the structure of solution grown crystals of lactide copolymers by means of chemical reactions, 251, 1973, p 980–990.

[59] Hartmann M. H, in D. L Kaplan (Ed.), Biopolymers from Renewable Resources, Springer-Verlag, Berlin, 1998, p 367–411.

[60] Bigg D. M, in Society of Plastics Engineers—Annual Technical Conference 54(2), 1996, p 2028–2039.

[61] Tsuji H and Ikada Y, Polymer, Properties and morphologies of poly(L-lactide), Anealling conditions effects on Properties and morphologies of poly(L-lactide), 36(14), 1995, p 2709–2716.

[62] Marega C, Marigo A, DiNoto V, and Zannetti R, Die Makromolekulare Chemie, Structure and crystallization kinetics of poly(L-lactic acid), 193, 1992, p 1599–1606.

[63] Kolstad J. J, Journal of Applied Polymer Science, Crystallization kinetics of poly(L-lactide-***co-meso***-lactide), 62, 1996, p 1079–1091.

[64] Mazzullo S, Paganetto G, and Celli A, Progress in Colloid and Polymer Science, Regime III crystallization in poly-(L-lactic) acid, 87, 1992, p 32–34.

[65] Migliaresi C, De Lollis A, Fambri L, and Cohn D, Clinical Materials, The effect of thermal history on the crystallinity of different molecular weight PLLA biodegradable polymers, 8, 1991, p 111–118

[66] Von Oepen R and Michaeli W, Clinical Materials, Injection moulding of biodegradable implants, 10, 1992, p 21–28

[67] Huang J, Buehler N, Hall E, Kean R, Kolstad J. J, Wu L and Runt J, Polymer Preprints, 37(2), 1996, p 370–371.

[68] Kishore K, Vasanthakumari R and Pennings A. J, Journal of Polymer Science: Polymer Physics Edition, Isothermal melting behavior of poly(L-lactic acid), 22(4), 1984, p 537–542.

[69] Kalb B and Pennings A. J, Polymer, General crystallization behaviour of poly(L-lactic acid), 21(6), 1980, p 607–612.

[70] Vasanthakumari R and Pennings A. J, Crystallization Kinetics of Poly (l-lactic acid), Polymer 24(2), 1983, 175–178.

[71] Urbanovici E, Schneider H. A and Cantow H. J, Some considerations concerning the temperature dependence of the bulk crystallization rate constants of polymeric materials, Journal of Polymer Science: Part B: Polymer Physics 35(2), 1997 359–369.

[72] Tsuji H, Crystallization from the melt of poly(lactide)s with different optical purities and their blends, Macromolecular Chemistry and Physics. 197, 1996, p 3483-3499.

[73] He Y, Fan Z, Wei J and Li S, Morphology and Melt Crystallization of Poly(L-lactide) Obtained by Ring Opening Polymerization of L-lactide With Zinc Catalyst., 46(2), 2006, p 1583–1589.

[74] Yasuniwa M, Subakihara S, Sugimoto Y, Nakafuku C, Thermal Analysis of the Double-Melting Behaviour of Poly(L-lactic acid), Journal of Polymer Science Part B: Polymer Physics, 42 (1), 2003, p 25-32.

[75] Di Lorenzo M, Crystallization behavior of poly(l-lactic acid), European Polymer, 41(3), 2005, p 569-575.

[76] Mazurin O. V, Glass Physics and Chemistry, Problems of compatibility of the values of glass transition temperatures published in the world literature, 33(1), 2007, p 22.

[77] Gibbs J. H and Di Marzio E, Nature of the glass transition and the glassy state, The Journal of Chemical Physics, 28 (3), 1958, p 373-383.

[78] Richardson M. J, “The glass transition region”, In: Mathot, V.B.F. (ed.) Calorimetry and thermal analysis of polymers, Munich: Hanser Publishers, 1994, p 169-188.

[79] Simon F, ergeb.Exact.Naturw, 9, 1930, p 222-274.

[80] Simon F, Z.Anorg. Chem., 203, 1931, p 220-227.

[81] Cowie J. M. G and Ferguson R, Physical ageing of poly(methyl methacrylate) from enthalpy relaxation measurements, Polymer, 34(10), 1993, p 2135-2141.

[82] Brunacci A, Cowie J. M. G, Ferguson, R & McEwenm I. J, Enthalpy relaxation in glassy polystyrenes: 1, Polymer, 38(4), 1997, p 865-870.

[83] Pyda M, Wunderlich B, Reversing and nonreversing heat capacity of poly(lactic acid) in the glass transition region by temperature-modulated differential scanning calorimetry, in: Proceedings of the 31st NATAS Annual Conference on Thermal Analysis and Applications, 2003, p 143/1–143/9.

[84] Pyda M, Nowak-Pyda E, Wunderlich B, Physical aging of amorphous poly(lactic acid) by temperature-modulated calorimetry, in: Proceedings of the 33rd NATAS Annual Conference on Thermal Analysis and Applications, 2005, p 135.47.662/1–135.47.662/10.

[85] Pyda M, Wunderlich B, Reversing and Nonreversing Heat Capacity of Poly(lactic acid) in the Glass Transition Region by TMDSC, Macromolecules, 38(25), 2005, p 10472–10479.

[86] Perego G, Cella G. D and Bastioli C, Effect of molecular weight and crystallinity on poly(lactic acid) mechanical properties , Journal of Applied Polymer Science, 59**,** 1996 p 37–43.

[87] Jamshidi K, Hyon S. H and Ikada Y, Thermal characterization of polylactides, 29(12), 1988, p 2229–2234.

[88] Jim R. White, Polymer ageing: physics, chemistry or engineering? Time to reflect, Elsevier, 9(11-12), 2006, p 1396-1408.

[89] Pan P. J, Zhu B, Inoue Y, Enthalpy Relaxation and Embrittlement of Poly(L-lactide) during Physical Aging Macromolecules, 40(26), 2007, p 9664–9671.

[90] Nicola A Bailey, James N. Hay, Duncan M Price, A study of enthalpic relaxation of poly(ethylene terephthalate) by conventional and modulated temperature DSC, Thermochimica Acta, 367-368, 2001, p 425-431.

[91] Aref-Azar A, Arnoux F, Biddlestone F, James N. Hay, Physical ageing in amorphous and crystalline polymers. Part 2, Polyethyelene Terephthalate, Thermochim. Acta, 273, 1996, p 217-229.

[92] Cowie J. M. G and Ferguson R, Polym. Commun., 27, 1986, p 258.

[93] Hutchinson J. M, Physical ageing of Polymers, Progress in Polymer Science, 20, 1995, p 703-760.

[94] Chen Z. Y, James N. Hay, and Jenkins M. J, FTIR spectroscopic analysis of poly(ethylene terephthalate) on crystallization, European Polymer Journal, 48(9), 2012, p 1586-1610.

[95] "Personal Communication" James N. Hay.

[96] Richardson M. J and Savill N. G, Polymer, 16, 753, (1975); Thermochimica Acta, 213, 12, (1975).

[97] http://www.thermo.com.20th Feb 2012.

[98] http://www.sintef.no/.5th May 2012.

[99] http://www.linkam.co.uk/.8th May 2012.

[100] Oneill M. J, Analysis of Temperature-Controlled Scanning Calorimeter. Analytical Chemistry, 36(7), 1964, p 1238-&.

[101] Wunderlich B, Thermal Analysis, 1990, New York: Academic Press.

[102] Felice D. S, Pantani R, Titomanlio G, Nucleation and crystallization kinetics of poly(lactic acid), Thermochimica Acta, 522, 2011, p 128– 134.

[103] Pantani R, Felice D. S, Sorrentino A, De Maio F, Polymer Degradation and Stability, Crystallization kinetics of virgin and processed poly(lactic acid), 95, 2010, p 1148-1159.

[104] Tadakazu M, Polymer Crystallization behaviour of poly(L-lactide), 39(22), 1998, p 5515–5521.

[105] Steven K, Chain Mobility, Thermal, and Mechanical Properties of Poly(ethylene furanoate) Compared to Poly(ethylene terephthalate), 47 (4), 2014**,** p 1383–1391.

[106] Allan R MacKintosch, Liggat John J, Dynamic mechanical analysis of poly(trimethylene terephthalate)—A comparison with poly(ethylene terephthalate) and poly(ethylene naphthalate), Journal of Applied Polymer Science, 92(5), 2004, p 2791–2796.

[107] Wiley M, Properties and Behavior of Polymers, 2 Volume Set, 2011, p 1259.

[108] Williams G and Watts D. C, Trans. Faraday Soc., 66, 1970, p 80-85.

[109] James N. Hay, The physical ageing of amorphous and crystalline polymers, Pure & Appl. Chern., Vol. 67, No. 11, 1995, p 1855-1858.

[110] Liu T, Petermann J, Multiple melting behaviour in Isothermally cold-crystallized isotatic polystyrene, Polymer 42, 2001, p 6453-6461.

[111] Bonnet M, Rogausch KD, Petermann J, The endothermic “annealing peak” of poly(phenylene sulphide) and poly(ethylene terephthalate), Colloid Polym Sci, 277 (6), 1999, p 513–518.

[112] Farrow G, Crystallinity, “Crystal size and Melting Point of polypropylene, Polymer, 4, 1963, p 191-197.

[113] Ninjenhuis A. J, Grijpma D. W, Pennings A. J, Highly crystalline as-polymerized poly(l-lactide), Polym. Bull., 1991, 26 91), p 71–77.

[114] Flory P. J and Vrij A, Melting Points of Linear-Chain Homologs – Normal Paraffin Hydrocarbons, Journal of the American Chemical Society, 85(22), 1963, p 3548-&.

[115] Flory P. J, Orwoll R. A and Vrij A, Statistical Thermodynamics of Chain Molecule Liquids 2. Liquid Mixtures of Normal Paraffin Hydrocarbons, Journal of the American Chemical Society, 86(17) 1964, p 3515-&.

[116] Flory P. J, Orwoll R. A and Vrij A, Statistical Thermodynamics of Chain Molecule Liquids I. Equation of State for Normal Paraffin Hydrocarbons, Journal of the American Chemical Society, 86(17), 1964, p 3507-&.

[117] James N. Hay and Wiles M, Surface Free-Energy of Extended Chain Crystals of Polyethylene, Makromolekulare Chemie-Macromolecular Chemistry and Physics, 178(2), 1977, p 623-630.

[118] Mills P. J and James N. Hay, The Lamella Size Distribution in Nonisothermally Crystallized Low-Density Polyethylene. Polymer, 25(9), 1984, p 1277-1280.

[119] Bulkin B. J, Lewin M, DeBlase F. J, Conformational change, chain orientation, and crystallinity in poly(ethylene terephthalate) yarns: Raman spectroscopic study, Macromolecules, 18 (12), 1985, p 2587–2594.

[120] Zhu X. Y, Yan D. Y, Fang Y. P, In Situ FTIR Spectroscopic Study of the Conformational Change of Isotactic Polypropylene during the Crystallization Process, J. Phys. Chem. B, 105 (50), **2**001, p 12461-12463.

[121] Chalmers J. M, Hannah R. W, Mayo D. W, Spectra-structure correlations: Polymer spectra. In Handbook of Vibrational Spectroscopy; Chalmers, J. M, Griffiths, P. R, Eds.; John Wiley & Sons: Chichester,UK,; 4, 2002, p 1893-1918.

[122] Koenig J. L, Spectroscopy of Polymers; American Chemical Society: Washington, DC, 1992.

[123] Mallapragada S. K, Narasimhan B, Infrared Spectroscopy in Analysis of Polymer Crystallinity, In Encyclopedia of Analytical Chemistry, Meyers, R. A, Ed.; John Wiley & Sons: Chichester, UK, 2000, p 7644-7658.

[124] Holland B. J, James N. Hay, Thermal degradation of nylon polymers, Polym. Int., 49(9), 2000, p 943–948.

[125] Holland B. J, James N. Hay, The kinetics and mechanisms of the thermal degradation of poly(methyl methacrylate) studied by thermal analysis – Fourier transform infrared spectroscopy, Polymer, 42 (11), 2001, p 4825–4835.

[126] Holland B. J, James N. Hay, The thermal degradation of poly (ethylene terephthalate) and analogous polyesters measured by thermal analysis – Fourier transform infrared spectroscopy, Polymer, 43, 2002, p 1835–1847.

[127] Jianming Z, Hideto T, Isao N and Yukihiro O, Weak Intermolecular Interactions during the Melt Crystallization of Poly(L-lactide) Investigated by Two-Dimensional Infrared Correlation Spectroscopy, J. Phys. Chem. B, 108(31), 2004, p 11514-11520.

[128] Jianming Z, Differences in the CH3/OaC interactions among poly(L-lactide), poly(L-lactide)/poly(D-lactide) stereocomplex, and poly(3-hydroxybutyrate) studied by infrared spectroscopy, Journal of Molecular Structure, 735–736, (2005), p 249–257.

[129] Meaurio E, Infrared Spectrum of Poly(L-lactide): Application to Crystallinity Studies, Macromolecules, 39(26), 2006, p 9291-9301.

[130] Meaurio E, Conformational Behavior of Poly(L-lactide) Studied by Infrared Spectroscopy, J. Phys. Chem. B, 110(11), 2006, p 5790-5800.

[131] Kister G, Effects of morphology, conformation and configuration on the IR and Raman spectra of various poly(lactic acid)s, Polymer, 39(2), 1998, p 267-273.

[132] Bellamy L. J, Infra-red Spectra of Complex Molecules. Volume 2. Advances in Infra-red Group Frequencies, Chapter 11. Published by Chapman and Hall, London 1980

[133] Chen Z. Y, James N. Hay, and Jenkins M. J, The Effect of Secondary Crystallization on Crystallization Kinetics – Polyethylene Terephthalate Revisited, European Polymer Journal, 81, 2016, p 216-223.

[134] Chan T. W and Isayev A. I, Quiescent polymer crystallization: Modelling and measurements, Polymer Engineering & Science, 34(6), 1994, p 461-471.

[135] Chen Z. Y, James N. Hay, and Jenkins M. J, The kinetics of crystallization of poly(ethylene terephthalate), measured by FTIR spectroscopy, European Polymer Journal, 49(6), 2013, p 1722–1730.

Appendix 1

Supported Publications:

1. Azizan A. Aziz, Sani A. Samsudin, James N. Hay* and Michael J. Jenkins, "The Effect of a secondary Process on Polymer Crystallization Kinetics – 3. Co-poly (lactic acid)". As submitted to European Polymer Journal for consideration to publish.